SHATIS'17
4th International Conference on
Structural Health Assessment of Timber Structures
20-22 September 2017 Istanbul, Turkey

DAMAGE EVOLUTION IN WOOD UNDER TENSILE LOADING MONITORED BY ACOUSTIC EMISSION

I.Yahyaoui[1], M.Perrin[1], X.J. Gong[1], H.Li[1]

[1] Institut Clément Ader (ICA), CNRS UMR 5312, University of Toulouse, UPS, 1 rue Lautréamont, 65000 Tarbes, France

Keywords: Wood, Acoustic Emission, Damage evolution, Failure mechanisms

Abstract

Considerable progress can be observed within recent years in timber structures. But, the development of damage in these structures may cause catastrophic events. Therefore, frequent monitoring should be conducted to estimate the health condition of these structures. In this context, the acoustic emission (AE) is an efficient method for real time monitoring as well as damage growth in both structural components and laboratory specimens.

In this study, tensile tests in the axial direction were performed on standardized wood specimens. Three wood species were tested including Douglas fir, silver fir and poplar. Actually, these woods have close density, but their structures and their mechanical behaviors are quite different, so conduce to different damage process. Douglas firs are softwoods with a pronounced distribution of earlywood and latewood, their high strength among softwoods explains their important application for structural purposes. Silver fir is also softwood and it is abundant in the Pyrenean region in France, so interested to study for economical reason. Moreover, its structure is quite different from that of Douglas fir. Finally, poplar wood is a hardwood and it's well known as a homogenous wood. This work aims to investigate their damage process with help of AE sensor. During the test loading data were recorded simultaneously with the transient AE signals. And then we try to correlate the AE sources to the damage mechanism in the woods tested.

According to results, the following conclusions can be stated: The AE data recorded from tensile tests indicate clearly that the scenario from damage initiation, accumulation up to final macroscopic failure is quite different from one wood to another one. It depends strongly on their distribution of earlywood and latewood. The forms and the magnitudes of AE activities are directly related to the annual rings structure. It is shown that the wood with abrupt transition from earlywood to latewood are more emissive than wood with gradual transition. Also, acoustic emission monitoring allows the early detection of damage and the establishment of damage scenarios.

1 INTRODUCTION

Due to the increase of ecological awareness, the use of wood in civil engineering structures like timber bridges has been recently raised. Nevertheless, wood is an anisotropic material which is organized in a complex hierarchical structure distributed across multiple spatial scales, from microscopic to macroscopic scale. Hence, a thorough comprehension of the failure evolution in wood structures is required to avoid critical situations and to maintain safety standards. Until today, there is a lack of information in literature about tracking back the evolution of wood fracture zone to its origin. Such research should determine the temporal-spatial occurrence of damage mechanisms and their interactions at different length scales [1].
Regarding this issue, acoustic emission (AE) method should be suitable which is defined as a transient elastic wave generated by the rapid release of energy. It is shown that the acoustic emission (AE) method is appropriate for characterizing wood fracture process because it is sensitive to damage mechanisms at different length scales [1-3]. This technique provides advantages of early detection of crack initiation [4]. Besides, detailed monitoring of the damage evolution is allowed by the high time resolution of AE technique.
This paper analyses the damage process of three softwood species based on acoustic emission signal parameters. Douglas fir *(Pseudotsuga Menziesii)*, silver fir *(Abies pectinata)* and poplar *(Populus)* were tested under tensile loading, the influence of the heterogeneity induced by the proportion of earlywood and latewood in annual rings on the acoustic emission response has been discussed.

2 EXPERIMENTAL DETAILS

2.1 Materials and specimens

The materials tested under tensile loading in this study are Douglas fir wood, silver fir wood and poplar wood. All of them have close density but different structure. Douglas fir has large growth rings and a sharp definition between the earlywood and latewood. For silver fir the transition between earlywood and latewood is more gradual. Only narrow bands of thicker latewood cells divide two regions of wide bands of earlywood. Silver fir structure is considered like uniform structure compared to Douglas fir structure. Poplar wood has different features compared to the two tested softwoods. Notable features for poplar wood are the diffuse pores in no specific arrangement, marginal parenchyma and nodded rays. The transition between earlywood and latewood is not distinct with naked eye so it is why poplar is considered as a homogenous wood.

Tensile specimens with dog-bone shape have been prepared from the three species of wood with nominal dimensions according to NF B51-017 (350 mm overall length, 100 mm length, 20 mm width and 20 mm thickness in grip section, 90 mm length, 20 mm width and 4 mm thickness in the calibrated section) (Figure 1). All specimens have the length in longitudinal direction and the width in radial direction. To prevent crushing on the specimen by the grips, four tabs in steel of length 60 mm were glued to the ends of the specimen using bicomponent epoxy resin (ESK-48).

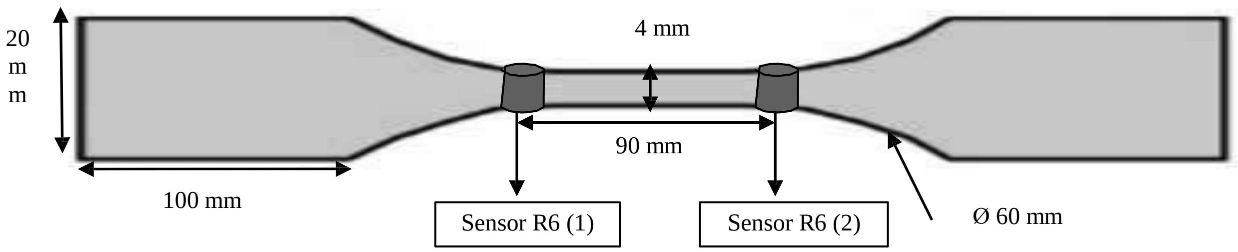

Figure 1: Tensile specimen and sensors position

2.2 Test conditions

Five specimens were tested for each wood species. The total number was 5x3= 15 samples. They were conditioned and stored at 20°C and 65% relative humidity before testing. Tensile tests were performed by using universal test machine MTS© 20M with a load cell calibrated in the load range of 100kN. In all tests, load was applied parallel to the grain of wood sample and under displacement control with a constant cross-head speed 2.5mm/min until the specimen failed. Strain gauges are used to measure the strain along the longitudinal and the transversal axis for the purpose to determine Young's modulus and Poisson's coefficient of the materials.

2.3 Acoustic emission equipments

Wood is a very heterogeneous and a highly attenuative material. For these reasons, a preliminary study was done to select the suitable sensors for wood materials. In the literature the sensors used for monitoring damage in wood have resonant frequencies between 150 and 300 kHz [1-5]. But a recent study [2] indicated that in the cases of wood fracture process the maximum Power Spectral Density (PSD) defined as the distribution of energy over the frequency, resided in a low frequency area around 60 kHz. So in order to properly assess the frequency portion of the signal, resonant frequency of the sensor should be carefully taken into account. In this context, four types of piezoelectric sensors were tested in order to select the suitable one: three resonant sensors R15α, R6α and R3α with resonant frequency respectively 150 kHz, 60 kHz and 30 kHz, and one wideband sensor (WD) (frequency band-width between 100 kHz and 1 MHz) are tested. Results of wideband sensor showed that the frequency of damage in wood is situated between 30 kHz and 50 kHz (Figure 2). Consequently, R3α and R6α sensors are the most convenient for wood damage monitoring. In this research work, both of R3α and R6α sensors were used simultaneously. After analyses of the signals recorded by these sensors, it is found that the R6α sensors gives better results concerning localization of the events. Therefore we will limit our analyses on the results recorded by R6α sensor in the next parts of this paper.

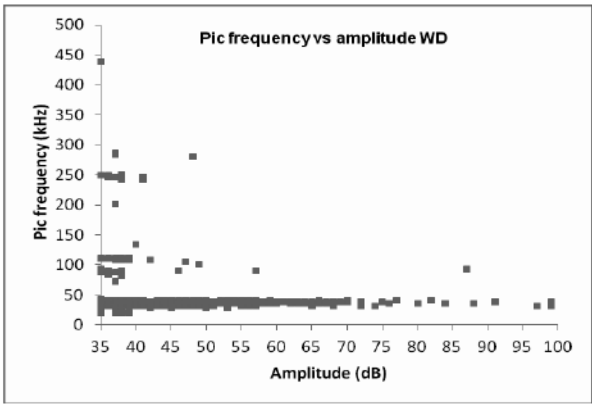

Figure 2: Pic frequency vs amplitude of WD sensor showing the concentration of hits in a frequency range between 30 kHz and 50 kHz.

Figure 1 schematizes also the positions of AE sensors on the tested specimen. In order to locate AE events, two R6α sensors were placed on the front side of the tensile specimen one on the top and another on the bottom of the calibrated section. Sensors were fixed with clamps. In order to avoid any loss of acoustic signal at the transducer-sample interface, silicone-free vacuum grease was used to couple the sensors to the surface of specimens. The AE data are recorded with help of an Euro Physical Acoustics system composed by a PCI8 board. The acquisition is computed by using AEwin/SAMOS software. The analog filter frequency is set up between 20 and 400 kHz and the acquired signals are preamplified by 40 dB. The environmental noise was filtered using a threshold of 35 dB. The timing parameters, peak definition time (PDT), hit definition time (HDT) and hit lockout time (HLT) are set at 40, 200 and 300 μs, respectively [6].These parameters are verified by Pencil-lead breaks (Hsu-Nielsen source) [7] before the beginning of tests. The same sources are used to calculate the wave velocities whose values are given in Table1. Wave velocity is species dependent. In fact, it increases with the increasing of raw density of the material [8].

Table 1: Wave velocities and raw densities of wood species

Wood species	Wave velocities (m/s)	Raw density (Kg/m^3)
Douglas fir	4747 ± 560	501 ± 22.25
Silver fir	4549 ± 164	446 ± 45.43
Poplar	4345 ± 115	410 ± 11.35

3 RESULTS AND DISCUSSIONS

3.1 Mechanical properties from stress stress-strain graph

The fracture stress and the modulus of elasticity for the three woods determined from the tensile tests are shown in Figure 3. It is shown that the tensile strength of Douglas fir is 65% greater than that of silver fir, and 8% greater than that of poplar, respectively. These results are compared with those obtained in reference [9] (Figure 3). Good correlation can be pronounced for Douglas fir, but not for silver fir and poplar wood. The failure stress for three woods in reference [9] seems following the same variation of their density. But it is not really the case regarding the measurement on the woods tested in our study. Concerning the

Young's modulus, it seems density dependent (Figure 3) since Douglas fir is stiffer than the two other species. Furthermore, silver fir and poplar have equivalent stiffness (Figure 3) and close densities (Table 1).

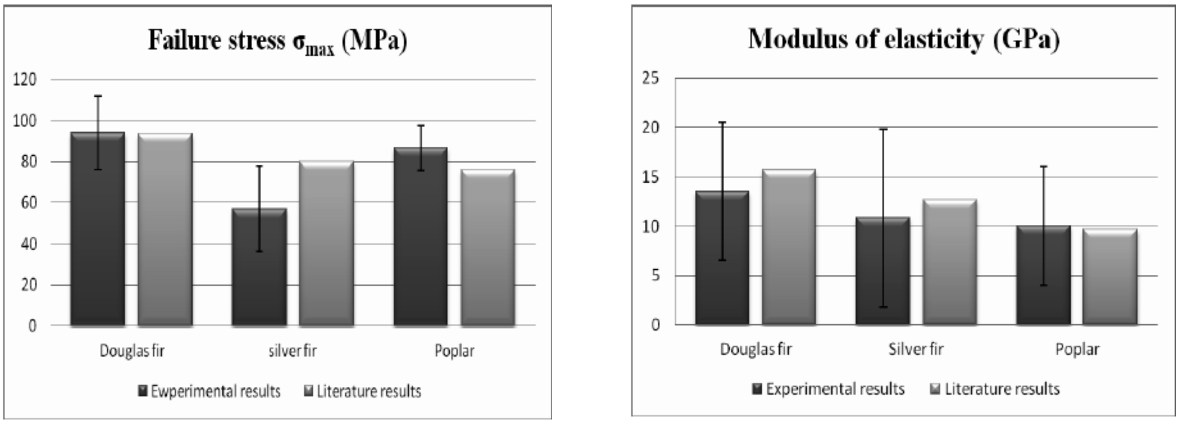

Figure 3: Mechanical properties for the three tested wood species

3.2 Failure scenario and damage indication by AE

3.2.1 Douglas fir

The examination of fracture surface of Douglas fir specimens reveals different damage mechanisms: transverse fracture in earlywood (EW) tracheid, transverse fracture in latewood tracheid (LW) and the parallel-to-grain crack propagation along the EW/LW interfaces and in the EW (Figure 4 a-b).

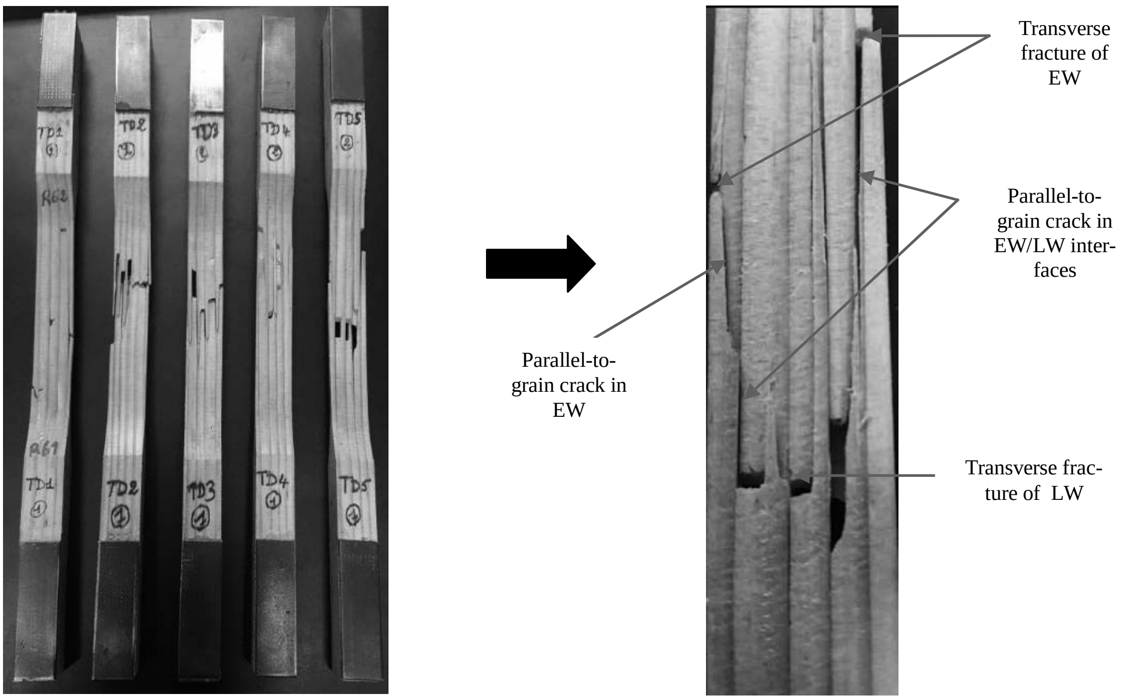

(a) (b)

Figure 4: (a) Failure patterns observed for Douglas fir specimens (b) Failure modes in TD5 fracture surface

As an example we will focus on TD5 specimen to correlate the AE data with damage mechanisms. Figure 5 shows the evolution of the load and of AE parameters in term of cumulative AE hits as a function of the testing time. In general, the load/time curve could be decomposed in three stages based on cumulative AE hits. In the linear deformation part, some emissions have been observed. In their study [10] suggested that the random AE signals observed in the elastic deformation stage are the result of the non uniform stress field resulting from non-homogeneity of wood structure. Actually, reorientations in wood structure are observed, which lead to adaptation for new conditions of loading [10]. When it entered into the non-linear deformation part (part II), the rate of cumulated AE hits increased. This rapid increase could be attributed to inter-laminar shear in planes of weakness like earlywood/latewood interfaces [8]. In this stage parallel-to grain micro-cracks in EW/LW transition zones are developed. Then, the specimen entered to the fracture stage (part III) which leads to a sharp increase in cumulative AE hit. As damage in the specimen intensified, macro-cracking took place and the first visible crack was found at t= 64.3s, herein a sharp drop of the load can be observed (Figure 5- Point B). A transverse crack in the EW appeared, and then the crack propagated longitudinally in the EW/LW interfaces. Successively, a second, a third visible crack across EW occurred at t= 68.2s and at t=69.47s, respectively (Figure 5 – Point C and Point D), they are accompanied by the longitudinal crack growth or in EW tracheid, or at the EW/LW interface. Thereafter, the rate of cumulated AE hits increased as the damage continued to progress until the fourth and final fracture at t=78.1 s (Figure 5- Point E). The several drops of load indicate that the specimen still had high load-bearing capacity after the first visible fracture [11].

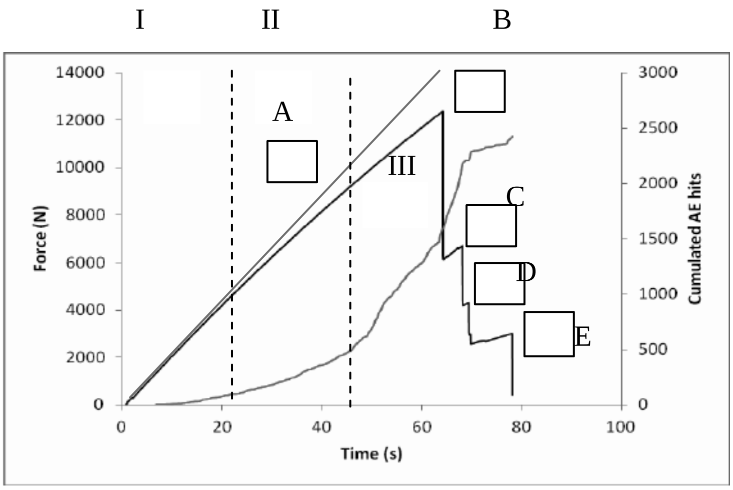

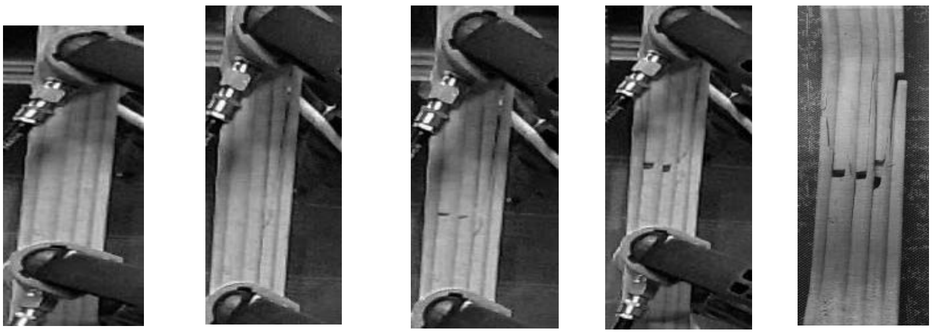

A B C D E

Figure 5: Force vs time, cumulative hits vs time and damage scenario of TD5 specimen

Even though the damage process for each Douglas specimen could not be exactly the same, a typical damage process in Douglas specimen can be proposed. Under tensile loading, the different stiffness between earlywood (EW) and latewood (LW) generates a shear stress at the EW/LW interfaces, which is the weakest layer because the density of wood between EW and LW changes abruptly [12]. Micro-cracks should initiate or at EW/LW interfaces or in EW, where the strength is much lower than that in LW. Their growth and coalescence conduce to longitudinal crack propagation. This process is sometimes accompanied by the fibre breaking in EW [13]. The transverse fracture in EW generates a tensile/flexion coupling effect, which accentuates even more the fibre breaking in EW. When the crack growth attains EW/LW interfaces levels, under shear stress (mode II) and peel stress (mode I), the longitudinal crack propagation (parallel-to-grain) along EW/LW interfaces will occur. And then, one of the latewood layers breaks, the rest of specimen cannot support the higher load and final fracture occurs [13]. On fracture surfaces, the longitudinal crack growth in EW and at EW/LW interfaces was evident, and the fiber breaking in EW is so shown stair-shaped.

3.2.2 Silver fir

Silver fir specimens under tensile loading failed usually in brittle manner (Figure 6). Much less crack propagation parallel-to-grain direction were observed along EW/LW interfaces or/and in the EW. The fracture surfaces appear more flat and demonstrate simultaneous transverse fracture in earlywood tracheid and in latewood tracheid.
The representative specimen TS4 (Figure 6-b) displays transverse crack that extend entirely through the sample width across the EW and the LW. Some longitudinal crack propagations have been also seen along EW/LW interfaces.

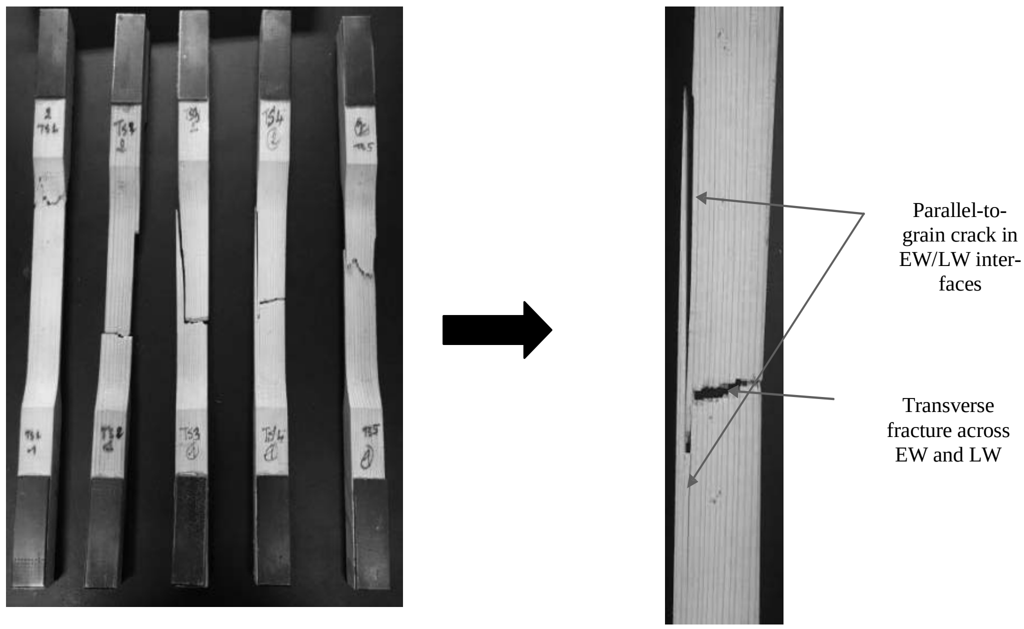

(a) (b)

Figure 6: (a) Failure patterns observed for silver fir specimens (b) Failure modes in TS4 specimen

Figure 7 shows the evolution of the load and of cumulative AE hits as a function of the testing time for the specimen TS4. Under low load (Part I), silver fir generated few emissions. In the second part (Part II), the cumulative AE hits increased with the load rise. Emissions in this stage can be attributed to micro-cracking in cells of earlywood since the structure of wood with narrow rings consists principally of earlywood tracheid [14]. The brittle fracture across EW starts with a significant increase in the rate of cumulated AE hits (Part III). When the EW is sufficiently damaged, the LW can no longer withstand the applied loads, the final fracture occurred. Actually the latewood has to be more resistant as in silver fir as the walls of latewood cells are much thicker than those of earlywood cells. Moreover at the last part of the test, the tensile/flexion coupling due to the transverse crack promotes the longitudinal crack propagation at EW/LW interface.

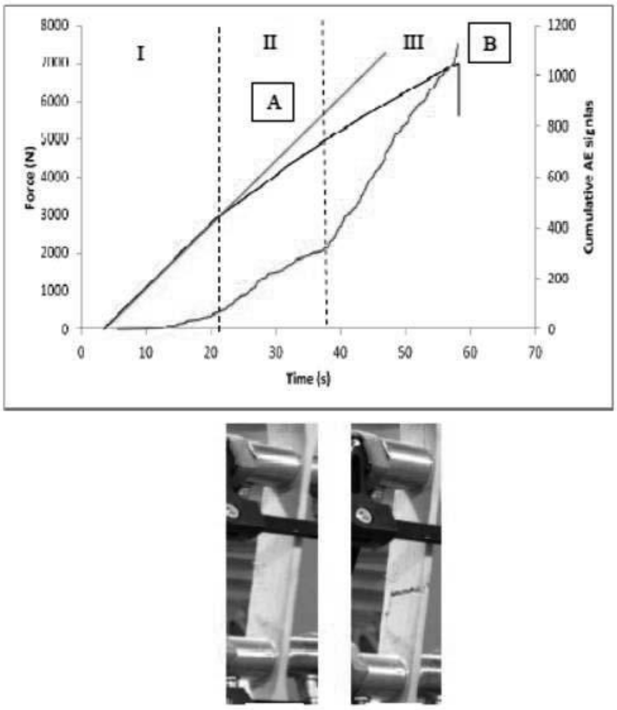

A B

Figure 7: Force vs time, cumulative hits vs time and damage scenario of TS4 specimen

In conclusion, silver fir has narrow growth rings, the specimens under tensile loading failed usually in brittle manner. The micro-cracking initiates firstly in the EW, the development of the micro-cracks leads to fiber breaking in the EW. When there are enough fibers broken in the EW, the transverse fracture in the LW occurs. The transverse crack across the section produces a tensile/flexion coupling effect, which promotes the longitudinal crack propagation at EW/LW interfaces, under mode I due to peel stress and mode II due to shear stress.

3.2.3 Poplar

Poplar is a hardwood and considered as quasi homogeneous material, because no transition from earlywood (EW) and latewood (LW) can be distinguished. The specimens shown in Figure 8-a display combination of tension and shear fracture, because the fracture surface of all specimens runs partially across wood grain and partially inclined to the grain direction. The specimens TP3 and TP4 display a large part of the shear fracture where the fracture sur- face is inclined to the fibers. Moreover, more or less longitudinal macro-cracking was also observed in the specimens.

For the representative specimen TP3 (Figure 8-b), the analysis of the AE cumulative hits during tensile test allows to divide the damage process in three parts (Figure 9). Part I is characterized by an absence of detectable acoustic emission. Poplar specimen (TP3) starts to generate acoustic signals at t=22.43s in part II. Then, the cumulative AE hit increased slightly with the load increase. At this stage the signals can come from the initiation and development of micro-cracking across wood cells since they are considered as the main spot of mechanical weakness in bulk wood specimens. The early stage in part III is characterized by a remarkable increase in cumulative AE hits, herein the damage mechanisms could be the growth of micro-cracks and the arrest of crack propagation at a vessel level, a mechanism specific to hardwood. At final fracture of the specimen, the load drops sharply and the cumulative AE hits suddenly rises when the visible cracks appeared at t=84.32s (Figure 9-Point B). Acoustic emission ac- tivity in this stage is mainly attributed to fiber breakage. Actually, in the final fracture process, under the effect of the stress concentration around the micro-cracks, the fibers of the wood could be broken, forming cross-grain macro-cracks. In the same time the growth and the coalescence of theses micro-cracks could also follow the direction parallel-to-grain due to the shear stress induced by wood structure at fiber/fiber interfaces. When a cross-grain crack meets a parallel-to-grain crack, their coalescence results in a crack inclined to the grain direction.

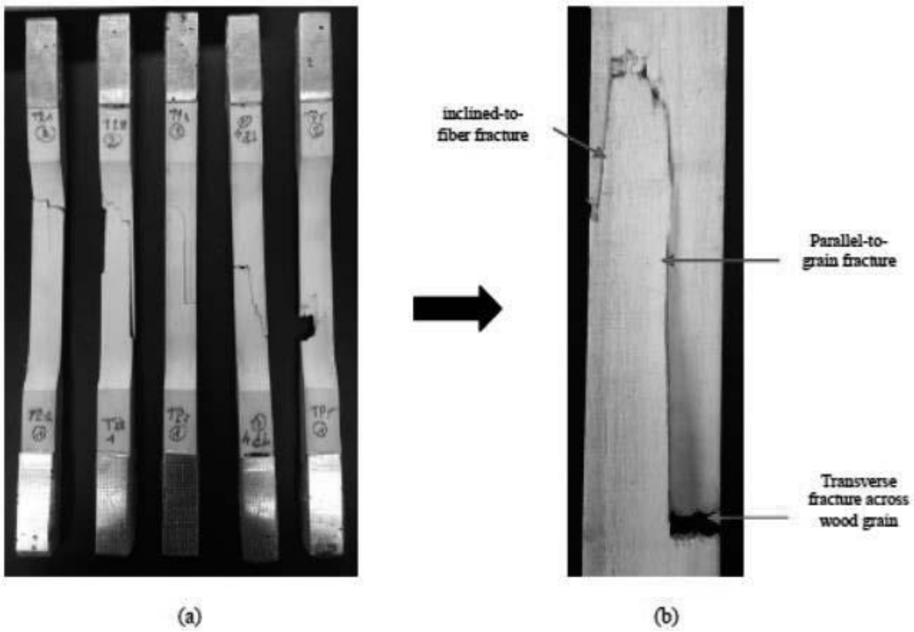

Figure 8: Failure patterns observed for poplar specimens (b) Failure modes in TP3 specimen

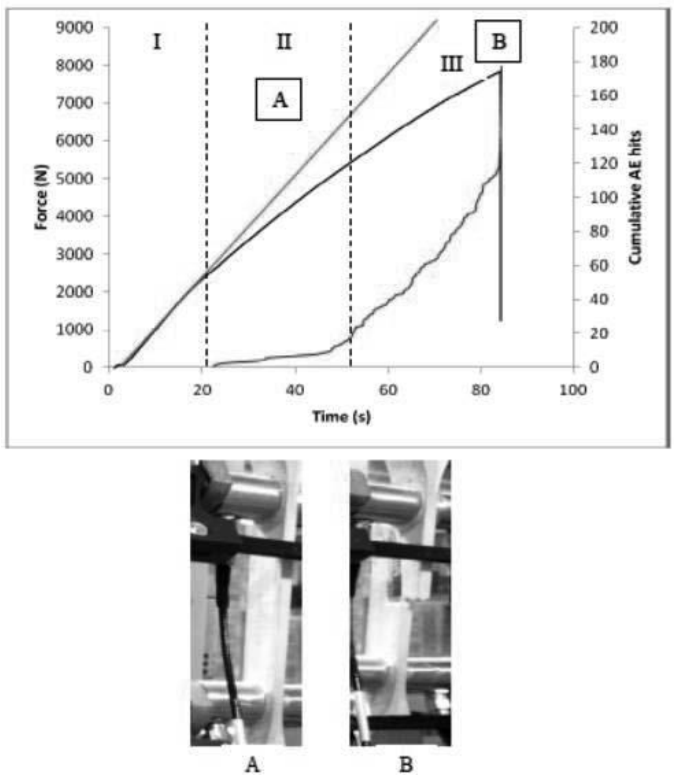

Figure 9: Force vs time, cumulative hits vs time and damage scenario of TP3 specimen

Consequently, the damage scenario of the tested poplar wood under tensile loading could be supposed as following: the damage process is started by micro-cracking in the wood cells. The growth of micro-cracks can be stopped at a vessel due to hardwood structure. Final fracture of the specimen occurs in a brittle manner. When a packet of fibers are broken simultaneously, instable crack propagation can be observed across-to-grain, parallel-to-grain as well as in the direction inclined to wood grain.

3.3 Comparison AE responses for species tested

The three wood species studied here show in general three stages of AE activity during tensile loading. But the total cumulative hits are quite different between species. Douglas fir generates higher total AE signals: more than twice of cumulated AE signals of silver fir and nine times more than cumulated AE signals of poplar (Figure 10). This investigation agrees well with the findings in reference [4], which indicated that the higher is the contrast between early and latewood in annual ring, the higher AE cumulative counts should be expected during tensile parallel to grain loading. Moreover the important difference in AE responses between softwoods (Douglas fir and silver fir) and hardwood (poplar) can be also explained by the higher energy consumed when the crack propagate in softwood [15]. Furthermore, hardwood requires a high stress levels for macro-crack initiation and its structure holds crack arrest components. In fact, vessels in hardwood species can stop the crack propagation [16]: the crack tends to open the vessel or deviates around the vessel and then stooped (Figure 11). Despite the crack arrest, the crack propagates in brittle manner in hardwood species [15]. These reasons explain why the poplar wood remained silent in early stage of loading and released less emission hits until the final fracture. Furthermore, wood structure contains radially oriented parenchyma called rays. They provide a mechanically strong structure which inhibits the crack propagation [17-18]. In fact, the volumetric proportion and the size of rays are different between soft and hardwood. The conifers wood contains around 5-10% of rays while it is around 10-32% in hardwood [19]. Therefore, the rays could strengthen poplar wood to crack growths more than the two softwoods (Douglas fir and silver fir) which explains the small AE signals generated during poplar damage.

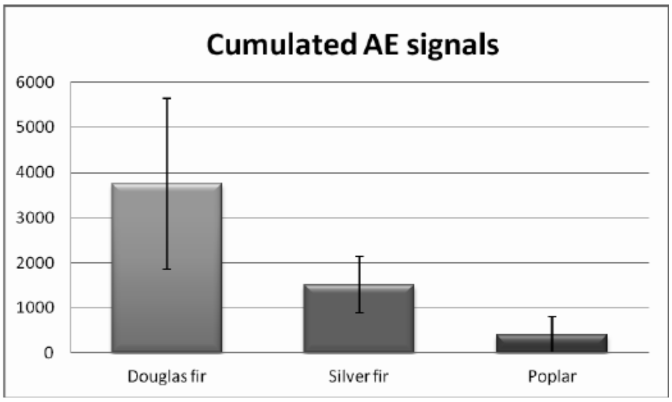

Figure 10: Cumulated AE signals of tested wood species

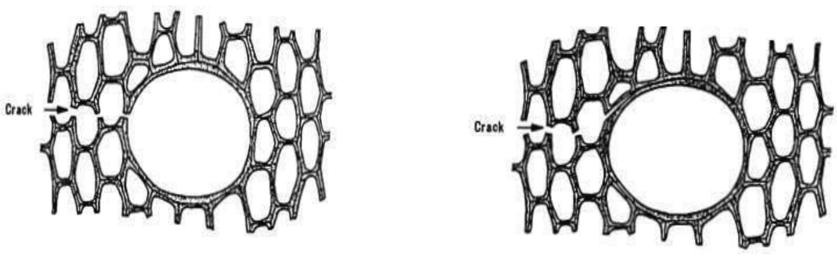

Figure 11: Crack arrest at a vessel [16]

4 CONCLUSIONS

In this study, the evolution of damage of three wood species under tensile loading was monitored by AE. The following conclusions can be stated:

- The magnitudes of AE activities as a function of time are directly related not only to the annual rings structure, but also to micro and meso-structures of woods. It is shown that the wood with well-defined growth rings is more emissive than wood with narrow rings and wood with homogeneous structure. The responses of AE are quite different between soft-wood and hardwood. More cumulative hits have been obtained during damage process in softwood than those in hardwood.
- AE is a promising technique for detecting the onset of micro and macro cracking. In fact, the AE data of tensile tests on three different wood species indicate clearly different scenarios from damage initiation and accumulation up to final macroscopic failure.
- There are many parameters that can affect the accuracy of AE monitoring of wood materials such as wood species, load types, geometry … So, to adapt AE technique to health monitoring of timber bridges, it is necessary at first to improve AE experimental protocol on laboratory scale.
- Actually, different parameters, such as forms and the energy of AE activities are worthy to study in future works in order to correlate different damage mechanisms to AE events.

REFERENCES

[1] Ritschel, F., Brunner, J. A. and Niemz, P. 2013. “Nondestructive evolution of damage accumulation in tensile test specimens made from solid wood and layered wood materials”. *J. composite structures*, 95, Pp: 44-52.

[2] Varner, D. 2012. “Acoustic emission during static bending of wood specimens”. *PhD the- sis.* Mendel University in Brno.

[3] Wu, Y., Shao, ZP. and Wang, F. 2014. “Acoustic emission characteristics and felicity ef- fect of wood fracture perpendicular to the grain”. *J. of tropical forest science*, 26 (4), Pp: 522- 531.

[4] Ansell, MP. 1982. “Acoustic emission from softwoods in tension”. *Wood Sci. technol*, 16, Pp: 35-58.

[5] Vautrin, A. 1987. “Acoustic emission characterization of flexural loading damage in wood”. *J. of materials science*, 22, Pp: 3707-3717.

[6] Lamy, F., Takarli, M., Angellier, N. and Dubois, F. 2015. “Acoustic emission technique for fracture analysis in wood materials”. *Int. J. Fract*, 190.

[7] Nilson, A. 1980. “Acoustic emission source based on pencil lead breaking”.

Svejsecntralen, 80.

[8] Bucur, V.2006. “Acoustics of wood”, Springer Series in Wood Science. Second Edition Germany.

[9] Hearmon, R.F.S. 1948. “The elasticity of wood and plywood”. *Dept. Sci. Ind. Res. For. Prod. Res. Spec.* Report No 7, HMSO, London.

[10] Raczkowski, J. and Molinski, W. 1994. **“**Acoustic emission in fracture machanics of wood”. *J. of theoretical and applied mechanics,* 2 (32).

[11] Liew, W.Y.H, Yeo, K.B and Ben Ismail, M.A. 2011. **“**Fracture behavior of tropical hardwood under tensile load”. *Int. Conference on advanced Science engineering and infor- mation technology*, Malaysia 14-15 January 2011.

[12] Kollmann, F.P. and Coté, W.A. 1968. “Principles of wood science and technology I: sol- id wood”, Springer-Verlag New York Inc.

[13] Sipolla,M. and Fruhmann,K.2001. “In situ longitudinal tensile tests of pine wood in ESEM”. *Holzforshung*, 56:669-675.

[14] Johnson, P.P.A and Brundage, M.R. 1934. “Properties of white fir and their relation to the manufacture and uses of the wood”. *Technical Bulletin* No. 408, Unites States Departement of Agriculture, Washington, D, C.

[15] Reiterer, M.F.Stanzl-Tschegg, SE. and Tschegg, E.K. 2000. **“**Mode I fracture and acous- tic emission of softwood and hardwood”. *Wood Science and Technology,* 34, Pp: 417-430.

[16] Ashby, A. and Gibson, L.J. 1988. **“**Cellular solids: Structure and properties”. Pergamon Press, New York, NY.

[17] Reiterer, A., Burgert, I., Sinn, G. and Tschegg, S.E. 2002b. “The radial reinforcement of the wood structure and its implication on mechanical and fracture mechanical properties-a comparison between two tree species”. *J. Mater. Sci*. 37, Pp: 935 – 940.

[18] Bordner, J., Schlag, M.G. and Grull, G. 1997. “Fracture initiation and progress in wood specimens stressed in tension: Part I: clear wood specimens stressed parallel to the grain”. *Holzforshung*. 51, Pp: 479-484.

[19] Ozden, S., Ennos, A.R. and Cattaneo, M.E.G.V. 2016. “Transverse fracture properties of green wood and the anatomy of six temperate tree species” *Forestry (Lond).* 90 (1), Pp: 58-69.

SHATIS'17
4th International Conference on
Structural Health Assessment of Timber Structures
20-22 September 2017 Istanbul, Turkey

MONITORING METHOD ANALYSIS FOR EFFECTIVE MEASURE OF WOODEN ARCHITECTURAL HERITAGE

L. Ha Na[1], A. Dai Whan[2], K. Hwan Chol[3], Y. Hyun Woo[4], K. Dong Yeol[1]

[1] National Research Institute of Cultural Heritage

[2] Chungbuk National University

[3] Sunmoon University

[4] Myungji University

Keywords: Wooden architecture, Cultural Heritage, Displacement, Monitoring method

Abstract

Methods for monitoring cultural heritages are getting more efficient and scientific with the development of technology and equipment. Thus, the monitoring methods currently experienced in Korea need to be examined from various aspects. In this study, monitoring method by 3D scan are compared with the method using total station and automatic measurement.

Among the East Asian wooden buildings, which are climate-sensitive such as change of temperature and humidity, the Geugnakbojeon of Muwi-sa Temple in Gangjin and the Jongmyo Jeongjeon in Seoul had been monitored. The advantage and disadvantage of each monitoring method were investigated by comparing the displacement measuring method and by analyzing the measurement cycle. Through this process, we propose an efficient displacement measuring method and a cycle with three of each measuring instruments.

Wooden cultural heritage should be monitored by using appropriate equipments depending on the importance of building and need for identifying periodic displacement. In this study, measurement trends of 3D scan and total station are similar, but 3D scan data analysis result in matching error can be occurred. Follow-up research is necessary to overcome the limit to suggest a specific measurement since the period of this study was too brief and objects were limited into few buildings.

1 INTRODUCTION

National Research Institute of Cultural Heritage has selected 56 samples for monitoring which are all popular and symbolic among National treasures and treasures in South Korea.These sites require special management because of damage and aging [2]. Among them, the wooden cultural heritages show historical characteristics in furniture and roof types according to the age of the building and even hint at the environment of the time. However, they are vulnerable to fire due to the nature of the material and structural problems arising from some members. These fires are likely to spread to the entire building because the members are intertwined.

Although the measurements and recording of cultural heritages using 3D scans are being promoted to research and record cultural assets, studies on the feasibility of using 3D scan data for monitoring are lacking. Few attempts have been made to use 3D scan data for monitoring, and research on the feasibility of using 3D scan data is still insufficient. In this study, therefore, 3D scanning was compared with existing monitoring methods to derive the advantages and disadvantages of 3D scanning and to verify the possibility of future developments.

2 MONITORING METHOD

2.1 Geugnakbojeon of Muwi-sa Temple in Gangjin

2.1.1. Monitoring model

Kangjin Muwi-sa is a temple in Mount Wolchulsan at 1174, Wolha-ri, Seongjeon-myeon, Gangjin-gun, Jeollanam-do, Republic of Korea. It was founded by Great Monk Wonhyo during the Silla Dynasty and has been rebuilt several times. Geugnakbojeon, which was selected as a monitoring model, was built in 1430 with a floor plan of 3-kans in front and 3 kans on the side. The single-floor structure is a jusimpo-style gable-roofed building with double eaves [3].

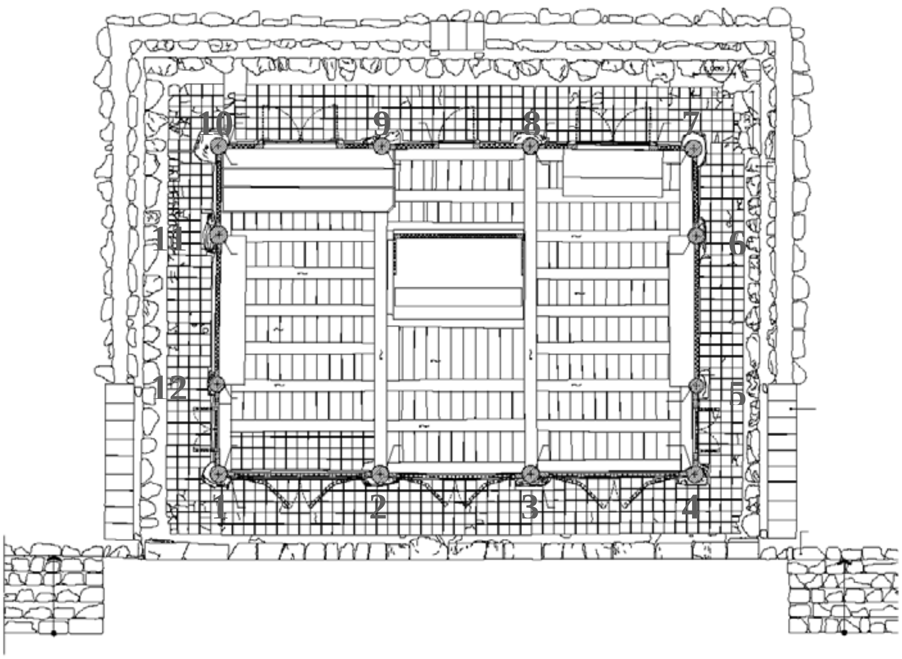

Figure 1 Measuring position

2.1.2. Monitoring method

In this study, we installed permanent boundary stones as reference points for displacement measurement; a total of 92 target points were considered: 23 in the front, 23 in the back, 23 on the right side, and 23 on the left side around the pillars and changbangs. To analyze the results, pillar numbers were assigned to them based on the southwest pillar as shown in [Figure 1].

3D scan was performed using Focus 3D × 330 from FARO. The research sequence was as follows: Install reference points → Install targets for displacement measurement reference points → 3D scan (first: all objects) → 3D scan (2^{nd}–6^{th}: displacement measurements) → Data post-processing → Comparison and analysis of displacement data(Table.1).

Table 1: 3D scan plan (Geugnakbojeon of Muwi-sa Temple in Gangjin)

Division	Date	Description
1st 3D scan	2016.08.31	All objects and surrounding environment
2nd 3D scan	2016.09.01	Displacement measurement part (pillar, changbang)
3rd 3D scan	2016.10.25	Displacement measurement part (pillar, changbang)
4th 3D scan	2016.10.26	Displacement measurement part (pillar, changbang)
5th 3D scan	2016.11.22	Displacement measurement part (pillar, changbang)
6th 3D scan	2016.11.23	Displacement measurement part (pillar, changbang)

The total station displacement was measured using FlexLine TS06 plus from Leica. The research sequence was as follows: Install reference points → Install reflectors for displacement measurement reference points →Total station measurement (first: displacement measurement part)→Total station measurement (2^{nd}–6^{th}: displacement measurement part)→Data backup (Excel and CAD interface) → Comparison and analysis of displacement data(Table.2).

Table 2: Total station plan (Geugnakbojeon of Muwi-sa Temple in Gangjin)

Division	Date	Description
1st total station	2016.09.01	All objects and surrounding environment
2nd total station	2016.10.25	Displacement measurement part (pillar, changbang)
3rd total station	2016.11.22	Displacement measurement part (pillar, changbang)

A two-axis inclinometer was installed to measure the displacement with an automatic measuring instrument, and the displacement measurement data was created using a data building program and the general-purpose application Excel. The research sequence was as follows: Install the measuring instrument and data logger → Acquire data (automatic measurement) → Compare and analyze displacement data(Table.3).

Table 3: Measuring sensor regularly plan (Geugnakbojeon of Muwi-sa Temple in Gangjin)

Division	Date	Description
Install an automatic measuring instrument	2016.10.14	Install a 2-axis inclinometer Set the data logger
Automatic measurement	2016.10.14 to 2016.11.30	Perform automatic measurement

2.2 Jongmyo Jeongjeon in Seoul

2.2.1 Monitoring model

Jongmyo Jeongjeon is a building for enshrining ancestral tablets of the kings of the Joseon Dynasty. Located at 157, Jong-ro, Jongno-gu, Seoul, Republic of Korea, it is the longest single building in South Korea. It has single eaves and a gable-roofed style with the shape of the Chinese character for human being (人) (Figure.2) [4].

Figure 2 Jongmyo Jeongjeon in Seoul

2.2.2 Monitoring method

In this study, the total displacement of the object was measured through a reference without targets installed for displacement measurement in the Jongmyo Jeongjeon, The 3D scan research method was the same as the one used for the Geugnakbojeon of Muwi-sa Temple in Gangjin(Table.4).

Table 4: 3D scan plan (Jongmyo Jeongjeon)

Division	Date	Description
1st 3D scan	2016.08.30	All objects and surrounding environment
2nd 3D scan	2016.09.06	Displacement measurement part
3rd 3D scan	2016.09.20	Displacement measurement part
4th 3D scan	2016.10.04	Displacement measurement part
5th 3D scan	2016.10.18	Displacement measurement part
6th 3D scan	2016.11.01	Displacement measurement part
7th 3D scan	2016.11.15	Displacement measurement part
8th 3D scan	2016.11.23	Displacement measurement part

3 MONITORING ANALYSIS

3.1 Analysis of results according to displacement measuring instrument employed

[Table 5] shows the result obtained by measuring the 12 pillars shown in [Figure 1] 8times. The left two graph shows the movement of 3D scan, and the right two graph shows the movement of the total station.

The analysis of the results for the displacement measurements of the 3D scan confirmed that each pillar showed different behaviors although the directions were similar. To examine the displacement behaviors in the southwest–northeast direction, pillars 1 and 6 showed displacement behaviors in round trip, pillars 3 and 5 showed displacement behaviors in the southwest → northeast direction, and pillar 6 showed displacement behaviors in the northeast → southwest direction. For the southeast–northwest displacement behaviors, pillar 4 showed displacement behaviors in the southeast → northwest direction and pillars 8 and 9 showed displacement behaviors in the northwest → southeast direction. Thus, pillars displacement behaviors appeared in opposite directions.

In the case of total station, pillars 6 and 11 showed displacement behaviors in the southwest ↔ northeast directions, and pillars 1, 3, and 9 showed displacement behaviors in the southwest → northeast direction. Pillar 12 showed displacement behaviors in the northeast → southwest direction, which is opposite to the direction the displacement behaviors of pillars 1, 3, and 9. Furthermore, pillars 7 and 8 showed displacement behaviors in the southeast ↔ northwest directions and pillar 4 showed displacement behaviors in the southeast → northwest direction(Table.5).

For automatic measurement, two 2-axis inclinometers were installed on pillars 7 and 10 to measure the displacement values. As a result, the minimum and maximum displacements of TL_X in the TL_XY values of pillar 7 were -0.002mm and 0.038mm, respectively, which were both measured on October 18. The minimum and maximum displacements of TL_Y were -0.026mm on October 15 and 0.012mm on November 1, respectively. The minimum and maximum displacements of TR_X of pillar 9 were -0.002mm on October 14 and 0.027mm on October 15, respectively. The minimum and maximum displacements of TR_Y were -0.026mm on October 18 and 0.012mm on November 1, respectively. Many of the minimum and maximum displacements occurred on October 18, and the cause for this should be investigated to determine the existence of any environmental factors.

Table 5: 1st–8th displacements of pillar inclination (3D scan, total station)

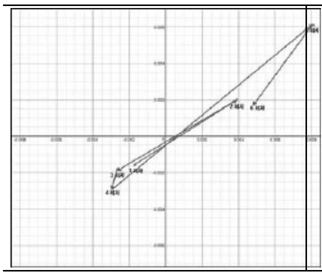 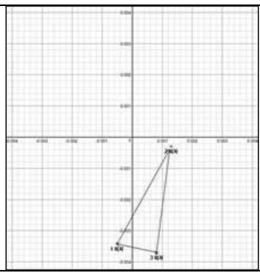	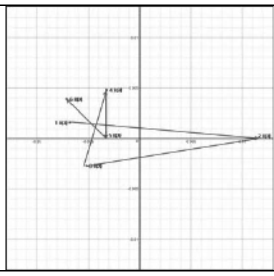 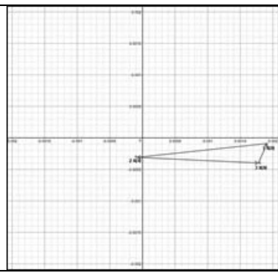
1 (Left: 3D scan, Right: Total station)	2 (Left: 3D scan, Right: Total station)

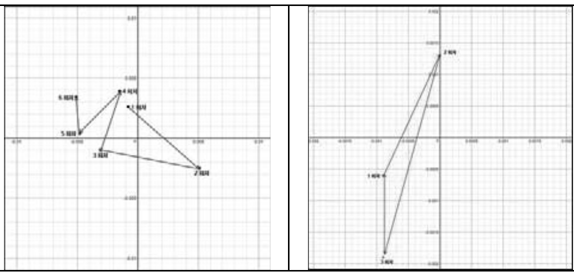	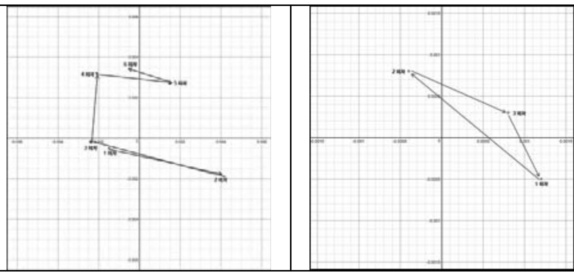
3 (Left: 3D scan, Right: Total station)	4 (Left: 3D scan, Right: Total station)
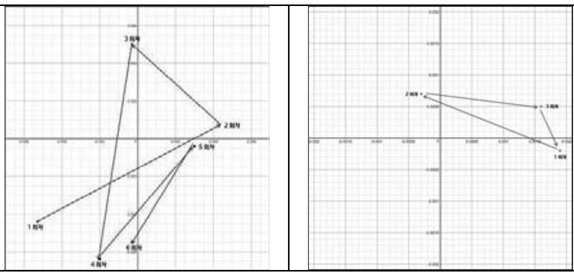	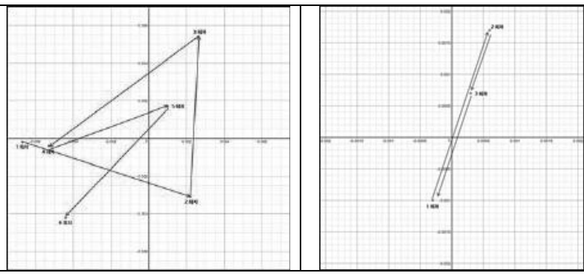
5 (Left: 3D scan, Right: Total station)	6 (Left: 3D scan, Right: Total station)
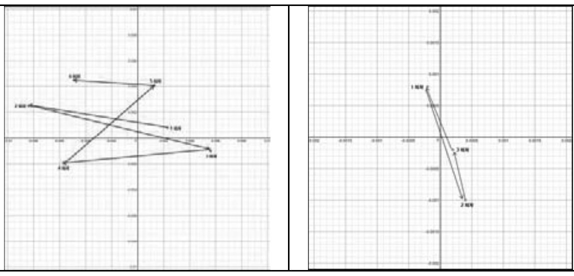	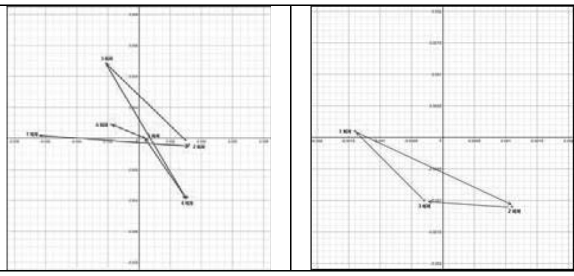
7 (Left: 3D scan, Right: Total station)	8 (Left: 3D scan, Right: Total station)
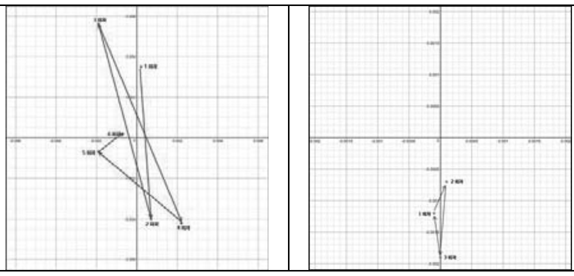	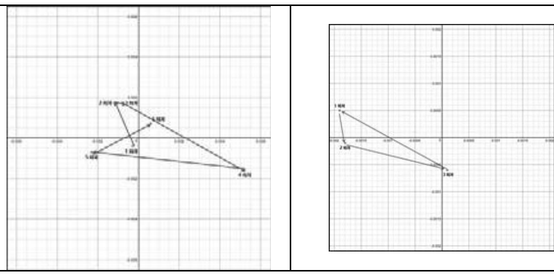
9 (Left: 3D scan, Right: Total station)	10 (Left: 3D scan, Right: Total station)
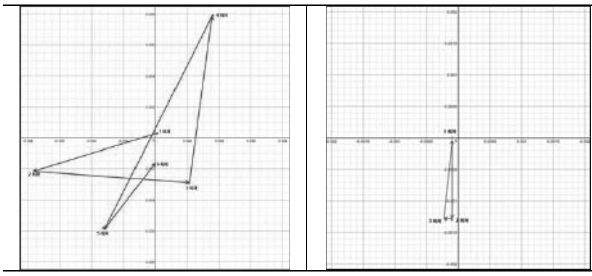	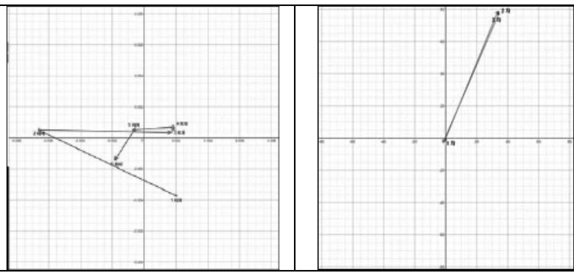
11 (Left: 3D scan, Right: Total station)	12 (Left: 3D scan, Right: Total station)

3.2 Displacement analysis using longitudinal section

[Table 6] shows the results obtained by scanning cross section of Jongmyo Jeongjeon 8times.

As a result of the first 3D scan of Jongmyo Jeongjeon, the measurement value of the pillar with the largest displacement was 0.46° in the front and 0.6° in the center. A comparison between the pillar inclinations based on these values showed no overall difference. In particular, the front pillar showed a displacement of 0.4mm in the 1st and 2nd measurements and -0.4mm in the 2nd and 3rd measurements; however, the 3rd–8th measurement values were identical to the value of the first measurement. In the case of the center pillar, the displacement values ranged from -0.07mm to 0.9mm for the 2nd to 8th measurements(Table.6).

Table 6 1st–8th displacements of pillar inclination

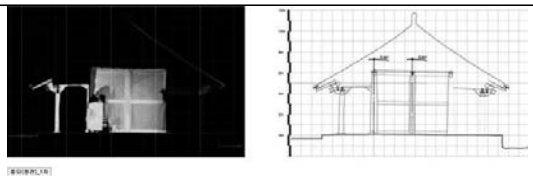

1st

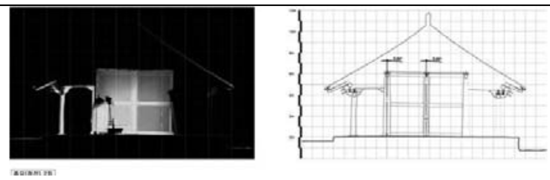

2nd

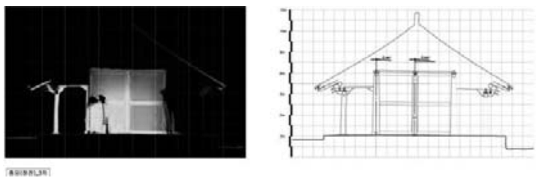

3rd

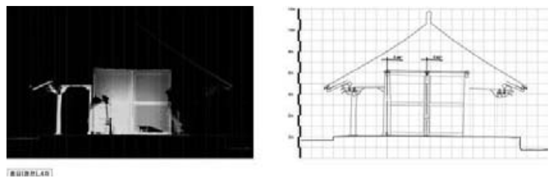

4th

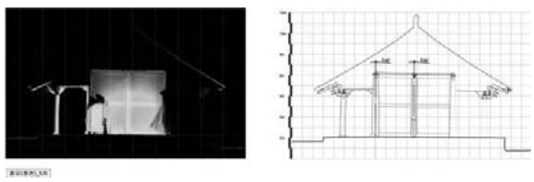

5th

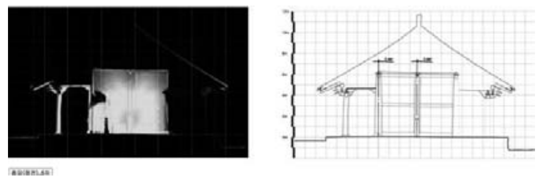

6th

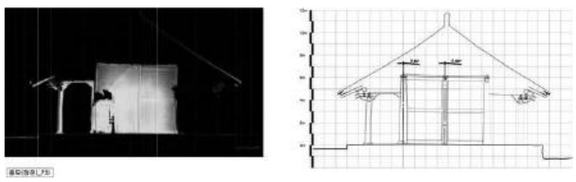

7th

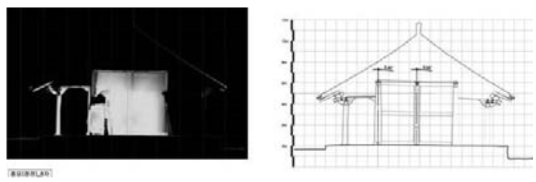

8th

3.3 Comprehensive analysis

In the case of automatic measurement, there was a limitation in analyzing the two data values and the result values, owing to a short research period. However, the pillar displacements of 3D scan and total station at pillars 5 and 9 showed behaviors in opposite directions. Pillars 2, 11, and 12 showed different types of displacement behaviors, but revealed similar trends in some iterations. The displacement behaviors of pillars 1, 3, 4, 6, 7, 8, and 10 appeared relatively similar in the southwest to northeast direction.

3D scan enables multilateral examination of the shape information using 3D data, which is very useful. Total station allows selective measurements of the necessary parts. Furthermore, automatic measurement offers the advantage of allowing constant measurement and the setting of a measurement period according to the purpose. However, total station provides limited numerical information. Furthermore, 3D scan takes more time to acquire experts and data. In the case of automatic measurement, a thorough review and preparation are required since the installed instrument is different depending on the data type to be obtained. Both methods have the disadvantage of high initial cost.

4 CONCLUSION

The displacements of wooden cultural heritages were measured using 3D scan, total station, and automatic measurement to obtain an efficient displacement measurement. Furthermore, a reasonable measurement period and a displacement measurement method were proposed by comparing the advantages and disadvantages of each measuring instrument.

Displacement Measurement results by 3D scanning and total station indicated 7 out of 12 pillars in Geugnakbojeon of Muwi-sa Temple in Gangjin has similar directional movements. Jongmyo Jeongjeon with 3D scan method had almost no difference on the 1^{st}, 2^{nd}, 5^{th} and 6^{th} measurement, but had 9.8mm of difference on the 4^{th} and 7^{th} order. Surely, matching error point must be concerned enough.

Since the period of study had been too short, with the periodic limit, for suggesting the compatible way of displacement measurement and analysis period, follow-up study to should be carried out especially consider efficient term of study, the advantage and disadvantage of additional part and equipment including participants, expenses concretely.

ACKNOWLEDGEMENT

This study was conducted as part of the research project supported by the National Research Institute of Cultural Heritage.

REFERENCES

[1] ***2016. “A Basic Study on Establishment of Displacement Measurement Method through Periodical 3D Scanning of Major Wooden Cultural Properties”. National Research Institute of Cultural Heritage. 2016.

[2] ***2016. “Report on the results of monitoring cultural properties targeted for 2015”. National Research Institute of Cultural Heritage. 2016

[3] ***2004. “The Geugnakbojeon of Muwi-sa Temple in Gangjin Survey Reports ”. Cultural Heritage Administration. 2004.

[4] HTTP://WWW.CHA.GO.KR/KOREA/HERITAGE/SEARCH/CULRESULT_DB_VIEW.JSP?MC=NS_04_03_01&VDKVGWKEY=11,02270000,11

SHATIS'17
4th International Conference on
Structural Health Assessment of Timber Structures
20-22 September 2017 Istanbul, Turkey

RESIDUAL LIFE PREDICTION OF ANCIENT TIMBER COMPONENTS BASED ON CUMULATIVE DAMAGE MODEL: A LITERATURE REVIEW

Wang Zhongcheng[1], Yang Na[2]

[1,2] School of Civil Engineering, Beijing Jiaotong University, Beijing 100044, China

Keywords: Residual Life, Ancient Timber Component, Cumulative Damage Model, Load duration

Abstract

Ancient timber structure is a common cultural heritage of mankind. How to be aware of the current working performance, make accurate maintenance plan and evaluate its residual life has become a common concern of the academic circles. This paper is a literature review of the development of cumulative damage models and the combination of these models and residual life prediction of ancient timber structures.

***Wood**'s experimental data (1951) showed that the mechanical property of timber would decreases over time. **Gerhards**(1979) proposed the cumulative damage model of $da/dt=exp(-a+b\sigma(t)/\sigma_s)$ that had been widely used around the world. During the last 30 years, the direction of research was more focused on the effects of environment based on the previous experimental data.*

*Most of the research did not take it into consideration that the σ_s in **Gerhards**'s model is not invariable, it will decrease over time like the description in Madison curve. And it is advised to perform a much more accurate and detailed test for current research.*

1 INTRODUCTION

China has a long history, during the past five thousand years, timber structure has been the main form of structures and a symbol of the wisdom and hardworking of our ancestor. Timber structure has been widely used because of the following advantages: timber is a kind of material which is convenient to obtain, it has good mechanical properties and outstanding seismic performance. There are many ancient architectures has experienced both environment and human destruction thousands of years and survive. Not only benefit from the form of the structure and carefully renovation, but also the specialty of timber as a kind of biological materials which has unusual properties. Nowadays, how to be aware of its current working performance, make accurate maintenance plan and evaluate its residual life reasonably has became a common concern of the academic circles. This paper is a literature review of the development of cumulative damage models and the combination of these models and residual life prediction of ancient timber structures.

2 EXPERIMENTAL STUDY ON CREEP RUPUTURE OF TIMBER

2.1 The Madison curve

The earliest studies of timber's cumulative model was the study of creep rupture of load-duration phenomenon began in the 1950s.

In 1951, **Wood**[1] published a report on the relationship between the bending strength and load duration of Douglas fir. Wood's experimental study was began in 1943 and lasted 8 years. The longest loading time of a single specimen was more than 5 years. As a comparison, Wood's tests were divided into two parts: a long-term loading test and a rapid loading test. In the long-term loading test, the standard static-bending test of about 5 minutes was first performed and this load was set as the standard load. Then, 126 specimens divided into 6% and 12% moisture content levels, respectively, were subjected to constant load ranging from 60% to 95% of the standard load. The failure time of each specimens was ranging from 6 minutes to more than 5 years. Unlike the long-term loading test, the rapid loading test was loaded with a fixed rate until the specimens were destroyed. Then the failure time was recording ranging from 1 second to 100 sec. The experimental bending strength of the testing specimens was 0% to 40% higher than the standard one. In addition, there was a compared test of impact loading. It was found that when the failure time was 0.015 seconds, the experimental bending strength of the specimen was 75% higher the standard strength.

The original intention of this study was to explore the design strength of the timber structure with different designing life. It is found that the bending strength of the long-term loading specimens is much lower than that of the specimens under standard tests. **Wood** then integrates the results of the two sets of experiments and obtain the curve shown in Figure 1.

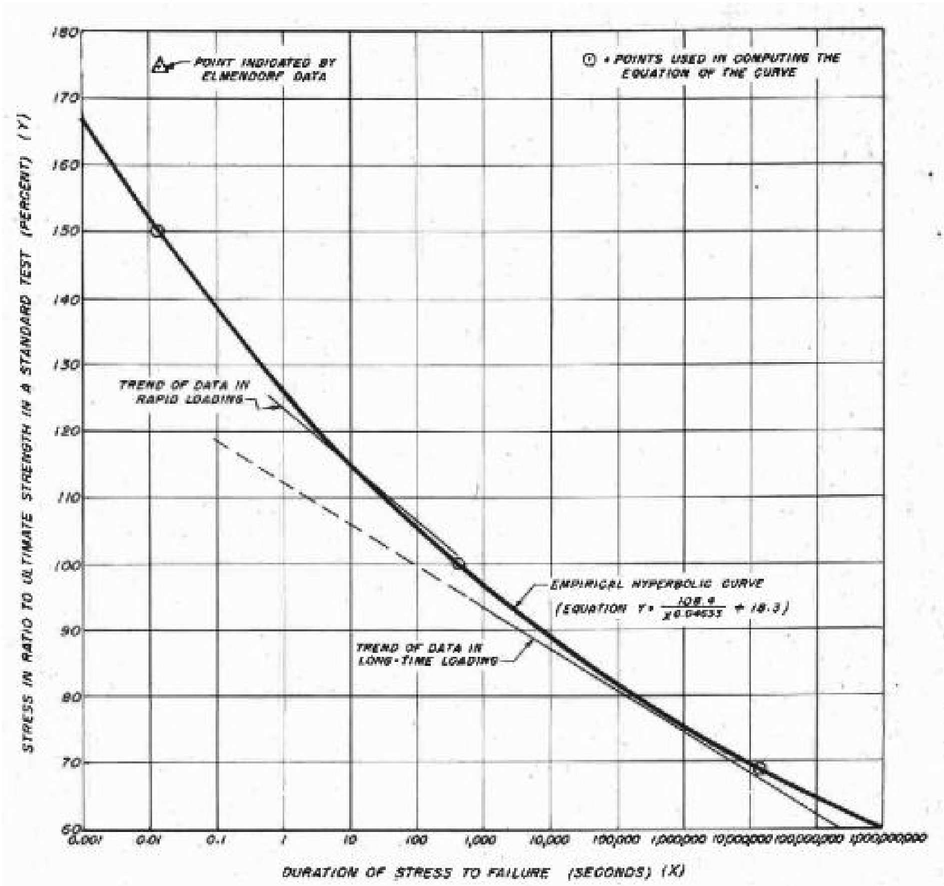

Figure 1: Madison curve

As it was shown in Figure 1, the bending strength of the specimens obtained by the rapid loading tests were higher than that of the long-term loading tests. The expression of the fitting curve is shown in equation (1), which is also called the Madison curve.

$$y = \frac{108.4}{x^{0.04635}} + 18.3 \tag{1}$$

Based on the experimental results, **Wood** proposed the earliest cumulative damage model, as in formula (2):

$$\frac{d\alpha}{dt} = A(\tau - \tau_0)^B \tag{2}$$

In the formula, τ is the ratio of the applied loads divided by the short term ultimate stress; τ_0 is a threshold below which the damage is assumed not to accumulate.

Barrett and **Foschi** (1978) used the experimental data of **Wood**'s, and proposed two kinds of cumulative damage model [2], as shown in the following formula (3) and (4):

$$\begin{cases} \dfrac{d\alpha}{dt} = a(\sigma - \sigma_0)^b \alpha^c & \sigma > \sigma_0 \\ \dfrac{d\alpha}{dt} = 0 & \sigma \le \sigma_0 \end{cases} \tag{3}$$

$$\begin{cases} \dfrac{d\alpha}{dt} = a(\sigma - \sigma_0)^b + \lambda\alpha & \sigma > \sigma_0 \\ \dfrac{d\alpha}{dt} = 0 & \sigma \le \sigma_0 \end{cases} \tag{4}$$

α is the damage state variable defined as zero in the undamaged state and unity at failure; σ is the applied load and σ_0 is a threshold stress below which the damage rate is zero; λ, a, b, c are constants based on the experimental data.

2.2 Gerhard's Cumulative Damage Model

From 1963 to 1974, **Gerhards** researched the strength of Hawaiian eucalyptus, white fir, Nepal alder, Western hemlock, black eucalyptus and southern pine[3]~[8]. And then he proposed the Gerhards cumulative damage model [9], as in formula (5):

$$\frac{d\alpha}{dt} = \exp[-a + b\frac{\sigma(t)}{\sigma_s}] \tag{5}$$

α is the same as in formula (4); σ_s is the static strength; $\sigma(t)$ is the applied load; a and b are constants.

In 1987, **Gerhards** conducted a further study of the model, he analyzed the effects of different ramp loads and constant loads on the damage model [10], and then discussed the parameters [11].

Gerhards has a wide range of research on the properties of timber, his cumulative damage model has been widely used by academics, and many studies have been improved on the basis of his cumulative damage model.

3 ENVIRONMENTAL EFFECTS ON CUMULATIVE DAMAGE MODEL

3.1 Effect of temperature and moisture content

Timber is exposed to the environment in the practical application. Its performance is affected by the ambient temperature and humidity, fungal corrosion, termite erosion and other environmental factors. The environmental impact was not considered to be in the cumulative damage model until 1990s.

Schniewind considered the cycle environmental impact of timber structure, he found that the environmental factors did shortened the failure time of timber under constant load [12]. Then, based on **Gerhards** cumulative damage model, **Schniewind** (1989~1991) improved the model under different constant temperature, cycle temperature and different relative humidity [13]~[15], and proposed the following formulas (6)~(8):

$$\frac{d\alpha}{dt} = \exp[-A + B\sigma + C(\tau - 1)] \tag{6}$$

τ is the ratio of the actual temperature divided by the standard temperature as in the test; A, B, and C are parameters based on the test.

$$\begin{cases} \Delta\alpha_i = \dfrac{1}{Ck_r}\{\exp[-A + B\sigma + Ck_\tau \Delta t_i] - \exp[-A + B\sigma]\} \\ \alpha(t) = \sum\limits_{i=1}^{m} \Delta\alpha_i \end{cases} \quad (7)$$

k_r is the rate of the changing temperature in one cycle. Other parameters are the same with formula (6).

$$\begin{cases} \dfrac{d\alpha}{dt} = \exp(-A + B\sigma + C\omega + D\omega^2) \\ \omega = (M - M_0)/M_0 \end{cases} \quad (8)$$

M is for the actual moisture content of timber; M_0 is the standard moisture content as in the test; Other parameters are the same with formula (6).

3.2 Effect of fungi

The effects of fungi were mainly on reducing the strength and the effective cross section of timber, and this study was carried out first by **Liese** and **Stamer** in 1943 as shown in Figure 2. It shows the strength of timber that had different species of fungi was changing over time.

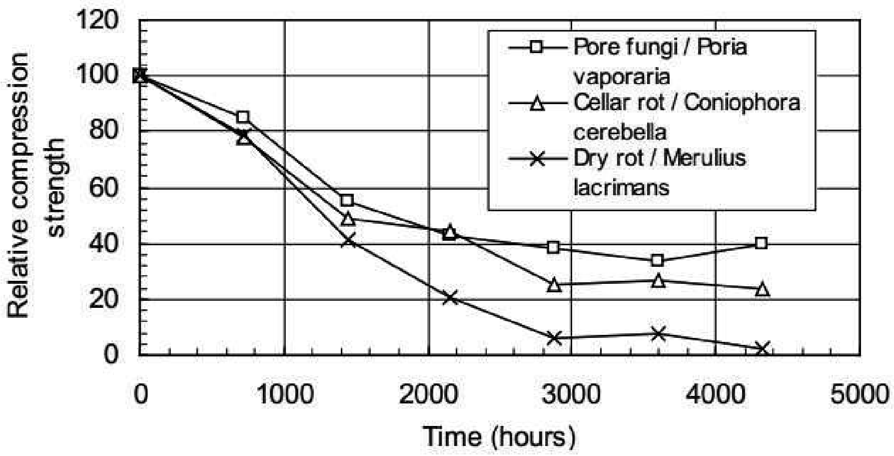

Figure 2: The strength of timber changing over time under the effect of fungi

Kuilen considered the reduction of the cross section of the timber and the reduction of the strength of σ_s in **Gerhards** cumulative damage model[16][17]. σ_s will reduce over time, as shown in formula (7):

$$F_u(t) = f_{c,0} \bullet A_{rem} + f_{c,0,dec} \bullet A_{dec} \quad (7)$$

$F_{c,0}$ is the initial compressive strength of timber; $F_{c,0,dec}$ is the compressive strength for the decayed part; A_{rem} is the area of the effective cross section and A_{dec} is the decayed cross sectional area.

4 TIMBER'S STRENGTH UNDER LONG-TERM LOADING IN CHINESE CODE

Chinese code [18][19] describe the strength of timber under long time loading with Long-term Strength, as in Figure (3).

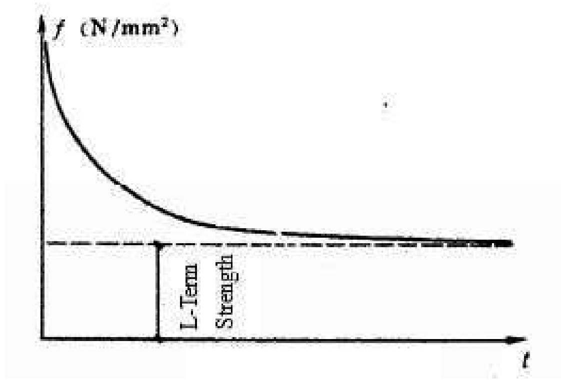

Figure 3: Long-term Strength in Chinese code

The ratio of the Long-term Strength and the impact strength of the timber varies depending on the species and mechanical properties of different kind of trees. The general values are shown in Table 1.

Table 1. The general value of Long-term (parallel-to-grain) Strength in Chinese code

Compressive strength	0.5~0.9	Tensile strength	0.5
Bending strength	0.5~0.64	Shearing strength	0.5~0.55

As an example, Chinese code gives the relationship between strength and time of pine in Table 2. The impact strength is measured under impact load.

Table 2. Relationship between strength and time (parallel-to-grain)

Strength type	Impact Strength (%)	The percentage of impact strength under the following days				
		1	10	100	1000	10000
Compressive	100	78.5	72.5	66.2	60.2	54.2
Bending	100	78.6	72.6	66.8	60.9	55.0
Shearing	100	73.2	66.0	58.5	51.2	43.8

With different designing life, the designing strength has been adjusted as in Table 3.

Table 3. Adjustment coefficient of the designing strength of timber arranging from the flowing years

Designing service life (Years)	Adjustment coefficient	
	Strength values	Modulus of elasticity
5	1.1	1.1
25	1.05	1.05
50	1.0	1.0
100 and above	0.9	0.9

5 CONCLUSION

- The earliest studies of cumulative damage model were based on experimental data. **Wood**'s and **Gerhards**'s experimental data made a great contribution to the studies of this researching area. Until now, part of the studies are still based on their data.
- During the last 30 years, especially after 2000, the direction of research is more focused on the effects of environment, such as temperature and humidity, fungal corrosion, termite erosion and other environmental factors. How to simulate the damage process of timber under environmental effect accounted for a large proportion.
- Although the consideration of environmental effect has been comprehensive, there are still aspect should be taken into consideration. For example, the $F_{c,0}$ in formula (7) is not invariable, it will decrease over time like the description in Madison curve. So the value of $f_u(t)$ in formula (7) is not conservative.
- Experimental research should be performed. The experimental data from **Wood** or **Gerhards** that has been widely used has been long ago. It is necessary to perform a much more accurate and detailed test for the current research of cumulative damage model.

REFERENCES

[1] Mark, R. and E. C. Robinson. 1994. "Vaults and Domes". In *Architectural Technology Up to the Scientific Revolution.* Edited by R. Mark. The MIT Press, Cambridge, Ma.

[1]: WOOD, L. 1951. "*Relation of strength of wood to duration of load*". In *Report No. 1916*. Forest Products Laboratory. Madison, WI, United States.

[2]: Barrett, J, D. Foschi, R, O. 1978. "*Duration of load and probability of failure in wood. Part I. Modeling creep rupture*". *J. Canadian Journal of Civil Engineering*, 5(5), Pp:505-514.

[3]: Gerhards, C, C. May 1963. "*Some strength and related properties of green wood of Hawaiian Eucalyptus saligna*". *Forest Service Research Notes*, *FPL-09*. U.S.

[4]: Gerhards, C, C. JUNE 1964. "*Strength and related properties of white fir*". *Forest Service Research Notes, FPL 14*. U.S.

[5]: Gerhards, C, C. May 1964. "*Limited evaluation of physical and mechanical properties of Nepal Alder grown in Hawaii*". *J. Forest Service Research Notes, FPL-036*. U.S.

[6]: Gerhards, C, C. 1965. "*Strength and related properties of Western hemlock*". *Forest Service Research Notes*. U.S.

[7]: Gerhards, C, C. August 1966. "*Physical and mechanical properties of blackbutt eucalyptus grown in Hawaii*". *Forest Service Research Notes*, *FPL-65*. U.S.

[8]: Gerhards, C, C. 1972. "*Relationship of tensile strength of southern pine dimension lumber to inherent characteristics*". *Forest Service Research Notes, FPL-174*. U.S.

[9]: Gerhards, C, C. 1979. "*Time-related effects of loading on wood strength: a linear cumulative damage theory*". *J. Wood Science.*
[10]: Gerhards, C, C. 1987. *Link C L.* "*A cumulative damage model to predict load duration characteristics of lumber*". *J. Wood & Fiber Science,* 19(2), Pp:147-164.
[11]: Link, C, L. Gerhards, C, C. Murphy, J, F. 1988. "*Estimation and confidence intervals for parameters of a cumulative damage model*". *Forest Service Research Notes, FPL-RP-484.* U.S.
[12]: SCHMEWIND, ARNO, P. "*Creep-rupture life of Douglas-fir under cyclic environmental conditions*". *J. Wood Science Technology,* 1(4), Pp:278-288.
[13]: Fridley, K, J. Tang, R, C. Soltis, L, A. 1989. "*Thermal effects on load duration behavior of lumber. Part I. Effect of constant temperature*". *J. Wood and Fiber Science,* 21(4), Pp:420-431.
[14]: Fridley, K, J. Tang, R, C. Soltis, L, A. 1990. "*Thermal effects on load duration behavior of lumber. Part II. Effect of cyclic temperature*". *J. Wood and Fiber Science,* 22(2), Pp:204-216.
[15]: Fridley, K, J. Tang, R, C. Soltis, L, A. 1991. "*Moisture effects on load duration behavior of lumber. Part I. Effect of constant relative humidity*". *J. Wood and Fiber Science,* 23(1), Pp:114-127.
[16]: Kuilen, V, D. J-W, G. 2007. "*Service life modeling of timber structures*". *J. Materials and Structures,* 40(1), Pp:151-161.
[17]: Kuilen, V, D. "*Lifetime modeling of timber structures*". *J.*
[18]: Ministry of Construction of the PRC. 2003. *Code for design of timber structures. M.* China Construction Industry Press.
[19]:Long Wei-guo. 2005. *Design manual of timber structure. M.* China Construction Industry Press.

ASSESSMENT OF THE *JUPITER JOINT*'S IN-PLANE AND OUT-OF-PLANE MECHANICAL BEHAVIOR UNDER COMBINED ACTIONS.

E. Perria[1], M. Kessel[1], M. Paradiso[2], M. Sieder[1]

[1] iBHolz, Institut für Baukonstruktion und Holzbau, Technische Universität Braunschweig

[2] DIDA, Dipartimento di Architettura, Università degli studi di Firenze

Keywords: Historical Timber, Woodwork joints, Jupiter joint, Structural Analysis

Abstract

Old timber structures are characterized by the complexity of structural elements and joints. The understanding of the basic working principles of the structural elements and joints is of basic importance for the definition of the load-carrying capacity and stiffness of the whole structure. Comprehensive and detailed information regarding design rules for the assessment and characterization of the carpentry joints are missing in the current scientific literature.

The paper presents experimental results on the behavior of the Jupiter joint (stop-splayed undersquinted & tabled with key joint), one among the most diffused elongation scarf joints. The tests are done on specimens with a specific geometry with inclination of the connecting surfaces of $\alpha = 60°$ and $\beta = 5°$ [Fig. 3]. Experimental in-plane and out-of-plane tests are proposed. The joint is loaded under external actions of pure compression, pure bending and combined compressive and bending stress. The failure modes and the qualitative influence of the geometry on the load-carrying capacity of the joint are described in detail. The paper concludes with the quantitative evaluation of the load-carrying capacity along both the strong and weak axis of the joint, expressed in min values, and represented in a N-M interaction diagram (pairs of normal force N and bending moment M).

The paper contains useful upgrades in the evaluation of carpentry connections' mechanical properties, more specifically in the field of the scarf joints. Useful pieces of information for the structural analysis of traditional timber constructional systems are presented.

1 INTRODUCTION

Timber historical buildings are diffused in many regions of the world. They are essential to the landscape of cities and countries, and constitute a precious example of both tangible and intangible historical heritage. For this reason, their maintenance and restoration is of basic importance. Nevertheless, historical buildings deserve particular attention at the moment of the intervention. In fact, old timber structures are characterized by the complexity of structural elements and joints. The understanding of the basic principles under which the structure works, is of basic importance for the definition of the correct restoration and strengthening work.

The carpentry structures and the joinery techniques are the result of a long-term process of evolution along the centuries and present a variety of constructional techniques that significantly vary according to regional building traditions. More than 600 different geometries of carpentry joints are known, and there are so many constructive techniques than cultures. According to the task they have to fulfill in the timber structure, the joints can be divided in different categories: lengthening, bearing, framing, angle and oblique shouldered joints. Among the most diffuse lengthening joint, the *stop-splayed undersquinted and tabled with key scarf* joint, also called *Jupiter joint*, has the function to enlarge the beams and other timbers along their longitudinal direction.

In the present paper, the load-bearing behavior and deformation behavior of the *Jupiter joint* carpentry connection, as found in historical wooden structures, is investigated.

1.1 Goals

The main aims pursued in the present paper are:

- Experimental evaluation of the load-carrying capacity of the *Jupiter joint* under combined compressive and bending action.
- Evaluation of the in-plane and out-of-plane behavior of the *Jupiter joint* under combined compressive and bending action.
- Representation of the experimental load-carrying capacity with a N-M interaction diagram (diagram that describes the interaction between normal force N and bending moment M).
- Evaluation of the failure modes for both the in-plane and out-of plane load directions.
- Quantification of the rotational stiffness' values to use in both the practice and structural analysis simulation.

1.2 Methodology

The adopted methodology is the scientific method. It consists of developed theories, systematic tests, measurements, observations, and modification of the initially adopted hypotheses. The adopted approach in this paper is experimental. The work consists of static in-plane and out-of-plane tests on scaled timber beams. The tests were carried out during the period April 2015 - July 2016, in the LHT Laboratory for wooden technology of the Faculty Building and Preserving in the HAWK Hildesheim (University of applied sciences), Germany.

2 MATERIAL AND METHODS

2.1 Equipment

The used machinery is Walter+Bai ag. (for forces up to $F_{c,max}$ = 250 kN and $F_{t,max}$ = 160 kN) controlled by a desktop computer with software Proteus. The equipment consists in the combination of two subsystems, two hydraulic jacks, one for vertical and the other for the horizontal loads. The Piston I is used for the application of axial forces ($F_{applied} = F_I$) and the Piston II for the application of bending moment ($F_{applied} = F_{II}$) (see equation (2) for the relation between applied force F_{II} and moment M). The force is exerted on the test specimens by means of movable cross-heads fixed to the frame. The head of the Piston II is provided with a head for the application of bending moment to the specimens.

2.2 Procedures

The procedure 2 tests (P2) follow a mixed force-controlled and displacement-controlled mode procedure. The P2 is described by the separate and consecutive loading of specimens by the Piston I and Piston II on the specimen's strong axis (Figure 1). The load F_I increases with force-controlled mode up to the chosen value of F_{target}; afterwards, the F_{II} with displacement-controlled mode is applied until the specimen's failure. During the loading the forces F_I and F_{II} and the correspondent pistons displacements w_I and w_{II} are measured. The relation among F_I force and the normal force (N) is defined in the equation (1). The one among the applied F_{II} force and the bending moment (M) by the equation (2).

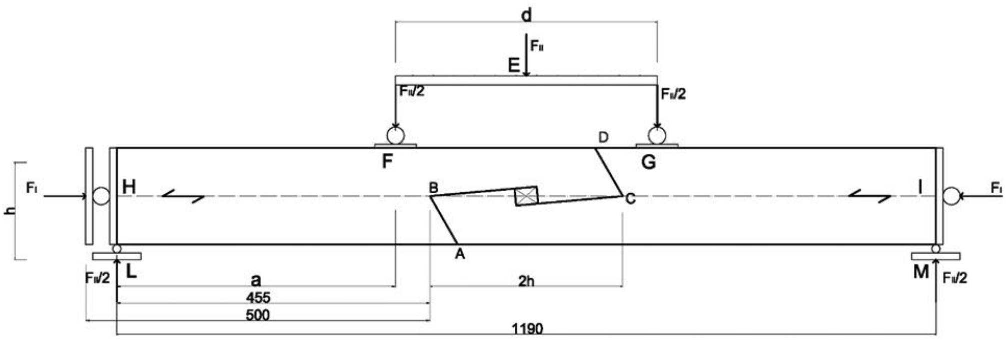

Figure 1: P2 tests asset for the application of compressive and bending force on the strong axis. All the dimensions are expressed in [mm]

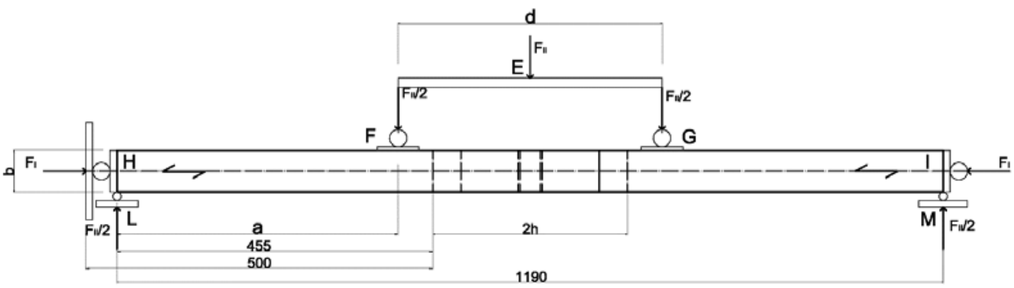

Figure 2: P3 tests asset for the application of compressive and bending force on the weak axis. All the dimensions are expressed in [mm]

The procedure 3 tests (P3) follow a mixed force-controlled and displacement-controlled mode procedure. The P3 is analogous to the Procedure 2, but the specimens are turned 90° and tested along the weak axis (Figure 2). The relation among F_I force and the normal force (N) is defined in the following equation (1). The one among the applied F_{II} force and the bending moment (M) by the equation (2).

$$N = F_I \qquad [kN] \tag{1}$$

$$M = \frac{F_{II}}{2} \cdot a \qquad [kN \cdot mm] \tag{2}$$

Where:

$$\begin{cases} a = 405\,mm & for \quad P1, P2 \\ a = 390\,mm & for \quad P3 \end{cases} \tag{3}$$

2.3 **Specimens**

The specimens are prepared from artificially dried solid timber beams of length 650 cm with a cross-section of b = 60 mm, h = 140 mm. The wood specie is spruce (*Picea abies*), timber strength class C24. The specimens are stored at a temperature of 20° C with relative humidity of 65%.

The specimen 6 (S6) is prepared for the analysis of the *Jupiter joint* along the strong and weak axis (Figure 3). The specimen surfaces are inclined of $\alpha = 60°$ and $\beta = 5°$. The joint is provided with a square-cut key.

The specimens' preparation consists of two different montages in the machinery according to the below described procedures.

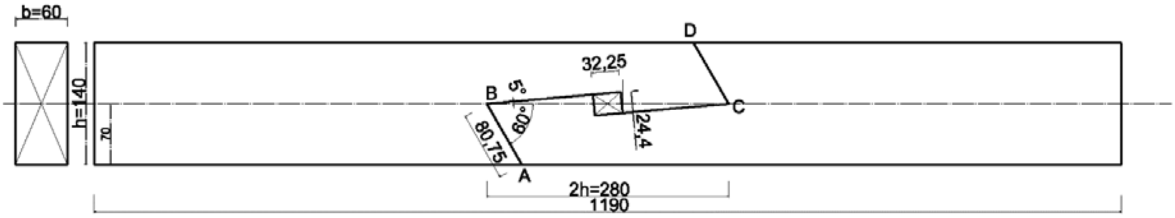

Figure 3: Specimen S6. Specimen used for the tests of the *Jupiter joint*. All the dimensions are in [mm]

3 TESTS

3.1 Strong axis tests

In Figure 4 are pictured the N-M interaction curves (interaction between the normal force N and the bending moment M) for the *Jupiter joint* (*stop-splayed undersquinted and tabled with key* scarf joint). The curves are the interpretation of the individual performed test results [1]. The strong axis tests are represented in colored results, while the weak axis tests are in bolt. The red line represents the strong axis' load-bearing interaction curve. The specimens are S6, performed with P2. The violet line describes the weak axis' load-bearing interaction curve. All the tests specimen are S6, and performed with P3.

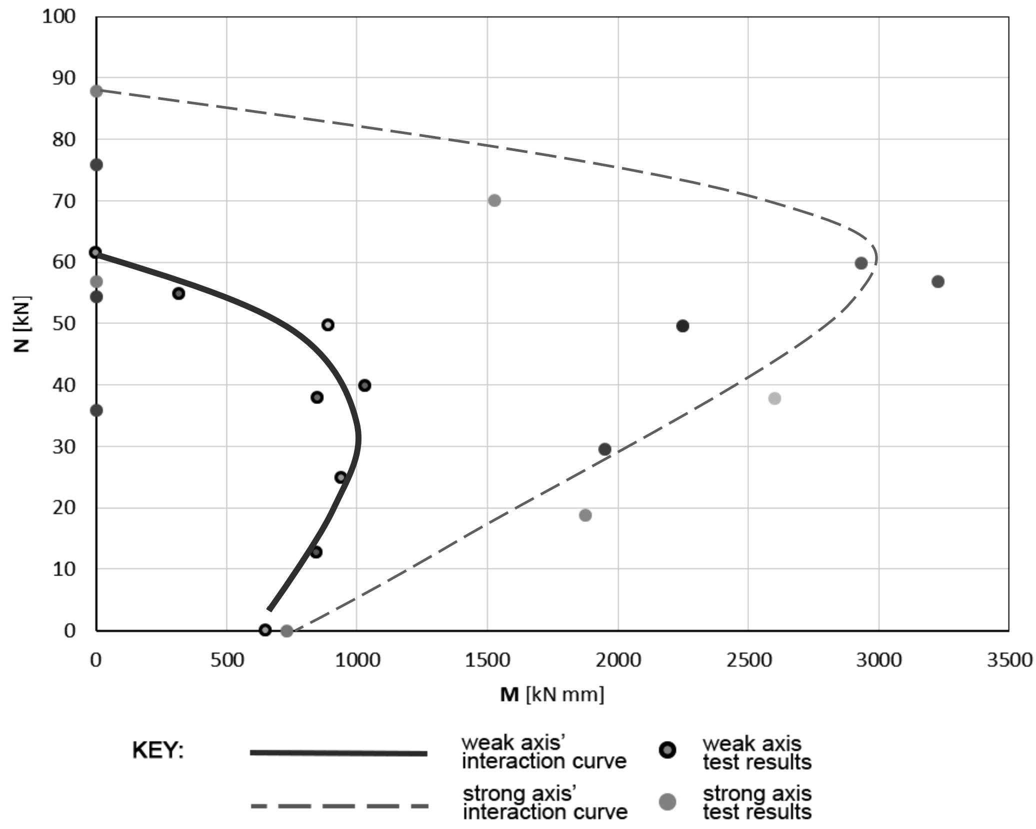

Figure 4: N-M interaction diagram for the *Jupiter joint* along the strong and weak axis

3.1.1 Failure modes (FM)

The failure modes observed in the weak axis' tests are mainly three, and are described as:

- FM II. Shear/tension perpendicular to the grain failure in the point B
- FM III Combined shear/tension perpendicular to the grain failure in the points B and C
- FM V. Shear failure in the BB''C'H prism.

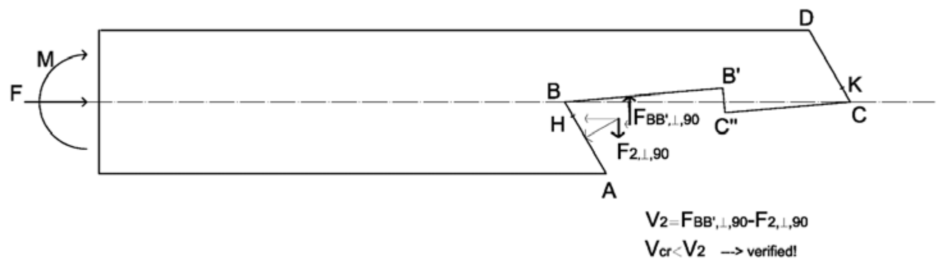

Figure 5: FM II. Shear/ tension perpendicular to the grains failure, active forces

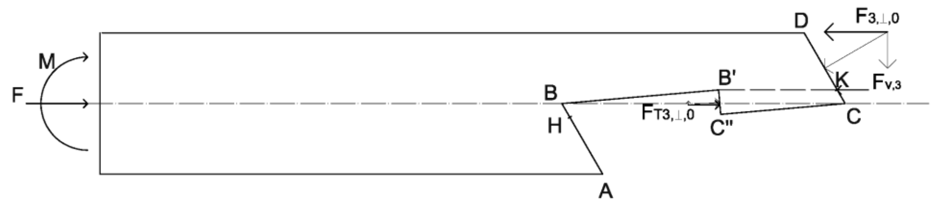

Figure 6: FM V Shear failure in the BB''C'H prism, active forces

FM I	FM II	FM III	FM IV	FM II + FM V	FM V
(…)			*(…)*		
	(a)	*(b)*		*(c)*	*(d)*

Figure 7: Failure mode of specimens of *Jupiter joint*, in-plane testing: (a): Specimen J60_5_S_F76_M α = 60° β = 5° 19/07/2016 compression force. (b): Specimen J60_5_S_F65_M α = 60° β = 5° 19/07/2016 compression force. (c): Specimen J60_5_S_F19_M α = 60° β = 5° 19/07/2016 compression and bending force. (d): Specimen J60_5_S_F0 α = 60° β = 5° 18/07/2016 pure bending

For all the specimens loaded along the strong axis, the main failure modes are the FM II and the combination of FM II and FM V. The failure modes are resumed in the Figure 7.

Referring to the Figure 6, the FM V is the shear failure in the lower timber piece's BB''C'H prism, for the whole depth *b* of the beam, and FM II happens in the lower timber piece along the fibers in correspondence of the point B, also for the whole depth *b* of the beam. It follows a more detailed description of the active forces on the surfaces that cause the failure.

FM II: The plain mechanism of fracture FM II on the compression and tension side is explained in the Figure 5. The failure is due to the contemporary action of the forces V_2 and V_{cr}:

$$\begin{aligned} V_2 &= F_{BB',\perp,90} - F_{2,\perp,90} \\ V_{cr} &\geq V_2 \rightarrow failure \end{aligned} \tag{4}$$

FM V: The shear failure is present both on the tensile and compressed side. The shear mechanism develops on the $\overline{B'K}$ shear plane. According to Figure 6, the shear force $F_{v,3}$ is dependent on the $F_{T3,0}$ and the $F_{3,\perp,0}$. The shear force acting on the shear plane $\overline{B'K}$ is:

$$F_{v,3} = F_{3,\perp,0} - F_{T3,\perp,0} \tag{5}$$

The section is verified when:

$$\frac{F_{v,3}}{b \cdot \overline{B'K}} \leq R_v \tag{6}$$

where: F_{pc} = pre - compression force; $F_{B'C'',\perp}$ = resultant force on the $\overline{B'C''}$ surface due to the external load, perpendicular to the surface; $F_{T3,\perp}$ = resultant force on the table 3 (T3 = surface $\overline{B'C''}$) of the joint, perpendicular to the surface; $F_{3,\perp}$ = resultant force on the face $\overline{DC}$ due to the external applied load, perpendicular to the surface; and $F_{T3,\perp,0} = F_{B'C'',\perp,0} + F_{pc,0}$.

3.2 Weak axis tests

The N-M interaction curve for the *stop-splayed undersquinted and tabled with key scarf* joint loaded along the weak axis is represented by the violet curve in Figure 4.

3.2.1 Failure modes

The observed weak axis's failure modes are mainly three and are following described:

- FM II. Shear/tension perpendicular to the grain failure in the point B
- FM III. Combined shear/tension perpendicular to the grain failure in the points B and C
- FM V. Shear failure in the BB''C'HBB''C'H prism.

According to the upper specimen in the Figure 10, the compression side is characterized by points A, H, B, B', B'', C', C'', C, K, D; while the tension side is characterized by the points A, H, B, B', B'', C', C'', C, D. For the specimens loaded along the weak axis the prevalent failure modes are the FM II, followed by the FM IV. The failure modes in the compression side are reported in Figure 9, and the ones observed in the tension side are in Figure 8.

The FM V is the shear failure in the lower timber piece's BB''C'H<u>BB</u>''<u>C</u>'<u>H</u> prism (Figure 10). The FM II happens in the upper timber piece's point B. The FM III is considered as secondary and due to the presence of the imperfections in the wood. It follows a more detailed description of the active forces on the surfaces that cause the failures, basing on test results and some basic equilibrium rules. The problem of the failure is very complicated because it implies some internal kinematic mechanisms that are explained in Figure 10 and brings both to the FM II and FM V.

FM II: Referring to Figure 10 and Figure 11, the FM II is explained through some three dimensional diagrams that consider the variation of the forces in the cross–section and the relative developed kinematic mechanisms. Here:

a) Because of $F_{T2,\perp,90}$ force, the grains in B are tensile-stressed in the upward direction.

b) Because of $F_{2,\perp,90}$ on the tension side, the fibers in <u>B</u> are tensile-stressed in the downward direction.

c) Because of $F_{T2,\perp,90}$ and $F_{2,\perp,90}$ forces, the clockwise torque $M_{BHC'B''}$ forms along the longitudinal direction of the compression side. The torque brings to the additional compression of the facing $\overline{AB}$ and $\overline{BB''}$ surfaces on the compressed side.

d) The force $F_{2,\perp,90}$ on the tension side, together with the $F_{2,\perp,90}$ on the compression side, bring to the formation of the anticlockwise torque $M_{\underline{BH}BH}$. The torque brings to the torsion of the specimen along the neutral axis that causes a non-homogeneous distribution of the compression force in the squint AB<u>AB</u> (Figure 11).

Because of the kinematic mechanisms above descripted in a), b), c), d), the FM II develops both in B, on the compression side, and in <u>B,</u> on the tension side.

FM I	FM II	FM III	FM IV	FM II + FM V	FM V
(...)	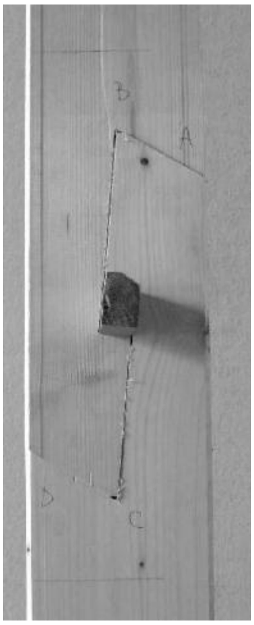 (a)	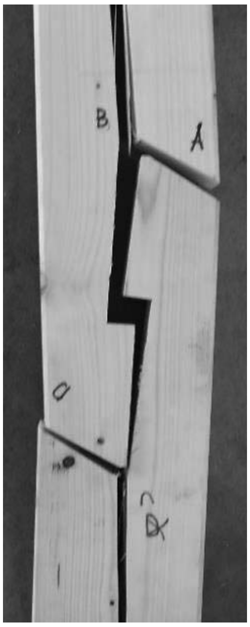 (b)	(…)	 (c)	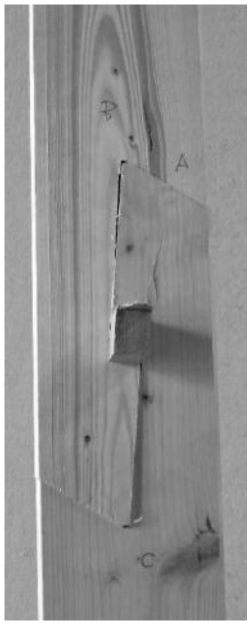 (d)

Figure 8: Failure mode on the tension side of specimens of *Jupiter joint*; out-of-plane tests: (a): Specimen J60_5_w_F50_M α = 60° β = 5° 21/07/2016 compression and tension stress. (b): Specimen J60_5_w_F55_M α = 60° β = 5° 21/07/2016 compression and tension stress. (c): Specimen J60_5_w_F12_M α = 60° β = 5° 21/07/2016, compression and tension stress. (d): Specimen J60_5_w_F25_M α = 60° β = 5° 21/07/2016 compression and tension stress

FM I	FM II	FM III	FM IV	FM II + FM IV	FM V
(…)	 (a)	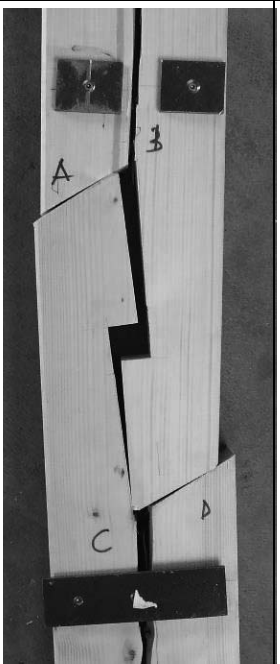 (b)	(…)	 (c)	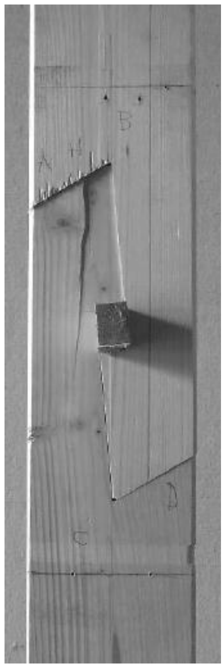 (d)

Figure 9: Failure modes on the compression side of specimens of *Jupiter joint*; out-of-plane tests: (a): Specimen J60_5_w_F50_M α = 60° β = 5° 21/07/2016 compression and tension stress. (b): Specimen J60_5_w_F55_M α = 60° β = 5° 21/07/2016 compression and tension stress. (c) Specimen J60_5_w_F38_M α = 60° β = 5° 21/07/2016, compression and tension stress. (d): Specimen J60_5_w_F12_M α = 60° β = 5° 21/07/2016 compression and tension stress

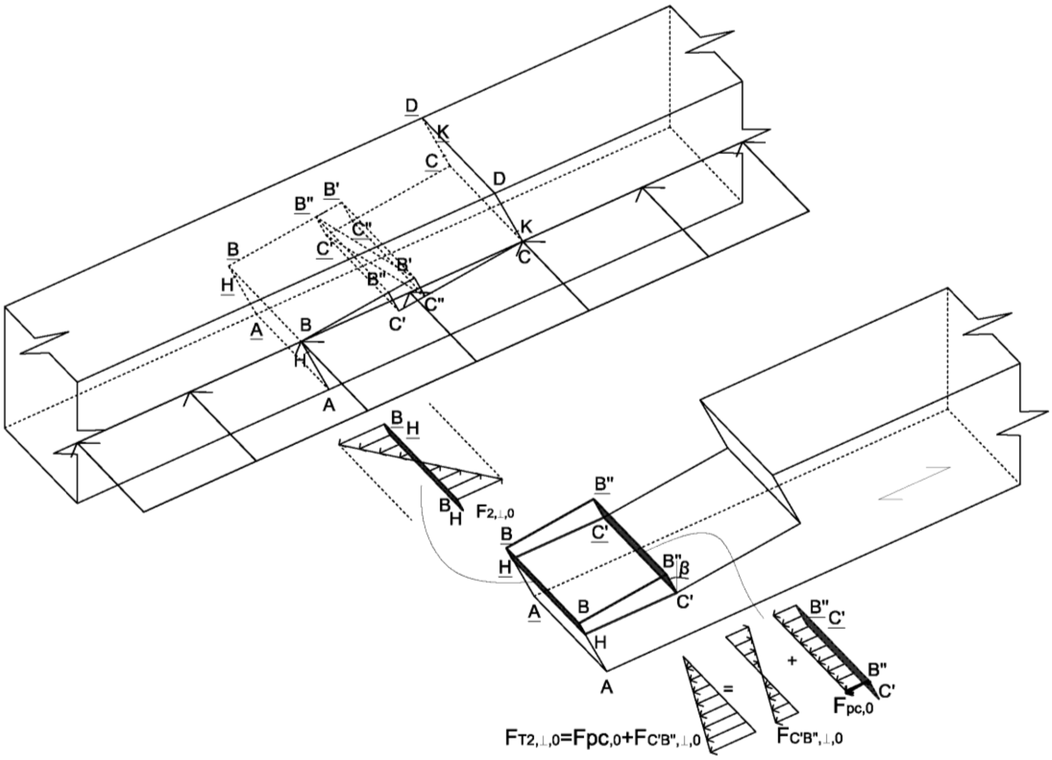

Figure 10: Upper specimen: three dimensional representation of the *Jupiter joint*s' specimen (loaded on the weak axis). Lower specimen: Complex mechanisms of transmission of the forces in the BB''C'HBB''C'H prism

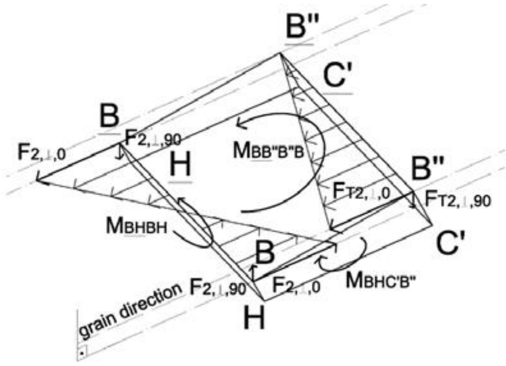

Figure 11: Detail of the forces in the BB''C'HBB''C'H prism and relative developed kinematic mechanisms

FM V: The shear failure is present both on the compressed and on the tension side. The shear mechanism develops even though on different shear planes.

Tension side: the shear plane $\overline{B'K}$. The shear failure can also verify on the tension side, on the fibers in $\overline{B'K}$, because of the compression on $\overline{CD}$ (specimen J60_5_w_F12, Figure 8 - c).

Compression side: the shear force acting on the shear plane $\overline{C'H}$ is described in equation (7) and depends on equation (8).

$$F_{v,2} = F_{2,\perp,0} - F_{T2,\perp,0} \tag{7}$$

$$F_{T2,\perp,0} = F_{pc,0} + F_{B''C',\perp,0} \tag{8}$$

where: $F_{C'B'',\perp}$ = resultant force on the $\overline{C'B''}$ surface due to the external load, perpendicular to the surface; $F_{T2,\perp}$ = resultant force on the table 2 (T2 = surface $\overline{C'B''}$) of the joint, perpendicular to the surface; $F_{2,\perp}$ = resultant force on the face $\overline{AB}$ due to the external applied load.

The section is verified when:

$$\frac{F_{v,2}}{b \cdot \overline{C'H}} \le R_v \tag{9}$$

Referring to Figure 11, the mechanism is further completed with some observations about the kinematic mechanisms in the third dimension. Because of both different resultant forces at the two compression and tension side, the anticlockwise torque MB’’B’BB’’ forms on the shear plane (transversal direction).

As an example that demonstrates the failure mechanisms in the beam, some images from the tests of the failure of the specimen J60_5_w_F0 [12] are proposed in the Figure 12:

(a) The upper timber part is rotated respect to the lower timber part due to the torque MBHBH that creates a torsion along the beam’s axis.

(b) The internal kinematic mechanisms (torque MBHC’B’’) causes a rotation that brings to the further compression of the segment $\overline{BB'}$ on the tension side and (c) the segment $\overline{AB}$ on the compression side. The key is a further fixed point that establish a horizontal rotation axis that causes the torsion of the upper respect to the lower part.

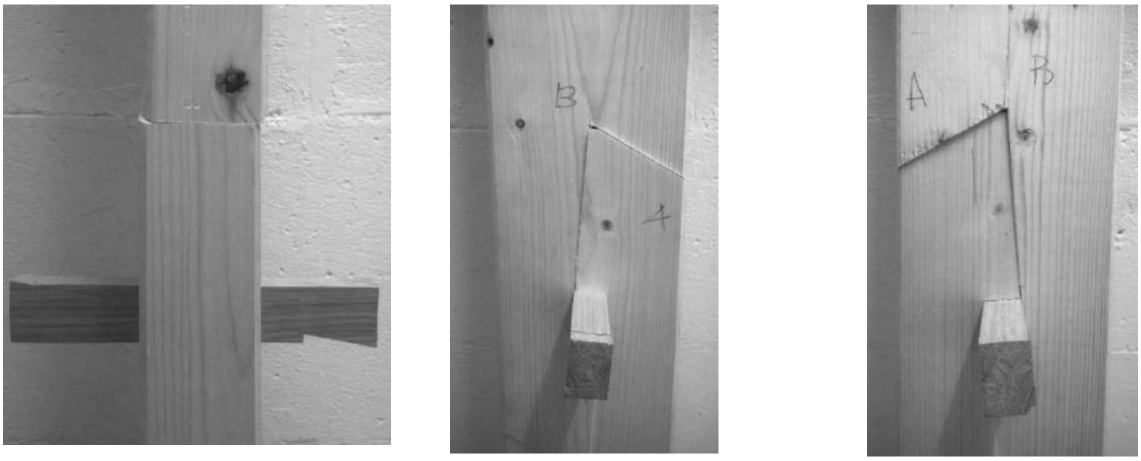

(a) (b) (c)

Figure 12: FM II on the specimen J60_5_w_F0 (a) Rotation of the upper to le lover side. The right part is compressed, the left is tensile-stressed. (b) Tension side. The segment BB’ is further compressed. (c) Compression side. The segment BA is further compressed

4 EVALUATION OF THE ROTATIONAL STIFFNESS

Referring to Figure 13, the calculation of the rotational stiffness k_φ in equation (15), is done according to the ultimate values of applied load and the displacements of the correspondent piston P_{II}. The calculation is performed as follows.

$$e = 0.405m \tag{10}$$

$$M_u = \frac{F_{II,u}}{2} \cdot e \tag{11}$$

$$u_{PII}(M_u) \tag{12}$$

$$\theta_{[\deg]} = arctg\left(\frac{u_{P2}}{l_b/2}\right) \tag{13}$$

$$\theta_{[rad]} = \frac{\theta_{[\deg]} \cdot \pi}{180°} \tag{14}$$

$$k_{\varphi} = \frac{M_u}{\theta_{[rad]}} \tag{15}$$

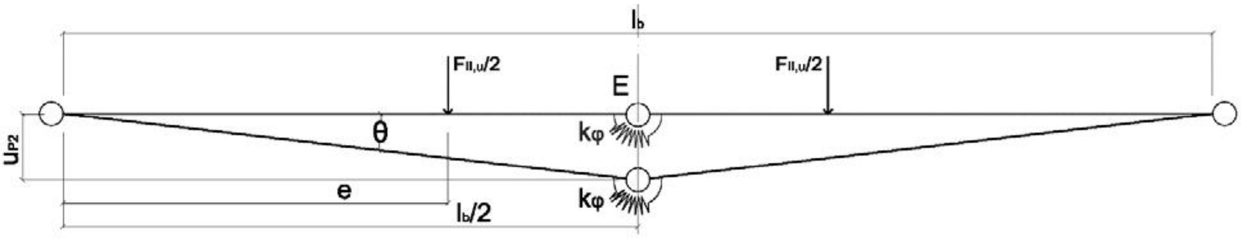

Figure 13: Scheme of the rotational stiffness of the hinge

The reference value of rotational stiffness for the *Jupiter joint* along both the strong and the weak axis is considered the rotational stiffness obtained in the pure bending tests, calculated according to equation (15). The tests of reference are the one performed in vertical position with the testing machine 2. The equation (16) gives a resume of the experimental values of rotational stiffness in the *Jupiter joint* for the strong and weak axis.

$$\begin{aligned} k\varphi y_{\exp} &= 663 \qquad (strong \quad axis) \\ k\varphi z_{\exp} &= 262 \qquad (weak \quad axis) \end{aligned} \tag{16}$$

5. GENERAL CONCLUSIONS ON THE *JUPITER JOINT*

5.1. Load-carrying capacity

The comparison of the tests of the *Jupiter joint* leads to the followings conclusions:

1. The load-carrying capacity of the *Jupiter joint* along both the strong and weak axis is the same for the specimens loaded in pure compression and in pure bending.
2. In pure compression, the test specimen loaded on the weak axis showed a smaller ultimate strength [*Fu*] respect to the one loaded on the strong axis. The reason of this difference in the load-carrying capacity of the specimen can rely in the specimen manufacturing, the timber's specific lower properties, and finally in the test asset.
3. The presence of imperfections in the test asset is a more significant factor for the specimen loaded on the weak axis; here, the minimum imperfection can really affect the test results.

5.2. Failure modes

The FM II. shear/tension perpendicular to the grain failure in the point B is the most recurrent, both on the weak and in the strong axis' tests. The basic reason of the failure is the same concluded and calculated for the *halved undersquinted scarf* joint [12]; nevertheless, in the *Jupiter joint* the problem is more complex because of the presence of more factors:

1. the presence of imperfections (that affect the weak axis more than the strong axis);
2. the pre-compression F_{pc} of the key;
3. the entity of both the angle α of the squint and β of the splayed surface;
4. the internal friction (not considered in the present section of the work);

Furthermore, the FM V is dependent on the length of the shear segment $\overline{C'H}$. The bigger is the surface of the shear plane (longer shear segment), the bigger is the load-carrying capacity of the specimen.

REFERENCES

[1] Blass H. J., Aune P. et alii. (1995). Timber Engineering, *STEP 1 (STEP 2), Basis of design, material properties, structural components and joints*, Centrum Hout, The Netherlands.

[2] Branco J. M., Descamps T. (2015). Analysis and strengthening of carpentry joints. in: *construction and building materials*, 97 (2015) 34–47.

[3] Collings G. (1992). Circular Work in Carpentry and Joinery, illustrated by Karl Shumaker, Roger Holmes, Canada.

[4] Fairham W., Roberts G. R. (1920). *Woodwork Joints: Carpentry, Joinery, Cabinet-Making*: The Woodworker Series, Ewan –Bros., London.

[5] Gatzelu L., D., (1899). *Carpinteria de armar*, Madrid.

[6] Gerner, M. (1983). *Fachwerk: Entwicklung, Gefüge, Instandsetzung*, Deutsche Verlags-Antstalt, Stuttgard.

[7] Gerner, M. (1992). *Handwerkliche Holzverbindungen für Zimmerer*, Deutsche Verlags-Antstalt, Stuttgard.

[8] Graubner W. (2004). *Holzverbindungen - Gegenüberstellungen japanischer und europäischer Lösungen*, Deutsche Verlags-Anstalt, München Stuttgard 2004.

[9] Gustafsson J., (ca. 1990). *A study of strenght of notched beams.* Division of Structural Mechanics, Lund Institute of Technology. Lund, Sweden

[10] Gustafsson P. (2003). *Fracture perpendicular to Grain – Structural applications*. In: Thelandersson and Larsen H., J., Timber Engineering, Wiley.

[11] Madsen B. (2000). *Behaviour of Timber Connections*. Vancouver, Canada: Timber engineering Ltd.

[12] Perria E. (2017). "*Characterization of halved undersquinted scarf joint and stop-splayed undersquinted & tabled scarf joint with key (Jupiter joint)".* Dissertation submitted to the Department of Architecture, Civil Engineering and Environmental Sciences University of Braunschweig – Institute of Technology and the Department of Civil and Environmental Engineering University of Florence".

[13] Sobon J. A. (2002). *Historic American Timber Joinery: A Graphic Guide*, Pub. By Timber Framers Guild, Ed. by Kenneth Rower. Retrived from https://www.ncptt.nps.gov/wp-content/uploads/2004-08.pdf.

[14] Tregold, T., (1858). *Elementary principles of carpentry*, John Weale, London.

SHATIS'17
4th International Conference on
Structural Health Assessment of Timber Structures
20-22 September 2017 Istanbul, Turkey

INDIRECT SONIC STRESS WAVES METHOD TO PREDICT THE CROSS-SECTIONAL VARIATION OF BENDING MODULUS OF ELASTICITY OF A TIMBER MEMBER

Morales-Conde, MJ[1], Saporiti Machado, J[2]

[1] Instituto Universitario de Arquitectura y Ciencias de la Construcción, Escuela Técnica Superior de Arquitectura, Universidad de Sevilla. Sevilla, Spain

[2] Structures department, Laboratório Nacional de Engenharia Civil, Lisboa, Portugal

Keywords: timber variability, stress waves, ultrasound, wood core, modulus of elasticity

Abstract

Wood is a natural material has been widely used throughout history in structural elements. The degradation of the material and mainly the deformation, related to serviceability limit states, are often the main reasons to assess existing structures.

For this purpose, the results obtained from visual inspection are combined with information from NDT and/or SDT methods, such as stress wave or ultrasound, thermography, screw withdrawal or drilling resistance. Stress wave testing methods are often used for prediction of timber elements' stiffness. However, timber's variability significantly affects the reliability of NDT/SDT capacity to predict their mechanical behaviour since these methods only provide information about the outer layers of the timber members. For a more reliable prediction assessment, one should acknowledge the spatial variability of timber's mechanical properties, especially considering the gross cross-section.

In this study, it was analysed the capacity of an indirect sonic stress wave method to predict the modulus of elasticity of a timber member, taking into consideration its cross-sectional spatial variability. The results show that the application of the new procedure provided a significantly increased capacity of prediction of the static modulus of elasticity (r^2 = 0.91–0.94) compared to the application of current ultrasonic measurements carried out on the surface of the specimens (r^2 between 0.72–0.73).

1 INTRODUCTION

Timber is a natural material often found in structural elements of historical constructions, given its good mechanical properties (e.g. the high strength/weight ratio). In these cases, timber inspection constitutes a crucial support decision tool regarding efficient repair or strengthening solutions, thus ensuring the safety of the structure [1]. Reliable tools for assessing mechanical behaviour of timber members are specially needed in the case of old timber structures where no information is available on wood species and mechanical properties.

Currently, assessment of timber structures is carried out by visual inspection to evaluate the condition of the structure (i.e. structural system, structural defects, deformation of timber members, signs of deterioration); the loading conditions (i.e. deviation from intended use that can result in overloading); the additions to the original structure and their effect on the original structural system; the quality of timber (knots, cracks, slope of grain, etc) and allocation of visual strength grade and consequent characteristic values or a strength class; and the location of critical areas for further inspection [2].

Frequently, the results obtained from visual inspection are combined with information from NDT and/or SDT methods, such as stress wave or ultrasound, thermography, screw withdrawal or drilling resistance [1].

Regarding the assessment of mechanical properties, stress waves are generally applied either using sonic or ultrasonic frequencies. Non-destructive testing (NDT) methods are used to predict the dynamic modulus of elasticity being affected by several factors such as moisture content, wood species and growth ring orientation [3]. Usually, stress wave testing is conducted in one or more surfaces of the member over an area showing no defects. The possibility of extrapolating the clear wood modulus of elasticity to the entire element is supported by the fact that the modulus of elasticity is mainly affected by the basic quality of a structural member and is less affected by local defects [4]. Stress wave testing onsite is based on an indirect method where the transducers are placed in the same surface. For this reason, only the outer layers of the timber members are tested. However, wood is an anisotropic material showing high variability in physical and mechanical properties in a same section and along its length [5].

The objective of this paper is to analyse the possibility of assessing the variation of bending modulus of elasticity across the cross section of structural timber members using a stress-wave semi-destructive method.

2 EXPERIMENTAL WORK

A sample of 30 clear wood pieces of Maritime pine (*Pinus Pinaster* Ait.) was used in this study. These test pieces (TP) had a size of 550 x 160 x 90 mm^3 and were divided into 2 groups of 15 samples (A and B) each according to growth ring curvature in the cross section. In sample A the growth rings are parallel to the larger longitudinal surface of the test pieces, whereas in sample B, the growth rings make an angle (of around 45º) with the same surface (Fig. 1). These pieces were tested using stress waves, ultrasound and core-drilling.

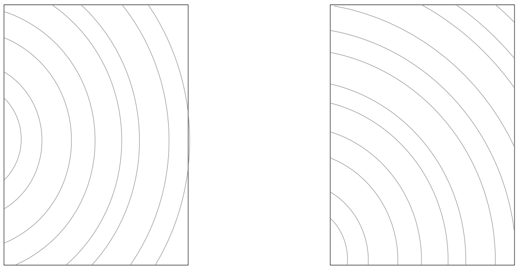

Samples A Samples B

Figure 1. The two types of test pieces (A and B) differentiated regarding the orientation of the growth rings in the cross section.

In each test piece, four stress wave measurements were carried out at different depths using a Fakopp Microsecond Timer equipment. The stress wave time-of-flight was determined by placing the transducers in the same surface (indirect method) (Fig. 2). The measurements were made in both edges of the specimen. For each edge, the first reading was made in the external layer by a spike penetration of approximately 10 mm. The transducers were placed 43 cm apart and were driven into the wood at an angle of ~45º (Fig. 2a). After the first readings, a larger hole was produced with a depth equal to the penetration of the spike using a drill bit diameter of 7.5 mm. In this case, the transducers were placed 40 cm apart. The diameter of the internal passage hole allowed the spike to be driven into the next 10 mm of wood, avoiding in the first 10 mm any contact between the spike and wood.

a) b)

Figure 2. a) Stress wave test; b) Ultrasound test

After stress waves measurements, ultrasound waves were generated using a PUNDIT plus equipment with two 54 KHz transducers. Coupling between the probes and timber's surface was achieved by means of a mineral gel. A one-shot impulse transmission was applied. The probes were placed 40 cm apart (minimum distance between probes perimeter) at the upper edge of the test specimens. Only one surface was tested and a compression spring placed on top of each transducer was used to maintain a constant pressure all over the tests (Fig. 2b).

The TOF was used along with the distance to predict the stress wave velocity parallel to the grain (v). The dynamic modulus of elasticity (E_{dyn}) was obtained from Eq. (1), using the average value of the density obtained from two wood cores taken in the vicinity of the transducers as density (ρ) estimation.

$$E_{dyn} = v^2 \cdot \rho \quad (\mathrm{N/m^2}) \qquad (1)$$

After performing this first stage, the pieces were cut to obtain 5 small clear wood specimens (SCWS) from each test piece. These pieces had a size of 20x20x550 mm^3 and were tested in static bending to obtain the static modulus of elasticity.

The bending modulus of elasticity (E_m) was determined according to static three-point load bending tests carried out according to the ISO 3133 standard [6]. The three-point bending test was accomplished with a span of 300 mm.

Density was determined over: the test pieces prior to being cut into small clear bending specimens (ρ_{TP}); the small clear specimens (ρ_{scws}); and, two wood cores taken near the ends of the specimen (ρ_{core}). The data are reported in Table 1. The density was determined based on the ratio of mass to volume at particular moisture content.

Table 1. Density of test pieces (TP), small clear wood specimens (SCWS) and wood cores (WC).

Test pieces (TP)			Small clear specimens (SCWS)			Wood cores (WC)		
Type	Number of specimens	Density (kg/m^3) Mean / CoV (%)	Type	Number of specimens	Density (kg/m^3) Mean / CoV (%)	Type	Number of specimens	Density (kg/m^3) Mean / CoV (%)
A	15	675.7 (11.7)	A	75	663.2 (14.4)	A	150	657.9 (14.8)
B	15	653.8 (11.6)	B	75	634.32 (15.3)	B	150	632.6 (15.3)

The moisture content was determined using the small clear wood specimens and the wood cores (Table 2). The samples were weighed and then placed in an oven at 103±2 °C until a mass variation of less than 0.1% in an interval of 2 hours is reached [7].

Table 2. Moisture content of small clear wood specimens (SCWS) and wood cores (WC).

Small clear specimens (SCWS)			Wood cores (WC)		
Type	Number of specimens	Moisture content (%) Mean / CoV (%)	Type	Number of specimens	Moisture content (%) Mean / CoV (%)
A	75	13.4 (2.0)	A	150	13.4 (2.9)
B	75	13.4 (4.2)	B	150	13.5 (4.7)

All the wood specimens was conditioned and tested inside a room with controlled temperature (20±2 ºC) and relative humidity (65±5%).

3 RESULTS AND DISCUSSION

The mean and the variability of the reference properties (f_m, E_m and ρ_{sc}) in the cross-section obtained from the small clear specimens cut at different locations inside specimens A and B are indicated in Table 3. A noticeable higher variability is found for modulus of elasticity than for density or strength. The variability found for density shows the importance of taken it into consideration when making predictions of the dynamic modulus of elasticity (equation 3) and in consequence of the static modulus of elasticity. Bending strength since is the property more connected to the presence of defects the result (very low variability) was expected given the fact that the results were obtained in clear wood specimens.

Table 3. Variability in the cross section measured by the coefficient of variation (mean, max and min) observed for each specimens A and B.

Test pieces Coefficients of variation		Reference properties		
			Bending	
		Density	Modulus of elasticity	Strength
A	Mean (%) Max (%) Min (%)	6.9 14.2 1.9	15.8 35.1 7.3	0.1 0.3 0.0
B	Mean (%) Max (%) Min (%)	6.4 11.9 2.2	12.2 24.8 4.7	0.1 0.2 0.0

The accuracy in the determination of the dynamic modulus of elasticity is influenced by the prediction of density, a property that varies along the cross section and the length of the element. A comparison is made with the density obtained from the initial test pieces and with that obtained from each small clear wood specimen (Fig. 3). The density information provided by two wood cores provides, on average, a good prediction of the overall density of the test pieces (i.e. a high correlation). This result is in accordance with previous works [8].

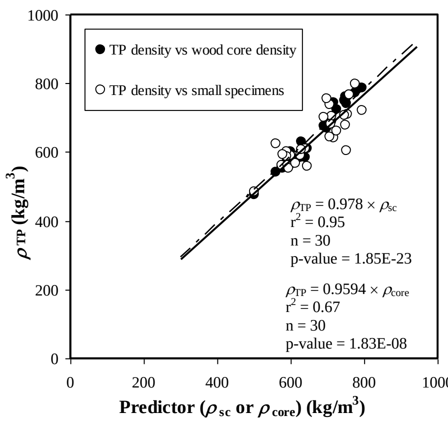

Figure 3. Prediction of TP density using as predictors the density obtained from the wood cores (ρ_{core}) and that from the small clear wood specimens (ρ_{sc}).

No significant difference is noted between the results obtained for each type of test piece (A and B) when tested using either the ultrasound or the sonic test method. Nevertheless, the sonic method results in a higher coefficient of determination when comparing the results in the same test pieces. The better capacity of the sonic method to predict the overall modulus of the elasticity made at different depths of the element is clear (Fig. 4). The result was consistent in both types of test pieces showing a coefficient of determination of ~0.70 and ~0.90 between the static and the ultrasonic or sonic dynamic modulus, respectively.

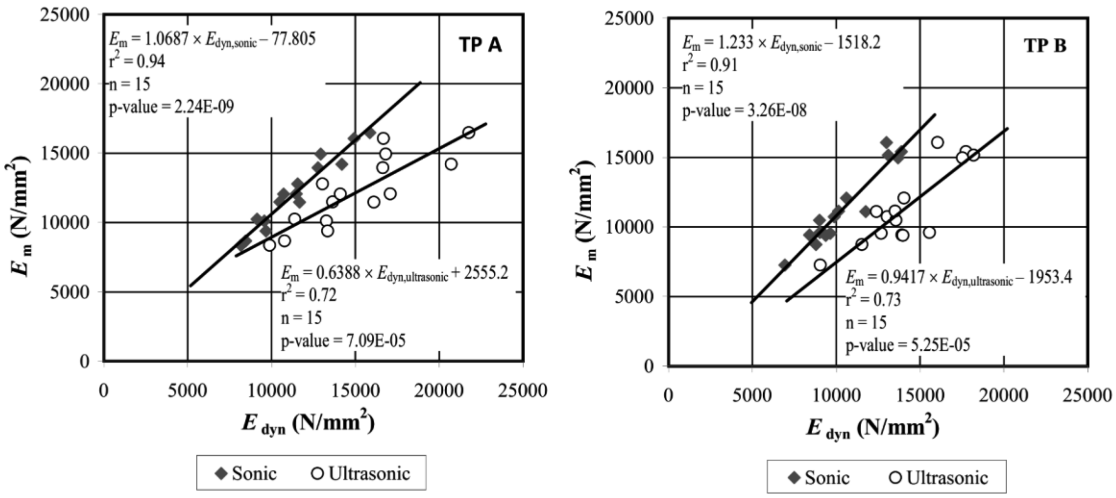

Figure 4. Correlation for the two types of specimens tested (A and B) between E_{dyn} and E_m.

The closer relationship obtained using the sonic method at different depths is also shown in Fig. 5. This figure compares the variation of the modulus of elasticity along the cross section for the different specimens and densities obtained directly from testing small clear wood specimens, and indirectly using sonic waves. As can be noted, in most cases a correlation exists between the dynamic modulus of elasticity (dynamic MOE) and the static modulus of elasticity (static MOE) obtained for the small clear specimens in each TP, A and B.

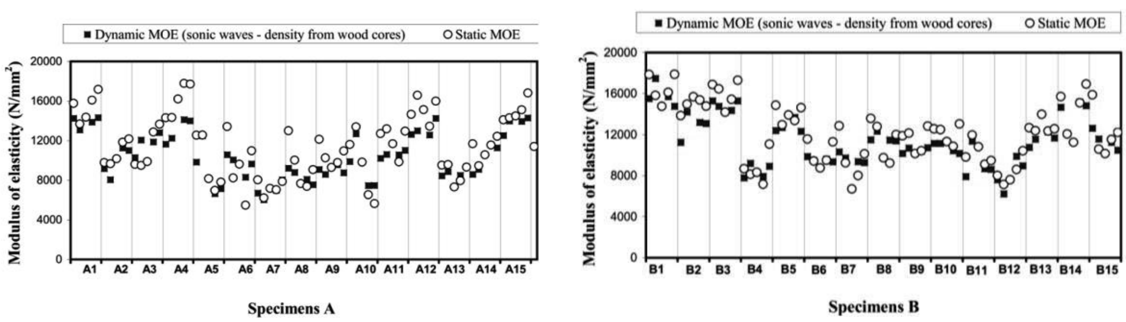

Figure 5. Cross-sectional variation of modulus of elasticity shown by specimen type A and B. For each TP specimen, five measurements are shown corresponding with the five small clear specimens obtained.

4 CONCLUSIONS

Timber's variability significantly affects the reliability of NDT/SDT capacity to predict its mechanical behaviour. This variability is high on timber members given the current gross section used and justify the present study which objective was to assess the capacity of a procedure based on an insertion of sonic probes at different depths into a piece of timber to obtain a better prediction of the static modulus of elasticity. The method was compared to the results obtained using a current indirect ultrasonic testing method. The application of the new procedure resulted in significantly increased capacity of prediction of the static modulus of elasticity (r^2 between 0.94 and 0.91, depending on the type of test piece tested) compared to the application of current ultrasonic measurements carried out on the surface of the specimens (r^2 between 0.72–0.73).

REFERENCES

[1] Feio A, Machado J S (2015) In-situ assessment of timber structural members: Combining information from visual strength grading and NDT/SDT methods – A review. *Construction and Building Materials*. 101, 1157–1165.

[2] Cruz, H., Yeomans, D., Tsakanika, E., Macchioni, N., Jorissen, A., Touza, M., Mannucci M. & Lourenco P. (2015). Guidelines for on-site assessment of historic timber structures, *International Journal of Architectural Heritage,* 9 (3), 277–289.

[3] U. Dackermann, K. Crews, B. Kasal, Jianchun Li, M. Riggio, F. Rinn, T. Tannert (2014), In-situ assessment of structural timber using stress-wave measurements, *Mater. Struct.* 47 787–803.

[4] Piazza M. Riggio M (2008) Visual strength-grading and NDT of timber in traditional structures. J Build Apprasil 3 267–296.

[5] Kasal. B. & Anthony. R. W. (2004). Advances in in situ evaluation of timber structures. *Progress in Structural Engineering and Materials, 6*(2), 94–103.

[6] ISO 3133:1975 (1975) Wood -- Determination of ultimate strength in static bending Available at:

[7] EN 13183-1:2002 (2002) Moisture content of a piece of sawn timber – Part 1: Determination by oven dry method. European Committee for Standardization.

[8] Machado, J S. (2015). Reliability of prediction by combining direct and indirect measurements. In J S Machado, M. Riggio and T. Descamps, eds., *Combined use of NDT/SDT methods for the assessment of structural timber members*. COST FP1101 State of the Art Report. Mons: Université de Mons, 1–13.

SHATIS'17
4th International Conference on
Structural Health Assessment of Timber Structures
20-22 September 2017 Istanbul, Turkey

MOISTURE CONTENT MONITORING IN GLULAM STRUCTURES BY EMBEDDED SENSORS

Hang Li[1], **Marianne Perrin**[1], **Florent Eyma**[1], **Xavier Jacob**[2] **and Vincent Gibiat**[2]

[1] Institut Clément Ader (ICA), CNRS UMR 5312, University of Toulouse, UPS, France

[2] PHASE Laboratory, EA 3028, University of Toulouse, UPS, Toulouse, France

Keywords: Moisture content monitoring, Glulam structures, Electrical measurements, Ultrasonic measurements, Embedded sensors

Abstract

Today, more and more timber structures (especially glulam structures) are used in civil engineering in respect of sustainable development and thanks to their competitive costs. However, the durability problem limits their development. Degradations related to excessive moisture content (MC) or to the wetting/drying cycles were observed and can lead to severe structural damages. In order to promote the use of wood in construction, infrastructure supervisors have expressed their need on continuous monitoring techniques of wood MC. However, no information exists in literature regarding the MC monitoring inside the lamellas of glulam.

In the light of this observation, we propose to transform glulam into "smart material" by embedding the MC monitoring system between the lamellas, on taking into account the major constraints of fabrication of this material (the small glue line thickness, the important bonding pressure, etc.). To achieve this, we have selected two families of methods: the electrical methods and the ultrasonic method. The former are based on resistive/capacitive measurements and the latter consists in the analysis of ultrasonic wave propagation in the material. 4 measurement configurations were identified for the electrical measurements using pin-type or surface-type sensors. Regarding the ultrasonic measurements, 2 configurations were proposed and tests were realized with two families of piezoelectric film sensors (PVDF (Polyvinylidene fluoride) and MFC (Macro Fiber Composite)).

Our results showed that it is possible to conduct electrical/ultrasonic measurements in wood with the proposed measurement configurations. The influence of bonding pressure and sensor distance was also investigated. Future study should be continued to investigate the feasibility of applying these identified measurement configurations for the local MC monitoring in the lamellas of glulam beams.

1 INTRODUCTION

Today, more and more glulam structures are used in building and civil engineering due to new challenges imposed by sustainable development. However, the problem of durability is a limiting factor for the development of these structures [1]. Pathologies such as cracks, delaminations or slots, as well as fungal or insect attacks have been observed. The majority of them can be attributed either to excessive moisture content (MC) (> 22%) or to the wetting/drying cycles in the material [2]. In order to promote the use of wood in construction, infrastructure supervisors have expressed their need on continuous monitoring techniques of wood MC.

A multitude number of techniques are reported to be able to measure the MC in wood [3,4]. However, a great number of them cannot respond to the constraints of continuous monitoring in engineering structures. According to our bibliographic research, two families of methods have the potential to be employed in long-term MC monitoring of glulam structures: the electrical methods (resistive/capacitive) [5,6] and the ultrasonic method [7].

Concerning the electrical methods, several studies have shown the possibilities of using different types of sensors for the continuous MC monitoring in wood [8]. With regard to the resistive method, it concerns the use of “pin-type electrodes” inserted in wood [5]. Regarding the capacitive method, it concerns the use of “surface electrodes” with two parallel metallic plates on the outer surfaces of wood [4].

Regarding the ultrasonic method, no studies exist in literature regarding sensors which can allow the continuous MC monitoring in wood. This might be explained by the fact that the conventional ultrasonic transducers are not compact enough to be permanently integrated in structures for long-term monitoring due to their size and cost [9]. Even though, referable information exists concerning structural health monitoring (SHM) using piezoelectric sensors. There exist two families of piezoelectric film sensors which are capable to be integrated in structures with relative moderate costs: the PVDF (Polyvinylidene fluoride) which is a piezoelectric polymer film; the MFC (Macro-fiber composite) which is composite with piezoelectric fibers integrated in an epoxy matrix [10].

According to studies cited above, no existing solutions allow the internal and local MC monitoring in the lamellas of glulam, which is essential to improve the structure durability. Given the industrial fabrication process of glulam [11], the major constraints for sensor integration are the small glue line thickness (0.3 mm) and the bonding pressure (10 bars).

In the light of these observations, we propose to transform the glulam into “smart material” by embedding MC monitoring systems in order to perform internal and local MC measurement in the lamellas. To achieve this, we have identified 4 measurement configurations for the electrical methods and 2 measurement configurations for the ultrasonic method. The objectives of this study are: 1) to verify the feasibility of conducting electrical/ultrasonic measurements in wood using the proposed measurement configurations; 2) to verify the influence of bonding pressure on sensor performance; 3) to investigate the influence of sensor distance on measured physical quantities.

2 MATERIAL AND METHODS

2.1. Electrical measurements

2.1.1. Measurement configurations

Four measurement configurations using different electrode set-ups were identified in this study (Figure 1). The specimens were prepared with Douglas fir because it is extensively used in construction. The Configuration 1 is a simple measurement configuration with stainless screws driven directly into the wood. However, loss of electrical contact between the electrodes and wood may arise due to the shrinkage and swelling of wood [5]. As a result, the Configuration 2 with conductive glue between the screws and wood was proposed to guarantee better electrical connection confronted with wood dimensional changes. It can also offer good repeatability for the measurements thanks to the mechanized drilling process and the precise dosage of glue. Furthermore, a similar configuration (Configuration 3) using directly the copper cables (stripped at the end) to conduct electrical measurement was also identified. At last, the Configuration 4 using copper patches (Ø50 mm, total thickness: 0.065 mm) was achieved because it is simple to realize in the glulam fabrication line and no additional machining is required. Moreover, it allows conducting both the resistive and capacitive measurements [3].

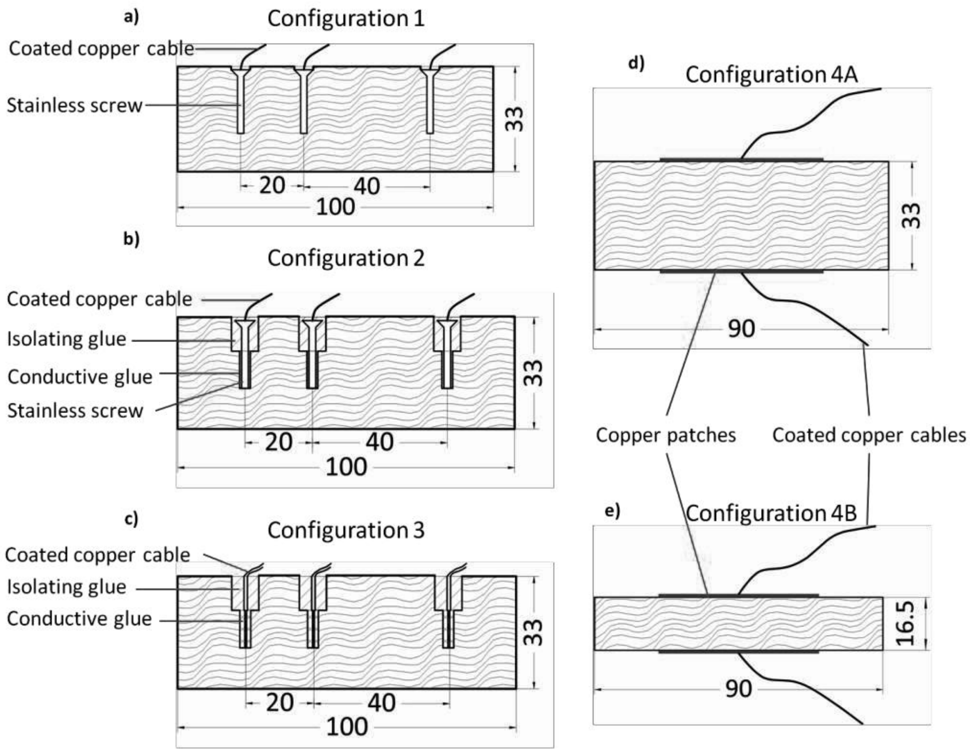

Figure 1: Measurement configurations: a) Configuration 1; b) Configuration 2; c) Configuration 3; d) Configuration 4A; e) Configuration 4B

2.1.2. Measurement devices

The electrical resistances were measured with a Giga-Ohmmeter developed at laboratory for specimens of all configurations. On the other hand, the capacitive measurements were only conducted on specimens of Configuration 4, with a LCR meter (GW INSTEK LCR-816). The frequency range of the LCR meter is from 100 Hz to 2 kHz. The frequency is fixed at 2 kHz in this study because according to James [12] who has realized the capacitive measurements at 4 different frequencies (0.2 kHz, 1kHz, 10 kHz, 100 kHz), the sensibility for MC monitoring increases with increasing frequency.

2.1.3. Investigation of the influence of bonding pressure and sensor distance

After the set-up of the sensors, solid wood specimens were prepared as described as follows. For the Configurations 2 and 3, the rest void in the top holes was filled with polyurethane glue used for glulam bonding. For the Configuration 4, a thin layer of polyurethane glue was applied on the patches to create electrical isolation and to prevent the patches from peeling off when moistening.

In order to investigate the influence of bonding pressure on sensor performance, glulam specimens were also prepared for each configuration. They were fabricated using a hydraulic press on setting the bonding pressure at 10 bars during 24 h. One more lamella (33 mm in thickness) was glued for the Configurations 1, 2 and 3 on the screwing/drilling side; two more lamellas (16.5 mm in thickness) were glued for the Configuration 4 on the two sides where patches were struck. In the end, it is important to point out that 5 identical specimens (for both solid wood and glulam specimens) were prepared for each configuration.

Furthermore, in order to verify the influence of sensor distance on MC measurements, specimens were prepared with two different electrode spacings (Figure 1).

2.2. Ultrasonic measurements

2.2.1. Tested piezoelectric film sensors and acquisition system

It was decided to test two families of piezoelectric film sensors: the PVDF and the MFC. As for the PVDF family, 3 models with different connection technologies and active areas were chosen: FLDT1, DT1-052K and DT2-052K (TE Connectivity Corporation). The former one has flexible leads while the latter two are connected to the cables by the penetrative eyelets. The total thickness of the 3 models is 0.21 mm and the thickness of the active area is 52 µm. The active area of the FLDT1 and DT1-052K is 41×12 mm² and that of the DT2-052K is 73×12 mm². Regarding the MFC family, two models working on two different vibration modes [13] were chosen: M4010 and M2814 (Smart Material Corporation). The thickness of both models is 0.3 mm. The M4010 works on d33 effect and it has an active area of 40×10 mm² while the M2814 works on d31 effect and it has an active area of 28×14 mm². The d33 and d31 are respectively the longitudinal and transverse piezoelectric coefficients, which means that the direction of deformation are respectively parallel (d33 effect) or perpendicular (d31 effect) to the direction of electric field [13].

The acquisition system is presented in Figure 2. The ultrasonic signal is generated with the help of a waveform generator (Agilent 33120A). It is connected to an amplifier (Amplifier Research Model 75A250A) and then the emitting sensor. The received ultrasonic signal is firstly amplified by a preamplifier at 40 dB (Sofranel 5660B) and it then arrives at an oscilloscope (Agilent DSO-X 2002A).

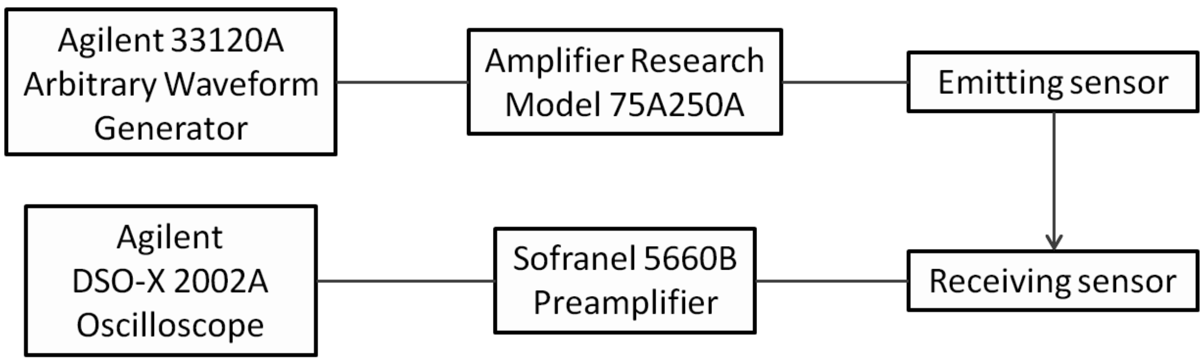

Figure 2: Acquisition System of ultrasonic measurements

2.2.2. Sensibility characterization of piezoelectric film sensors

As a first step, all the sensors were tested in 2 measurement configurations as presented in Figure 3. In the Configuration 5 (Transmission in the lamella), the propagation of waves through the thickness of one lamella is studied; in the Configuration 6 (Transmission at interface) the propagation of waves in the fiber direction of wood is analyzed. 3 Douglas fir planks of 500×90×33 mm^3 (Longitudinal (L)*Tangential (T)*Radial(R)) were used in this study. A 10-bar pressure was assured by a clamping equipment based on screw-assembly principle (Figure 4). A conventional piezoelectric sensor (R15α, MISTRAS Group) was also used in this study. It was selected because it presents good sensitivity in the range from 50 kHz to 400 kHz with a resonant frequency at 150 kHz. Firstly, tests of sweep frequency were carried out using R15α as emitter and a piezoelectric film sensor as receiver in the frequency range from 50 kHz to 400 kHz. Secondly, tests were conducted in the same condition but with the piezoelectric film as emitter and with the R15α as receiver. For these tests, modulated harmonic signals were used in order to make sure that the sensors generate and respond to acoustic waves with frequencies corresponding to the excitation electrical signals. The RMS (root mean square) amplitude was used to compare the performance of each sensor.

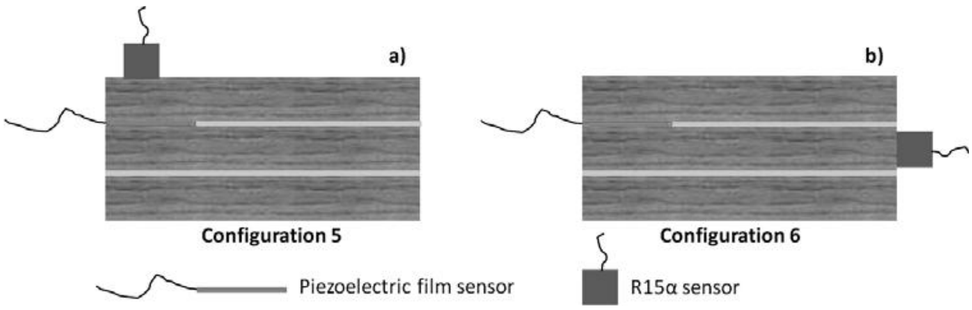

Figure 3: Measurement configurations of ultrasonic method: a) Configuration 5: Transmission in the lamella; b) Configuration 6: Transmission at interface

Figure 4: Clamping equipment for the ultrasonic measurements

2.2.3. Investigation of the optimal frequency

Following the first step, the piezoelectric film sensor presenting the best performance was tested in the 2 measurement configurations (Figure 5) in order to investigate the optimal frequency when two piezoelectric film sensors were used. Tests of sweep frequency were conducted with modulated harmonic signals in the frequency range from 50 kHz to 400 kHz. The RMS amplitude was used as an indicator of sensor performance. Once the optimal frequency was determined, test was then realized with impulse signal in order to calculate the ultrasonic propagation velocity using the equation below:

$$V=D/t \quad (1)$$

where V is the ultrasonic velocity (m/s), D is the propagation distance (m) and t is the TOF (time of flight) (s).

The impulse signal was used in order to have a clear separation of emitting and receiving signals.

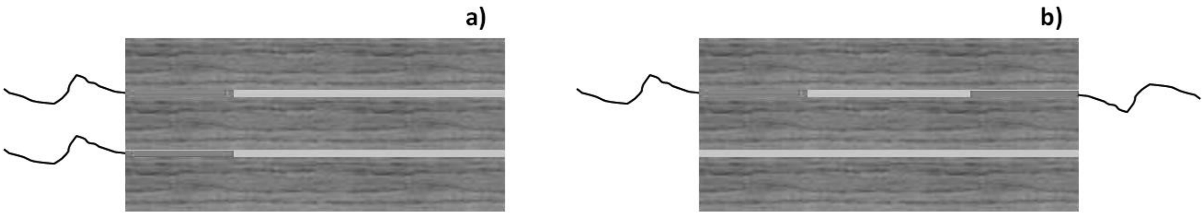

Figure 5: Test with 2 piezoelectric film sensors: a) Transmission in the lamella; b) Transmission at interface

2.2.4. Investigation of the influence of bonding pressure and sensor distance

In order to investigate the influence of bonding pressure on sensor performance, test was realized with experimental set-ups determined in previous step but without exerting extra pressure.

Furthermore, tests were conducted in order to investigate the influence of sensor distance. Regarding the in-situ monitoring of glulam structures, since the lamella thickness is standardized, it is only possible to position sensors with different distances in the length direction. As a result, there is no need to conduct this test for the Configuration 5. Regarding the Configuration 6, tests were realized by approaching two piezoelectric film sensors 50 mm each time until the distance left between sensors is comparable to the sensor dimension (50 mm in length).

3 RESULTS AND DISCUSSION

3.1. Electrical measurements

3.1.1. Feasibility of electrical measurements in wood

The implementation of different measurement configurations was firstly achieved on solid wood specimens. The measurements at initial state (10% in MC) on these specimens have shown the possibility to realize the electrical measurements in wood. As for the resistive measurements, it was found that electrical resistance is in the order of 10^9 Ω for the Configurations 1, 2 and 3 and 10^{10} Ω for the Configuration 4 (Figure 6). These values are in the same order of magnitude with information available in literature [14,15]. The different values obtained can be attributed to the different shapes of the electrodes (Configurations 1, 2 and 3: pin-type electrodes; Configuration 4: surface electrodes) and also to the fact that measurements were conducted in different wood orthotropic directions (Configurations 1, 2 and 3: Longitudinal direction; Configuration 4: Tangential direction) [3]. Regarding the capacitive measurements, the values of capacitance measured (Figure 7) were also in the same order of magnitude with information available in literature using similar frequency [16]. In our study, the capacitance measured on the 33 mm thick specimen is 3.1 pF on average while it is 5.0 pF by extrapolating the results of James at 1 kHz [16]. The difference can be explained by the different frequencies used since our results were measured at 2 kHz.

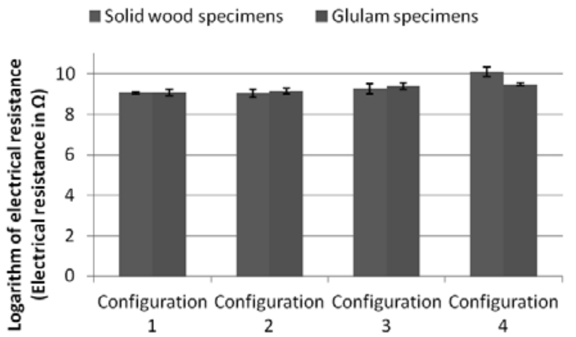

Figure 6: Comparison between results of electrical resistance measured on solid wood specimens and glulam specimens (Configurations 1, 2 and 3: sensor distance = 20 mm; Configuration 4: sensor distance = 16.5 mm)

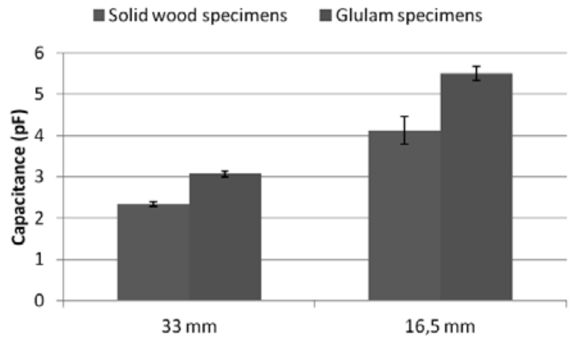

Figure 7: Comparison between results of capacitance measured on solid wood specimens and glulam specimens for Configuration 4

3.1.2. Influence of bonding pressure

Regarding the Configurations 1, 2 and 3, no difference on electrical resistance was observed between solid wood and glulam specimens (Figure 6). It can be explained by the fact that the bonding pressure was not directly applied on the sensors so that the condition of electrical connection between the electrodes and wood was not changed by the pressure. As for the Configuration 4, the resistance was observed to be reduced by 5.2 times (calculated with resistance in Ω) on average (Figure 6) and the capacitance was observed to have increased by 1.3 times on average (Figure 7). These observations can be attributed to the fact that the effective contact area between wood and sensors has increased due to the application of the bonding pressure, leading to a lower resistance [17] and higher capacitance measured [18].

3.1.3. Influence of distance between sensors

Regarding the resistive measurements, no difference was observed on resistance measured using sensors of different spacings. For the Configurations 1, 2 and 3 (Figure 8), this observation was also made by other authors and can be explained by the fact that the contact resistance associated with wood/electrode interface contributes to the majority of the total resistance measured so that the distance between electrodes does not influence the resistance measured in the case of pin-type electrodes [3].

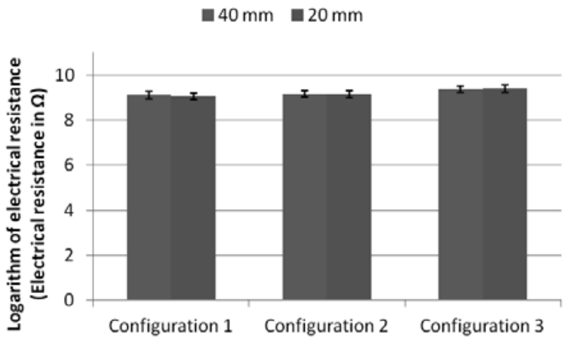

Figure 8: Comparison between results of electrical resistance measured with different sensor distances (Glulam specimens)

Concerning the Configuration 4 (Figure 9), this observation can be related to the surface roughness which can cause smaller effective contact area, leading to higher resistance measured compared to the theory, i.e. the contact resistance [17]. As a result, in view of the small thickness of our specimens, we could not observe the influence of sensor distance.

On the other hand, it was observed that the capacitance measured on the 16.5 mm thick specimens is on average 1.8 times of that of the 33 mm thick specimens (Figure 10). This observation can be explained by the theoretical equation which shows that the material capacitance is doubled if the material thickness is halved [3]:

$$C = \varepsilon_0 \varepsilon_r \frac{A}{d} \tag{2}$$

where C is the capacitance (F), ε_0 is absolute permittivity of vacuum ($\approx 8{,}854 \cdot 10^{-12}$ F•m^{-1}), ε_r is the dielectric constant which determines some kind of ability to store electrical charge, A is the area of the plates (m²) and d is the distance (m) between them.

Our results do not show an exact two-fold relationship. It can be related to the heterogeneity of wood material and can also be explained by the existence of contact capacitance associated with wood/electrode interface [18].

Figure 9: Comparison between results of electrical resistance measured with different sensor distances (Configuration 4)

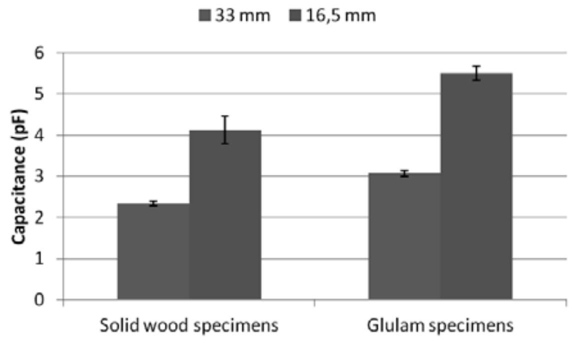

Figure 10: Comparison between results of capacitance measured with different sensor distances (Configuration 4)

3.2. Ultrasonic measurements

3.2.1. Sensibility characterization of piezoelectric film sensors

The results of the sensibility characterization for the MFC M4010 and the PVDF FLDT1 are presented in Figure 11 and Figure 12. The results of the MFC M2814, PVDF DT1-052K and DT2-052K are not included in the figure because their responses are not sufficient enough to conduct ultrasonic measurement in wood. For the MFC M2814, the weaker response compared to the M4010 can be related to their different working modes: the d31 effect used by the M2814 is weaker than the d33 effect used by the M4010 [13]. The difference in responses among the PVDF sensors might be attributed to their different connection technologies. The metallic connection of DT1-052K and DT2-052K have penetrated the protective coating. As a result, the sensor response might have been influenced by the parasitic electromagnetic signals in the environment captured by the exposed metallic connection. On the other hand, the connection of FLDT1 is non-penetrative (flexible circuit), thus the response is less affected by the parasitic electromagnetic signals.

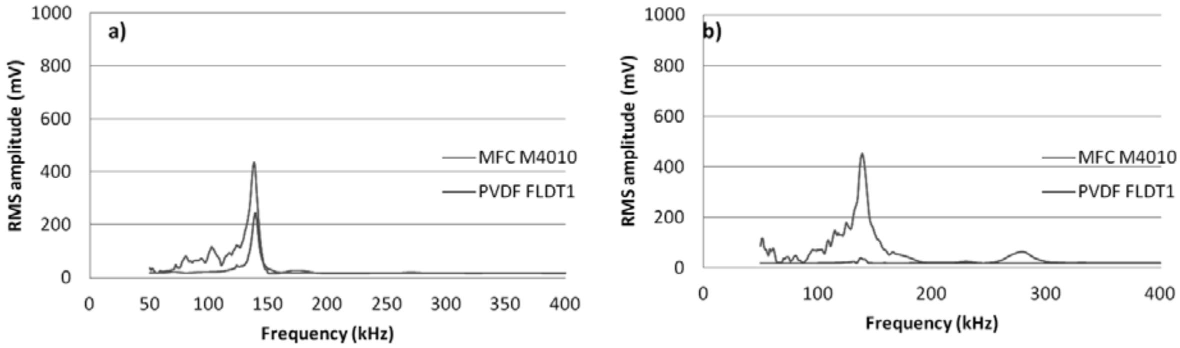

Figure 11: Sensitivity curves when piezoelectric film sensors are used as receiver: a) in Configuration 5(Transmission in the lamella); b) in Configuration 6(Transmission at interface)

The Figure 11 shows the sensitivity curves when piezoelectric film sensors are used as receiver (R15α is the emitter). It can be seen that MFC M4010 exhibits almost the same receiving performance in the two measurement configurations while the PVDF FLDT1 functions only in transmission in the lamella (Configuration 5). The curves present maximum peaks at 150 kHz because it is the resonant frequency of the R15α sensor.

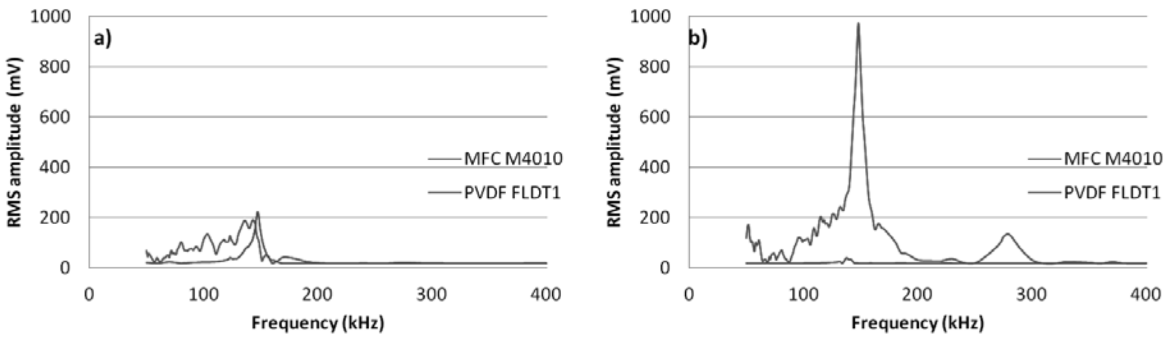

Figure 12: Sensitivity curves of when piezoelectric film sensors are used as emitter: a) in Configuration 5(Transmission in the lamella); b) in Configuration 6(Transmission at interface)

The Figure 12 presents the sensitivity curves when piezoelectric film sensors are used as emitter (R15α is the receiver). It can be observed that the emitting performance of MFC M4010 is greater when it is used for transmission at interface (Figure 12b) than for transmission in the lamella (Figure 12a). The PVDF FLDT1 works in transmission in the lamella (Figure 12a) but not in transmission at interface (Figure 12b). The curves present maximum peaks at 150 kHz because it is the resonant frequency of the R15α sensor.

It can be concluded that when conducting measurements in transmission at interface, MFC M4010 presents better performance both in emission (Figure 11b) and in reception (Figure 12b) than PVDF FLDT1 from 50 kHz to 400 kHz. When conducting measurements in transmission in the lamella, MFC M4010 exhibits better performance in reception than PVDF FLDT1 from 50 kHz to 400 kHz (Figure 11a). Regarding the performance in emission, although the highest amplitude is obtained by PVDF FLDT1 at around 150 kHz (Figure 12a), the performance of MFC M4010 can still be considered better since its characteristic curve is more wideband in the range from 50 kHz to 400 kHz. As a result, in the following step, the test was realised with two MFC M4010 sensors.

3.2.2. Investigation of the optimal frequency

Following the previous step, frequency sweep test was conducted with 2 MFC M4010 sensors in both measurement configurations (Figure 5). The objective is to find out the optimal frequency when two MFC M4010 sensors are used. Results showed that the highest amplitude is obtained at 60 kHz for both configurations (Figure 13). Considering the fact that considerable attenuation will happen when wood increases in MC [19], a better signal strength is desired to guarantee the feasibility of ultrasonic measurement in high MC. As a result, 60 kHz was used for the measurement of ultrasonic velocities in the following study in both measurement configurations.

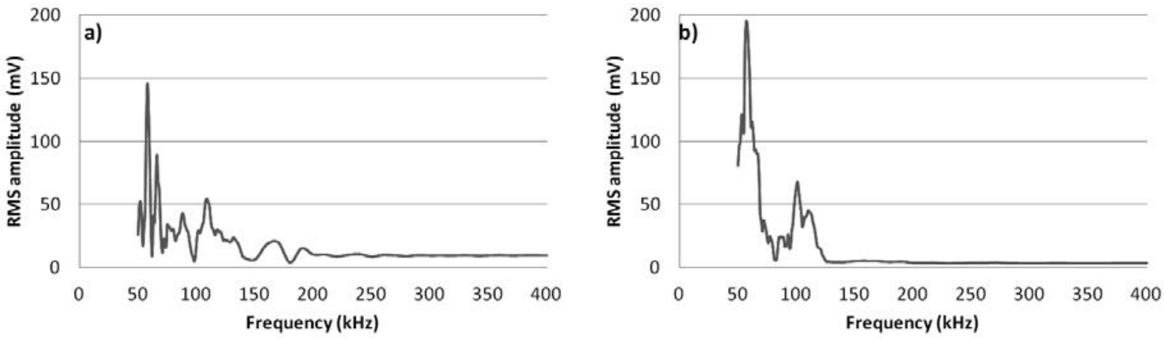

Figure 13: Test of frequency sweep with 2 MFC M4010 sensors: a) in Configuration 5(Transmission in the lamella); b) in Configuration 6(Transmission at interface)

3.2.3. Influence of bonding pressure

Tests were then conducted at 60 kHz with two MFC M4010 sensors using impulse signal to compare the sensor response with or without the pressure of 10 bars. It was found that the pressure can improve the facility of TOF measurement since the amplitude is increased. An example is given in Figure 14 which presents the result of Configuration 6. In the figure, the response without pressure is multiplied by 10. The explanation for this observation is that the pressure has improved the acoustic coupling between wood and sensors.

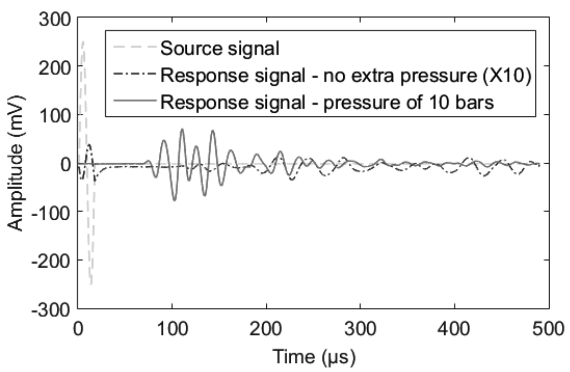

Figure 14: Comparison of results between measurement without extra pressure and with a pressure of 10 bars

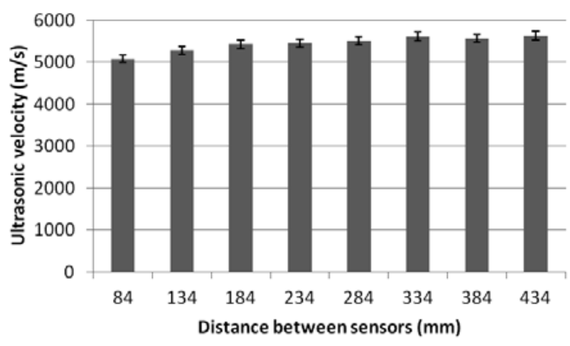

Figure 15: Ultrasonic velocity measured with different sensor distances

3.2.4. Influence of distance between sensors

In order to investigate the influence of sensor distance, tests were realized in transmission at interface at 60 kHz with two MFC M4010 sensors by approaching them 50 mm each time. The results are presented in Figure 15. The velocities are in the same order of magnitude with information available in literature concerning the longitudinal velocity [19]. It can be observed that the ultrasonic velocity remains almost stable as a function of distance between sensors, except for the small distances (84 and 134 mm). This difference can be explained by the fact that at these distances (from center to center of sensors), the length of wood left between sensors (44 and 94 mm) is comparable with the sensor dimension (50 mm in length). As a result, we could not have a clear separation of emitting and receiving signals, which is important for a precise measurement of ultrasonic velocity. As a result, it is better to not reduce the sensor distance smaller than 184 mm in order to have a clear separation of emitting and receiving signals for a precise measurement of ultrasonic velocity.

4 CONCLUSIONS

In order to extend the service life of glulam structures, it is necessary to embed MC measurement systems in the lamellas because it is more precise and furthermore it can provide a link between the MC (or wetting/drying cycles) and the durability of the structures in order to inform the infrastructure supervisors as early as possible with the potential risk of damage so that appropriate maintenance operations can be made in advance. As a result, within this framework, 4 measurements configurations using electrical methods and 2 configurations using ultrasonic method were tested in this study.

4.1. Electrical measurements

Results showed that it is possible to conduct electrical measurements in wood with the proposed configurations. On the other hand, it was found that when surface electrodes were used (Configuration 4), the glulam specimens exhibit lower electrical resistance and higher capacitance compared to the solid wood specimens. At last, with the decreasing sensor distance, no influence was observed for the resistive measurements and the capacitance was found to have increased.

4.2. Ultrasonic measurements

The performance of 5 piezoelectric film sensors from 2 families (PVDF and MFC) was tested in this study in two measurement configurations. It turned out that the MFC M4010 presents the best performance in both emission and reception. The optimal frequency for the measurement of ultrasonic velocity using two M4010 sensors was found to be 60 kHz. On the other hand, the M4010 was observed to be able to resist the pressure of 10 bars, and in fact the signal amplitude can be improved thanks to the pressure. At last, measurements were conducted with different sensor distances and it turned out that the ultrasonic velocity remains almost stable except for distances comparable with the sensor length.

Future study should be continued to investigate the feasibility using the 4 electrical configurations and the 2 ultrasonic configurations to monitor the MC variation in glulam specimens.

ACKNOWLEDGMENT

Special thanks should be addressed to Emannuel Laught for his contribution in developing the Giga-Ohmmeter and to Tommy Vilella and Frédéric Leroy for their help in experimentation.

REFERENCES

[1] Kasal, B. 2013. “Assessment, Reinforcement and Monitoring of Timber Structures–COST FP1101”. *Adv. Mater. Res.*, 778, Pp:1037–1040.

[2] Dietsch, P., Gamper, A., Merk, M., and Winter, S. 2014. “Monitoring Building Climate and Timber Moisture Gradient in Large-Span Timber Structures”. *J. Civ. Struct. Health Monit.*, 5(2), Pp:153–165.

[3] Skaar, C. 1988. *Wood-Water Relations*, Springer-Verlag, Berlin Heidelberg.

[4] Moron, C., Garcia-Fuentevilla, L., Garcia, A., and Moron, A. 2016. “Measurement of Moisture in Wood for Application in the Restoration of Old Buildings,” *Sensors*, 16(5), Pp: 697-705.

[5] Brischke, C., Rapp, A. O., and Bayerbach, R. 2008. “Measurement System for Long-Term Recording of Wood Moisture Content with Internal Conductively Glued Electrodes”. *Build. Environ.*, 43(10), Pp:1566–1574.

[6] Kabir, M. F., Daud, W. M., Khalid, K., and Sidek, H. a. A. 1998. “Dielectric and Ultra- sonic Properties of Rubber Wood. Effect of Moisture Content Grain Direction and Frequen- cy”. *Holz Als Roh- Werkst.*, 56(4), Pp:223–227.

[7] Goncalves, R., and Leme da Costa, O. A. 2008. “Influence of Moisture Content on Longi- tudinal, Radial, and Tangential Ultrasonic Velocity for Two Brazilian Wood Species”. *Wood Fiber Sci.*, 40(4), Pp:580–586.

[8] Brischke, C., Rapp, A. O., Bayerbach, R., Morsing, N., Fynholm, P., and Welzbacher, C.

R. 2008. “Monitoring The ‘material Climate’ of Wood to Predict the Potential for Decay: Re- sults from in Situ Measurements on Buildings”. *Build. Environ.*, 43(10), Pp:1575–1582.

[9] Raghavan, A., and Cesnik, C. E.. 2007. “Review of Guided-Wave Structural Health Mon- itoring”. *Shock Vib. Dig.*, 39(2), Pp:91–116.

[10] Cai, J., Qiu, L., Yuan, S., Shi, L., Liu, P., and Liang, D. 2012. “Structural Health Moni- toring for Composite Materials”. In *Composites and Their Applications*. Edited by N. Hu, InTech, Croatia.

[11] AFNOR, 2013. “NF EN 14080, Timber structures - Glued laminated timber and glued solid timber - Requirements”.

[12] James, W. 1986. “The Interaction of Electrode Design and Moisture Gradients in Dielec- tric Measurements on Wood”. *Wood Fiber Sci.*, 18(2), Pp:264–275.

[13] Kholkin, A. L., Pertsev, N. A., and Goltsev, A. V. 2008. “Piezoelectricity and Crystal Symmetry”. In *Piezoelectric and Acoustic Materials for Transducer Applications*, Edited by A. Safari and E.K. Akdogan, Springer US

[14] Brown, J. ., Davidson, R. W., and Skaar, C. 1963. “Mechanism of Electrical Conduction in Wood”. *For. Prod. J.*, 13(10), Pp:455–459.

[15] James, W. L. 1963. *Electric Moisture Meters for Wood*, Dept. of Agriculture, Forest Ser- vice, Forest Products Laboratory, Madison, Wisconsin.

[16] James, W. L. 1977. “Dielectric Behavior of Douglas-Fir at Various Combinations of Temperature, Frequency, and Moisture-Content”. *For. Prod. J.*, 27(6), Pp:44–48.

[17] Holm, R. 1967. *Electric Contacts - Theory and Application*, Springer-Verlag, Berlin Heidelberg.

[18] Dervos, C. T., and Michaelides, J. M. 1998. “The Effect of Contact Capacitance on Cur- rent-Voltage Characteristics of Stationary Metal Contacts”. In *43rd IEEE Holm Conference on Electrical Contacts*. 20-22 October, Philadelphie, Pennsylvania, Pp:530–540.

[19] Bucur, V., 2006, *Acoustics of Wood*, Springer-Verlag, Berlin Heidelberg.

SHATIS'17
4th International Conference on
Structural Health Assessment of Timber Structures
20-22 September 2017 Istanbul, Turkey

THE ANALYSIS OF THE LONG-TERM STRUCTURAL HEALTH MONITORING OF A TYPICAL ANCIENT TIBETAN BUILDING

Guo Ting[1], **Yang Na**[1]

[1] School of Civil Engineering, Beijing Jiaotong University, Beijing 100044, China

Keywords: Ancient Tibetan building, Structural health monitoring, Strain, Temperature

Abstract

Ancient Tibetan buildings, some of which have been assessed as the world's cultural heritage, are of high historical and cultural value.

These existing ancient Tibetan buildings, subjected to earthquake, environmental and operational loading, have been built at several hundred years or even a thousand years ago. Because of the effect of natural external forces such as corrosion and the degradation of the properties of structural materials, the bearing capacity and stability of the structural component decreased. There are even serious damage that threaten the safety of structures. Structural health monitoring, as a effective method, can obtain structural response in real time to learn current condition of them. A long-term monitoring system has been installed in a typical ancient Tibetan timber building, which is located in Tibet, China, to collect data on strains and temperatures of the structural components (columns, beams and connections) since September 2012.

This paper will present the first analyses and interpretation from the monitoring, mainly focusing on collected data of columns and beam-column connections.

1 INTRODUCTION

Ancient Tibetan buildings, some of which are listed as world cultural heritage, were built at several hundred years or even a thousand years ago. These structures are subjected to earthquake, environmental and operational loading as well as material deterioration and they have experienced large environmental changes in last few centuries, both bearing capacity and stability of these structures have decreased. At present, most historic Tibetan buildings appear to different degree damage[1]and some of them even collapsed. There are serious safety problems in some ancient Tibetan buildings, and many structures have been maintained for several times. Thanks to highly value of history, culture, art and science of these ancient Tibetan architectures, it is very important to assess the condition of these historic structures in operational environments to protect them. However, because of the remoteness of Tibet, there is little literature on Tibetan structures. Most existing researches focus on the architectural art and construction technology and a few are on the mechanics and material properties of Tibetan structures. Jiang et al. [2]summarized the damage situation of Potala Palace before its first maintenance and detailed the construction mode and structure characteristics of Potala Palace. Yang et al.[1] studied the basic mechanical properties of Tibetan timber structures, concluding the physical material parameters, the law of degradation of wood, and the mechanical properties and failure modes of beam-column joint. On the other hand, because of the structural complexity of ancient Tibetan buildings, it will be a long time to understand the structural performance fully.

Structural health monitoring(SHM) is a very important method for realizing the structural behavior in real time based on feedback information from the structure during its service life, in terms of response and performance under operational and environmental loadings[3]. SHM method is therefore applicable to historic Tibetan buildings to obtain current behavior of these structures under operational condition. This method is widely used in modern engineering such as bridges, buildings etc.previously. In recent years, some ancient structures have been also installed SHM system to monitor the stresses, strains and deflections etc. of structures. Shi Y.L. presented a study on distributed optical fiber monitoring for platform of Donghua Gate in the Forbidden City, Beijing and obtained successfully data in two years to analyze totally the deformation and leakage of wall[4]. Wei D.M. *et al*. analyzed the primary reasons and fundamental features of emergence and development of the existing damage of Yingxian Wood Pagoda based on monitoring strain data[5]. Recently, non-destructive(NDT) monitoring methods are developed for monitoring structural information. N.P. van Dijk *et al*. [6] measured displacement of a Vasa ship with laser-assisted total stations.

Wooden structure of an typical ancient Tibetan building has been installed SHM for mainly monitoring the strain and relative deformation of elements(beams, columns, connections) as well as temperatures around sensors. This paper will describe the SHM and analyze the structural behavior based on collected data preliminarily.

2 OVERVIEW OF THE ANCIENT BUILDING

2.1 Structural characteristics

Ancient Tibetan buildings, differing from other historic architecture, have unique characteristics. Typical Tibetan heritage buildings consist of many rooms, and each room is an independent structural unit with traditional framework within it and full height walls on two opposite sides. The framework within room all consist of wooden components including beams, columns, queti (typical beam – column joint in Tibetan buildings) concluding Gongmu and Dianmu, rafters except special floor system made of Agatu(a type of local soil mixture that is commonly used in Tibet for floor slab construction), pebbles and clay, while walls refer to the thick walls made of bricks and stones. A sketch on the layout of typical ancient Tibetan building is shown in Figure 1.

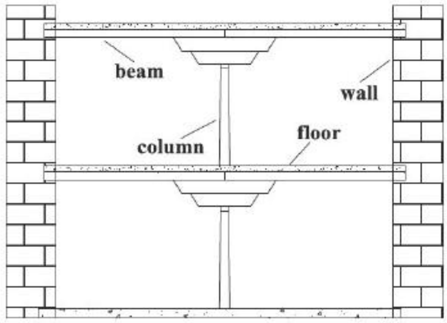

Figure 1: Typical ancient Tibetan building[7]

Figure 2 shows the components layout of wooden framework, which is column, Ludou, Dianmu, Gongmu and beam from bottom to top. Dianmu and Gongmu constitute distinctive beam-column connection, called ‘Que Ti’, which is the key component of ancient Tibetan timber buildings to transfer shear, compression and bending loads from beam to column[8]. Quiti is not only decorative, but also helps for improving the bearing capacity and stability of beam-column connection because of its large sizes of section and length.

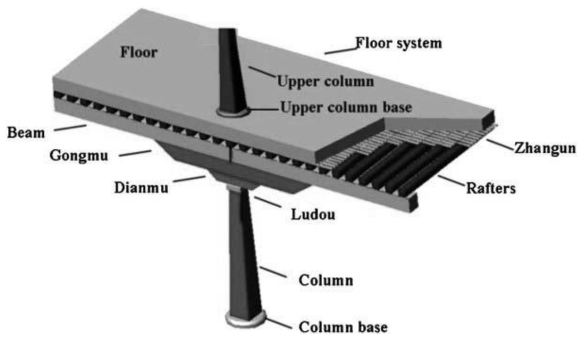

Figure 2: Typical Tibetan timber frame and floor arrangement[7]

Mortise-tenon connection is adopted between one beam and another, and other elements are arranged directly layer by layer, positioned with the dowel only. Figure 3 detailed the layout of beam-column connection. The connections in frame system can be considered as semi-rigid joints[7], which makes the connection between components not close enough and results relative displacement between components easily.

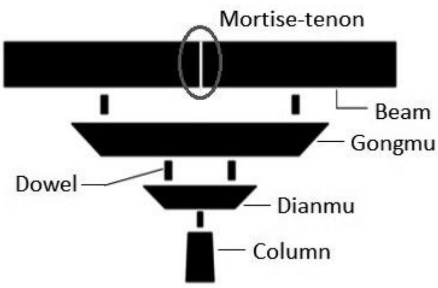

Figure 3: Detail view of typical beam-column connection

2.2 Main damage

Ancient Tibetan building, subjected to earthquake, environmental and operational loading, have experienced exchanging environment more than several hundred years or even a thousand years. Many historic Tibetan buildings appear to damage in different degree. In addition, wood are the materials of components of historic Tibetan buildings except stone wall and special floor, and degradation of wood is an irreversible process[9]caused by mechanical, environmental or biological agents (bacteria, fungi and insects), because of the biological nature of the material. In recent years, the growing increasing of tourists also aggravate the structural damage. Figure 4 shows the actual damage form of timber structure of ancient Tibetan building, mainly focusing on following form：(a) components(column, beam, Queti) crack; (b) beams deflect excessively; (c) columns torsion; and (d) beam-column connection strongly skew distortion.

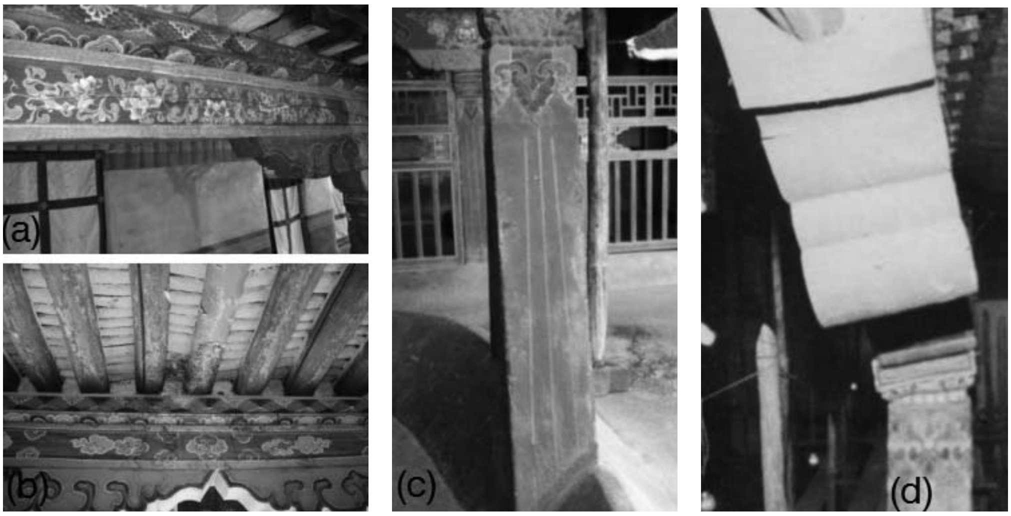

Figure 4: Main damage form of timber structure of ancient Tibetan building. (a)beam cracks; (b) beam deflects excessively; (c) columns torsion; and (d) beam-column connection strongly skew distortion.

3 SYSTEM OF SHM

3.1 The monitored building

The long-term monitoring system has been installed in a typical Tibetan heritage building in the city of Lhasa, and it has a history of 1300 years. The building complex is on top of a hill with a height of 117m and 13 levels in total including three levels of underground basement. There are many exhibition rooms in the building, and some of them are opened to the public[7].Wooden framework of the monitored building is constructed of Tibetan Populus cathayana. Previous study [1] found that the physical and mechanical properties of Tibetan Populus cathayana have degraded greatly after hundreds of years. The existing building, maintained several times, have different degree damages of most components.

3.2 Structural monitoring system

The data monitoring system composes of three subsystems, namely, sensor subsystem, data acquisition and transmission subsystem, and the data management and analysis subsystem. The sensor subsystem consists of more than 350 optical fiber grating strain sensors installed at different locations of the building[7]. Each sensor can collect the strain of components response between two elements as well as the temperature reading around the sensor. It has to be pointed out that all measurements are related to the first measurement and they are all relative to this starting point. Locations for the sensors have been selected with the following criteria: (a) positions that are known to be significant in load transfer within the structure; (b) positions that are significantly affected by the crowd load; and (c) positions that are critical to the structure, that is, damage around the location will lead to large deformation of the structure[7]. All sensors started to collect data at Sep.18th, 2012. The strain and temperature were collected once every hour, and there are 24 strain readings and 24 temperature readings in 1 day from one sensor.

This paper mainly looks at the collected data of Xida Palace, a chamber in the building. The sensor placement of it is shown in Figure 5. The box represents two sensors on column in-plane and out-of-plane and a corresponding arrow represents a sensor on pointing beam. The circle represents two sensors on column in-plane and out-of-plane and a corresponding arrow represents a torsion sensor that one end is installed on Gongmu and the other end is installed on Dianmu or beam. The sensors installed on columns located the middle of the member. The beam sensors are installed at the bottom of the member. The torsion sensor, installed on beam-column connection(queti), measure the relative deformation between Gongmu and Dianmu or beam. Labels C1 to C44 are for the columns.

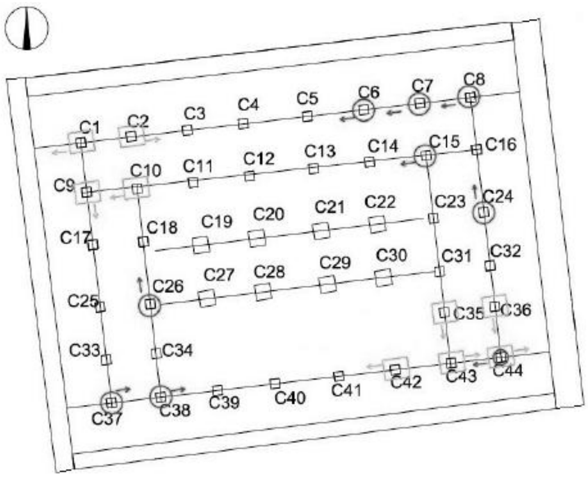

Figure 5: The sensor placement in Xida palace

4 DATA ANALYSIS

4.1 Strain of column

The strain of structure is resulted by thermal and moisture effect, crowd load, and snow load in winter season. Figure 6 shows strain time history for sensors of column C1. The data are collected four years from Sep.18th, 2012 to Sep.18th 2016. It can be seen that the strain variations of column C1, both in-plane and out-of-plane, increase firstly, followed by decrease and go back to the initial value almost in the first year. The strain variations show good periodicity with the year. However, the strain variations of column C1 in-plane is different from out-of-plane, which means the column is not axially loaded. Because of the special construction of ancient Tibetan building, Column C1 is not connected to its corresponding upper column and not strictly aligned with it. Thus, loads from upper column are usually eccentric. In addition, the upper structure of Xida palace is corridor, and the loads from upper floor are also eccentric. Moreover, there is a beam above the column on the south side but no beam on the north side, which lead to eccentricity loading on column out-of-plane. For these reasons, the column is in a complex state of stress.

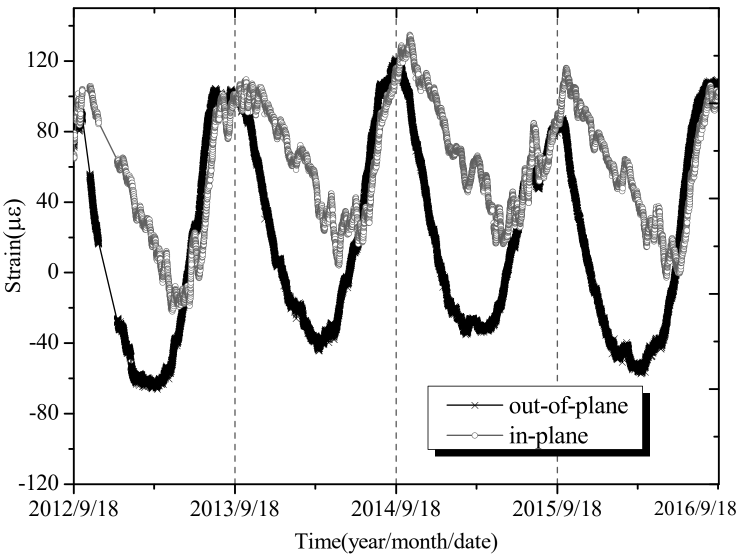

Figure 6: Strain time history for sensors of column C1 in four years

Most sensors of column show the similar behavior, but significant difference can be detected from column C26. Figure 7 gives the strain time history of sensors installed on column C26. In this case, the strain variation of column C26 in-plane increased firstly in a short period of time and decreased always until Feb. 2013, then increased to the initial position basically at the end of the year. While the strain variation of column C26 out-of-plane increased firstly until Feb. 2013, then decreased to the initial position basically at the end of the year. Looking at the evolution of strain measurements along following three years, two sensors also show totally opposite variation, which means tension in one side and pressure in another side of column simultaneously. From four years collected data, it can be concluded that strain variations roughly follow the yearly cycle and measurements can be broadly defined as periodic.

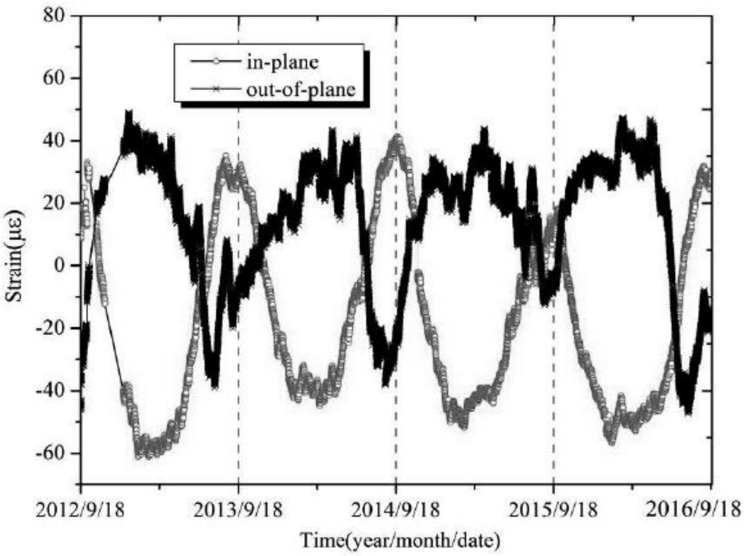

Figure 7: Strain time history for sensors of column C26 in four years

4.2 Relative deformation of connection

Joints are often one of the weakest points in a timber structure as they cause the loss of perfect continuity in the structure, resulting in a reduction of the global strength [10]. From a mechanical point of view, the resistance and the durability of ancient Tibetan timber structures are mainly dependent on the design of the connections between the elements, namely, beam-column connection, column base connection, and Dougong connection. The behavior of column base connection is very hard to monitor in a full-scale structure and only a few Dougong connections in the monitored building. Therefore, there are just beam-column connections installed sensors in the monitored building. Depending on the complexity and present damage situation of the structure, the relative deformation is measured through the strain sensor between Queti(Gongmu and Dianmu).Figure 8 shows the strain and temperature increments of Queti connected to column C26 in four years. It is noted that the trends of strain variation and temperature variation are very similar with a correlation coefficient of 0.915.

The relation between stain and relative deformation can expressed as following:

$$\Delta = \varepsilon \cdot l \tag{1}$$

where Δ , ε , l represent the relative deformation value, strain variation value, and the gauge length of sensor, respectively. From four years data of torsion sensor, the maximum strain increment is 983.4 $\mu\varepsilon$, and the gauge length of sensor is 150mm, according to equation 1, the maximum relative deformation is 0.148mm that is a very small value.

Figure 8 also shows that the strain variation is periodic and almost come back to the initial value at the end of each year, which means basically no residual deformation is observed in Queti in four years under current operational condition.

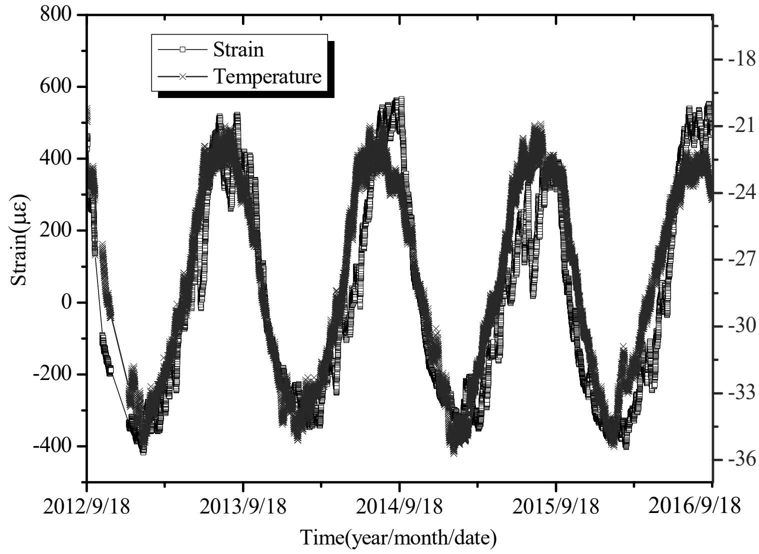

Figure 8: Strain and temperature variations of Queti connected to column C26 in four years

5 CONCLUSIONS

Structural health monitoring method is applicable to ancient Tibetan buildings, with distinctive and complicated structural characteristics, different degree damages, as well as little understanding of it. This paper described a typical historic Tibetan building installed sensors and analyzed the strain and temperature response based on collected data from Xida palace in this building. Major observations of this research are as follows:

1.The strain variations of column are periodic and basically come to the initial value at end of each year; the strain variations of column in-plane is different from out-of-plane, which means the column is compressed eccentrically; and the behavior of each column is different.

2.The trends of strain variation and temperature variation are very similar with a correlation coefficient of 0.915; the maximum relative deformations in Queti connected to column C26 and all columns are 0.148mm and 0.220mm respectively, which inclines the relative deformation is very small in four years; and there is basically no residual deformation existed in beam-column connection in Xida palace.

6 ACKNOWLEDGMENTS

The authors gratefully acknowledge the financial support of the Beijing Natural Science Foundation of China (Key Program) (No. 8151003), the National Natural Science Foundation of China for Excellent Young Scholars (No. 51422801), the National Natural Science Foundation of China (Key Program) (No. 51338001), and the National Key Technology R&D Program (No. 2015BAK01B02).

REFERENCES

[1]Yang N., Li P., Law S.S. and Yang Q.S. 2012. "Experimental research on mechanical properties of timber in ancient Tibetan building". *J. Mater. Civil Eng.*, Asce, 24, Pp:635–643.

[2]Jiang H.Y. 1994. "The Maintenance Report of Potala Palace". Cultural Relics Publishing House: Beijing.

[3]Francesca Lanata and Ecole Supérieure du Bois. 2015. "The analysis of the long-term behaviour of a timber truss structure: the case of the ESB building". *3rd International Conference on Structural Health Assessment of Timber Structures*, Wroclaw-Poland, September 9-11.

[4]SHI Y.L. 2016. "A study on distributed optical fiber monitoring for platform of Donghua Gate in the Forbidden City, Beijing". Master Thesis of Nanjing University.

[5]Wei D.M. and Li S.W. 2002. "An Investigation into the Dam age Characteristics of the Wooden Pagoda in Yingxian County". *Journal of South China University of Technology (Natural Science Edition)*, 30(11), Pp:119-121.

[6]N.P. van Dijk, E.K. Gamstedt and I. Bjurhager. 2016. "Monitoring archaeological wooden structures- Non-contact measurement systems and interpretation as average strain fields". *Journal of cultural heritage*, 17, Pp:102-113.

[7]Dai L., Yang N., Zhang L., Yang Q.S. And Law S.S. 2016. "Monitored crowd load effect on typical ancient Tibetan building". *Struct. Control Health Monit*, 23, Pp:998–1014.

[8]Lyu M.N., Zhu X.Q. and Yang Q.S. 2017. "Connection stiffness identification of historic timber buildings using temperature-based sensitivity analysis". *Engineering Structures*, 131, Pp:180-191.

[9] Thomas Nilsson and Roger Rowell. 2012. "Historical wood-structure and properties". *Journal of cultural heritages.* 13S, Pp: S5-S9.

[10]Xu B., Bouchair A., Taazount M. And Vega E. 2009. "Numerical and experimental analyses of multiple-dowel steel-to-timber joints in tension perpendicular to grain". *Engineering Structures*, 31, Pp:2357-2367.

STRENGTHENING OF TRADITIONAL BUILDINGS WITH SLIM PANELS OF CROSS-LAMINATED TIMBER (CLT)

Anders Bjørnfot[1], Francesco Boggian[2], Anders Steinsvik Nygård[1] and Roberto Tomasi[1]

[1] Faculty of Science and Technology, Norwegian University of Life Science, Norway

[2] Department of Civil, environmental and mechanical engineering, University of Trento, Italy

Keywords: Rehabilitation of traditional buildings, Cross-Laminated Timber (CLT) panels, In-plane shear test method

Abstract

The Cross-Laminated Timber (CLT) panel is a relatively new construction product that has earned wide use in the construction industry, mostly for new constructions. The crosswise build-up of the CLT panel means that it has both high in-plane and flexural characteristics, making the CLT panel useful in a multitude of applications. A relatively new application is strengthening of traditional buildings where the CLT panel can be used as both vertical and horizontal elements, with and without any remaining load-bearing structure. In addition, the ability of the CLT panel to redistribute stresses around openings and notches makes it especially suitable for complex geometries with many interrelating constructive element, which often is the case in older traditional buildings.

*The research presented in this paper is part of a larger research projects aiming to analyze the applicability of slim CLT panels for strengthening of traditional buildings that require a high strength and stiffness in combination with flexibility in use. The project contains three main phases, 1) verification of the in-plane shear characteristics of slim CLT panels, 2) development of a flexible and robust in-plane shear connection system for slim CLT panels and 3) verification of flexural characteristics and connection systems with and without opening*s. *This paper reports on experimental results from the first phase.*

*The shear stiffness of 12 specimens of five layers CLT panels where tested in a newly developed direct shear test method. The test method is composed of a pinned steel frame where rectangular CLT panels of 600x600 mm are placed. The CLT panels are bolted at the edge and then a compressive force is applied at the corner to creat*e a field of pure shear stress. *The results from the test shows promising results with high in-plane shear stiffness of relatively thin CLT panels.*

1 INTRODUCTION

In historical or - more generally - existing structures, retrofit systems conventionally are in concrete or in steel. More recently, the use of timber has been proposed as an alternative “dry” and sustainable solution with interesting results in compatibility, reversibility, and/or recoverability of the intervention. The use of timber slabs for the refurbishment of the flexural behavior of existing timber beams has been proposed by Riggio et al. [1], creating a T-beam composite section, where the original timber behaves like a web, and a new element, placed on the floors upper side and connected to the existing beam, works as a flange. Cross-laminated timber panels (CLT) can be an interesting product used as “timber slab” in retrofitting techniques, because they have both flexural and in-plane stiffness. Therefore, CLT panels can also be used as bracing systems in order to stabilize a building against horizontal shear forces caused by earthquakes while giving the building lower additional masses than in the case of steel and concrete.

This concept has been proposed and adopted for the in-plane stiffening of both horizontal and vertical bracing systems in existing buildings. The first case was investigated by Branco et al. [2], among others, who proposed rigid connections with inclined screws between the slab and the beam. Five full-scale timber floors were subjected to in-plane monotonic tests, including one un-strengthened reference floor. As illustrated in Figure 1a, the flexibility of the lateral connection system between the CLT panels is also crucial to characterize the global in-plane behavior of the timber diaphragm.

Other Authors, for example Sustersic and Dujic [3], have proposed retrofitting systems employing CLT panels to stabilize a building against horizontal shear forces. These retrofitting methods could be applied both in masonry and concrete frame building. For masonry shear walls the CLT panel acts like a new outer jacket applied externally to the existing masonry walls, fixed to them with a special connections. The same technique can be applied to the infill masonry in concrete frames or, better, the masonry panels can be completely substituted by the new CLT walls (see Figure 1b).

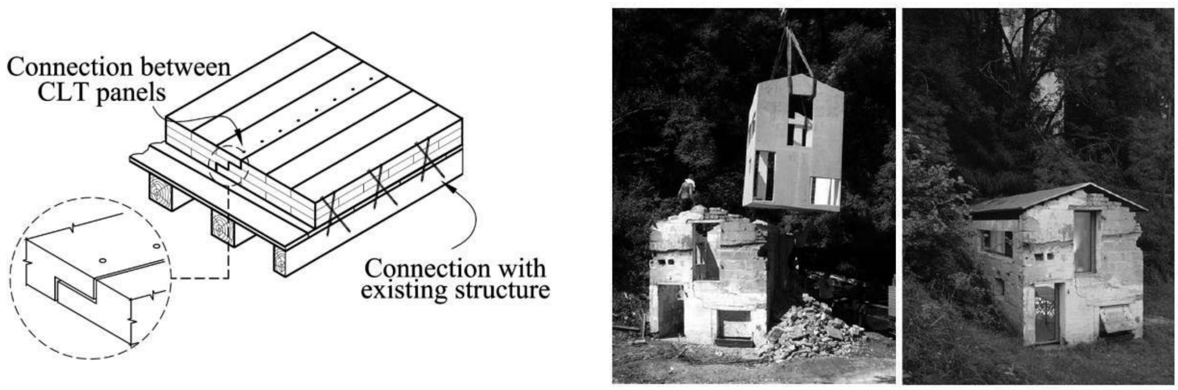

a) b)

Figure 1: Possibility to retrofit with CLT panels as a) horizontal timber diaphragms, or b) as masonry shear walls (Illustrations from www.promolegno.it).

In all these application it is crucial to assess the in-plane stiffness of the CLT bracing system, which depends on the in-plane stiffness of the CLT panels itself, and on the in-plane connection system between the panels. The project contains three main phases:

1. verification of the in-plane shear characteristics of slim CLT panels;

2. development of a flexible and robust in-plane shear connection system for slim CLT panels, and;
3. verification of flexural characteristics and connection systems with and without opening.

This paper reports on the first experimental results from the first phase, where the shear stiffness of 12 specimens of five-layered CLT panels where tested in a newly developed direct shear test method.

2 CLT IN-PLANE SHEAR STRENGTH & STIFFNESS

The shear stresses in the CLT panel can be expressed by a Representative Volume Element (RVE), representing the intersection between orthogonal boards through the thickness of the panel [4; 5]. The stress state of the RVE represents the global stress pattern of the whole CLT element. By assuming no influence from finite number of layers, no edge gluing, and equal board layer widths and thicknesses, it is possible to further detail the stress state of the RVE by defining a Representative Volume Sub Element (RVSE) that represents the intersection of two orthogonally glued boards (Figure 2).

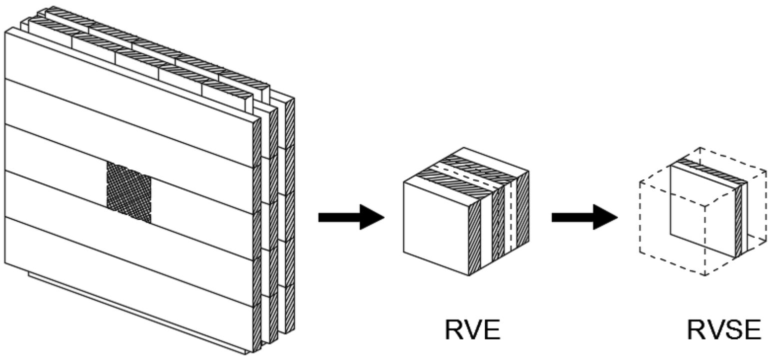

Figure 2: In-plane shear stresses in the CLT panel expressed as a Representative Volume Element (RVE) and a Representative Volume Sub-Element (RVSE). Illustration from [6].

Through the expression of the CLT panel in the representative elements RVE and RVSE (Figure 2), three failure mechanisms can be defined; gross shear failure, net shear failure, and torsional shear failure (Figure 3). Gross shear failure considers a constant distribution of shear stresses over the whole cross section of the panel, which means that shear failure parallel to the grain may occur in all layers. In order for this mechanism to take place, it is necessary that the shear stresses can be transferred between adjacent boards by edge gluing and that no cracks exists between the layers. A commonly agreed upon value of the gross shear strength is in between 3.5 and 4.0 MPa.

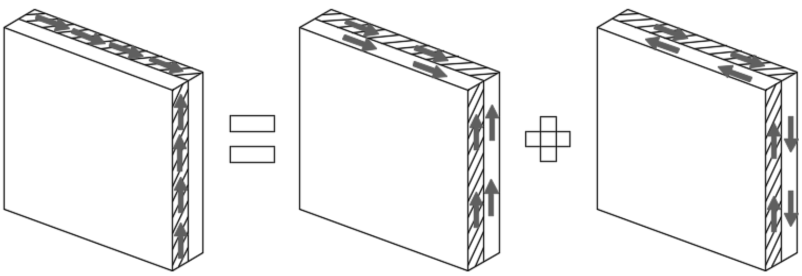

Figure 3: Internal stresses in the RVSE element resulting of net and torsional shear. Illustration from [6].

If there is a gap between the boards, or if the boards are put side by side without gluing, the shear stresses are transferred through the cross section of each board and the glued interface between the layers. In this case, the failure is perpendicular to grain, called "net" shear (Figure 3) since only the layers orthogonal to the direction of the applied shears force is considered. In the literature, there is no common agreement on the “net” shear strength. For torsion mechanism (Figure 3), the shear stress is transferred via the glued interface between layers. A characteristic value of 2.5 MPa is a commonly used value for torsional shear even though these values are based on tests of single glued interfaces and not full scale models [7].

2.1 Testing methods for CLT in-plane stiffness

Two, in principle, different approaches have been presented to this date; small-scale tests and full scale panel tests [6]. Small-scale tests are used to verify only parts of the mechanisms that can occur in CLT elements. However, by doing so the system effects that are present in CLT will not be accounted for. In Figure 4, three typical small-scale test setups are depicted. Jöbstl et al. (2004) [7] presented an experimental setup consisting of two orthogonally glued boards (Figure 4a). The boards are then loaded in a torsion. Through tests it was concluded that the strength and stiffness of orthogonally glued boards are higher than for rolling shear and lower than for shear parallel to the grain

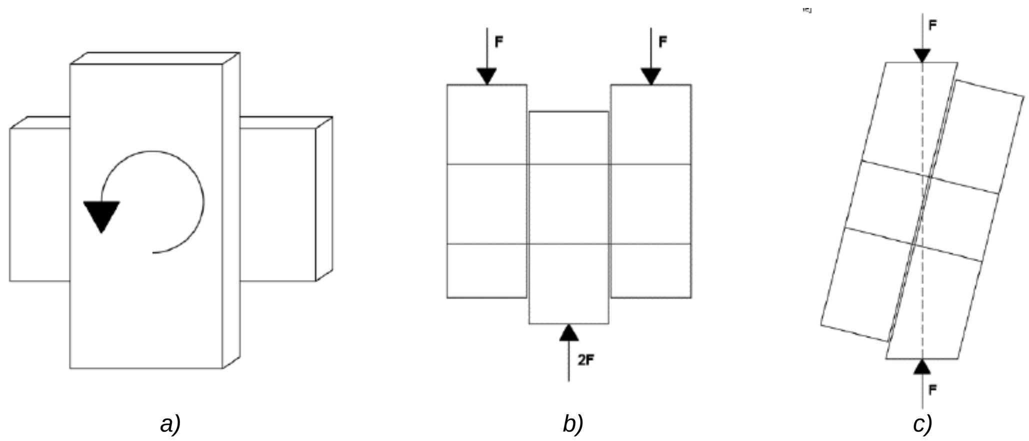

Figure 4: a) Torsion test setup of Jöbstl et al. (2004) [7]. b) shear test setup of Jöbstl et al. (2008) [8]. c) Shear test setup of Brandner et al. (2013) [9]. All illustration from [6].

Jöbstl et al. (2008) [8] describe a test procedure (Figure 4b) to verify the lamella board’s shear strength perpendicular to the grain. The setup consisted of a three board wide element that is loaded vertically such that the shear force is transferred through two shear planes perpendicular to the grain in the horizontal board. Brandner et al. (2013) [9] presented a test configuration consisting of a single shear plane that is obtained by rotating two parallel lamella by 14 degrees, such that the shear force is transferred through the perpendicular board (Figure 4c). Combined failure of shear perpendicular and torsion was identified. From the tests, it was concluded that the shear strength from this setup is somewhat overestimated. The other approach is to test a larger parts of the full CLT panel (Figure 5).

Bogensperger et al. (2007) [10] presented a test setup consisting of two side by side hinged steel frames, each containing a CLT element that are connected to the rig with glued-in steel plates (Figure 4a). The force is applied through the steel plates along the narrow side of the outer boards. The test specimens failed close to the load introduction and the authors therefore suggested the application of a correction factor based on FE analysis. Andreolli et al. (2014) [11] presented a test procedure in which a square CLT element placed in steel brackets is loaded in compression in two opposing corners (Figure 5b). To account for the combined shear and compression stresses in the tested specimens, a correction factor was suggested.

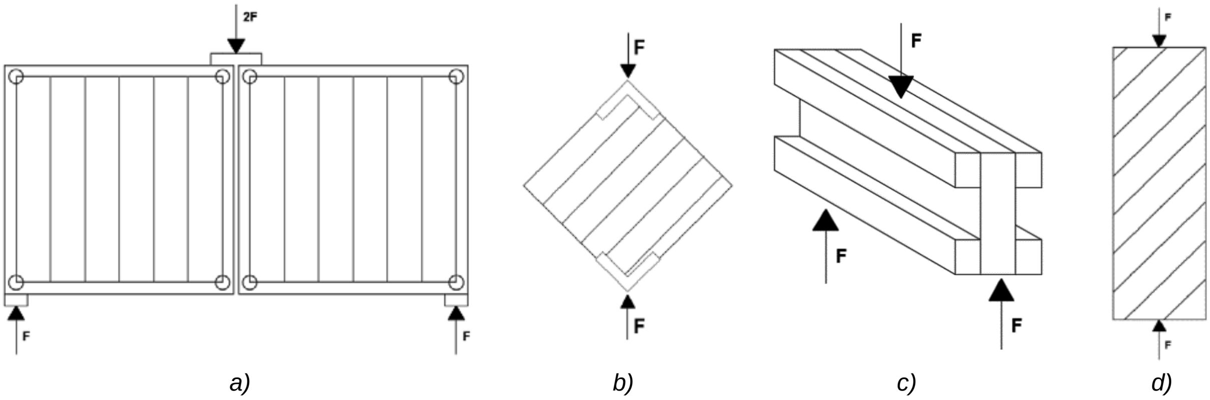

Figure 5: Test setups of a) Bogensperger et al. (2007) [10], b) Andreolli et al. (2014) [11], c) Gagnon et al. (2014) [12], and d) Brandner et al. (2015) [13]. All illustration from [6].

Gagnon et al. (2014) [12] presented a test method which is a modified version of a three-point beam bending test (Figure 5c). The tested specimen is cut into the shape of a beam, reinforced with LVL strips in the top and bottom to avoid bending failure. From the tests, the shear strength can be evaluated based solely on geometrical considerations. Brandner et al. (2015) [13] proposes a test setup based on a diagonally cut strip of CLT that is tested under compression (Figure 5d). Even though preparing the test specimens are not straight forward, the authors conclude that the test procedure demonstrate functional and operational efficiency and yields reliable shear failures, and suggested that this test setup is implemented in the EN 16351 standard [14].

2.2 Direct shear test procedure

Tests on single nodes does not provide information on the stiffness of the CLT panel, and although it is useful to know the capacities for different failure modes, it is not clear if the values are representative for the complete CLT panel [11]. In addition, none of the test methods that are published today is able to isolate the in-plane shear stress. Consequently, the results have to be modified by correction factors that might lead to reservations in the validity of the results [6]. Therefore, a direct shear test procedure is looked for that is able to isolate the in-plane shear stress so that the shear strength and stiffness can be directly evaluated. Vecchio et al. [15], in their process of verifying the modified compression-field theory for reinforced concrete, proposed a direct shear test procedure.

The testing rig [15] had the possibility to apply any combination of membrane shear, compression and tension by coupling hydraulic jacks to shear keys that was cast into the edges of the concrete specimen and anchored with shear studs. As this kind of anchoring is not applicable for CLT, a method with continuous bonding along the edge to a hinged steel frame was proposed in [6]. The suggested method aims to deform a panel directly into a parallelogram through the edge bonds to a hinged steel frame. The combined forces applied through the edge bond will apply “pure” membrane shear forces to the tested element, which can be visualized by Mohr’s circle (Figure 6) as only shear stresses τ are generated when the idealized element is turned 45 and the compression and tension stress along the diagonal are equal.

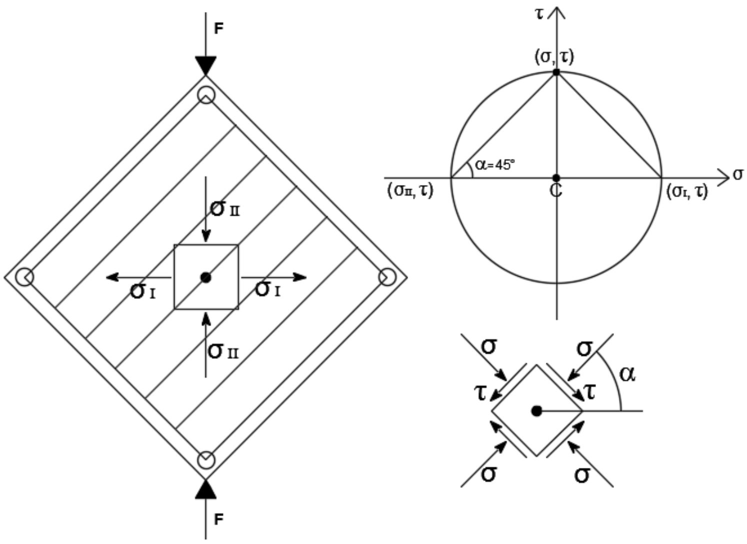

Figure 6: Mohr's circle and 45 degree rotated element. Illustration from [6].

3 TEST DESCRIPTION

The aim of the performed tests is twofold; 1) assess the applicability of the new test procedure for direct evaluation of shear stiffness, and 2) evaluate the stiffness of the CLT panels loaded with pure in plane shear. The test was conducted in the elastic field and consisted of the compression of a square panel rotated 45 degrees. The timber specimen was inserted in a specifically built steel frame (Figure 7) that was hinged at the four corners and the specimen was cut in a circular shape at the corners (Figure 8) to obtain the desired distribution of load. As the timber specimen is not in contact with the corners of the frame, the compression load from the press was transferred to the specimen only on the edge of the panel, which then, at least in theory (Figure 6), implies a pure shear field in the middle of the panel.

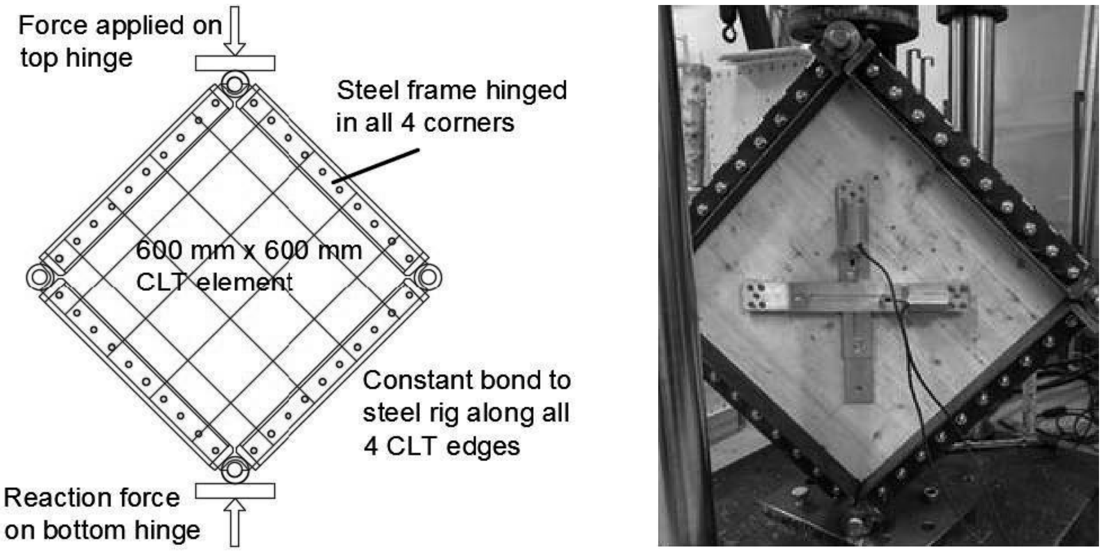

Figure 7: Proposed setup of the direct shear test procedure.

3.1 Materials and method

A total of 12 square CLT elements were tested (Figure 8). The CLT panel has five layers of 20 mm board thickness giving a total panel thickness of 100 mm. All of the board in each of the 12 tested specimens where made out of C24 strength graded spruce. Each specimen were precut using in a CNC machine to give the right geometry (600 by 600 mm), placement (10 per side) and size of bolt holes (12 mm) as well as the circular cut-out of the corners (40 mm radius). The bolts used was also 12 mm in diameter, which means that the tolerances obtained from CNC manufacturing was critical. The steel frame for transferring the load to the specimen consisted of 8 L-shaped profiles with 10 aligned holes on one side and two rings at the ends in order to assemble the frame using one bolt at each corner (Figure 7).

Number of specimens	12
Dimension [mm]	600
Thickness [mm]	100
Number of Layers	5
Board width [mm]	120
Board thickness [mm]	20
Edge bonding	No
Holes diameter[mm]	12
Corner radius [mm]	40
Strength class	C24

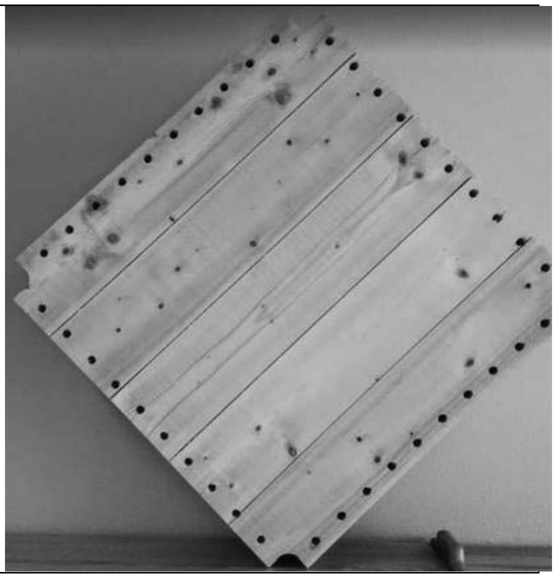

Figure 8: Specimen geometry and material data.

The CLT panel was first placed on top of one side of the steel frame and then the other side of the steel frame was placed on top before the four bolts at the corners were inserted to hold the frame together. A total of 40 bolts with washers were then placed in the predrilled holes and tightened so as to assure a continuous contact and load transfer between the steel frame and the timber specimen. Every specimen was loaded in four cycles in the linear elastic range (i.e. 65-150 kN) through a constant displacement of 3 mm/min. During every loading cycle, the applied load was measured by the load cell and displacement was measured by displacement gauges mounted in a cross shape on each side of the CLT element to measure vertical and horizontal displacements in the core of the specimen. The core was evaluated as 0.4 times the length of the side as was suggested by Andreolli et al. (2014) [11].

4 RESULTS AND ANALYSIS

An example of the force-displacement diagram for one of the tested specimens is illustrated in Figure 9. The displacements are in this case evaluated based on the average of the measured displacement from both sides of the specimen. The behavior of the specimen in the load range is clearly linear. For each specimen, a stiffness was evaluated as the least squares regression line slope with $R^2 \geq 0.99$. The first cycle was always excluded since it was considered as adjustment for the specimen so only cycle 2-3-4.

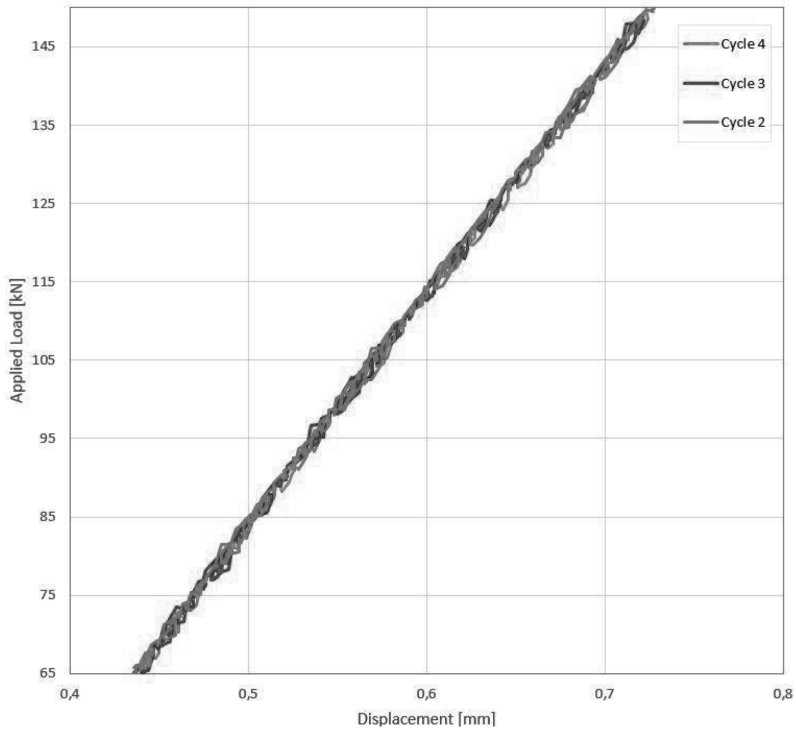

Figure 9: Example of a load-displacement curve for one of the tested specimens.

The shear modulus G for each specimen as presented in Table 1 was evaluated as $G = \tau / \gamma$ where τ is the shear stress in the element and γ is the shear strain. The shear stresses were considered constant in the core section (0.4 times the panel length) of the panel. The shear strain γ was evaluated using the cosine rule in the core region of the specimen with each side $a = 0{,}4 \cdot l$, diagonal $d = \sqrt{2}a$, and Δ is the change in length (Figure 10):

$$(d-\Delta)^2 = a^2 + a^2 - 2a^2\cos(90-\gamma)$$

Considering small displacements ($\cos(90-\gamma) \approx \sin\gamma\,;\ \Delta^2 \approx 0$) gives:

$$G = \frac{\tau}{\gamma} = \frac{F}{\Delta} \cdot \frac{0{,}4}{2 \cdot t_{clt}} = K \cdot \frac{0{,}4}{2 \cdot t_{clt}}$$

where K is the stiffness value evaluated from the test results (Figure 9). The evaluated shear modulus for each of the 12 tested specimens is presented in Table 1.

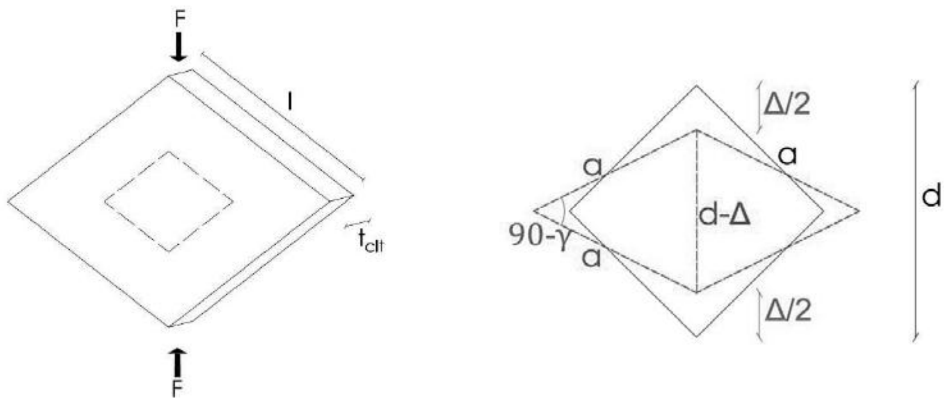

Figure 10: Notations for the evaluation of shear strain γ in the core of the specimen.

Table 1: Calculated shear modulus for each of the tested specimen.

Specimen	G [MPa]
1	558,2
2	543,1
3	590,4
4	535,4
5	544,8
6	566,5
7	574,7
8	565,8
9	568,2
10	556,4
11	517,8
12	513,7
Avg. [MPa]	552,9
St. Dev [MPa]	22,9
COV [%]	4,13

4.1 Discussion

The value of in plane shear stiffness obtained from the experiments is now compared with some existing formulas and other experiments analyzed during the literature review. The most used formula is the one proposed by Bogensperger [4]:

$$G_{clt} = \frac{G_0}{1 + 6 \cdot \alpha_{FE-FIT} \left(\frac{t}{a}\right)^2}$$

where α_{FE-FIT} is a correctional function depending on the number of layers, in this case for 5 layers:

$$\alpha_{FE-FIT,5} = 0{,}4253 \cdot \left(\frac{t}{a}\right)^{-0{,}7941}$$

With this formula the value obtained would be G_{clt} = 533,2 MPa. From the experimental campaign presented the value G_{clt} = 552,9MPa was obtained which is in line with the Bogensperger formula. Three other experimental values are considered in Table 2 based on Dujic [16], Andreolli [11] and Brandner [7].

These values are compared with the value of G modulus obtained from the experiments presented in this paper. From the comparison it can be seen that the G modulus result is aligned with other values present in literature, so G = 550 MPa is a realistic value.

Table 2: Comparison with values from literature.

G_{clt}	[MPa]
Dujic [16]	500
Andreolli [11]	550
Brandner [7]	540
Experimental	553

5 CONCLUSIONS AND FUTURE WORK

The research presented in this paper is part of a larger research projects aiming to analyses the applicability of slim CLT panels for strengthening of traditional buildings that require a high strength and stiffness in combination with flexibility in use. The first goal of the research was to assess the in-plane stiffness of CLT panels by means of a new general direct shear test method, than can generate a stress state of pure shear within the specimen to be tested. The method proved to be effective and to give experimental results in terms of CLT in-plane stiffness consistent with other methods proposed in literature.

The CLT in-plane stiffness is not per se sufficient to characterize the in-plane stiffness of existing floor diaphragms refurbished with the described technique, because other deflection contributions related to the connection system between slab and floor and between CLT panels can be more relevant. To this purpose the second stage of this research will be dedicate to the assessment of stiffness of the connection system described in Figure 11, at the present under investigation at the timber laboratory of the Norwegian University of Life Science.

Figure 11: Test on connection between CLT panels.

REFERENCES

[1] Riggio, M., Tomasi, R., Piazza, M. Refurbishment of a traditional timber floor with a reversible technique: Importance of the investigation campaign for design and control of the intervention (2014) International Journal of Architectural Heritage, 8 (1), pp. 74-93

[2] Branco, J.M., Kekeliak, M., Lourenço, P.B. In-plane stiffness of timber floors strengthened with CLT (2015) European Journal of Wood and Wood Products, 73 (3), pp. 313-323

[3] Sustersic, I., Dujic, B. Seismic Strengthening of Existing Concrete and Masonry Buildings with Crosslam Timber Panels (2014) RILEM Bookseries, 9, pp. 713-723.

[4] Moosbrugger, T., Guggenberger, W. and T. Bogensperger. 2006. "Cross-Laminated Timber Wall Segments under homogeneous Shear — with and without Openings". In *Proceedings of WCTE 2006 – World Conference on Timber Engineering*.

[5] Bogensperger, T., Moosbrugger, T. and G. Silly. 2010. "Verification of CLT-plates under loads in plane". In *Proceedings of WCTE 2010 – World Conference on Timber Engineering*.

[6] Nygård, A., Björnfot, A., Tsalikatidis, T. and R. Tomasi. 2016. "Test Method for Determining the In-Plane Shear Strength and Stiffness of Cross Laminated Timber (CLT)". In *Proceedings of WCTE 2016 – World Conference on Timber Engineering*.

[7] Jöbstl, R.A., Bogensperger, T., Schickhofer, G. and G. Jeitler. 2004. "Mechanical Behaviour of Two Orthogonally Glued Boards". In *Proceedings of WCTE 2004 – World Conference on Timber Engineering*.

[8] Jöbstl, R.A., Bogensperger, T. and G. Schickhofer. 2008. "In-Plane Shear Strength of Cross Laminated Timber. In *Proceedings of CIB-W18/41-12-3, 2008*.

[9] Brandner, R., Bogensperger, T. and G. Schickhofer. 2013. "In-Plane Shear Strength of Cross Laminated Timber (CLT): Test Configuration, Quantification and Influencing Parameters." In *Proceedings of CIB-W18/46-12-2, 2013*.

[10] Bogensperger, T., Moosbrugger, T. and G. Schickhofer. 2007. "New Test Configuration for CLT-Wall-Elements under Shear Load". In *Proceedings of CIB-W18/40-21-2, 2007*.

[11] Andreolli, M., Rigamonti, M. and R. Tomasi. 2014. "Diagonal Compression Test on Cross-Laminated Timber Panels". In. *Proceedings of WCTE 2014 – World Conference on Timber Engineering*

[12] Gagnon, S., Mohammad, M, Toro, W.M. and M. Popovski. 2014. "Evaluation of In-Plane Shear Strength of CLT". In *Proceedings of WCTE 2014 – World Conference on Timber Engineering*.

[13] Brandner, R., Dietsch, P., Dröscher, J., Schulte-Wrede, M., Kreuzinger, H., Sieder, M., Schickhofer, G. and S. Winter. 2015. "Shear Properties of Cross Laminated Timber (CLT) under In-Plane Load: Test Configuration and Experimental Study". In *Proceedings of INTER 2015 – International Network on Timber Engineering Research*.

[14] EN 16351:2015 Timber structures - Cross laminated timber – Requirements. *European Committee for Standardization*.

[15] Vecchio, F. J. and M. P. Collins. 1986. "The Modified Compression-Field Theory for Reinforced Concrete Elements Subjected to Shear". In *ACI Journal – Technical paper, Title no. 83-22, p 219-231, 1986*.

[16] Dujic, B., Klobcar, S., and Zarnic, R. Influence of Openings on Shear Capacity of Wooden Walls. In Proceedings of CIB-W18 (2007).

CHAPTER V

STRUCTURAL EVALUATION AND SAFETY ASSESSMENT

SHATIS'17
4th International Conference on
Structural Health Assessment of Timber Structures
20-22 September 2017 Istanbul, Turkey

SAFETY ASSESSMENT AND STRENGTHENING OF ICA CATHEDRAL IN PERU: THE HIDDEN TIMBER SKELETON

Paulo B. Lourenço[1], Maria Pia Ciocci[1], and Satyadhrik Sharma[2]

[1] ISISE, Department of Civil Engineering, University of Minho, Guimarães, Portugal

[2] UME School, Istituto Universitario di Studi Superiori (IUSS), Pavia, Italy

Keywords: Half-timber Construction, Quincha Technique, Nonlinear Analysis, Finite Element Modelling, Safety Assessment, Strengthening

Abstract

The Cathedral of Ica, Peru, is one of the buildings involved in the ongoing "Seismic Retrofitting Project: Assessment of Prototype Buildings (SRP)", initiative of the Getty Conservation Institute (GCI). The complex historical building is composed of two sub-structures – an external masonry envelope and an internal timber structure – and was heavily damaged by earthquakes experienced in 2007 and 2009. The aim of this work is the seismic assessment of the structure in its current condition and the proposal of an effective strengthening to reduce its vulnerabilities.

A model of the representative bay of Ica Cathedral is first constructed in SAP 2000 software. The structural performance of the representative bay is investigated by performing linear elastic analysis under different loading conditions. Advanced modelling of the entire structure of Ica Cathedral is carried out in Midas FX+ for DIANA. Nonlinear behaviour is assumed for the different types of masonry, while isotropic homogeneous and linear behaviour is adopted for timber. Nonlinear static under gravity loading, mass proportional pushover and time history analyses are performed to study the interaction of the timber structure with the masonry envelope. The model is validated by comparing the existing damage observed in–situ with the numerical results and the safety assessment of the building is carried out.

After the main vulnerabilities of the structure have been identified, a global strengthening of the structure is proposed guaranteeing the principles of minimum intervention and reversibility, as well as the use of technologies that are easy to implement in future projects.

1 INTRODUCTION

Half-timber constructions emerged as a fairly recurring typology in Peru during the Hispanic Viceroyalty and the early Republic periods (16^{th}-19^{th} century), with the application of the so-called *quincha* technique. Used even before the Incan empire, after the Spanish conquest the quincha technique was developed technologically and widely diffused in Peru to erect both monumental and vernacular buildings [1, 2]. It was only after the destructive earthquakes that occurred in Peru in 1868 and in 1908 that the Peruvian state banned the use of adobe and quincha for urban housing and recommended constructions in brick, masonry and reinforced concrete. However, these half-timber constructions continued to be still very much in use in the rural areas and they still form a large percentage of the total number of Peruvian buildings [3].

Today, these half-timber structures represent an important part of the historical heritage of Peru. However, they are at a high risk of being irrevocably lost and damaged because of several reasons, importantly earthquakes. Typically classified as unreinforced masonry (URM) structures, under seismic action their structural response is characterized by the formation of isolated parts that suddenly collapse as rigid blocks. On the other hand, the collapse of quincha timber frames is usually due to insufficient structural performance and significant state of decay of the timber connections. The combination of masonry and quincha techniques used for these constructions adds considerable complexity at any attempt to characterise their global response.

Being representative of ecclesial buildings in coastal cities during the Viceroyalty of Peru, the Cathedral of Ica was selected by the Getty Conservation Institute (GCI) for the Seismic Retrofitting Project (SRP). Using the Cathedral of Ica as a prototype building, a methodology that can be applied to carry out the safety assessment and to develop efficient strengthening techniques for similar constructions is presented in this paper. A deep insight into the main features responsible for the intrinsic complexity that characterises the structure is first presented according to the information provided by the GCI [4] and additional knowledge derived from an experimental campaign carried out by the University of Minho [5]. The material properties are assumed considering the extensive laboratory testing campaign conducted by the Pontifical Catholic University of Peru (PUPC) [6] and the dynamic identification tests carried out in-situ by the University of Minho [5]. Afterwards, advanced numerical modelling and structural analysis are performed considering partial and global models to carry out the safety assessment in its current condition. Finally, a global strengthening of the structure is proposed and implemented in the numerical model to verify its efficiency.

2 DESCRIPTION OF THE STRUCTURE

Located at the corner of an urban block in the historic centre of Ica, the Cathedral has a rectangular plan of 22.5 x 48.5 m^2 following the Jesuit typology established by the Church of the Gesù in Rome (Figure 1): an atrium; a main nave; two side aisles; a transept; and an altar flanked by two chapels on its lateral sides. A series of spaces, including a sacristy and offices, is located to its western side, while it is adjacent to a concrete portico to the south.

The Cathedral can be divided structurally into two main sub-structures: an external masonry envelope and an internal timber frame. The masonry structure consists mainly of the front façade, two bell towers, the lateral walls and the back façade. The 21 m long Neoclassical front façade is made of fired brick masonry in lime mortar, with a thickness ranging from 2.25 m at the base to approximately 0.60 m at the top. The 20 m high bell towers are composed of timber frames that rest on fired brick bases, each approximately 3.80 x 3.80 m^2 in plan. The lateral walls are of adobe masonry, over a base course of fired brick and rubble stone masonry. Their thickness range between 1.0 m and 2.0 m and their total height is about 6.75 m.

The internal timber structure is composed of a series of pillars, pilasters – i.e. engaged pillars – and piers which support a system of longitudinal and transversal beams, that in turn carry a complex vaulted roofing system. These timber members are made of cedar (*Cedrelaodorata*), sapele (*Entandrophagmasp*) or huarango (*Prosopissp*). The pillars and the pilasters are composed of numerous posts, which are braced by means of horizontal and diagonal elements and are wrapped with flattened cane reeds (c*aña chancada*). The vaulted roofing system includes a main umbrella dome, barrel vaults and small domes. In particular, the barrel vaults covering the central nave are characterized by lunettes corresponding to the location of the windows in the upper nave walls. In general, the domes are composed of ribs and two ring beams located at the top and at the bottom, while the barrel vaults are constructed by a system of principal and secondary arches composed of several timber elements made of nailed planks. Caña chancada and cane reeds finished with layers of mud plaster (*caña brava*) cover the intrados and the extrados of the vaulted roofing frame respectively. Layers of fired brick masonry and sand, lime and cement mortar cover the flat wooden ceiling, which surrounds the small domes lying above the lateral aisles.

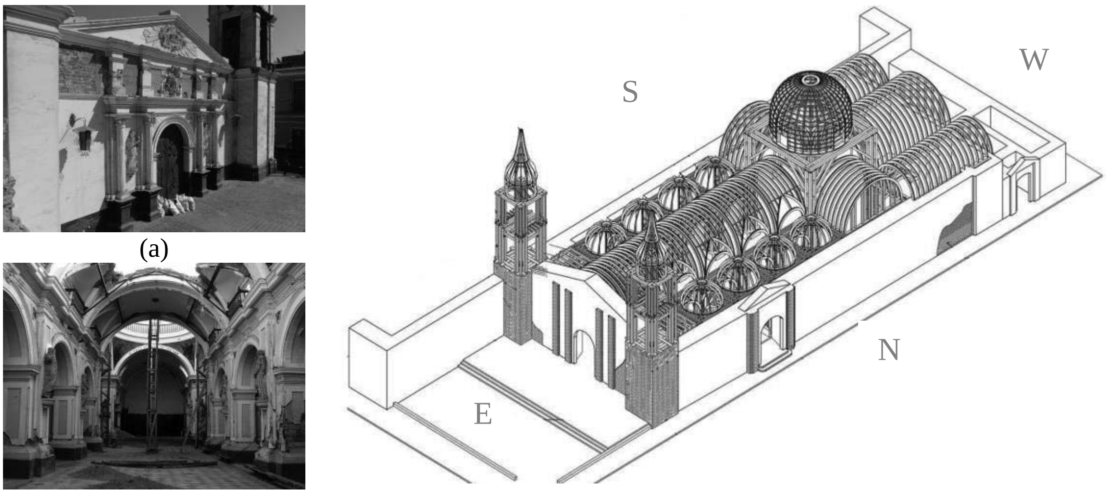

(a) (b) (c)

Figure 1: Ica Cathedral: (a) front façade; (b) main nave; (c) overall structural scheme

The structural parts composing the representative bay, studied in detail in Section 4, are shown in Figure 2. Each pillar is composed of eight posts and a huarango tree trunk located in the central part, while each pilaster consists of four posts. These posts are connected to the system of beams and to the bracing elements by means of mortise and tenon, half–lap and nailed joints. The lunettes of the barrel vault are composed of timber members connected mainly by means of mortise and tenon joints which are different in dimension and layout for each connection. In particular, the beams located at the top of the lunettes are characterized by multiple mortise holes to receive the tenons of the secondary arches of the barrel vault and the lunettes' ribs.

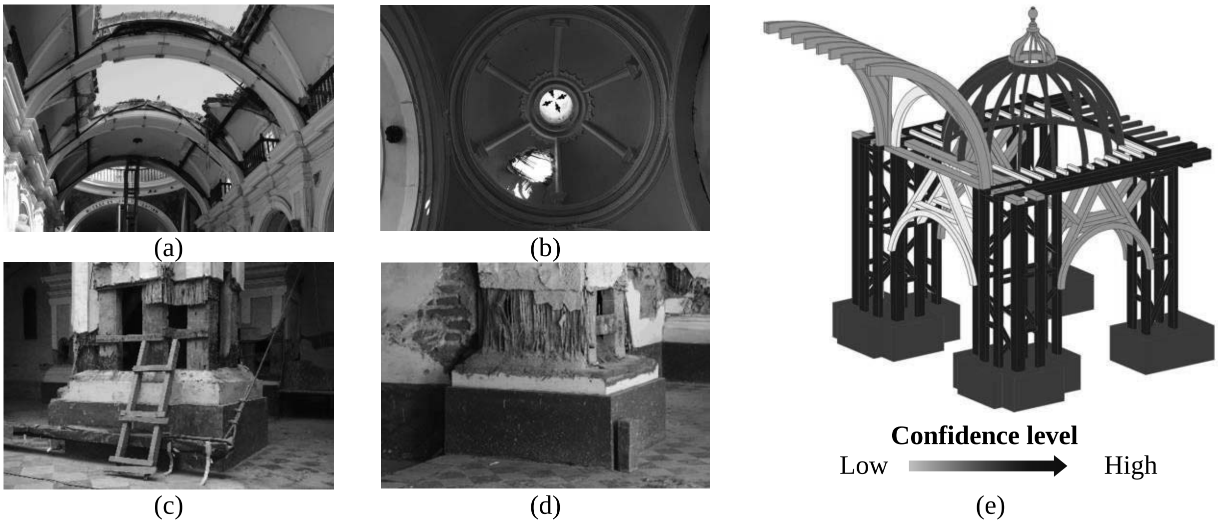

Figure 2: The representative bay: (a) barrel vaults with lunettes; (b) aisle dome; (c) pillar; (d) pilaster; (e) structural scheme

3 MATERIAL PROPERTIES

3.1 Timber

The density and the mean value of modulus of elasticity of existing timber – i.e. huarango, cedar and sapele – were assumed on the basis of the experimental results obtained by PUCP. It should be mentioned that, in order to take into account the weight of the quincha covering layers, an increase in the density value was assumed for the timber sub-structure by calculating an equivalent specific weight assigned to the timber elements carrying them [7]. The strengthening timber members presented in Section 6.1 were assumed made of tornillo (*Cedrelinga catenaeformi*). The density and the mean value of the modulus of elasticity of tornillo were assumed according to the recommended values provided for the corresponding structural wood class in the Peruvian Code [8]. A summary of the material properties adopted for the different wood species is presented in Table 1.

All the timber elements were assumed to have isotropic homogeneous and linear elastic behaviour in the numerical models, except for the connecting elements between the two sub-structures, as discussed in Section 6.2. The von Mises criterion was applied to them, assuming a yield stress equal to the lower value of axial capacity. In order to evaluate the von Mises yield stress, to carry out the verifications for the representative bay (Section 4.3) and for the strengthening elements (Section 6.3), the load-carrying capacities were assumed considering the classification into the structural classes recommended by the Peruvian Code [8]. In particular, huarango was evaluated corresponding to Class A, sapele and cedar to Class B, and tornillo to Class C. Further details can be found in [7].

Table 1: Density and modulus of elasticity adopted for the different wood species.

Properties	Huarango	Cedar	Sapele	Tornillo
Density [kg/m^3]	1040	380	490	550
Modulus of Elasticity [MPa]	16900	9380	8610	8826
Poisson's ratio [–]	0.30	0.30	0.30	0.30

3.2 Masonry

The material properties of existing masonry – i.e. rubble stone, fired brick and adobe – were primarily derived from bibliographic resources and national technical building standards [7], considering also the results of the experimental campaign performed by PUCP [6]. It should be mentioned that the modulus of elasticity of the different masonries was updated according to the results obtained from the model updating which was performed on the basis of dynamic identification tests. Please refer to [7].

According to the strengthening proposal (Section 6.1), new brick masonry was suggested to substitute the existing masonry in selected parts. The new brick masonry was assumed to be made of brick units similar to the existing bricks from Ica Cathedral and a new sand lime mortar. The compression strength of the new brick masonry was derived from the compression tests performed by PUPC on brick wallets constructed using fired brick units from the Hotel El Comercio, another prototype building from the SRP project. The tensile strength, the modulus of elasticity and the fracture energy were assumed on the basis of existing literature [7]. A summary of the material properties adopted for the different types of masonry is presented in Table 2.

In order to simulate the mechanical behaviour of masonry, the Total Strain Rotating Crack (TSCR) material model, that is available in DIANA software [9], was used in this study. In particular, for all typologies of masonry, the tensile and the compression softening of masonry were defined by an exponential curve and a predefined parabolic curve.

Table 2: Material properties adopted for the different types of masonry.

Properties	Adobe	Fired Brick	Rubble Stone	New Fired Brick
Specific weight [kN/m^3]	19	19	19	19
Modulus of Elasticity [MPa]	220*	850*	720*	1200
Poisson's ratio [–]	0.20	0.20	0.20	0.20
Compressive strength [MPa]	0.46	1.70	1.00	6.00
Tensile strength [MPa]	0.05	0.10	0.06	0.25
Fracture energy (compression) [N/mm]	1.00	3.50	1.50	12.40
Fracture energy (tension) [N/mm]	0.01	0.01	0.01	0.02

*Value obtained from model updating

4 THE REPRESENTATIVE BAY

4.1 Numerical model

As an initial step towards understanding the global behaviour of the structure, a 3D finite element (FE) model of a representative bay was first constructed in SAP 2000 software [10]. Figure 3a presents the FE model of the representative bay, composed of 1136 nodes and 1344 *Frame* elements. Translational displacements were restrained at the base of posts and the timber joints were modelled as hinges or rigid connections according to the mechanical behaviour of the timber joints present in the representative bay. Moreover, suitable restraints were applied in terms of horizontal displacement and rotation, defined by the symmetry of the structure. It should be noted that the representative bay was assumed to be self-supported and no restraint was assumed in correspondence to the connection with the longitudinal masonry walls in this model.

4.2 Parametric analysis

Parametric analyses were first carried out by applying self-weight and mass proportional lateral load (representative of the seismic action) in the transversal direction of the numerical model in order to evaluate the relative importance of the various joints to the global behaviour of the representative bay. The reference model described in Section 4.1 was compared to several models differing only by the assumptions made for specific sets of timber connections [7]. The structural response of the representative bay was investigated in terms of structural stiffness defined as the slope from load-displacement diagrams. In particular, the control node was assumed at the top of the lunette, where the maximum lateral displacement was observed. According to the obtained results, the timber joints of the barrel vault with lunettes have the most significant influence on the structural behaviour of the representative bay under transversal lateral loading (Figure 3b), whereas the pillars stiffness are rather insensitive the connections of their timber elements.

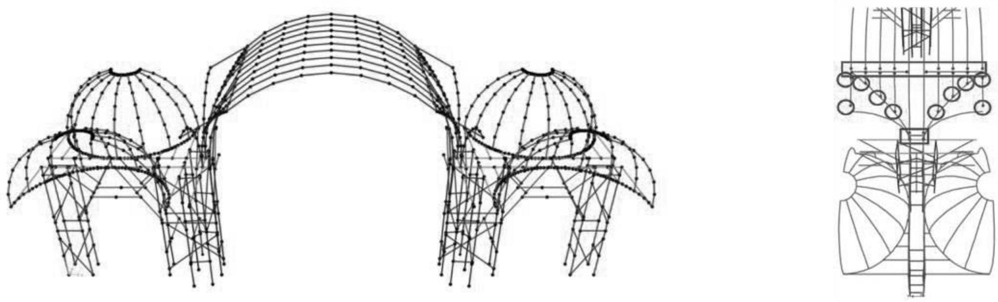

(a) (b)

Figure 3: The model of the representative bay: (a) FE mesh in SAP 2000 software; (b) critical timber joints

4.3 Compliance with Eurocode 5

The capacity of sustaining vertical and horizontal actions was investigated by performing linear elastic analyses on the model of the representative bay, and the compliance with the various criteria specified by the Eurocode 5 [11] was evaluated both for Serviceability Limit State (SLS) and Ultimate Limit State (ULS).

Global verifications were carried out on all the straight elements of the representative bay for SLS under self-weight (G) and live load (Q), and for ULS under vertical load (1.35G) and under earthquake load combination (G+E). In particular, a value of 0.50 kN/m^2 was adopted for the live load (Q) since access to the roofing system was assumed only for maintenance, while the seismic action (E) was considered by applying mass proportional lateral loading after having introduced the self-weight (G). In addition to global verifications, local verifications for ULS were carried out on the mortise and tenon connections of the beams at the top of the lunettes as they are thought to be the main reason of the collapse of the roofing system of Ica Cathedral during the 2007 Pisco earthquake.

On the basis of the results obtained for SLS, the values of displacement which occurred in the beams at the top of the lunettes and those close to the masonry were slightly higher than the limit values calculated for instantaneous and final deflections according to Eurocode 5 [11]. However, existing historical timber structures often show high values of deformation without affecting significantly their usage. As regards the global and local verifications for ULS, they were satisfied for all the timber members under vertical load, while the beams at the top of the lunettes and their connections were not verified under earthquake load combination.

5 COMBINED MODEL

5.1 Numerical model

In order to investigate the interaction between the two sub-structures and its effect on the global response of Ica Cathedral, a 3D FE model of the entire structure was constructed in Midas FX+ Version 3.3.0 Customized Pre/Post processor for DIANA software [9]. The FE mesh of the combined model was composed of 96,340 nodes in total.

The masonry envelope of the Cathedral was included in the numerical model by using *3D isoparametric solid linear* four-noded (TE12L) elements. The effect of the cloister adjacent to the building was included in the numerical model by using one-noded *translation spring dashpot* (SP1TR) elements along the entire length of the southern lateral wall. Full connectivity was assumed between intersecting walls, horizontal layers of different masonries and the elements composing the bell towers. As regards boundary conditions, translational displacements were restrained at the base of the model of the masonry envelope. For the internal timber frame, all the structural parts were modelled by using *class–I beam* two-noded (L13BE) elements with shear deformation. The base of the posts composing the timber structure was pinned, while rigid connection was assumed for all the timber joints, given the need to simplify the model.

A crucial aspect was the definition of the connections existing between the two sub-structures, for which little information was available [4]. Connections between the two sub-structures were assumed to exist between: (1) the wooden beams in the upper part of the main entrance and the fired brick façade and the lateral longitudinal masonry walls; (2) the transversal wooden beams of the bays and the lateral longitudinal masonry walls; and (3) the wooden beams supporting the barrel vaults of the chapels and altar and the masonry walls. These connections were modelled by merging the nodes of *class–I beam* elements with those of *3D isoparametric solid linear* elements and restraining their torsional rotation degree of freedom to avoid compatibility problems.

5.2 Nonlinear static analysis

In order to assess the seismic capacity of the whole structure of Ica Cathedral, nonlinear static (pushover) analyses were performed by applying a mass proportional approach, after having introduced the self-weight. According to the results obtained from the nonlinear static analysis under self-weight, the highest values of displacement were observed for the barrel vaults and the main dome, ranging from 1.0 cm to 2.0 cm, and no cracking was observed throughout the masonry envelope.

Consequently, the lateral load was applied in the XX– (longitudinal) and YY– (transversal) directions of the model, considering the absence of any adjoining structures in these directions. The lateral load-carrying capacity was assessed from load-displacement curves, which were obtained assuming the nodes exhibiting high displacement in the direction of the applied load as control points, and was compared to the peak ground acceleration (PGA) provided in the Peruvian Code [12], or the ultimate state. According to the results obtained from the pushover analysis in the XX– direction, the maximum lateral load-carrying capacity was calculated with a value of 0.45g and the failure mechanism in the masonry envelope was identified as the out-of-plane failure of both the front façade and the bell towers. When the lateral load was applied in the YY– direction, the maximum lateral load-carrying capacity was calculated to be a value of 0.28g and the failure mechanism consisted of the out-of-plane failure of the northern lateral wall. It should be mentioned that these values of lateral load-carrying capacities were found 25% higher than those obtained for the only masonry envelope, implying that the connection between the two sub-structures has a significant influence on the global behaviour of the structure [7]. However, the seismic capacity of the combined model calculated when the lateral load was applied in the YY– direction was considerably lower than the PGA (0.45g).

5.3 Nonlinear dynamic analysis

Nonlinear dynamic analysis (time-history) analysis was carried out on the combined model mainly to validate it with respect to damage observed in-situ due to past seismic activity – particularly, the MW 7.9-8.0 Pisco earthquake in 2007 and a later seismic event in 2009, both of which greatly damaged the structure – and to compare the obtained results with those derived from nonlinear static analyses.

The time history analysis was performed on the combined model considering Rayleigh viscous damping. The Rayleigh damping parameters for the structure were calculated by considering all the natural modes of vibration until 80% mass participation was reached. Implicit time step integration using the Hilber-Hughes-Taylor method, also so-called α method, was used to perform this analysis, adopting a value for α equal to -0.1 and a time step Δt equal to 0.0045s. The seismic input was simulated by means of two artificial accelerograms, applied in two orthogonal directions to each other (XX and YY). These accelerograms were generated on the basis of the elastic response spectrum provided by the Peruvian Code [12] for the region of Ica, using the software SeismoArtif v2.1 [13]. More details can be found in [7].

A plot of scan of the maximum principal strains that occurred in the history of the applied loading showed that the model underwent severe damage. Critical cracking present in the structure after the earthquakes, such as parallel cracking in the adobe masonry of the northern lateral wall, diagonal cracks in the front façade and separation cracks at the base of the pediment were reproduced by this analysis, confirming the validity of the model. Additionally, damage similar to the failure mechanisms predicted by the pushover analysis was observed. It should be mentioned that the nonlinear dynamic analysis also reproduced cracks existing currently in the structure which were not obtained from pushover analyses, where the lateral load was applied monotonically, increased up until the failure and in only one direction (Figure 4).

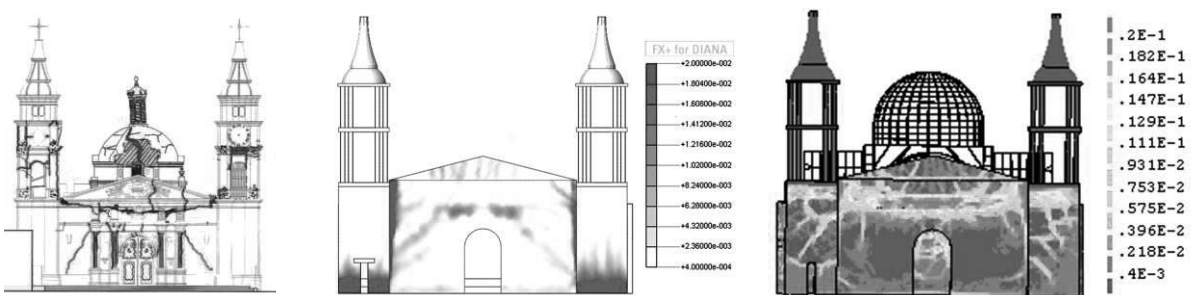

(a) (b) (c)

Figure 4: Correlation of cracks observed in the numerical model and in-situ: (a) crack survey after the 2007 Pisco earthquake [4]; (b) crack pattern from pushover analysis in the XX– direction and (c) crack pattern from time history analysis

6 STRENGTHENED MODEL

6.1 Strengthening proposal

The safety assessment of the whole structure of Ica Cathedral pointed out the need to strengthen the most vulnerable regions, i.e. the northern lateral wall of the Cathedral as well as other out-of-plane mechanisms. Based on the criteria recommended by [14], strengthening measures were kept to the minimum necessary to guarantee safety, durability and the least damage to the historic fabric. Moreover, the design methodology included the state of the art research being performed by GCI and PUCP on traditional, low tech yet highly effective methods that have been historically used for the retrofitting Peruvian structures.

The strengthening proposal for the Cathedral included: (1) replacing of existing masonry with new brick masonry in selected parts to ensure limited long-term deterioration; (2) steel anchoring systems to address the out-of-plane mechanism of the front façade; (3) timber anchoring systems to connect the internal timber frame more strongly with the external masonry envelope; and (4) a timber collar beam to address the out-of-plane mechanism of the wall at the north-western corner. A brief overview of the timber anchoring systems and the collar beam proposed for the structure is presented in this paper (Figure 5). More details regarding the other suggested strengthening techniques can be found in [15].

The timber anchoring systems are embedded in new brick columns and are composed of: (1) three lower levels of anchors with a cross-section of 75 x 75 mm^2, which are connected to the posts of the quincha pilasters; and (2) an upper level of anchors with a cross-section of 150 x 150 mm^2, which are connected to the transversal beams of the internal timber structure. In order to improve the resisting mechanism, the timber anchoring systems located at the uppermost level are also embedded in adobe masonry for a length of 70 cm and have vertical keys embedded downward for a length of about 60 cm. The frame of the collar beam is composed of longitudinal and transversal timber elements with a cross-section of 150 x 150 mm^2. All the strengthening timber members are connected by means of half-lap joints with pegs to each other and to the internal timber structure.

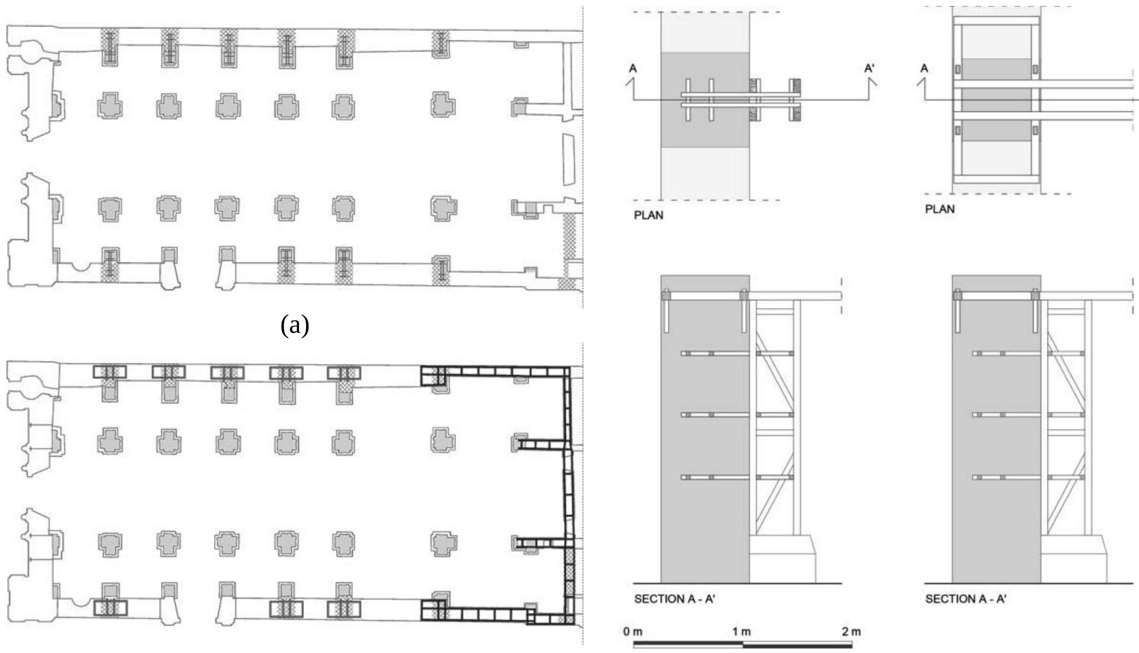

(b) (c)

Figure 5: Timber strengthening systems: (a) anchors at the lower levels (red); (b) anchors at the upper level (red) and the timber collar beam (blue); (c) detail of the anchors at the lower levels (left) and at the upper level (right)

6.2 Numerical model

Based on the hypotheses assumed for the combined model and the strengthening proposal, a 3D FE model of the strengthened structure was constructed in Midas FX+ Version 3.3.0 Customized Pre/Post processor for DIANA software [9], as shown in Figure 6. Additionally, the timber anchoring systems as well as the elements composing the collar beam were modelled by using *class–I beam* two-noded elements which were fully embedded in the masonry. *Flat shell* three-noded (T15SH) elements were used to model the steel plates of the anchoring system on the front façade. The elements connecting the *fully embedded class–I beam* elements with the *class–I beam* elements modelling the internal timber structure were modelled by using *enhanced truss* two-noded (L6TRU) elements and applying the von Mises criterion. As discussed in [15], this modelling hypothesis was made to assume a more conservative scenario when a lateral load was applied to the structure. In order to allow a better comparison, the combined model described in Section 5.1 was updated using *enhanced truss* elements for the connecting elements between the two sub-structures, and it will be referred in this paper as the unstrengthened model of the structure.

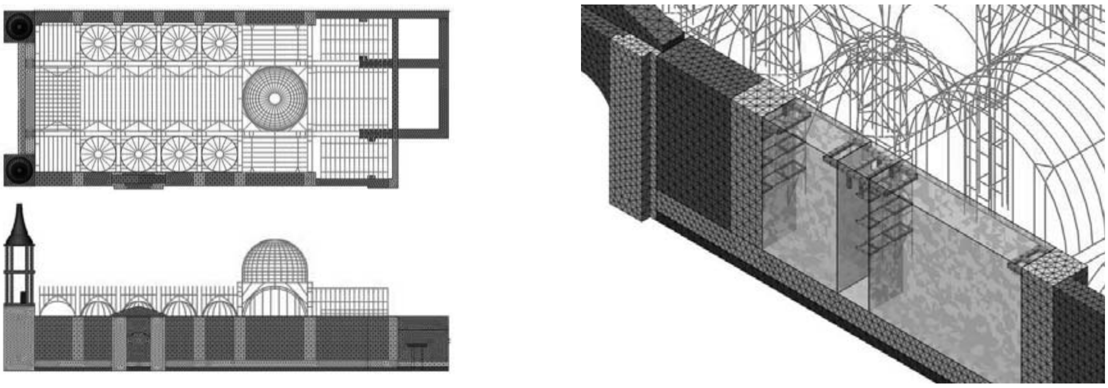

(a) (b)

Figure 6: Strengthened model: (a) FE mesh in Midas FX+ for DIANA; (b) detail of the embedded elements

6.3 Nonlinear static analysis

The efficiency of the proposed strengthening was mainly evaluated comparing the results obtained for the strengthened model (SM) and unstrengthened model (UM) under mass proportional lateral load in the XX– and YY– directions. Moreover, verifications of all the timber strengthening elements were carried out to validate the assumption made on their linear elastic behaviour considering the internal forces which occurred when the strengthened model was subjected to a lateral load equal to the PGA.

In the XX– direction, the maximum lateral load that could be applied to UM was 0.39g, while a maximum capacity of 0.45g was calculated for SM. Compared to the out-of-plane mechanism of the front façade and the bell towers observed for UM, the failure mechanism of SM was identified as the out-of-plane mechanism of only the southern bell tower. In the YY– direction, the maximum lateral load was calculated as a value of 0.25g for UM, while a lateral load higher than 0.45g could be applied to SM. While the out-of-plane mechanism of the northern lateral wall was observed for UM, a progressive flexural failure of the north-western corner was identified for SM (Figure 7).

For both the analysed directions, the highest values of internal forces throughout the strengthened model under the lateral load of 0.45g occurred in the elements corresponding to the elements of the collar beam. While the verifications were satisfied for the strengthening timber elements when a lateral load of 0.45g was applied in the XX– direction, when this lateral load was applied in the other direction the elements of the collar beam were subjected to tensile axial forces and shear which were higher than the corresponding capacities. Therefore, the behaviour of the structure was investigated adopting a higher wood structural class (Class B) for the strengthening timber elements. Although no relevant difference was observed in terms of capacity curve and internal forces in the timber strengthening elements, the load-carrying capacities obtained for a wood species classified as Class B are much higher than those obtained considering Class C and the verifications were satisfied for all the strengthening timber elements.

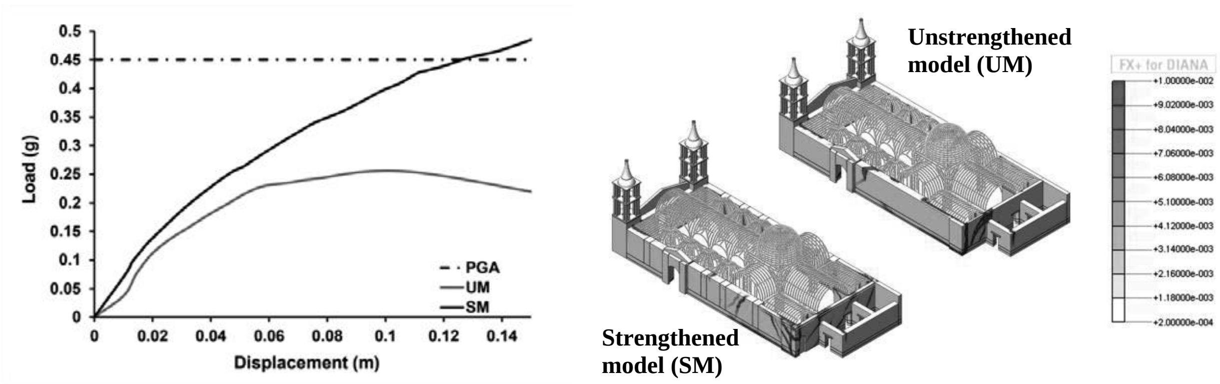

(a) (a)

Figure 7: Pushover analysis in the YY– direction: (a) load-displacement diagram. Control node at the top of the northern lateral wall; (b) failure mechanisms in terms of maximum principal strains observed for the strengthened and unstrengthened models

7 CONCLUSIONS

This paper presented the safety assessment and the seismic retrofitting of the Cathedral Ica, a complex half-timber structure built during the Viceroyalty period in Peru by applying the quincha technique. Within the Seismic Retrofitting Project (SRP), initiative of the Getty Conservation Institute (GCI), a multidisciplinary approach was applied with an organization in steps which are similar to those used in medicine: condition survey (anamnesis), identification of causes and decay (diagnosis), choice of remedial measures (therapy) and control of the efficiency of the interventions (controls). In such a scenario, a full understanding of the structural behaviour was essential and it was performed by means of several numerical models which were created on the basis of geometric surveys, laboratory and in-situ tests.

A single representative bay was first studied by performing linear elastic analysis under different loading conditions and verifying the compliance with the various criteria specified by Eurocode 5. Under seismic action, the verifications were not satisfied for the beams at the top of the lunettes and their connections. Subsequently, the structural behaviour of the whole Cathedral was investigated performing nonlinear static and dynamic analyses, and the lower bound capacity of the structure was found much lower that the PGA recommended by the Peruvian Code for the region of Ica. Therefore, strengthening measures were proposed to address the most vulnerable parts of the structure guaranteeing minimal and compatible interventions. The results obtained from the nonlinear static analysis performed on the model implementing the strengthening showed an improved global seismic behaviour of the structure, with a significant reduction of the out-of-plane vulnerabilities and higher capacities.

ACKNOWLEDGEMENTS

This work was carried out with funding from the Getty Seismic Retrofitting Project under the auspices of the Getty Conservation Institute (GCI). This work is also partially financed by FEDER funds through the Competitivity Factors Operational Programme - COMPETE and by national funds through FCT – Foundation for Science and Technology within the scope of the projects POCI-01-0145-FEDER-007633 and PTDC/ECMEST/2777/2014.

REFERENCES

[1] Rodríguez Camilloni, H. 2003. “Quincha Architecture: The development of an antiseismic structural system in seventeenth century Lima”. In *Proceedings of the First International Congress on Construction History, Madrid, 20th – 24th January 2003.*

[2] Hurtado Valdez, P. 2009. “Masonry or Wooden Vaults?: The Technical Discussion to Re-built the Vaults of the Cathedral of Lima in the Seventeenth Century”. In *Proceedings of the Third International Congress on Construction History, Cottbus, 20th – 24th May 2009.*

[3] Cancino, C., Farneth, S., Garnier, P., Vargas Neumann, J. and Webster, F. 2009. “Damage Assessment of Historic Earthen Buildings after the August 15, 2007 Pisco, Peru Earthquake”. The Getty Conservation Institute, Los Angeles, USA.

[4] Cancino, C., Lardinois, S., D’Ayala, D., Ferreira, C. F., Dávila, D. T., Meléndez, E. V. and Santamato, L. V. 2012. “Seismic Retrofitting Project: Assessment of Prototype Buildings”. The Getty Conservation Institute, Los Angeles, USA.

[5] Greco, F., Karanikoloudis, G., Mendes, N. and Lourenço, P. B. 2015. “Experimental in situ testing campaign on adobe historic structures in Peru, within the Getty SR Project. Report 2015-DEC/E-30”. University of Minho – TecMinho, Guimaraes, Portugal.

[6] Vicente, E. and Torrealva, D. E. 2014. “Mechanical Properties of Adobe Masonry of Historical Buildings in Peru”. In *Proceedings of the 9th International Conference on Structural Analysis of Historical Constructions (SAHC 2014), Mexico City, 14th-17th October 2014.*

[7] Lourenço, P. B., Sharma, S., Ciocci, M. P. and Greco, F. 2015. “Seismic Assessment of Ica Cathedral (Current Condition), Peru. Report 2015-DEC/E-34”. University of Minho – TecMinho, Guimaraes, Portugal.

[8] RNE E.010. 2006. “Reglamento Nacional de Edificaciones: Norma Técnica E.010 "Madera". Decreto Supremo N° 011-2006-vivienda (05-03-2006)”. Ministerio de Vivienda, Construcción y Saneamiento, Peru (in Spanish).

[9] TNO DIANA. 2014. “Diana Manuals”. http://tnodiana.com/DIANA-manuals

[10] CSI. 2014. “Analysis Reference Manual for SAP 2000, ETABS, SAFE and CSiBrisge”. Berkeley.

[11] EN 1995-1-1. 2004. “Eurocode 5: Design of timber structures - Part 1-1: General - Common rules and rules for buildings”. CEN, Brussels.

[12] RNE E0.30. 2016. “Reglamento Nacional de Edificaciones: Norma Técnica E.030 "Diseño Sismorresistente". Decreto Supremo N° 003-2016-vivienda (24/01/2016)”. Ministerio de Vivienda, Construcción y Saneamiento, Peru (in Spanish).

[13] SEiSMOSOFT. 2013. “Seismoartif v2.1”. Pavia, Italy.

[14] ICOMOS. 2003. “Recommendations for the analysis, conservation and structural restoration of architectural heritage”.

[15] Ciocci, M. P., Sharma, S., Lourenço, P. B. 2016. “Assessment of the strengthening proposal for Ica Cathedral, Peru. Report 2016-DEC/E-11”. University of Minho-TecMinho, Guimaraes, Portugal.

SHATIS'17
4th International Conference on
Structural Health Assessment of Timber Structures
20-22 September 2017 Istanbul, Turkey

EXPERIMENTAL AND NUMERICAL INVESTIGATIONS ON TIMBER-CONCRETE CONNECTIONS WITH INCLINED SCREWS

B. Berardinucci[1], S. Di Nino[1], A. Gregori[1], M. Fragiacomo[1], F. Moar[2]

[1] Department of Civil, Architectural-Construction and Environmental Engineering, University of l'Aquila, Italy

[2] Head of the Technical Consulting Department – Rothoblaas

Keywords: Timber-concrete composite beams, connections, inclined screws, mechanical model, parametric analysis

Abstract

In new and existing buildings, it is important that floors are sufficiently strong and stiff in plane. A possibility is to connect a concrete topping to the flexural elements of the floor. When retrofitting existing building, timber–concrete composite structures are often used to combine acoustic separation and thermal insulation with increased stiffness and load-carrying capacity.

The use of inclined screws to connect the existing timber beam with the concrete topping represents a promising solution to maximize the slip modulus. This paper investigates the mechanical behavior of such a type of timber–concrete connection. 10+10 pushout tests have been carried out at the Laboratory of the Department of Civil, Building and Environmental Engineering of the University of L'Aquila. Each specimen consisted of a timber block connected to two concrete slabs by means of two inclined screws per side. To reproduce the timber flooring used in real practice as permanent formwork for the placement of the concrete topping, an OSB layer was introduced between the timber block and the concrete slabs of the specimens. Two different OSB thicknesses and screw lengths were investigated. Screws measuring 8 mm in diameter and produced by Rothoblaas were used.

Experimental results were statistically assessed to compute the mean slip moduli and the characteristic values of the shear strength. An extension of the original European Yielding Model has been proposed to include the effect of interlayer flooring between timber beams and concrete slab connected by inclined screw. An accurate estimation of the characteristic shear strength was obtained for the actual failure mode observed during the tests.

1 INTRODUCTION

1.1 State of the art

Timber-concrete composite structures (TCCs) have become widely used in construction due to improvement in mechanical behavior and ease of assembly. TCCs are often used for upgrading of existing floors to mitigate problems resulting from excessive vibrations and deflections, to improve acoustic separation and thermal insulation, and to attain a rigid diaphragm in seismic areas. TCCs are also used in new construction, in order to obtained im-improved acoustic separation and thermal comfort, to reduce the weight (dead load) and to reduce costs. The advantage of using TCCs is to exploit the combined action of two different materials that contribute together to resist to external stresses. Replacing the structurally ineffective cracked part of concrete (non-resisting in tension) with timber leads to a fully resisting section. A typical configuration of a TCC includes a lower timber element (principally loaded in tension), a concrete topping (mainly loaded in compression) and a connection system (mainly subjected to shear stresses).

In some cases, a timber flooring is interposed between the concrete topping and the timber beams: it corresponds either to the permanent formwork used for the placement of the concrete slab in the case of a new building, or to the pre-existing timber flooring when retrofitting and existing timber-only floor.

The most common connection system is represented by metal fasteners, which have the advantage of being readily available off-the-shelf and easily installed. The mechanical properties and geometrical configuration of shear connectors affect the mechanical behavior of the TCCs due to the inherent flexibility of this connection system. The fasteners (e.g. screws) can be placed either perpendicular to the timber-concrete interface, or inclined. Using screws inclined at 45° has been proved to result in higher values of stiffness and load-carrying capacities compared to those placed perpendicularly. For a given geometrical and loading condition, this leads to a reduced number of fasteners needed 0-0.

The load-carrying capacity of timber-to-timber joints using inclined screw connectors can be determined using the yielding theory (Johansen yielding theory) which assumes plasticity in both the wood and the fastener. K. W. Johansen first applied the theory of plasticity to dowel-type connectors in wood arranged perpendicular to the interlayer. Those design criteria for the single connector now form the basis for the design of nailed and screwed timber-to-timber joints given in the Eurocode 5 0. In accordance with the Eurocode 5, the load-carrying capacity can be calculated by combined two effects: the “dowel effect” which depends on the bending resistance of the screw and the embedding resistance of the wood; and the “rope effect”, which depends on the tensile resistance of the screw and on the presence of friction between at the concrete-timber interlayer. This model can also be applied to timber-to-steel and timber-to-concrete connections. In order to obtain the load-carrying capacity of timber-to-concrete connection with inclined screws, which are principally loaded in tension, the Eurocode 5 theory has to be extended, by taking into the account the withdrawal capacity of fastener and friction between contact interfaces of connected members. Due to the lack of adequate method concerning the case of inclined screws, it [7] is recommended that load carrying capacity of inclined screws are derived from experimental test according to 0.

In 0, Kavaliauskas et al. proposed to adopt the Johansen’s yielding theory as a method to predict the load-carrying capacity of timber-to-concrete joints when the timber element bears directly to the concrete topping and threaded screws are used as inclined connectors. According to this method, the ultimate load-carrying capacity of a single connector is assumed to correspond to the condition such that either the stress in the wood attains the embedding strength, or plasticization is attained in both wood and metal dowel. In order to determine the load-carrying capacity, the kinematical possible failure modes are determined. The screw length embedded in the concrete part of connection was assumed to be rigidly fixed and so to remain undeformed. In the present paper, an extension of the aforementioned model has been developed, referring to an alternative timber to concrete connection configuration in which a non-structural interlayer (e.g. an OSB panel) is interposed between the timber beam and the concrete topping.

2 EXPERIMENTAL PROGRAMME

2.1 Experimental setup

Push-out tests were carried-out at the Laboratory for Structure and Material Testing of the Department of Civil, Architectural-Construction and Environmental Engineering, at the University of L'Aquila. Rothoblass Srl provided the specimens and commissioned the tests. Two sets of specimens of timber-to-concrete connections (named CLC8240 and CLC8160 respectively) were tested in push-out configuration under short-term loading. Each set of specimen consisted of ten samples, produced with the same materials in accordance to the geometrical configurations shown in 0and in 0respectively. Each sample consists of a central timber element (glue laminated pine, strength class Gl24h) connected to two adjacent concrete slabs (strength class C25/30) by means of two 45° inclined full threaded screws per side (0. Between the timber element and the concrete slabs an OSB flooring panel was interposed, measuring 22 mm in thickness for specimens type CL8160 and 44 mm for specimens type CLC8240 respectively.

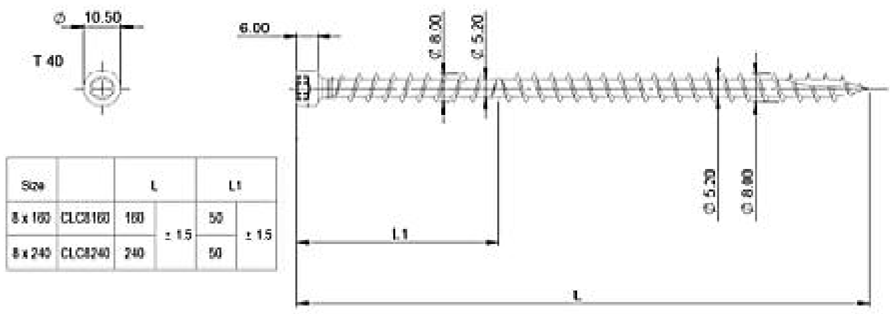

Figure 1: Geometry of a full threaded screw (measures in mm)

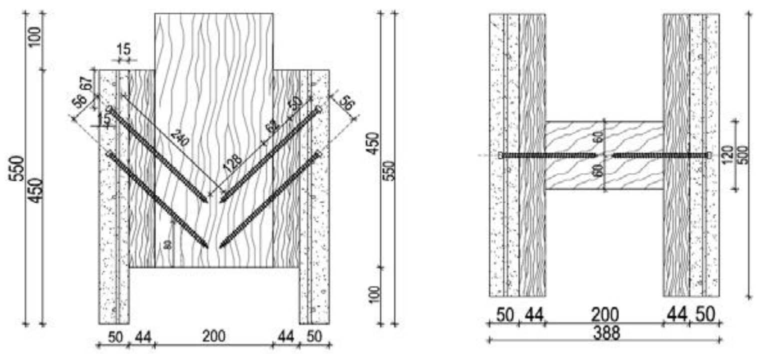

Figure 2: Typical dimensions of specimen clc8240 (measures in mm)

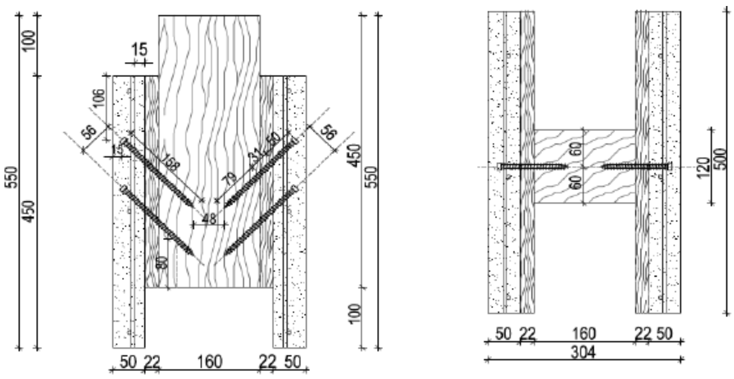

Figure 3: Typical dimensions of specimen clc8160 (measures in mm)

The specimens were placed under the loading machine and the push-out test procedure was followed in accordance with the standard 0: the load was increased to 0,4 Fest (maximum estimated load, estimated on the basis of past experience, or based on preliminary tests) and maintained for 30 s, then reduced to 0,1 Fest and also maintained for 30 s, thereafter the load was increased until the deformation of 15 mm was achieved. In order to assess the relative slip between timber and concrete, four displacement piezoelectric transducers were placed at the four corners of the sample and the average of the four measurements was taken. Tension rods were used in the upper and lower part of each sample to prevent elements separation during the test (Figure 4).

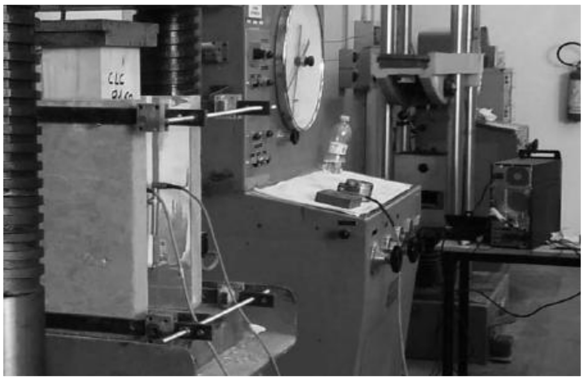

Figure 4: Photo of a sample during the push-out test

2.2 Results

A load – displacement (slip) curve was obtained for each sample, where the peak value represents the ultimate load (Figure 5).

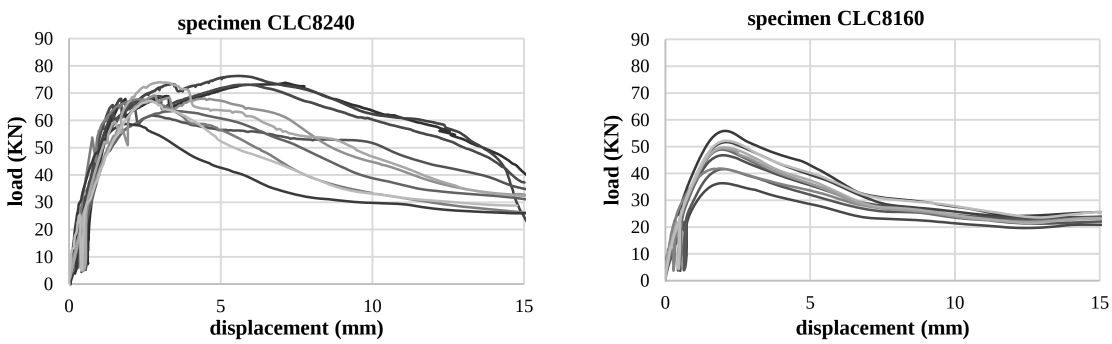

Figure 5: Load-displacement (slip) curves

According to 0, characteristic values of the load-carrying capacity F_u per specimen were calculated assuming a log-normal distribution: these values are shown in Table 1.

Specimen CLC8240	
$F_{u,max}$	19,083 kN
$F_{u,min}$	14,682 kN
$F_{u,mean\ value}$	17,255 kN
$F_{u,k}$	14,535 kN
S_y	0,08

Specimen CLC8160	
$F_{u,max}$	13,974 kN
$F_{u,min}$	9,086 kN
$F_{u,mean\ value}$	11,860 kN
$F_{u,k}$	8,962 kN
S_y	0,129

Table 1: Calculation of characteristic values of load-carrying capacity per connector

At the end of the push-out tests, the concrete slabs did not show any evident crack, but vertical displacement at interface between timber and concrete slab resulting in timber crushing, as shown in Figure 7. Specifically, two combined failure modes were observed: the ultimate load-carrying capacity was reached when the timber crushed at the interface with the screw, and the screw exceeded its withdrawal capacity. In all cases, no plastic hinges appeared along the screws length.

Figure 7: Evidence of the failure mode: no hinges formed along the embedded screw length into concrete.

3 MECHANICAL MODEL FOR STRENGTH PREDICTION

In this section the Johansen's yielding theory is adopted to predict the ultimate load for timber-to-concrete joints using self-tapping threaded connectors screwed at an angle into the wood, as done in 0. The ultimate load-carrying capacity of a single connector is assumed to correspond with the condition where either the stress in the wood attains the plastic value (the embedding strength) or the plastic failure is attained in both the wood and the dowel. In order to determine the load-carrying capacity for a specific connector geometrical configuration, the possible kinematical failure modes are first determined. The screw in the concrete part of connection is assumed to be rigidly fixed and so to remain undeformed.

Unlike 0, in the present study timber and concrete are considered not in direct contact, but separated by an OSB flooring (see Figures 2-3). Thus, a different, proper model is required to determine the (modified) load-carrying capacity and possible additional failure modes. In general the OSB flooring has mechanical properties different from timber, and depending on that it can contribute more or less significantly to the whole system capacity. However, in this study, the mechanical analysis is performed by referring only to the following limit cases:

- *Limit case 1*: OSB modeled as fully resisting and, therefore, as an extension of the timber;
- *Limit case 2*: OSB modelled as a fully non-resisting material and, thus, as an empty gap between timber and concrete.

Limit case 1 refers to the case of a high quality OSB (comparable to timber) fully connected to the timber. Limit case 2 occurs when either a low quality OSB is used (and therefore its strength contribution can be neglected) or the OSB is not connected to both the timber element and the concrete topping, and thus it can freely move with respect to both timber and concrete. The load-carrying capacity calculated according to limit case 2 conservative.

3.1 Failure modes

The initial geometrical configuration of the system is described by the screw diameter d, the screw inclination angle α with respect to the timber-concrete interlayer, the screw length l (with $t = l\sin\alpha$ representing the horizontal projection) and the length s inserted in the OSB. The quantity $t_s = s\sin\alpha$ denotes the horizontal projection of the length s, which also signifies the OSB thickness.

By referring to timber-concrete joints with inclined screws, schematics of the kinematically possible failure modes, together with the internal forces and the plastic hinges occurring in the screw length, are displayed in Figure 8 and 9 for the limit cases 1 and 2, respectively.

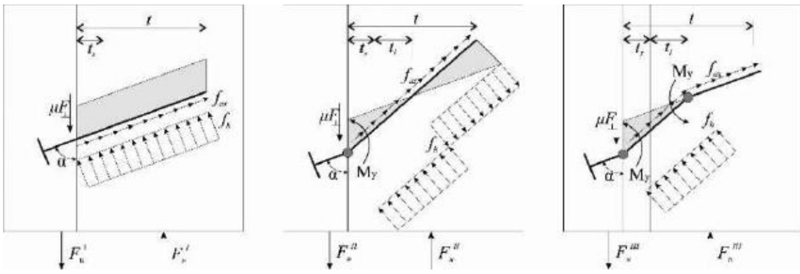

Figure 8: Failure Modes (Limit case 1)

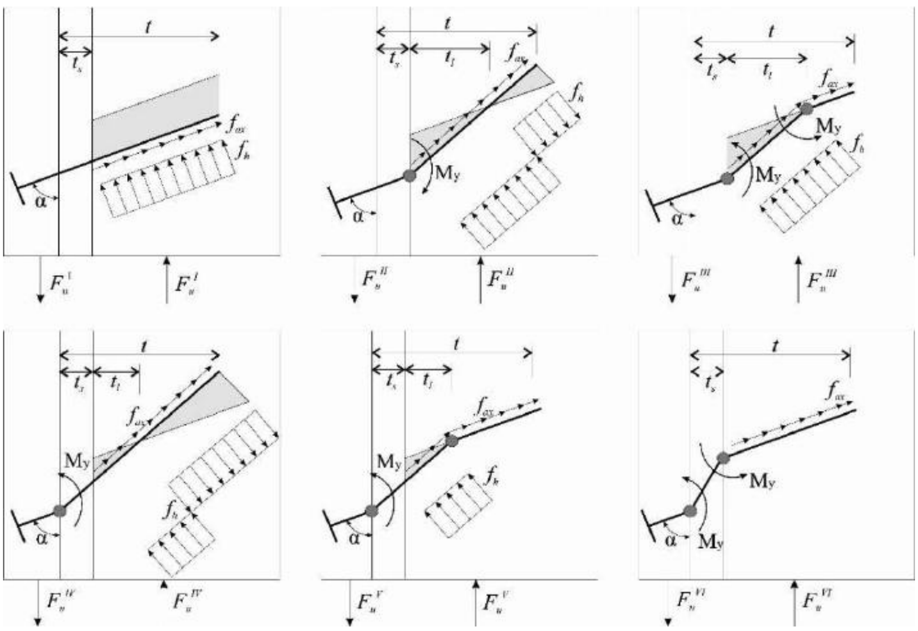

Figure 9: Failure Modes (Limit case 2)

In the second limit case, Figure 9,0 modes I, II, III are similar to the failure modes determined in 0. In Mode I the ultimate load-carrying capacity is reached when the wood yields plastically along the screw and attains the embedding strength f_h. Mode II is attained when the embedment stresses are distributed over the length of the screw so that a plastic hinge at the interface between timber and OSB is formed and the screw rotates as a stiff member in the wood. Such failure mode is possible if the embedded length $(l - s)$ of the fastener in wood is enough to enable the plastic hinge formation in the screw. Mode III failure occurs when the embedding stresses are distributed over a length x_l (t_l signifying its horizontal projection) of the screw, forming an additional plastic hinge. Modes IV, V, VI can only occur when a gap is considered. Mode IV is similar to Mode II, but the plastic hinge is formed at the interface between concrete and OSB. Mode V is similar to Mode III, but also in this case the plastic hinge is formed at the interface between concrete and OSB. Finally, Mode VI is an extension of Mode V, where the second hinge is located at the timber-OSB interface.

In the first limit case, Figure 8, modes I, II, III are the same failure modes determined in 0, where timber and concrete are in contact; the only difference is that the screw is not completely inserted in the timber, but it is in part also inserted in the OSB.

Each failure mode can be determined by imposing the equilibrium of a system of forces given by the fastener withdrawal strength f_{ax}, the timber embedding strength f_h, and the fastener yield moment M_y. In the limit case 1 also the friction force $\mu F_\perp$ at the concrete-OSB interface (with μ signifying the friction coefficient and $F_\perp$ the axial compression force) must be considered.

3.2 Formulas derivation

The ultimate load-carrying capacity F_u^h (where the superscript $h = I, II, III$ for the limit case 1 and $h = I, II, III, IV, V, VI$ for the limit case 2) for each failure mode is here determined by using the Principle of the Virtual Work. The theorem states that the virtual work spent by a system of balanced, active $\boldsymbol{f}$ and restraint $\boldsymbol{r}$, forces is zero for each kinematically admissible virtual field of displacements $\delta\boldsymbol{u}$ and restraint displacements $\delta\boldsymbol{s}$:

$$L_e = \boldsymbol{f}^T \delta\boldsymbol{u} + \boldsymbol{r}^T \delta\boldsymbol{s} = 0 \qquad \forall\ (\delta\boldsymbol{u}, \delta\boldsymbol{s}) \tag{1}$$

The Principle of Virtual Work can be applied as described in the following section.

3.2.1. Application of the principle of virtual work to Mode II

Figure 10 displays the (virtual) kinematic problem corresponding to the (real) static problem shown in Figure 9.

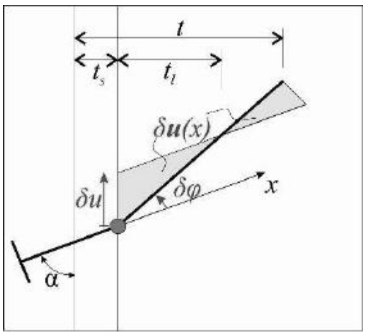

Figure 10: Virtual kinematic problem of Mode II

It can be obtained by the superposition of the rigid vertical translation mode of the timber (with displacement δu) and of the rigid rotation mode of the screw around the plastic hinge (with rotation angle $\delta\varphi$), which produce the relative displacement field $\delta\boldsymbol{u}(x)$ between timber and screw.

By applying the principle of the virtual work:

$$L_e = F_u^{II}\delta u - \left(M_y\delta\varphi + \int_0^{x_l}\boldsymbol{f}_1{}^T\delta\boldsymbol{u}\,(x)dx + \int_{x_l}^{l-s}\boldsymbol{f}_2{}^T\delta\boldsymbol{u}\,(x)dx\right) = 0 \quad \forall\,(\delta u,\delta\varphi) \tag{2}$$

where:

$$\delta\boldsymbol{u}(x) = \begin{pmatrix}\delta u\sin\alpha\\ \delta u\cos\alpha - \delta\varphi x\end{pmatrix}$$
$$\boldsymbol{f}_1 = \begin{pmatrix}f_{ax}d\\ f_h d\end{pmatrix}, \boldsymbol{f}_2 = \begin{pmatrix}f_{ax}d\\ -f_h d\end{pmatrix} \tag{3}$$

the equilibrium equations are derived by collecting all terms in eqn (2) for any δu and $\delta\varphi$, and then by imposing they are equal to zero.

$$(eqn1)\delta u + (eqn2)\delta\varphi = 0 \qquad \forall\,(\delta u,\delta\varphi) \tag{4}$$

In particular, $eqn2 = 0$ expresses the rotation equilibrium, from which eqn (5) is derived for x_l.

$$x_l = \frac{(t-t_s)}{\sqrt{2}\sin\alpha}\left(\sqrt{1+\frac{2M\sin\alpha^2}{df_h(t-t_s)^2}}\right) \tag{5}$$

Then, $eqn1 = 0$ expresses the translation equilibrium, from which, by substituting eqn (5), the ultimate load-carrying capacity F_u^{II} is found (eqn (6)).

$$F_u^{II} = df_{ax}(t-t_s)\cot\alpha + df_h(t-t_s)\left(-1+\sqrt{2}\sqrt{1+\frac{2M\sin\alpha^2}{df_h(t-t_s)^2}}\right) \tag{6}$$

3.2.2. Load-carrying capacity equations

The equations of ultimate load-carrying capacity for each failure mode in the limit cases 1 and 2 can be derived similarly to the procedure detailed before, see respectively eqns (7-9) and eqns (10-15).

Limit case 1

$$F_u^{I} = df_{ax}t(\mu+\cot\alpha) + df_h t(1-\mu\cot\alpha) \tag{7}$$

$$F_u^{II} = df_{ax}t(\mu+\cot\alpha) + df_h t(1-\mu\cot\alpha)\left(-1+\sqrt{2}\sqrt{1+\frac{2M\sin\alpha^2}{df_h(t-t_s)^2}}\right) \tag{8}$$

$$F_u^{III} = df_{ax}t(\mu+\cot\alpha) + 2(1-\mu\cot\alpha)\sqrt{df_h M}\sin\alpha \tag{9}$$

Limit case 2

$$F_u^{I} = df_{ax}(t-t_s)\cot\alpha + df_h(t-t_s) \tag{10}$$

$$F_u^{II} = df_{ax}(t-t_s)\cot\alpha + df_h(t-t_s)\left(-1+\sqrt{2}\sqrt{1+\frac{2M\sin\alpha^2}{df_h(t-t_s)^2}}\right) \tag{11}$$

$$F_u^{III} = df_{ax}(t-t_s)\cot\alpha + 2\sqrt{df_h M}\sin\alpha \tag{12}$$

$$F_u^{IV} = df_{ax}(t-t_s)\cot\alpha + df_h(t+t_s)\left(-1+\sqrt{2}\sqrt{\frac{2M\sin\alpha^2}{df_h(t-t_s)^2}+\frac{t^2+{t_s}^2}{df_h(t+t_s)^2}}\right) \tag{13}$$

$$F_u^{V} = df_{ax}(t-t_s)\cot\alpha + df_h t_s\left(-1+\sqrt{\frac{4M\sin\alpha^2}{df_h {t_s}^2}+1}\right) \tag{14}$$

$$F_u^{VI} = df_{ax}(t-t_s)\cot\alpha + \frac{2M\sin\alpha^2}{t_s} \tag{15}$$

where the characteristic withdrawal capacity [N] at an angle α to the grain according to the Eurocode 5 0 should be taken as:

$$F_{ax,k,Rk} = \frac{n_{ef}\, f_{ax,k}\, d\, l_{ef}\, k_d}{1{,}2\, cos^2\alpha + sin^2\alpha} \tag{16}$$

with:

$$f_{ax,k} = \ 0{,}52\, d^{-0{,}5}\, l_{ef}^{-0{,}1}\, \rho_k^{0.8} \tag{17}$$

d is the outer diameter measured on the threaded part [mm];
l_{ef} is the pointside penetration length of the threaded part minus one screw diameter [mm];
n_{ef} is the effective number of screws (in our case equal to the actual number of screws, *n*);
$k_d = min.\begin{cases} d/8 \\ 1 \end{cases}$;
$f_{ax,k}$ is the characteristic withdrawal strength perpendicular to the grain [N/mm^2].

The characteristic embedding strength [N/mm^2] according to Eurocode 5 0 should be taken as:

$$f_{h,k} = 0{,}082\, \rho_k\, d^{-0{,}3} \tag{18}$$

The characteristic values of the yield moment [Nmm] according to Eurocode 5 0 should be taken as:

$$M_{y,Rk} = \ 0{,}3\, f_u\, d^{2{,}6} \tag{19}$$

where f_u is the tensile strength of the screw [N/mm²].

It should be noted that the presence of the withdrawal strength f_{ax} in this system of equations is justified when a significant axial displacement component affects the screw, due to its inclination. The problem may become inconsistent for small values of inclinations α, for which the timber is not likely to yield for withdrawal.

3.3 Analytical-experimental comparison

A first comparison between the experimental value of the load-carrying capacity of the connection, and those resulting from the aforementioned equations for limit case 2, shows that the mechanical model is unable to predict the correct failure mode. In Table 20 results are shown for the specimen CLC8160.

Theoretically, the connection failure mode should be Mode *V* characterized by two plastic hinges in the fastener. However, the tests show that no plastic hinge could be developed in the fastener at the interface between timber and concrete, which means a failure Mode *I*.

	Calculated values					
Experimental Value	MODE I	MODE II	MODE III	MODE IV	MODE V	MODE VI
8,962 kN	8,509 kN	5,795 kN	4,550 kN	4,810 kN	3,895 kN	3,896 kN

Table 2: Analytical-experimental comparison

3.4 Parametric study

The dependency of the ultimate load upon the geometrical configuration and the dimensions of the connector has been investigated using the aforementioned analytical solutions. The first study (Figure 11) explores the dependency of the load-carrying capacity upon the screw inclination α. In limit case 1, a friction coefficient $\mu = 0.4$ is considered.

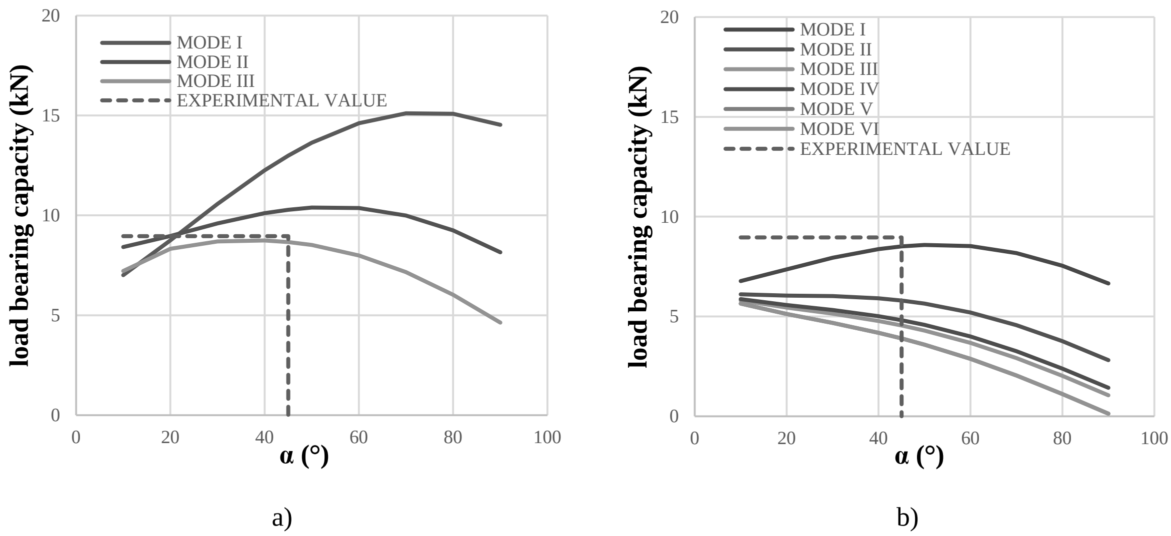

Figure 11: Variation of the load-carrying capacity with the screw's inclination. a) Limit case 1, b) Limit case 2

The following remarks can be done:

- in Limit case 1, the predicted values of the load-carrying capacity are less conservative compared to Limit case 2;
- in Limit case 1, the load-carrying capacity of the connection reaches a maximum when the screw is arranged at an angle of 50°;
- in Limit case 2, the load-carrying capacity of the connection decreases with the inclination of the screw, except for Mode *I* when it reaches a maximum at an angle of 50°.

Figure 12 shows the variation of the load-carrying capacity of an inclined screw (α=45°) with the non-dimensional t_s/t ratio, and with a friction coefficient $\mu = 0.4$ (Limit case 1). By incrementing the thickness of the OSB panel (gap), the ultimate load decreases and tends to zero when the penetration length of the threaded part in the timber element is null. When this ratio is equal to zero, and no gap is considered in the model, the ultimate load is maximum and the failure modes are reduced to three: the model tends towards Limit case 1. When the

t_s/t ratio goes to one and no connection between timber and concrete is considered, then the load-carrying capacity is null.

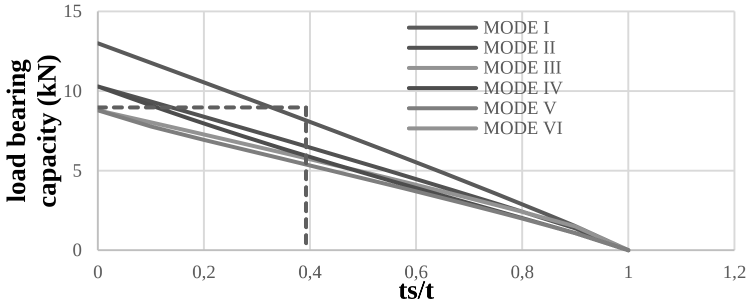

Figure 12: Variation of the load-carrying capacity with the $^{t_s}/_{t}$ ratio

Figure 13 displays the variation of the load-carrying capacity of an inclined screw (α=45°) with the non-dimensional d/t ratio assuming a friction coefficient μ=0.4 (Limit case 1). By increasing the outer diameter measured on the threaded part, the ultimate load increases. In this case, the thickness of the OSB panel (gap) has been assumed equal to the experimental configuration in Limit case 2, and null in Limit case 1.

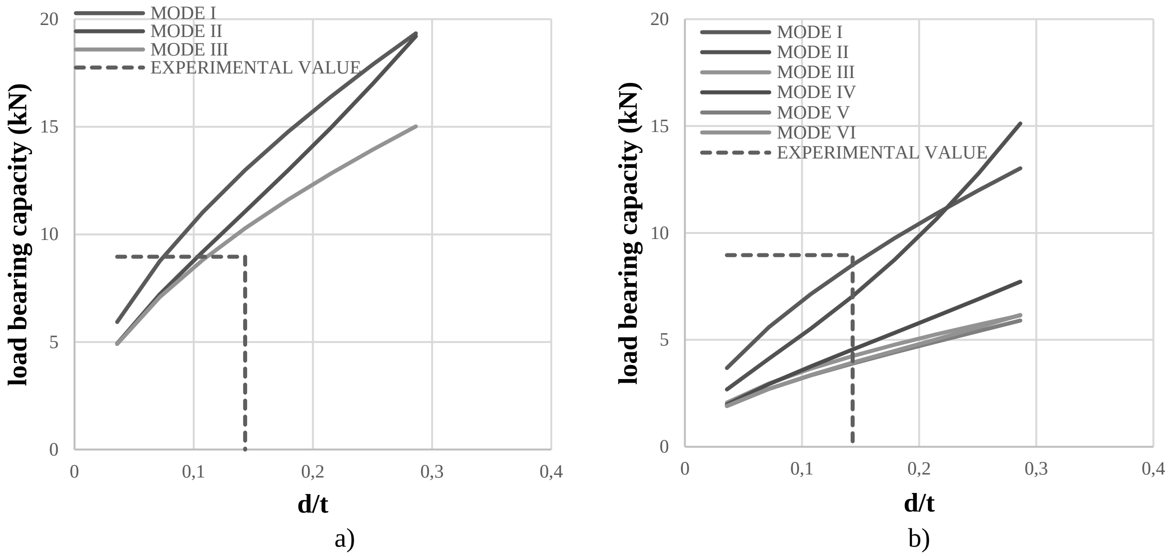

Figure 13: Variation of load-carrying capacity with the $^{d}/_{t}$ ratio: a) Limit case 1; b) Limit case 2

4 CONCLUSIONS

In this paper a mechanical model for calculating the load-carrying capacity of inclined screw was proposed, according to the Johansen's theory. In order to validate the analytic formulations, push-out tests were performed. Furthermore, parametric studies have shown how the ultimate load varies depending upon the geometrical configuration and dimensions of the connector.

In all investigations, the influence of the withdrawal and embedding strengths was found to be significant. An estimated value of the withdrawal and embedding strengths of screws were used for computing the theoretical value, according to the Eurocode 5. Although the theoretical ultimate load of the connection is close to the experimental one, the failure mode differs. Theoretically the connection failure mode should be characterized by two plastic hinges occurring in the fastener, but the tests showed that no plastic hinge developed in the fastener at the interface between timber and concrete, meaning a failure Mode *I*.

Better predictions of the load-carrying capacity of timber-to-concrete connections with inclined screws would require a previous identification of the actual mechanical properties of the timber and the screws (withdrawal and embedding strengths) using appropriate experimental tests.

ACKNOWLEDGEMENTS

Special thanks to Rothoblaas Srl for the financial and technical support provided, without which the present research would not have been possible.

REFERENCES

[1] Saulius Kavaliauskas, Audronis Kazimieras Kvedaras, Balys Valiūnas. Mechanical behavior of timber-to-concrete connections with inclined screws. Journal of civil engineering and management, 2007, Vol XIII, No 3, pp. 193–199.

[2] Roberto Tomasi, Alessandro Crosatti, Maurizio Piazza. Theoretical and experimental analysis of timber-to-timber joints connected with inclined screws. Construction and Building Materials 24 (2010), pp. 1560–1571.

[3] Fragiacomo, M., and Lukaszewska, E. Development of prefabricated timber-concrete composite floor systems." Struct. Build., 2011, 164(2), pp. 117–129.

[4] Bejtka I, Blaß HJ. Joints with inclined screws. Proceedings from meeting thirty-five of the international council for building research studies and documentation, CIB, Working Commission W18 – Timber Structure, Kyoto, Japan; 2002.

[5] Bejtka I, Blaß HJ. Screws with continuous threads in timber connections. RILEM, Proceedings PRO 22, Stuttgartl, 2001.

[6] Ceccotti A, Fragiacomo M and Gutkowski. On the design of timber–concrete composite beams according to the new versions of Eurocode 5. 35th Meeting of the Working Commission W18–Timber Structures, International Council for Research and Innovation in Building and Construction, Kyoto, Japan, 2002, pp. 10–24.

[7] EN 1995-1-1, Eurocode 5: Design of timber structures - Part 1-1: General - Common rules and rules for buildings. CEN, 2004.

[8] UNI EN 26891, Timber structure – Joints made with mechanical fasteners – General principles for the determination of strength and deformation characteristic. CEN, 1991

[9] BS EN 14358:2016, Timber structures - Calculation and verification of characteristic values. CEN, 2016.

[10] EN 13183-1, Moisture content of a piece of sawn timber - Determination by oven dry method. CEN, 2002.

SHATIS'17
4th International Conference on
Structural Health Assessment of Timber Structures
20-22 September 2017 Istanbul, Turkey

ASSESSMENT OF THE STRUCTURAL PERFORMANCE OF A NORWEGIAN HISTORIC TIMBER STRUCTURE: VÆRNES CHURCH.

Filippo Frontini[1], Jan Siem[1], and Dag Nilsen[1]

[1] Department of Architectural Design, History and Technology, Norwegian University of Science and Technology

Keywords: Historic timber structure, Structural Analysis, Medieval roof.

Abstract

In Norway, the architectural heritage is comprised mainly of wooden buildings. Besides the stave churches and log timber houses, the third largest group of wooden medieval structures in Norway is the surviving roofs of stone churches. In the Trøndelag region of Norway, five stone churches still preserve wooden roofs dating from the period c. AD 1140 – AD 1350.

Værnes church is one of these buildings, and has the largest roof span amongst them. The roof over the choir section in Værnes church dates back to AD 1140 and the nave roof back to AD 1191. During the middle ages, timber structures represented the most advanced construction techniques. Their characteristics were influenced by both local traditions and material availability. Gaining knowledge about the techniques used in the construction of historic structures is of paramount value towards the devel- opment of restoration and renovation of buildings.

The present work discusses results from a study on Værnes Church focusing on the assessment of the structural performance of the two-dimensional structure and plans investigations of the possible three-dimensional effect of the timber roof. A computational model of the church's structure was developed to better understand the behaviour of the two-dimensional roof structure. Future work will focus on experimental investigation of tim- ber dowelled connections, and aim to increase the knowledge on three-dimensional effects of this kind of structures.

1 INTRODUCTION

Historical timber roof trusses are often complex systems; attics of many churches, cathedrals, castles and medieval halls hide timber roofs. They are an important cultural heritage, being bearers of information from a period of which direct sources of information are scarce. During the middle ages, timber roof trusses represented the most advanced construction technique of the time. Their characteristics were influenced by local traditions, available materials, and construction techniques. Wooden structures were built by carpenters and craftsmen using methods based on experience.

In Norway, an important group of wooden medieval structures is the surviving roofs of stone churches. These structures testify the great craftsmanship of medieval carpenters. They have a remarkable cultural and technical value, but unfortunately, detailed investigations and assessments have not been carried out so far.

Misunderstanding of the structural behaviour can lead to an incorrect intervention that may change the overall distribution of the stresses with severe consequences for the building, causing additional problems. The purpose of the rehabilitation work is not only to assess the stability of the structure and ensure its safety, but it is also a way to preserve and transmit the cultural heritage of historical construction systems to the future,[1].

A correct understanding of the behaviour and the reliability level of the structure is important to avoid unnecessary and visually disturbing changes of the construction. Regarding the structural aspect of historic structure, it is easier to find papers and works about masonry structures than timber structures or the interaction between timber and masonry. Courtenay [2] investigated the behaviour of the interaction between roof and masonry wall and Heyman the effect of the deflection under wind load,[3, 4]. Mainstone focused on different types of buildings and in particular in masonry structure, such as Hagia Sophia in Istanbul and the dome of St. Peter in Rome,[5-7]. More recently Morris et al. used modern computer tools and the finite element method (FEM) to analyse the Westminster Hall in London,[8]. They pointed out the importance of the FEM in historical and technical exploration. Sandin, Olsson, and Thelin conducted research on the structural analysis of historic timber structures defining mechanical pattern and performing finite element analysis (FEA) on case studies of old Swedish churches,[9].

2 MOVITATION

The first aim of this paper is to test a methodology for analysing historic timber structures in order to evaluate if the structure satisfy today's reliability level design. The second aim is to study the design principles of the Trøndelag family of churches. This group of churches has an inestimable heritage value, in particular Værnes church that is almost 900 years old. The original wooden structure is still standing. The last aim is to lay the foundation for further steps to understand the global three-dimensional behaviour of the roof structure involving both the trusses and the stiffening effect of the outer roof.

3 THE TRØNDELAG FAMILY OF CHURCHES

The surviving roof of stone churches make up the third largest group of medieval wooden building structures in Norway, after Stave Churches and timber houses. A Ph.D. thesis carried out by Ola Storsletten recorded that, among approximately 150 stone churches dating from the period between 1030 to 1537, only 17 original roof designs survived partly or entirely. Traces and remains of surviving medieval roof designs are also known in further four churches,[10].

The Trøndelag family of churches is dated between 1100 and 1350. In its pure form, it is represented by five structures. The main five churches of this family are located in Trøndelag (Fig. 1), but it is possible to find similarities in other churches in the central part of Norway and also in Sweden. Today's Norway borders do not correspond to the borders of the Norwegian Kingdom during the middle ages. The kingdom of Norway extent comprised part of the current Sweden and this had a direct impact on the work of medieval timber churches.

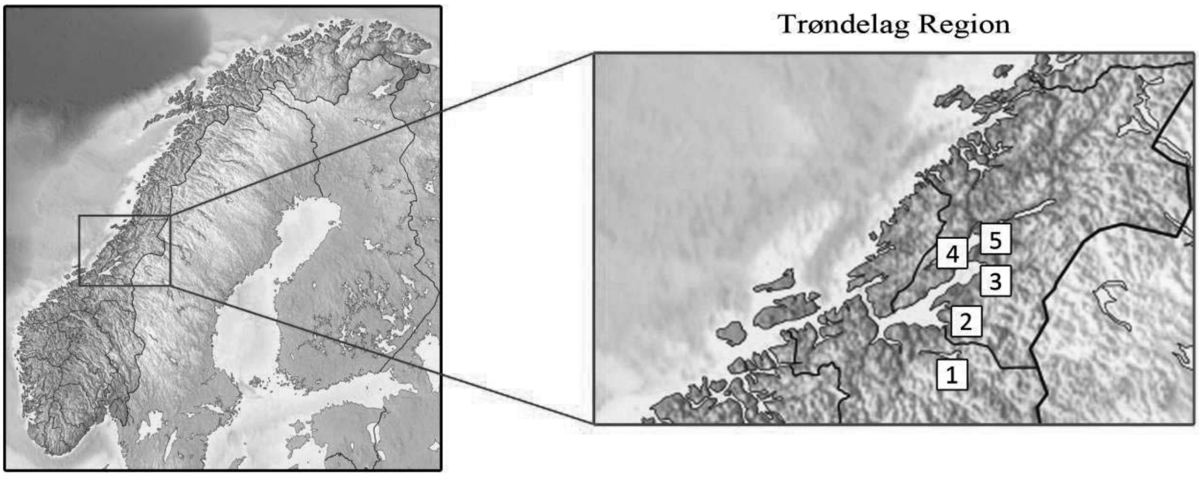

Figure 1: Trøndelag family of churches.1)Selbu Church, 2)Værnes Church, 3)Alstadhaug Church, 4)Hustad Church, 5)Mære Church. (Derivative work of "Relief map of Norway", www.maps-of-europe.net licensed under CC BY-SA 3.0)

The starting period of the construction activity is associated with the introduction of the tithe in the first decades of the 1100s and the ending with the Black Death in 1349-50,[11]. The design of trusses remains strikingly uniform throughout this period. It is only after the plague that noticeable changes occurred in the structures, in the form of more advanced timber connections. In medieval times, timber trusses were used in several types of buildings: bridges, relatively large rooms, halls, castles or boathouse. With regarding to churches from 1100-1350, the preserved and documented examples are limited. This type of churches has wooden roof structures whose task is to cover a relatively large room while taking into account natural conditions such as rain, snow and wind. The Norwegian stone church is a result of foreign influence.

The stone churches construction in 1200s Norway is influenced by the gothic roof trusses present in masonry churches in England and on the Continent. The carpentry in medieval stone buildings, in Norway, represents a continuation of an existing building construction technique and the local crafts tradition. Previously, trusses might have been of a simpler kind.

Before Christianity arrived, masonry of stone laid in the mortar was comparatively unknown in Norway, but since this was the common material for churches in Europe, it was not long time before the first stone churches were erected on Norwegian soil. They were built at the same time as the Stave Churches, and some are dated as far back as before the reign of Olav Kyrre (1066-93). During the 12th Century, numerous large and small stone churches and monasteries were erected all over the country, and many of the churches are still standing. Those in Western Norway and Trøndelag derive mostly from the Anglo-Romanesque type. Outside the core area, there is no longer a clear dominance of this type even though some roof trusses in Sweden and other areas of centre Norway have many similarities to Trøndelag churches.

The Trøndelag type is named after the area of distribution. Within this area, the five main stone churches were built during the period 1100-1350, and they are preserved with original wooden roofs from that period. Today Selbu church is located in Sør-Trøndelag while Værnes, Alstadhaug, Hustad and Mære churches are in Nord-Trøndelag. Although the dimensions of the churches vary, each of them consists of a rectangular nave and a narrower chancel. The oldest building of this group of churches is Værnes Church, of which the chancel roof has been dated from ca. 1140 through dendrochronological dating. The youngest nave structure is in Mære church, dating from ca. 1199. At least two generations of artisans have worked on the construction of these stone churches.

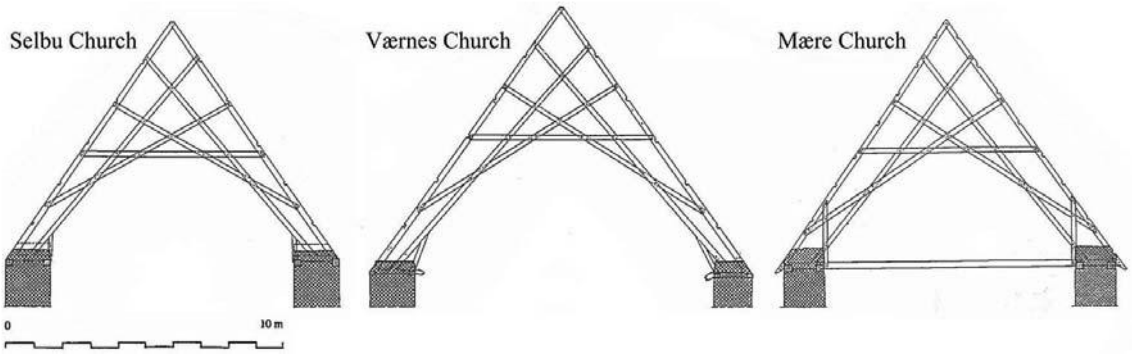

Figure 2: Examples of Trøndelag roof trusses. Selbu church, Værnes church, Mære church.

The key feature of the Trøndelag type frames is the superposition system of rafters and collar beams that form a sort of "grid", with many connection points. This characteristic makes the structure stiff in the upper part. Another hallmark of the Trøndelag type churches is the distance between the principal rafter and the secondary rafter. The distance between these two elements is in some way proportional to the span. The cross sections of principal rafters, secondary rafters, and collar beams are different either within the same church and from church to church. All roof constructions consist of a roof truss that in principle forms a rigid triangular framework. The structure is the trademark of the Trøndelag-type. Three of the roofs are shown in Fig. 2.

Værnes church is discussed more in detail (see Figs. 5-7). The typical angle of the main rafters in the Trøndelag churches is approximately 54° (only in Alstadhaug is lower). In the bottom part of the frame, there is a pair of wooden wall plates embedded in the masonry that runs longitudinally along the entire length of the wall. The outer wall plate is connected with the main rafter while the inner one supports the lower strut and the sole piece. These elements have a considerable size; they are rectangular or square shaped and have a section where the edges vary between 15 cm and 20 cm. The two wall plates are connected by sole piece. The collar beams are always present, usually located at the middle height of the frame or above.

4 VÆRNES CHURCH

4.1 Assessment

Værnes church is one of the largest and best preserved Norwegian medieval churches with western tower, nave, chancel and sacristy from the middle ages. The church is oriented with the choir to the east. The choir of Værnes Church has been dated from ca. 1141 through dendrochronological dating while the nave has been dated from ca. 1191,[12]. The timber roof structure of the nave is substantially preserved. The church was renovated in 1960. Drawings of the original construction have been made by Erlin Gjone, [13], but none structural assessments or documentations of changes for the work done. The drawings presented in this article are derived from this work and the visual survey carried out.

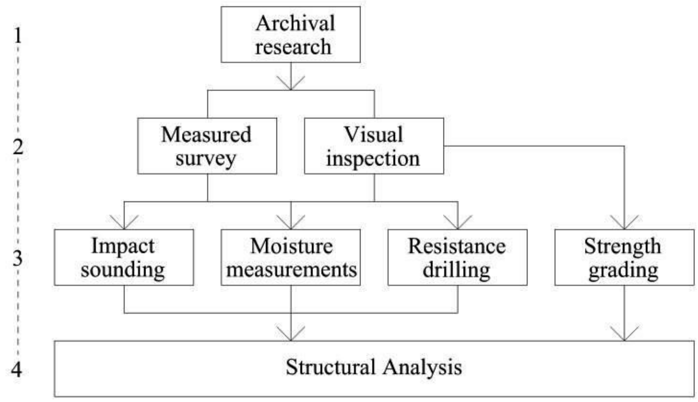

Figure 3: Methodology of Assesment.

The church has a stone structure with a continuous foundation and a timber pitched roof constituted by 21 trusses as shown in Fig. 4. All the elements are made of pine, [12]. The longitudinal system is composed by 5 parallel purlins that connect the main rafters and run along all longitudinal length. In the structure the secondary members, the struts, and the collar beams cross each other as shown in Fig. 5.

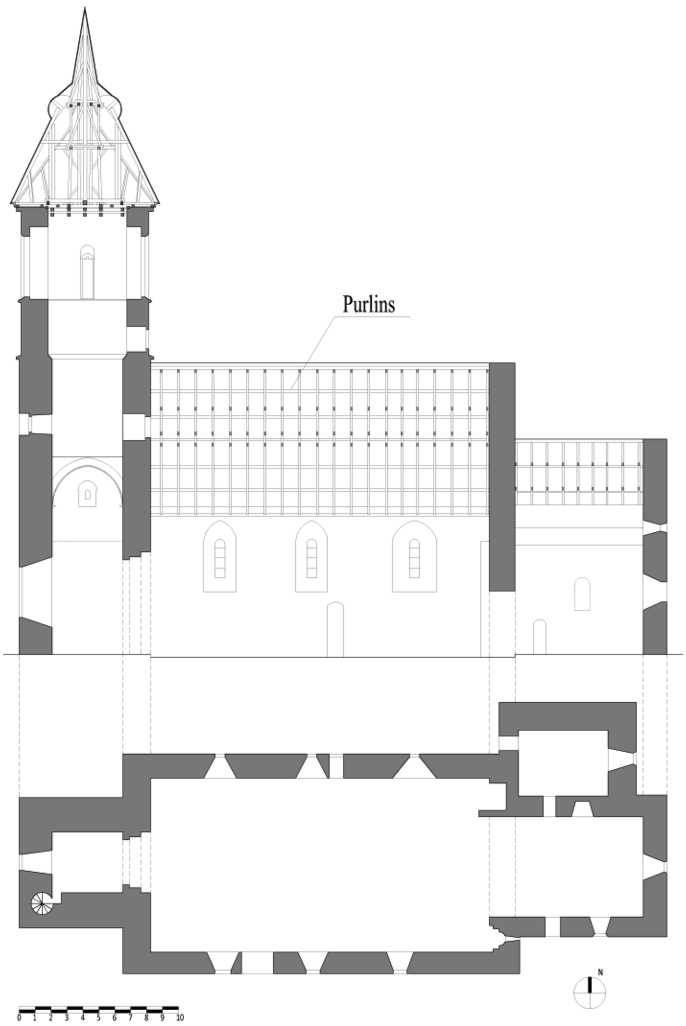

Figure 4: Section and plan of Værnes Church.

The structure is approximately 14.1 m wide; the angle of the roof is approximately 54°. The structure consists of the main rafters, secondary rafters, wall plates embedded in the walls, collar beams and struts. The main rafters and the secondary rafters are connected to the wall plates on top of the longitudinal walls. The angle of the secondary rafters is about 50°. In the bottom of the truss, an lower strut is present. On top of the wall, a sole piece is connecting the rafters, the lower strut and the wall plates.

A detailed survey is carried out. The new survey in addition to the drawings of Erling Gjone is useful to know the overall position of the structural elements and their dimensions (Fig. 5). The main rafters have a rectangular section 12x20 cm, the secondary rafter 12x18 cm, the struts 12x17 cm, the collar beam 12x16 cm and the sole piece embedded in the wall have a section 18x18 cm.

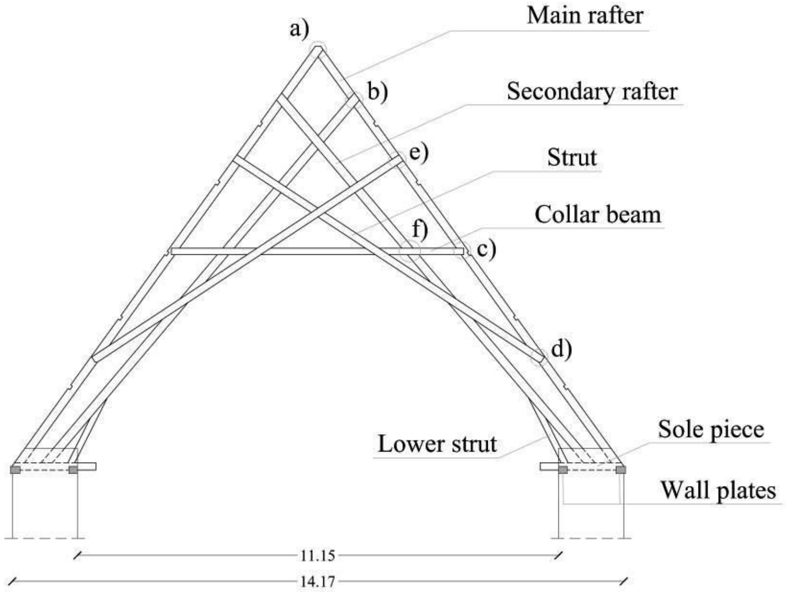

Figure 5: Værnes Church structure.

In Værnes Church, all the connection are made with single or double pegged half lap joints as shown in Fig. 6 a)-f) (the letters in Fig. 6 correspond to the letters in Fig. 5).

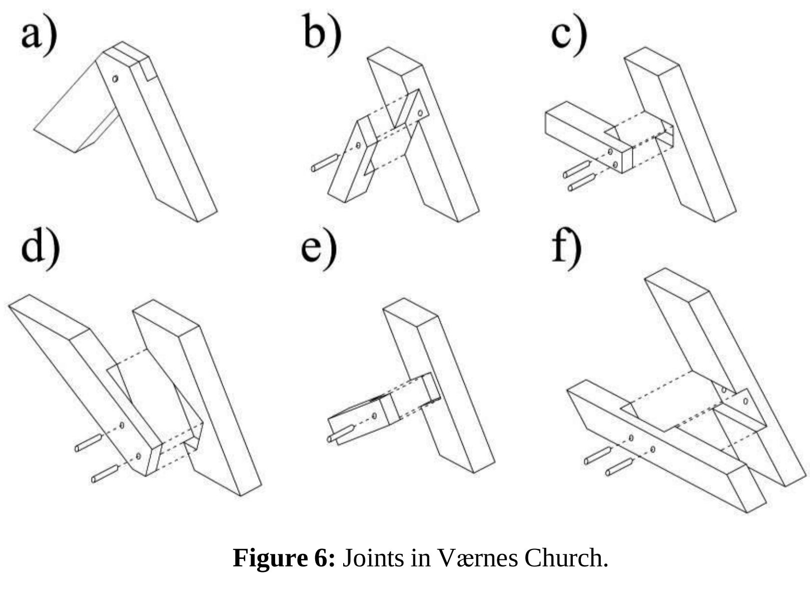

Figure 6: Joints in Værnes Church.

The support of the timber structure on the masonry wall is shown on figure 7. The wall provides the vertical support for both main and secondary rafter. The secondary rafter is joined to the sole piece with a step joint which can transfer horizontal loads. The sole piece is joined to the inner wall plate with a lap joint which also can transfer horizontal loads. The inner wall plate can transfer horizontal loads to the masonry wall by compression. Thus, the secondary rafter can transfer horizontal loads to the masonry wall. The main rafter can transfer horizontal loads through the lap joint in the outer wall plate, but the outer wall plate can just transfer horizontal loads to the masonry walls through friction. Thus, the main rafter and the outer wall plate can slide on top of the masonry wall when the horizontal load exceeds the friction capacity. The lower strut can also transfer both horizontal and vertical loads.

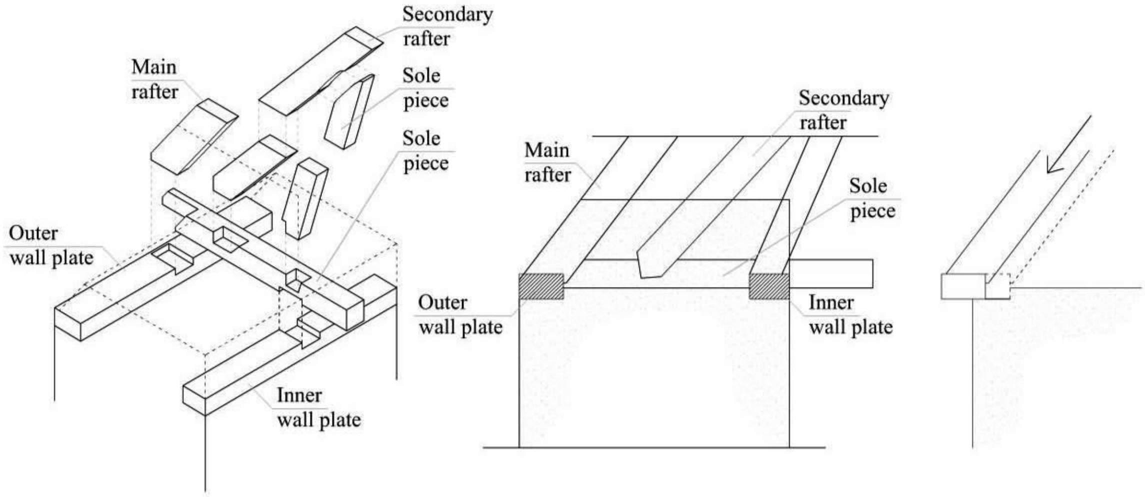

Figure 7: The connection between the trusses and the walls in Værnes church.

The objective of the assessment was to gather information on material and deterioration state and on structure and geometry to evaluate the structural system and the safety. The methodology adopted is shown in Fig. 3 and earlier used in [14]. First an archival research was done to survey the structure geometry using methods described by Tampone, [15], and to understand the load history of the building and the repairs carried out during its lifetime.

The walls were scanned with a 3D laser measuring system (Leica 3D Disto) to investigate if forces from the wood structure could have deformed the walls. The walls were secondly scanned with points in a squared pattern with measurements every 10 cm with an accuracy of 1 mm. The outcomes was two detailed profiles of the two wall sides of the church. The north side of the church had a maximum displacement of about 4 cm compared with a straight line along the top of the wall while the south side showed about 6 cm of maximum displacement. The outer wall plates exhibit a displacement that varies between 3 and 4 cm along the wall. Since they are not fastened to the walls or hold in place by anything, they can shift horizontally so they do not contribute to the horizontal resistance. They simply lay on the walls.

The survey showed that in the beginning, that there were just two layers of wooden boards in the roof stratigraphy. The bottom layer of boards is set from the top of the roof to the bottom, and the top layer is in the longitudinal direction, orthogonal to the bottom layer. The roof configuration was designed to drain the water and prevent infiltrations. The two board layers were bonded together to form a rigid surface with a lot of wooden dowels,[16]. This configuration lasted for about 150 years up to the late 1200s when they added a third level of wood and then wooden shingles. The roof was very light since each layer was just about 3 cm. In 1869, on the northern side of the roof, a layer of stone slates has been added. The southern side was covered with stones in the 1895/96 forcing the structure to work asymmetrically for almost 25 years. In the last intervention, in the 1960s, they completely changed the stratigraphy of the roof again, adding a layer of insulation and other wooden layers.

Two important aspects needed to be assessed on site: the soundness and the strength of the wood. Since the building is cultural heritage, it is subject to several restrictions that prevent the majority of accessible tests for the evaluation of the mechanical properties of the timber truss, thus the soundness of the material was checked through visual inspection, impact sounding by hammer and minimized use of a resistance drilling. The moisture content was checked with hygrometer. The average moisture content of the elements is below 25%. The strength of the timber evaluated with visual grading. The Norwegian standard NS-INSTA 142:2009 in combination with the European standard EN 338 was applied, [17, 18]. The grades refer to commercial classification that differ from the traditional carpentry works, and they can underestimate the true strength of the timber elements, [19]. The elements was classified as C24.

The survey of the structure on site, showed two important interventions. The first, a structural element was placed between the main and the secondary rafter on top of the masonry walls as shown on figure 8b). This element was probably installed in the 1960s, to avoid the development of the observed displacement of the main rafter on the outer wall plate discussed earlier.

Secondly it has been noticed that the joints connecting the main rafters and the struts earlier shown in Fig. 6 d) were reinforced as shown in Fig. 8a).

Figure 8: a) Shifted joint connecting the main rafter and the strut (reproduced with permission from Pasi Aalto). b) Repair intervention installed during the 1960s.

4.2 Structural analysis

In order to perform a preliminary structural analysis of a historic timber structure, a simple model has been chosen. To evaluate the reliability level, the structure analysed according to the Eurocodes. Five main levels of assumptions are to be made: the loads, the material properties, the geometry, the joint behaviour and the supports, [20].

The three different loads on the roof are the dead load, the snow load and the wind load. The five changes through the history in dead load of the roof earlier described is given in table 1 with numbers for the load.

The roof is steep and, on one hand, it prevents the deposition of snow, but on the other hand it exposes a greater surface to the action of the wind. The design rules in the Eurocodes, has been used to simulate the intensity of these loads.

As a result of the assessment, the material properties are based on the values in EN 338 for C24. The geometry is chosen as described in Fig. 5.

A fundamental part of accurate modelling of the structure is the configuration of the joints. Timber joints have a semi-rigid behaviour and a good ductility that make them an excellent solution to transfer the loads, [21-24]. A preliminary analysis was carried out with hinged connections. This was done in order to avoid an over estimation of local forces, [25]. The hinges are located along the elements centrelines not introducing eccentricities in the preliminary model.

Table 1. Dead loads chronology.

	Stratigraphy configuration	Period	Load
1)	2 layers of wooden boards (2 cm thick)	1140 - late 1200s	0.16 kN/m
2)	3 layers of wooden boards + 1 layer of wooden shingles	late 1200s - 1869	0.32 kN/m
3)	3 layers of wooden boards + 1 layer of stone tiles (only on one side)	1869 – 1895/96	Asymmetric load: 0.32 kN/m / 1 kN/m
4)	3 layers of wooden boards + 1 layer of stone tiles (only both sides)	1895/96 – 1960s	1 kN/m
5)	3 layers of wooden boards + 1 layer of insulation + 2 layers of wooden boards + 1 layers of stone tiles	1960s - now	1.4 kN/m

The roof structure is connected to the walls in three points on each side. As a result of the discussions in connection with Fig. 7, the outer supports are modelled as rollers and the other two as hinged support.

The Ultimate limit states (STR) was checked for each stratigraphy (see Tab. 1). The structural analyses were performed on each typology of stratigraphy to observe the evolution of the loads during the life of the structure. Fig 9. shows an example of the results of the analysis for the fifth configuration.

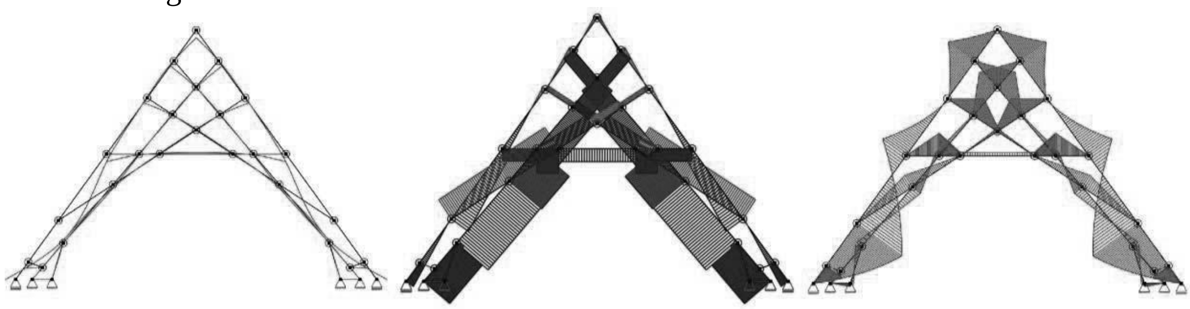

Figure 9: Displacement, axial forces and bending moment diagrams for the fifth configuration.

5 OBSERVATION AND CONCLUSIONS

The assessment done gave a good overview of the structure and was an effective method to understand the complexity of the structural health and behaviour. The method proved efficient in attaining a structural assessment of a historic timber structure.

The grid of joints, the hallmark of the structure typology, reduces the effective length of the elements and also redistributed the bending moments

The structural analysis of the case study, representing the church family, showed that the main rafter works as a continuous beam. The analysis also showed that the secondary rafter carry most of the load in compression transferring forces to the inner part of the top of the masonry wall.

The axial force diagram from the calculations showed that the strut carried load in tension. This type of joint is not able to bear high tensile stresses. The observation of the repaired damage, Fig. 8, confirmed that the connection had been too weak to transfer the tension forces. This point represent a in the design.

The design of the support connecting the main rafter with the top of the wall showed that the outer wall plate was pushed outwards from the edge of the masonry wall. The reinforcement on

Fig. 8 showed that this has been considered as a problem earlier. This support design can be a general problem for the family of churches.

The archive research showed that during the lifetime of the structure, the dead loads on the roof increased and therefore the internal stresses increased as well.

In this evaluation a simple model for the joints is chosen. An accurate study of the joints would be valuable to increase the knowledge on this structural type. In order to study the semi-rigid behaviour of a joint accurately it should be taken into account both axial and rotational stiffness of the joints. Another topic to investigate is the three-dimensional diaphragm effect in the roof. Thus, the study of the outer roof effect on the structure is planned as the next step. The outer roof effect will be studied both with an experimental campaign on wooden dowels and with numerical analysis.

REFERENCES

[1] N. Lombardini, "Assessment of Deformability and Collapse Load of Timber Structures Built According to Treatises of the First Half of Nineteenth Century: the Case of the Truss Structures on the Roof of the Town Hall in Ravenna." presented at the Mechanical Behaviour and Failures of the Timber Structures. ICOMOS IWC - XVI International Symposium Florence, Venice and Vicenza, 2007.

[2] L. T. Courtenay and R. Mark, "The Westminster Hall roof: A historiographic and structural study.", The Journal of the Society of Architectural Historians, pp. 374-393, 1987.

[3] L. T. Courtenay, "Where Roof Meets Wall: Structural Innovations and Hammer-Beam Antecedents, 1150–1250.", Annals of the New York Academy of Sciences, vol. 441, no. 1, pp. 89-124, 1985.

[4] J. Heyman, "An apsidal timber roof at Westminster.", Gesta, pp. 53-60, 1976.

[5] R. J. Mainstone, "The Dome of St Peter's: Structural Aspects of its Design and Construction, and Inquiries into its Stability.", AA files, pp. 21-39, 1999.

[6] R. J. Mainstone and R. J. Mainstone, "Structure in architecture: history, design and innovation.", Ashgate, 1999.

[7] R. J. Mainstone, "The structure of the church of St. Sophia, Istanbul. Science Museum.", 1965.

[8] E. T. Morris, R. G. Black, and S. O. Tobriner, "Report on the Application of Finite Element Analysis to Historic Structures: Westminster Hall, London.", The Journal of the Society of Architectural Historians, pp. 336-347, 1995.

[9] C. Thelin and K.-G. Olsson, "Static Behavior of a Historic Roof Structure.", Journal Of Architectural Engineering, 2005.

[10] O. Storsletten, "Takene taler: norske takstoler 1100-1350 klassifisering og opprinnelse.", Arkitekthøgskolen i Oslo, 2002.

[11] A. Gunnarsjaa, "Norges arkitekturhistorie.", Abstrakt, 2006.

[12] M. Stige, K. E. Pettersson, and K. Hauglid, "Værnes kirke : en kulturskatt i stein og tre.", Stjørdal historielag Instituttet for sammenlignende kulturforskning 2016.

[13] "Archives of the Directorate for Cultural Heritage, Norway. (Riksantikvaren)." ed.

[14] F. Frontini, "In situ evaluation of a timber structure using a drilling resistance device. Case study: Kjøpmannsgata 27, Trondheim (Norway).", International Wood Products

Journal, pp. 1-7, 2017.

[15] G. Tampone, "Il restauro delle strutture di legno: il legname da costruzione, le strutture lignee e il loro studio, restauro, tecniche di esecuzione del restauro.", Hoepli Editore, 1996.

[16] "Værnes kirke 900 år: kirkebygg og menighetsliv i Stjørdal.", Stjørdal: Menighetsrådet, 1985, p. 336 s. ill.

[17] Norsk Standard, "NS-INSTA 142:2009. Nordiske regler for visuell styrkesortering av trelast. Nordic visual strength grading rules for timber.", ed, 2009.

[18] EN 338: Structural timber-Strength classes.

[19] H. Cruz et al., "Guidelines for the on-site assessment of historic timber structures." International Journal of Architectural Heritage, 2013.

[20] N. Van, E. Verstrynge, K. Brosens, and K. Van, "Quality management of structural repair of traditional timber roof structures." in Structural Analysis of Historical Constructions: Anamnesis, diagnosis, therapy, controls: CRC Press, 2016, pp. 209-215.

[21] T. Descamps, Lambion, J. and Laplume, D., "Timber structures: Rotational stiffness of carpentry joints." presented at the Proceedings of the 9th World Conference on Timber Engineering. Portland, OR.

[22] J. M. Branco and T. Descamps, "Analysis and strengthening of carpentry joints." Construction and Building Materials, 2015.

[23] T. Descamps, L. Van Parys, and S. Datoussaid, "Development of a Specific Finite Element for Timber Joint Modeling." International Journal for Computational Methods in Engineering Science and Mechanics, vol. 12, no. 1, pp. 1-13, 2011.

[24] T. Descamps and J. Noël, "Semi-rigid analysis of old timber frames: definition of equivalent springs for joints modeling. Enhancement of the method, numerical and experimental validation." International Review of Mechanical Engineering, 2009.

[25] S. M. Holzer, "Analysis of historical timber structures." in Structural Analysis of Historical Constructions: CRC Press, 2016, pp. 1203-1210.

SHATIS'17
4th International Conference on
Structural Health Assessment of Timber Structures
20-22 September 2017 Istanbul, Turkey

SEISMIC PERFORMANCE EVALUATION OF TRADITIONAL QUINCHA PANELS USING THE CAPACITY SPECTRUM METHOD

Daniel E. Torrealva[1], **Roberto M. Silva**[1]

[1] Pontificia Universidad Católica del Perú

Keywords: Quincha Construction System, Cyclic Tests, Capacity Based Assessment, Capacity Spectrum Method

Abstract

The Historical Center of Lima, a World Heritage city owes its survival to earthquakes, in great part to a timber construction system called "quincha". This lightweight construction system was implemented during the time of the Colony in an attempt to cope with the frequent destructive earthquakes that devastated the city every time.
The system is composed of timber posts spaced every 60cm, a bottom and top timber girders and a woven cane infilled with mud; the surface of the wall is then coated with additional layers of mud plaster and then finished with a fine layer of gypsum. It is widely accepted by the "limeños" that the system is earthquake resistant in spite of being old and frequently poorly maintained.

An experimental evaluation of the seismic behavior of quincha walls from typical houses of the Historic Center of Lima was performed at Pontificia Universidad Católica del Perú. Reproductions of the original system at natural scale were constructed and tested to lateral cyclic load in order to evaluate its in-plane shear stiffness and strength capacity. Twelve specimens were constructed representing two different models from the second and third stories from the Hotel Comercio, a typical house from the Historical Center of Lima. An additional panel was tested under the same type of loads. It was an original quincha panel extracted directly from the second story of the Hotel Comercio.

The experimental results showed that the quincha system has large capacity of lateral displacement without diminishing the capacity to stand the vertical load. The experimental data was later used to compute the capacity/demand ratio using the Capacity Spectrum Method and the Peruvian Seismic Code to determine its seismic performance. The results showed that the structural system of traditional quincha walls possess a wide range of deformation, allowing them to successfully cope seismic demands requested by the Peruvian Code.

1 INTRODUCTION

Historical structures are buildings that survive in the middle of the urban environment and modern buildings. They are recognized as an important part of the culture of a nation because they constitute remembrances and memories of the birth of a society that has been able to survive over time.

Construction in times of the Spanish colony consisted primarily in the use of quincha and adobe as building materials, especially in Lima, capital of the viceroyalty. After the Spaniards arrival to Peru in 1532, the earth buildings - adobe, rammed earth - were replaced by brick and stone constructions, on the lookout for a dignified and majestic city that could live up to a Viceroyalty capital [1]. Nevertheless, after the 1699 earthquake in Lima, authorities demanded to retake the already known constructive system known as quincha - essentially composed of cane, wood and mud - for its convenient characteristics among them for being lighter than current constructions. Furthermore, constructions began to limit the use of adobe to the first story, using quincha for the upper stories [2].

Thus, the proliferation of quincha structural system on the coast of Peru is bound to Peruvian seismic predisposition since it is located in the Pacific Fire Belt, characterized by its intense subduction process between the Oceanic Plate under the Continental.

Although it is accepted that the quincha structural system has a good behavior in response to seismic forces [3], there are no much studies that quantitatively evidence these premises. Therefore, the present article seeks to know the performance of traditional quincha walls against seismic forces represented by demand spectra according to the Peruvian Seismic Code, based on the structural capacity of the traditional quincha walls acquired from experimental results.

2 EXPERIMENTAL TESTING OF REPRODUCED PANELS

2.1 Construction of Specimens

The purpose of the experimental testing was to obtain important information on the capacity of the traditional quincha walls. For this matter, the Hotel Comercio, a representative building of the Historic Center of Lima was chosen as the prototype to create the specimens that would be tested.

Constructions located in the Historic Center of Lima present, in most of the cases, a first story made out of adobe with quincha in the upper stories, ranging from one to three levels at most. The structural system of quincha walls of the upper stories displays different geometric arranges, within which a general pattern stands out: vertical wooden posts joined by an upper and a lower beam. These walls also have timber-stiffening elements within their structural system; the most common are the struts and diagonals [4].

The second level of Hotel Comercio has walls with heights of 4 meters with a stiffener known as “citara” composed by struts at the bottom of the wall, while the third level presents walls of 3.2 meters high with one wooden diagonal as stiffener.

Six panels were constructed replicating the structural system from the second story of the Hotel Comercio, denoted as MA; and six more for the third story denoted as MB.

The construction process of the specimens is similar in both structural systems. The cutting procedure of the wood is required to obtain the posts and beams with its respective transversal section. The distance between posts is typically 60 cm in both systems and its connection with the upper and lower beams is achieved by mortise and tenon joints.

In the case of the specimen with struts, while adobe masonry is added at the bottom of the panel - citara - the rest of the wall is filled with woven cane and mud mortar to be later covered by mud plaster on its surface applying a final layer of gypsum.

In the case of panels with diagonal, the stiffener element crosses the entire panel functioning as a cross brace. Similar to the walls with citara, woven canes and mud mortar are filled, as well as the mud plaster and the layer of gypsum.

Figures 1 and 2 display images of the panels constructive process, whereas Figures 3 and 4 show MA and MB specimens, respectively.

Figure 1: Construction of MA quincha panels. a) assembly of mortise and tenon connection; b) fastening of citara with lower beam and post (using nails); c) mud mortar applied as infilling in the panel

Figure 2: Construction of MB quincha panels. a) assembly of wooden posts with upper beam; b) transversal canes are introduced into the posts; c) view of structural system of third story quincha wall

2.2 Testing procedures

The specimens were tested under lateral cyclic loads with controlled displacement using a servo-hydraulic actuator with a capacity of 490 kN and maximum displacement of +/- 150 mm located at the top of the panels.

In addition to lateral loads, tests also included vertical loads on some of the panels as an additional phase conducted before the application of cyclic displacement. MA3 and MA4, as well as MB3 and MB4, were tested under vertical loads that represent the weight of an external wall. As for panels MA5, MA6, MB5 and MB6, vertical loads were also applied and they represent the weight of an internal wall. At last, no vertical loads were applied in panels MA1, MA2, MB1 and MB2 as shown in Table 1.

The test had considered four symmetrical cyclic phases in every panel; however, slight damage after concluding the phases forced the addition of a final one with a shift of the center of the actuator to provide more displacement capacity in one direction. This additional phase was considered in all MA specimens with the exception for panel MA1 and for specimens MB5 and MB6, as seen in Table 1.

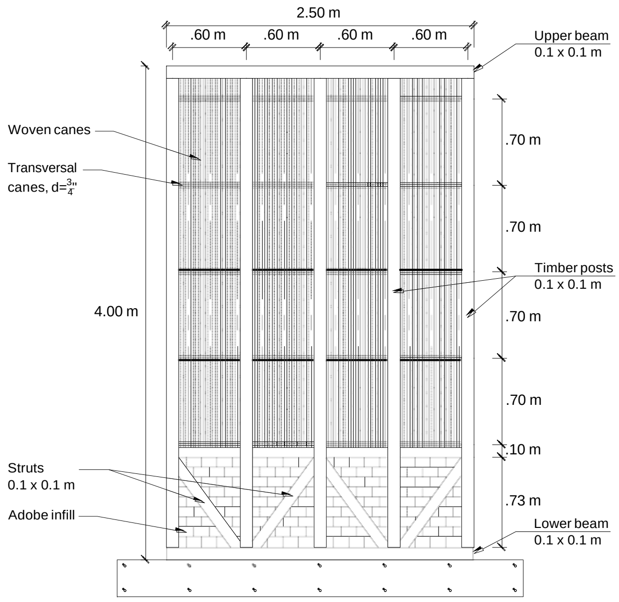

Figure 3: MA panel

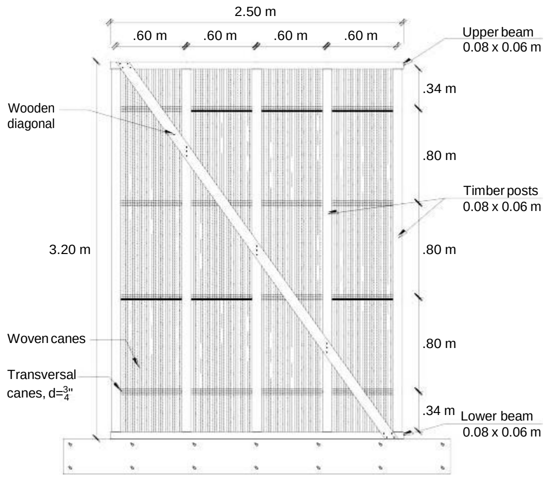

Figure 4: MB panel

Table 1: Test phases in MA and MB specimens.

Specimens	Vertical load (kN)	Max. displacement (mm)				
	Phase 0	Phase 1	Phase 2	Phase 3	Phase 4	Phase 5
MA1	-	+/-25	+/-50	+/-100	+/-140	-
MA2	-	+/-25	+/-50	+/-100	+/-140	+200/-100
MA3	39	+/-25	+/-50	+/-100	+/-140	+250/-50
MA4	39	+/-25	+/-50	+/-100	+/-140	+230/-70
MA5	78	+/-25	+/-50	+/-100	+/-140	+220/-80
MA6	78	+/-25	+/-50	+/-100	+/-140	+230/-70
MB1	-	+/-25	+/-50	+/-100	+/-140	-
MB2	-	+/-25	+/-50	+/-100	+/-140	-
MB3	15	+/-25	+/-50	+/-100	+/-140	-
MB4	15	+/-25	+/-50	+/-100	+/-140	-
MB5	31	+/-25	+/-50	+/-100	+/-140	+300/0
MB6	31	+/-25	+/-50	+/-100	+/-140	+300/0

2.3 Experimental results

The tests performed in MA quincha panels displayed slight damage, presenting the highest deterioration in the layer of mud plaster and perceptible cracks at the location of all timber elements. The mortise and tenon joint became loose because of the cyclic movement, but it always remained in place. Concerning MB quincha panels, the results of their tests displayed similar outcomes regarding MA panels with exception of the aftermath of the stiffener element since the timber diagonal of the panel cracked in both ends at the nailed connection in some MB panels. Even though the wooden stiffener failed, the structure did not collapse at any moment of the test since the mortise and tenon joint was yet working between posts and beams of the structure.

Numeric data obtained from tests allowed the development of hysteretic curves, which for the case of MA6 and MB6 panels are presented in Figure 5 through a basal shear force vs. the displacement at the top of the panel.

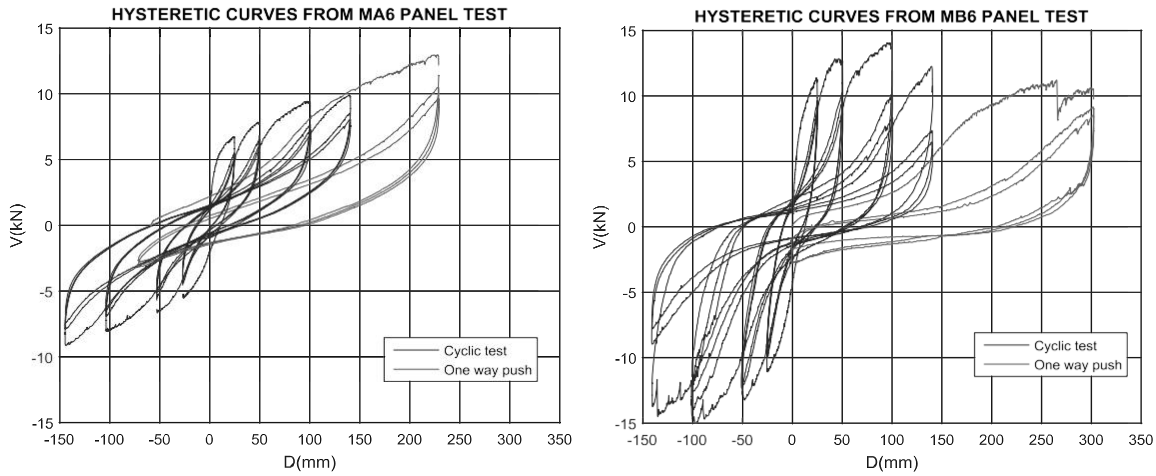

Figure 5: Hysteretic curves from MA6 and MB6 panels respectively, tested under the greatest vertical loads and reaching the greatest displacement of MB panels, for MB6 and the second greatest displacement of MA panels, for MA6

2.4 Capacity based assessment

The performance assessment of quincha panels is attained based on the capacity spectrum method (CSM), which allows the evaluation of the performance of a structure through a graph that relates the seismic demand to its capacity. The purpose of the methodology is to find the point of performance, understood as the demand for displacement of a structure when submitted to a seismic movement [5].

A curve that relates the basal shear force to the displacement at the top represents the capacity of a structure and is generally obtained by a non-linear static analysis, also known as pushover. The cyclical tests carried out on the quincha specimens allow the actual capacity of the panels to be obtained through an envelope from the hysteretic curves, so it is no longer necessary to perform the non-linear static analysis. These envelopes are presented in Figure 6 for all of MA and MB panels.

The CSM demands values of elastic and hysteretic damping obtained from the structure's capacity, so it can take into account the inelastic characteristics of the structure when capacity demands are beyond the elastic range [6]. This is accomplished through damping values known as elastic or viscous damping - inherent to the system - and hysteretic damping, related to the area under the hysteresis loop. These values allow obtaining factors that reduce the seismic demand spectrum, considered as elastic and for a 5% damping, in order to represent an inelastic demand.

Concerning the seismic demand, Peruvian Seismic Code E.030 was used to build the spectra [7] with maximum horizontal acceleration on the ground of 0.25g, 0.4g and 0.5g. These values correspond to earthquakes cataloged as occasional, rare and very rare. Figure 7 shows spectra demand in a format spectral acceleration vs. period.

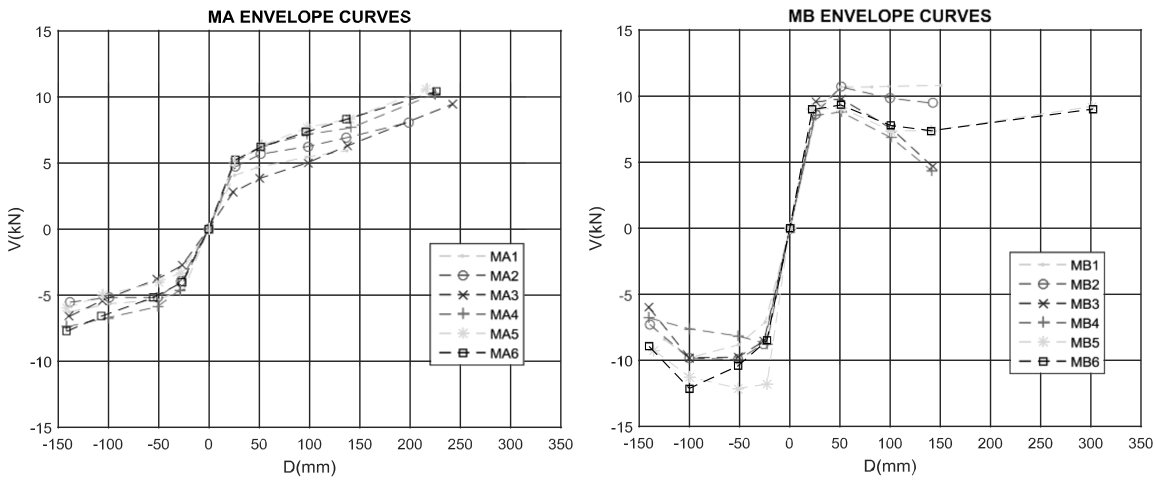

Figure 6: Envelope curves from quincha specimens

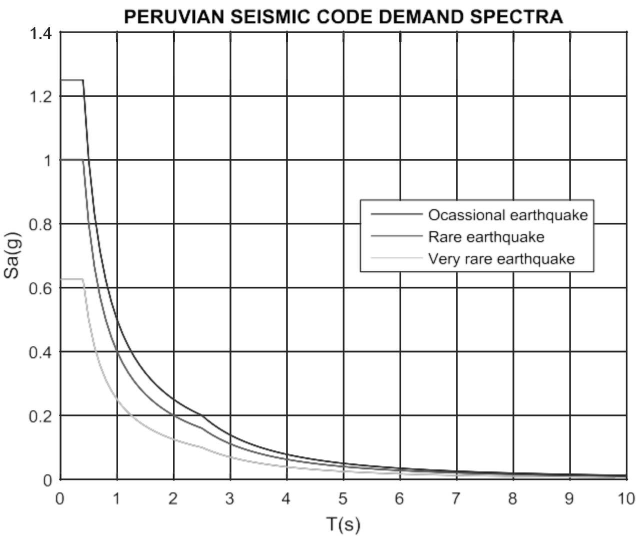

Figure 7: Peruvian Seismic Code demand spectra

After performing capacity based performance evaluation in the quincha panels, a comparison was made between behavior observed and recorded during the tests and the results obtained through the capacity spectrum method. This comparison will allow predicting physical behavior in the quincha wall when subjected to seismic demand.

The performance graphs of the specimens MA6 and MB6 are shown in Figure 8 and Figure 9, where it is possible to observe the performance point of the walls for each level of earthquake among the photographic records obtained during the tests.

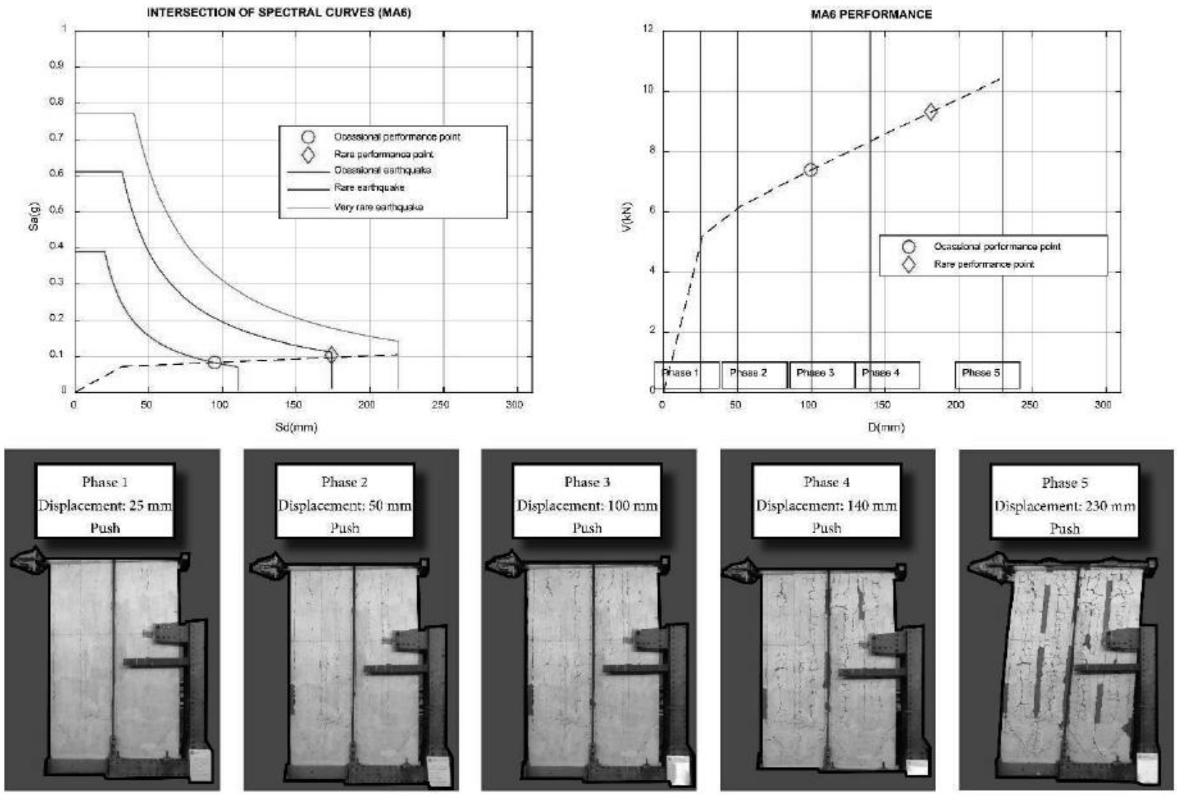

Figure 8: Performance graphs for panel MA6 for Occasional, Rare and Very rare earthquakes. There is no point of performance for Very rare earthquakes since the maximum displacement capacity of the actuator during the test was not enough for the seismic demand

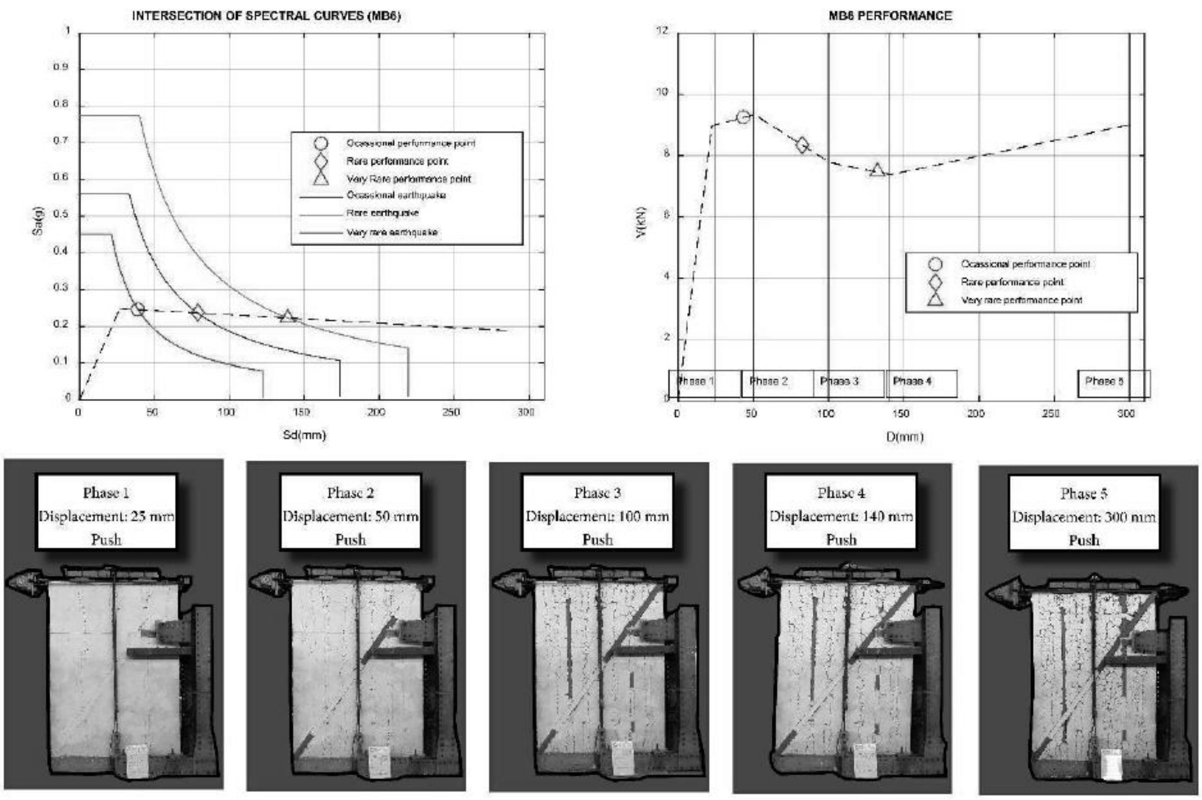

Figure 9: Performance graphs for panel MB6 for Occasional, Rare and Very rare earthquakes

3 EXPERIMENTAL TESTING OF ORIGINAL QUINCHA PANEL

3.1 Original Specimen

A final test was conducted on a wall directly extracted from the second story of Hotel Comercio. The panel was 4.72 m high, 2.72 m wide and 20 cm thick. Since the panel belonged to the second story of the building, its structural system possessed the posts, beams and struts representative for a traditional quincha wall.

Initially, the aim was to extract the panel intact for which the mud was removed from the surface of the wall with the objective of reducing the weight of the structure. Since the panel was still heavy to handle at such height and given the collapses occurred on this story, disassembling of the panel was the way to proceed.

The process started by pulling off the upper beam enabling the removal of canes and posts and lastly extracting the sill plate from the wall. All elements were kept separated and registered so they could be distinguished from each other in the reconstruction process.

For the assembly of the wall, the sill plate and upper beam were identified at first. The upper beam had to be replaced for its deplorable condition. Its replacement was taken from the rubble of the collapsed area at the Hotel Comercio, with characteristics similar to the replaced element. The main timber frame was assembled from posts and beams through mortise and tenon joints. Then, canes were placed horizontally through the posts; vertically canes were also plaited.

Once the assembly was over, the frame was bolted to a wooden beam located at the bottom of the wall in order to provide stability. Then, two rows of brick and seven rows of adobe blocks were placed in the bottom of the wall with one-inch thick mud mortar to perform the union of the bricks. Finally, the surface of the panel was settled by mud and straw in two stages. The first step placed a thick layer of mud among the canes, reaching the bottom of the posts; while the second, the layer was coated in order to patch the cracks originated by the contraction of the mud. A layer of plaster was applied on the surface of the wall, with the intention to perceive the cracks during the test and point out these fissures with the help of colored chalks. Figure 10 illustrate the obtainment of the original specimen.

3.2 Testing procedures

The original quincha wall was denoted as MC and alike as MA and MB tests, it was submitted to four phases; three of them were symmetrical cyclic phases reaching displacements of 30, 60 and 140 mm. The last phase was performed moving the center of the actuator to provide more displacement in one direction, reaching 290 mm in a single direction. There was no vertical load applied to the panel.

3.3 Experimental results

Through the first two phases of the test, the specimen demonstrated cracks in the mud plaster at the surface of the wall. They were more visible in wooden elements; posts, beams, strut and in places where the horizontal canes were placed. The third phase caused loss of mud coating in certain areas of the panel and an uprising of 2 cm from the mortise and tenon joint, among the outermost posts and lower beam. The last phase, enlarged the existing cracks, clearly displaying the structural system of the panel; greater - but not considerable - mud detachment occurred as well, and a lifting of 7 cm befell in the connection of extreme posts and lower beam.

A graphic of the hysteretic loops obtained from processing numeric data from the tests is presented in Figure 11, along with its correspondent envelope.

Figure 10: Extraction of original quincha panel. a) original location of the specimen: second story of Hotel Comercio; b) disassembling process began by extracting upper beam; c) assembled timber frame from original panel

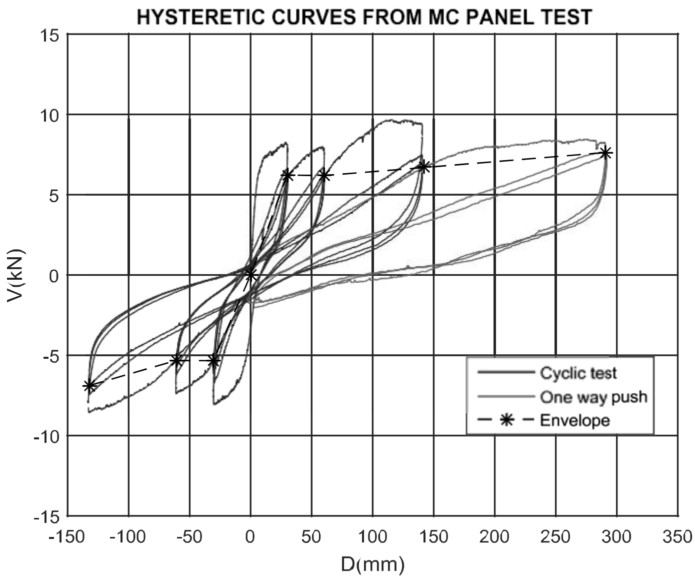

Figure 11: Hysteretic curves from MC and the envelope obtained

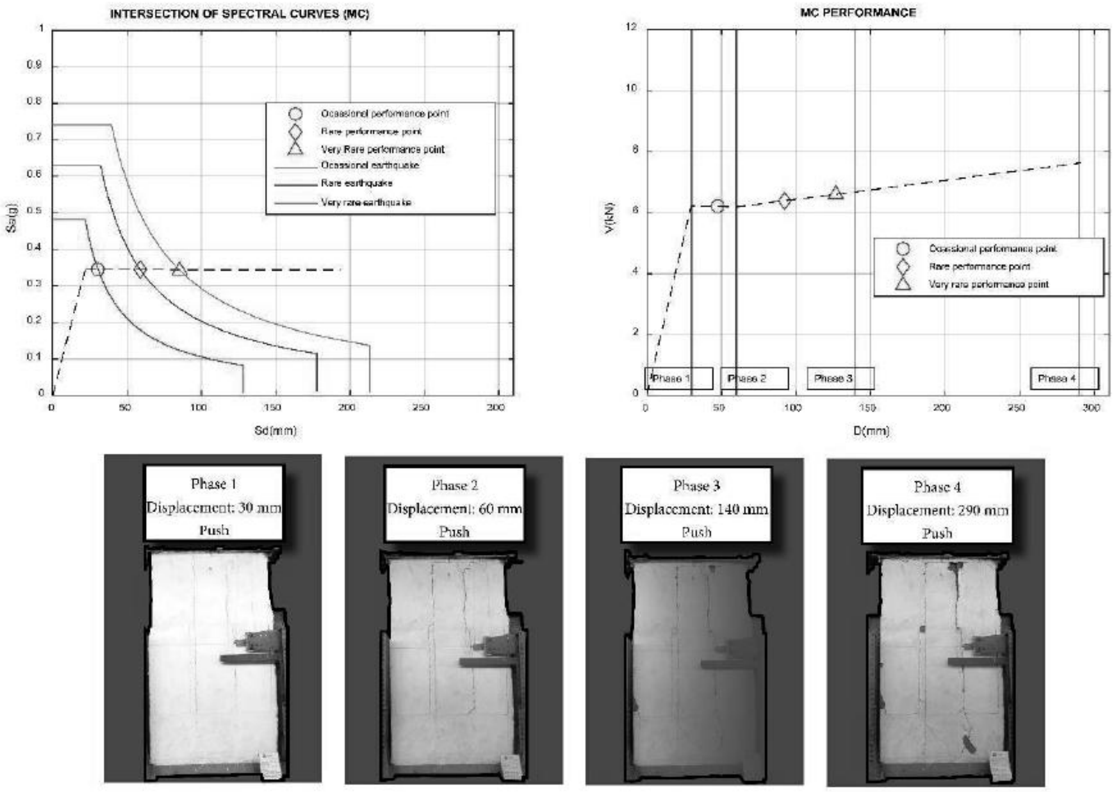

Figure 12: Performance graph for MC panel for Occasional, Rare and Very rare earthquakes

3.4 Capacity based assessment

The capacity spectrum method was applied as well in the original wall to analyse its performance against seismic loadings. The results show the wall possesses the capacity of displacement to cope with occasional, rare and very rare earthquakes in the range of non-linear behaviour.

Figure 12 shows the original quincha panel - MC - would demand, for an occasional earthquake, a displacement capacity similar to the displacements applied in Phase 2. Regarding rare and very rare earthquakes, the required displacement is lower than the assigned for Stage 3 of the cyclic tests.

There was no damage of the structural elements throughout all phases of the test, nor considerable detachment of the covering, as seen in the photographic record of Figure 12. The actuator’s capacity for displacement is not enough to generate collapse in the original wall.

4 COMPARISON OF RESULTS

Results were compared among those walls that presented similar conditions during their tests. Panels MA1 and MB1 were chosen to compare with MC since they were tested under no vertical load.

Since the panels had different dimensions, the curves were plotted using lateral force per unit width against the angular distortion. Figure 13 shows capacity from panels MA, MB and MC, where the higher lateral force capacity is achieved by the wall with the timber diagonal. Panels MA and MC possess similar structural typology therefore their capacity is similar, although MC has a slightly higher capacity.

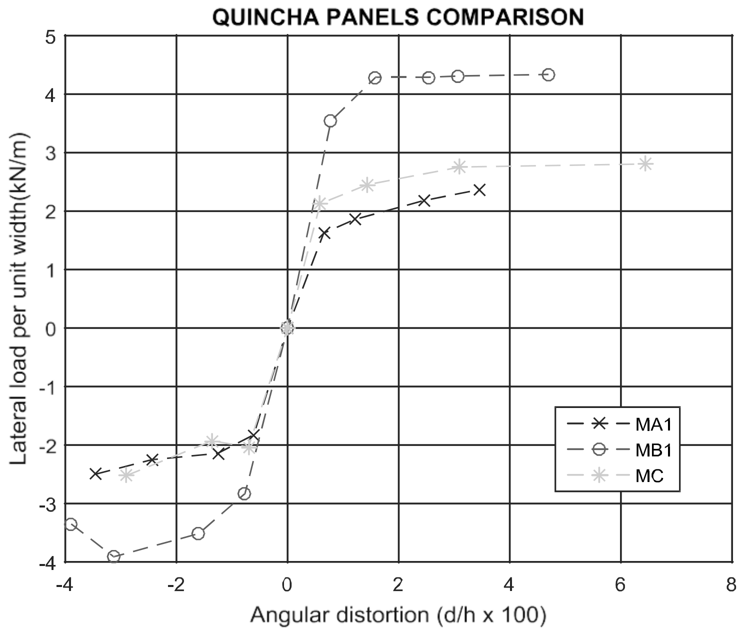

Figure 13: Capacity from MA, MB and MC panels

Envelopes from MA and MB specimens displayed in Figure 6 provide important information regarding the behaviour of quincha panels for both typologies tested. MA panels show similar resistance to lateral loads despite the vertical load applied while tested, reaching a maximum lateral force of 10.6kN achieved by MA5 wall. Initial lateral stiffness is also similar in all of the walls, obtaining an average in both directions of analysis of 0.17kN/mm for panels with no vertical load, 0.14kN/mm for external walls and 0.17kN/mm for internal walls. Concerning MB specimens, the behaviour is similar while analyzed in elastic range; however, there is a marked difference between the capacities of the walls depending on the type of vertical load applied. The lower resistance was observed in the walls that carried the greater vertical load (internal walls), while the walls with no vertical load applied, achieved the highest resistance. This difference is not clearly visible in the negative direction of displacement tested. For a 150 mm displacement, the maximum lateral force reaches a value of 10.84kN, while for a 300 mm displacement, the lateral force achieved is 9kN. Lateral stiffness is very similar in the positive direction of displacement of the test, while on the negative side that statement does not occur. Internal panels have an average stiffness of 0.42kN/mm in both directions of analysis, 0.36kN/mm is the stiffness for external walls, while 0.33kN/mm for panels with no vertical loads.

Figures 8, 9 and 12 show the results relative to the capacity based assessment performed in the panels. The three panels show enough displacement capacity to cope with occasional and rare earthquakes in the non-linear range. In the case of the MA6 wall, cyclic displacement tests do not offer enough information to recognize the performance of this panel against very rare earthquakes because the maximum displacement of the actuator during the test was not enough to reach the point of performance; nonetheless, the panel had capacity to endure higher displacements as it was not near failure. Both the MB6 wall and the MC wall show enough displacement capacity to deal with very rare earthquakes. MB6 has an approximate displacement of 130 mm, which is less than the displacement applied during phase 4 of the cyclic test. Finally, MC panel requests a displacement of approximately 127 mm for the very rare earthquake, less than the 140 mm of displacement applied during phase 3 of the test.

5 CONCLUSIONS

From the experimental tests and the assessment performed in the historical panels, it is concluded that the traditional quincha walls have the necessary displacement capacity to cope with the demands of the design earthquakes according to the Peruvian seismic- resistant standards E.030, in the three levels of intensity analyzed. It is worth to remember that the experimental tests were performed under controlled displacements and none of the panels reach failure under testing. This indicates that, despite not having obtained a performance point, as it is the case of the wall MA6, the walls would not collapse for a demand of very rare earthquake.

The performance of the walls against the design earthquakes was found within their nonlinear range, meaning that they suffer from damage as reported in the photographic records. The hysteretic curves obtained from each of the walls show a great capacity to dissipate the energy that comes from the seismic demands, so the damages are minor and do not seriously compromise the structural system of the panels.

6 ACKNOWLEDGEMENT

The authors are grateful to the Seismic Retrofitting Project (SRP), a project carried out through an agreement between the Getty Conservation Institute (GCI) and the Pontificia Universidad Católica del Perú (PUCP) in which the experimental testing was performed. The authors would also like to thank Alexis Rossi, Oswaldo Sáenz, María Lourdes Mogollón, Diego Relagado and Christian Chacón for their contributions in the testing of the panels.

REFERENCES

[1] Schilder, C. 2000. "La herencia española: las bóvedas y cúpulas de quincha en El Perú". In *Actas del Tercer Congreso Nacional de Historia de la construcción*. Juan de Herrera Institute, Sevilla, Pp: 1019-1026.

[2] Linder, A. 2002. "El Primer Reglamento de Construcciones Asísmicas". In *Revista Ingeniería Civil Año 6 N°27-2002*. Cabildos de Lima, Lima, Tomo 33.

[3] Diaz, A. 1984. "Prefabricated Cane Lathing Construction System". In *Informes de la Construcción*. Number 36. Pp: 25-34.

[4] Torrealva, D. and Vicente, E. 2012. "Proyecto de Reforzamiento Sísmico: Evaluación experimental del comportamiento sísmico de muros de quincha del Centro Histórico de Lima - Perú". In *11th International Conference on the Study and Conservation of Earthen Architectural Heritage*. TERRA 2012. Lima. Pp: 23-26.

[5] Bonett, R. 2003. "Vulnerabilidad y riesgo sísmico de edificios. Aplicación a entornos urbanos en zonas de amenza alta y moderada". In *Departamento de Ingeniería del Terreno, Cartografía y Geofísica*. Universidad Politécnica de Catalunya. Doctoral Thesis.

[6] Comartin, C. And Niewiarowski, R. 1996. "Seismic evaluation and retrofit of concrete buildings". In *Applied Technology Council*. Redwood City. California.

[7] NTP E.030. 2016. "Norma Técnica E.030 Diseño Sismorresistente". In *Proyecto de Norma Técnica de Edificación E.030*. Lima. Perú.

SHATIS'17
4th International Conference on
Structural Health Assessment of Timber Structures
20-22 September 2017 Istanbul, Turkey

PROBLEMS OF DURABILITY IN TIMBER STRUCTURES UNDER USE CLASS 2 CONDITIONS

A. Lozano[1], D. Lorenzo[2], M. Alonso[3], J. Benito[4]

[1] University of Oviedo

[2] University of Santiago de Compostela

[3] University of Oviedo

[4] Tecnalia Research and Innovation

Keywords: Timber structures, Use Class 2, Condensation, Decay

Abstract

Last years a number of pools and wineries have been built using timber elements, due to the good performance of this material in atmospheres with of aggressive chemicals, those are much more harmful to other structures such as concrete or steel.

However, lately there are appearing degradations by wood destroying fungi or termites in buildings of this type, several of which have even collapse. The origin of these kinds of degradation was not related to water leaks, but to the condensation of the water vapor over the steel connections and other construction elements without thermal insulation.

The paper shows three different examples of degradations by decay organisms in timber structures under conditions of Use Class 2, the sand presents the results of the experimental study of the reasons that have caused such damages, including the measurements of the indoor air conditions and other non-destructive tests carried out on each building.

1. *INTRODUCTION*

Use Class concept is based on differences in environment exposures that can make the wood susceptible to biological deterioration. Indoor or covered swimming pools and wineries are examples of Use Class 2 according to European Standard EN 335: 2013 [1], situations in which the wood is under risk of occasional wetting and therefore there is a real possibility of attacks by wood destroying fungi or even termites, depending on the air temperature, relative humidity (RH), design and maintenance.

In the case of covered pools structures, built in sawn and glued laminated wood fir (*Abies alba*) and spruce (*Picea abies*) during the last years there had been detected a certain number of constructions in Spain of this kind, that had suffered several wood decay attacks. In some cases damages were so critical and the safety of the structure was so affected, that closing of the building was mandatory.

This paper shows three cases of biological deterioration in covered pools built in different points of the geography of Spain.

The first one was built in the 1980s, but the other two were less than twenty years old. However, in all cases, first damages had appeared with less than ten years of service life.

As it can be seen, regardless of the region, the warm and humid environment of the indoor heated swimming pools, combined with an incorrect design of the building so that thermal bridges were formed in certain areas, were the origin of the degradation of the timber components. In these three cases the level of destruction was such that there was no choice but to replace most of the affected wood elements.

Therefore, the objectives of this paper are to understand the cause of the early severe decay, so that these types of buildings are properly designed not only by experts in structural wood, but also by professionals of the air conditioning, in order to guarantee the maximum durability for the construction.

2. WOOD SERVICE LIFE

2.1 Durability and treatability of sawn and glued laminated wood

Sawn and glue-lam wood, due to its organic nature, are supposed to be degraded and returned to nature because of the degrading action of biological and/or abiotic agents that directly or indirectly are involved in its degradation.

Biological agents are composed by living organisms that degrade wood, including moulds, wood disfiguring fungi, wood destroying fungi, wood destroying insects and marine borers; and abiotic comprising mainly to atmospheric agents, i.e., the sun and rain, as well as chemicals products.

They are responsible for attacks that cause reductions in the resistance of wood elements and consequently their physical and mechanical properties that should be taken into consideration when using the wood and its protection.

The action of wood destroying insects is characterized by perforations and tunnels, while fungi attack produces a variety of defects, including destruction of anatomical elements. Abiotic agents themselves do not cause serious damage.

However unsuitable environmental conditions, particularly high temperature and humidity of the inner air, allow biological agents attacks and affect the final service life of certain indoor timber constructions. In addition, the indirect action of water on structural elements (water from condensation), leads to the appearance of fungal decay. So that means that good indoor conditions and correct thermal insulating (in order to avoid thermal bridges), are a key element to consider on the construction and design of covered swimming pools, wineries and other buildings with similar environmental conditions.

The natural durability of wood species is defined as the inherent resistance to attack by wood destroying organisms, while the treatability is the ability which a liquid penetrates inside the material.

In terms of biological susceptibility, fir and spruce are classified as not durable heartwood (durability class 3-4 with regard to fungal decay as reported in the European Standard EN 350:2016 [2]) which means that their longevity without any preservative treatment for outdoor purposes, may be limited.

However, when we talk about covered constructions, the choice of wood species with good natural durability is not a priority to be considered. And the same happens with the implementation of a preventive preservation treatment.

Unfortunately, in terms of treatability, fir and spruce are classified as very difficult wood species to treat (treatability class 3 with regard to classification in the European Standard EN 350[2]), which means that their longevity without any preservative treatment for environmental conditions where the development of wood destroying fungi is possible, should be limited.

2.2 Indoor air conditions and thermal insulation

High temperatures and RH, make possible the formation of interior condensations that allow the development of fungi decay of wood used in covered pools structures.

Despite the great variations among geographical locations, the consideration of correct indoor climatic conditions inside this kind of buildings and their insulation are a key step in the service life of the structure. That means that the risk for wood components in this type of pools to be moistened due to condensation water depends on local climatic conditions.

In Spain, with the exception of most of the Canary Islands and certain areas of the south of the peninsula, in any construction of the rest of the country there can be indoor condensations in covered swimming pools.

Moreover, all the wood decay organisms are present in Spain, including fungi, insects and marine borers. It has been precisely this diversity of wood species, constructive designs and construction procedures, combined with similar hygrothermal parameters of the inner air inside covered pools, which has led to the emergence of associated pathological processes of decay fungi and insects attacks.

Therefore, the most important parameters to evaluate are the accuracy of projects details related to thermal bridges and the correct renovation of the indoor air.

2.3 Design of the enclosure and joints

Another very important item to ensure service life and the good performance of timber structures exposed to Use Class 2 is the design of the building enclosure. This factor includes design details related to breaking thermal bridging, cross sectional area of the thermal bridge, condensation control, etc.; and above all, the choice of materials with low thermal conductivity, specially through the outer insulation layer.

Regarding covered pools, one problem focuses precisely in the retention of the condensation water. This pathological process occurs in the joints between wood elements and other water trapping points, due to the incorrect design details. In those parts where water is retained, rots, fungi fruiting bodies and serious damages are frequently observed. The problem is especially severe in parts with more unfavorable situation (water traps located in poorly visible or inaccessible zones), with rot damages to the point that sometimes have come to completely degrade all the pieces by wood destroying fungi, which directly affects the structural safety of the structure.

Because all these questions it is really important to design the connections between the different construction elements on the purpose to avoid the retention of water, and ensure ventilation and rapid evacuation of water. This matter should be especially taking into account in the main structural components and joints, in order to avoid the water traps. The examples that will be shown below perfectly serve to understand the relevance of this issue.

2.4 Standards

The European Standard EN 350:2016 [2] provides information on the natural durability of wood species of importance in Europe. The European Standard EN 335: 2013 [1] defines the use classes, and also provides information on biological agents susceptible to attack the wood. The European Standard EN 460:1995 [4] indicates the requirements for wood to be used in use classes.

In the case of CTE [3] (Technical Building Code), the basic document of Wood Structural Safety of Spanish Building Technical Code (CTE-SE-M), in paragraph 3: "Durability", reflects the different use classes for wood elements that are part of the structure of a building; and also can be applied to timber bridges.

3. DECAY IN TIMBER STRUCTURES OF COVERED POOLS: CASES OF STUDY

Three different structures, corresponding to as many covered swimming pools, constructed with timber elements and located in three Spanish regions, have been surveyed: two of them are located in the north of the country (Galicia and Cantabria – Figures 1 and 2), and the third one in the interior (Burgos).

Figures 1 and 2: timber structures of the pools located in northern Spain

In these three particular cases, all these buildings were built between eighties and nineties, used fir and spruce wood structures (solid and glue-lam main beams), and early decay problems due to wood destroying fungi began after only less than ten years of service life.

Damages appeared in all their timber elements, including the main structural pieces, and they were always similar, regardless of the location of the building: severe loss of resistant section in the main beams (Figure 3), that had caused the collapse of some of them (Figure 4). It was also possible to observe rots, which were most noticeable in connections and joints between main and secondary beams (water trapping – Figures 5 and 6). Fungal mycelium was even visible on the surface of different wood elements (Figures 7 and 8).

Figures 3 and 4: severe damages (Cantabria´s pool) and collapse of the main beam (pool in Galicia)

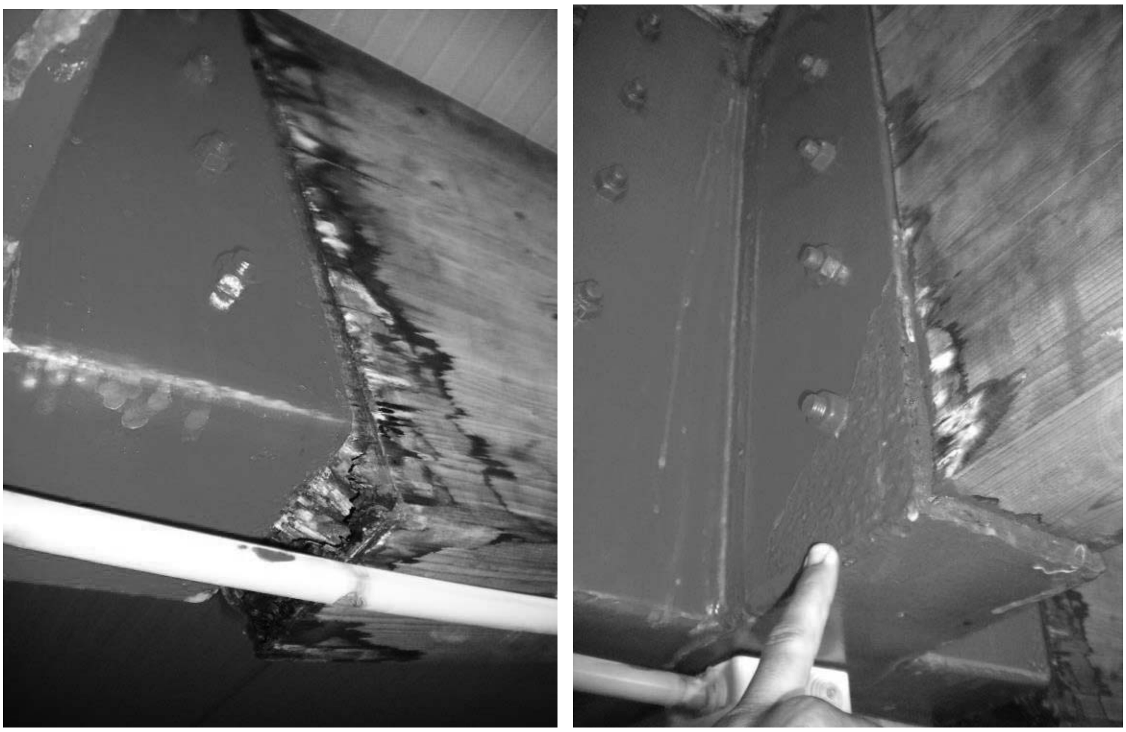

Figures 5 and 6: important fungal decay in the water traps (swimming pool in Galicia)

Figures 7 and 8: important fungal decay in the water traps (swimming pool in Burgos)

In addition, there was also significant local crushing of the heads in some beams, which showed that there were serious damage caused by rotting fungi (Figures 9 and 10).

Figures 9 and 10: local crushing in the heads of main beams (swimming pool in Burgos)

During these inspections it was found that in addition to the water traps, the presence of moisture spots in different areas was also observed, coinciding in many occasions with the joints between enclosure panels (Figures 11 and 12). However, in none of these cases were detected degradations by fungi, no doubt because at these points there were no joints that favored water retention.


Figures 11 and 12: water spots in different timber elements and absence of damages
(Swimming pools in Burgos and Galicia, respectively)

Finally, moisture content of all these elements was measured using both resistance and capacitance devices. Values above 30% where always detected near the metal joints (Figure 13). In cases where there were doubts about the level of damage, a resistograph instrument was used to analyze the extent of the fungal decay (Figure 14 and 15).

Figures 13 and 14: measuring the moisture content and resistograph device (swimming pool in Galicia).

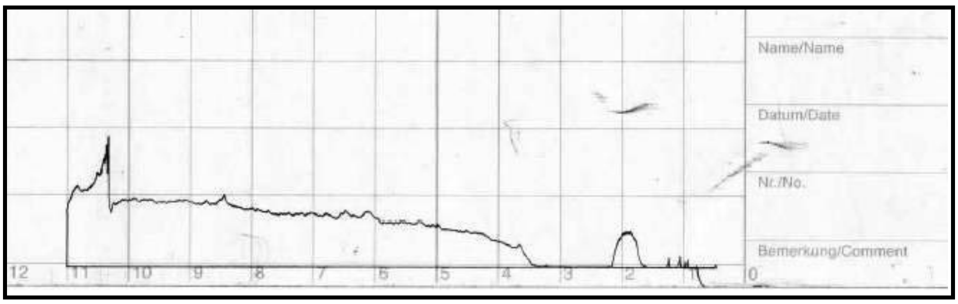

Figure 15: information about the decay of the timber beam near the joint (swimming pool in Galicia).

Therefore the degree of damage to the timber elements on these buildings was directly related to the design details and connections (thermal bridges and water traps), the humidity of the inner air, the wood species used in their structure, the impossibility of applying preventive preservative treatment, and the climatic conditions of middle and northern areas of Spain.

At the end, the situations of these three installations presented so severe wood decay attacks and were so critical, that the closing of them due to several structural damages was mandatory.

So the influence of the lack of maintenance should always be considered, otherwise it would have allowed to stop the deterioration of the structures, avoiding the replacement of the pieces.

4. ON SITE SURVEY

After analyzing the damage level of the structures, the immediate corrective measures were considered in order to allow keeping the swimming pools in use.

Subsequently, surface thermometers were placed at certain points in two of these buildings (pools in Galicia and Burgos), in order to check if there were indeed condensations on several points of the enclosure panels. The choice of these points was determined precisely from the visible water spots on some wooden beams (see Figures 11 and 12 above).

The equipment remained in operation over a period of time ranging from four and five months, depending on the building.

These data, together with the humidity and temperature registers of each installation, allowed studying the possibility of condensation humidity occurring on certain points of the enclosure. And that was precisely why water would appear on several joints and connections.

The graphs below show (Figures 16 and 17) the results obtained in the pools of Galicia and Burgos, respectively. As can be seen, condensations occur continuously and consistently over all months, including the warmest ones. So in this type of installations, the control of the interior environmental humidity and the design of the enclosure to avoid the thermal bridges, are decisive factors to guarantee the durability of the structure.

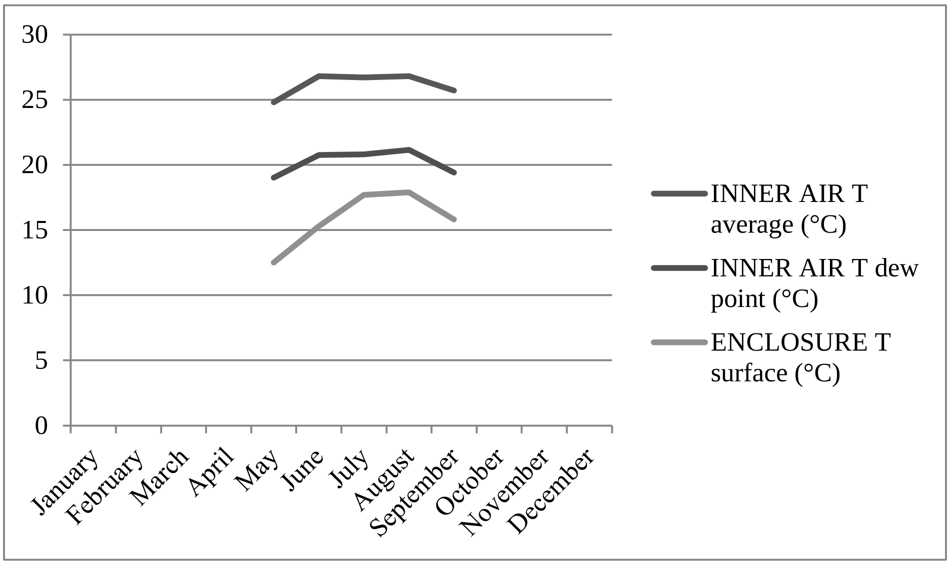

Figure 16: on site survey results (swimming pool in Galicia)

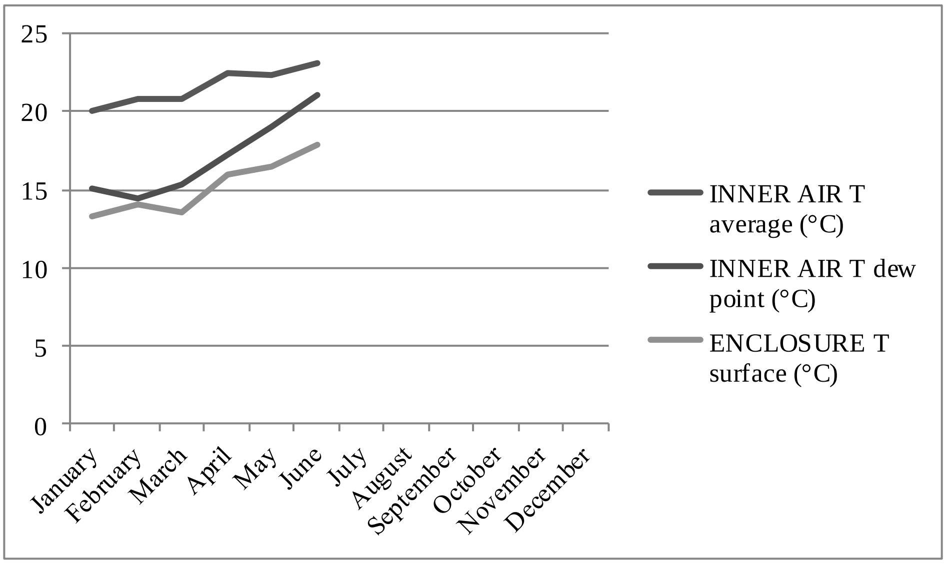

Figure 17: on site survey results (swimming pool in Burgos)

5. CONCLUSIONS

Currently in Spain serious structural damages are being detected in several covered pools built during the 80-90s with wooden structure. In most cases, the problems are due to fungal decay and are located in the joints between beams.

The origin of these damages is related to the retention of the water from the condensation, on the steel connections of the mentioned unions. This means that these are a really Use Class 3 situation, instead of a 2. In contrast, other areas where there was ventilation, only aesthetics or disfiguring stains and muds have been observed, but no decay or loss of mass.

In addition, in the three cases analyzed, the species used had been fir and spruce, which further aggravated the situation, due to its low durability and difficult treatment. Both have a low natural durability according to the standard EN 350:2016 [2], so these wood species are not proper in use classes related to high moisture content, due they are not durable and it should be necessary to apply a protective preservative product, according to EN 460:1995.

And in terms of treatability, fir and spruce are classified as very difficult wood species to treat (treatability class 3 with regard to classification in the European Standard EN 350:2016 [2]). Currently the CTE[3] does not allow to use a non impregnable wood specie above use class 3.1.

Therefore, with regard to wood structures used in covered swimming pools, and in general for buildings exposed to a Class of Use 2, it is recommended:

- Carefully analyze and solve properly the possible thermal bridges that exist in the envelope of the building.
- Check the indoor humidity.
- Design joints and connections, avoiding water traps. All the variables that can affect an increase in moisture content of the structural component have to be considered to prevent fungal decay and help to achieve the desirable service life of these interior structures in these geographical locations. The design of details is crucial for the durability of covered swimming pools. In case of doubt, provide joints with drainage holes or construction details that have the same effect, similar to those defined for EN ISO 12944 - 3[5] steel structures.

- In certain cases, design the structures so that the sawn and glue-lam wood would be placed in use class 3. Perhaps should be interesting to consider the using of wood species with enough natural durability; or likely to improve with the application of preventive preservative treatments, in order to increase their natural durability.
- This consideration should be absolutely necessary in covered swimming pools with low efficiency air renovation systems.

REFERENCES

[1] EN 335:2013. Durability of wood and wood based products. Use classes: Definitions, application to solid wood and wood-based products.

[2] EN 350: 2016. Durability of wood and wood based products. Natural durability of wood. Part 2: Guide to natural durability and treatability of selected wood species of importance in Europe.

[3] CTE Technical Building Code. Government of Spain, Madrid, 2009.

[4] EN 460: 1995. Durability of wood and wood-based products. Natural durability of solid wood. Guide to the durability requirements for wood to be used in hazard classes.

[5] ISO 12944-3:1998. Paints and varnishes. Corrosion protection on steel structures by protective paint systems – Part 3: Design considerations.

SHATIS'17
4th International Conference on
Structural Health Assessment of Timber Structures
20-22 September 2017 Istanbul, Turkey

STRUCTURAL ASSESSMENT OF TIMBER HANGING TRUSS IN SALT MAGAZINES IN PAG

Juraj Pojatina[1], MSc; David Anđić[1], MSc; Prof. Hrvoje Turkulin[2], PhD; Assist. Prof. Marin Hasan[2], PhD

[1] STUDIO ARHING Ltd., Zagreb, Croatia

[2] University of Zagreb Faculty of Forestry, Zagreb, Croatia

Keywords: Assessment, Structural Timber, Salt Magazines, Restoration

Abstract

The examination, research and evaluation of historical trusses in Pag, Croatia was implemented in 2016. In this assessment project, vernicular roof structure of salt magazines was evaluated. Magazines were built between 17th and mid 19th century. The hanging truss is composed of two rafters and tie beam with central post and two diagonal members. The main purpose of the assessment was to examine the impact of aging and salt on wooden construction elements in order to restore and reinforce the existing structure. As assessment tools, visual examination, sampling and laboratory testing were performed. Laboratory tests included examination of the physical properties of withdrawn samples: density, growth-ring width, proportion of latewood, determination of timber strength class, determination of moisture content, and biological soundness assessment of samples using "screening-test" for fungal infestation or colonisation.

As a result of visual examination, various deficiencies were determined: missing central posts of the hanging trusses followed by substantial deformations, moisture content of wooden members, metal connections yielding and metal connectors' corrosion. Salt induced severe surface degradation of timber beams. According to the tradition of building with wood at that time in the region of island of Pag and according to the macroscopic properties of taken specimens, wooden constructions were built of Scots pine (Pinus sylvestris) and black pine (Pinus nigra) with strength class of C50.

With completed research results and visual examination outcomes, a thorough plan for future designing activities for reinforcement and restoration is given. Reinforcement techniques and tools are adjusted according to damage grading and possibilities of restoration. Strengthening of existing roof members, metal connections replacements and full or partial replacements of wooden hanging truss members have been proposed.

1 INTRODUCTION

Salt magazines in Pag is a nine-unit warehouse complex linked together with roof passages (Fig. 1 and 5). Magazines were built from 17^{th} to 19^{th} century. Three central magazines were built under Republic of Venice around year 1632. Pag salt pans were the largest salt producer in Republic of Venice. Rest of the complex was built during Austro-Hungarian Empire around the year 1845 [1]. Salt from nearby salt pans was stored in these magazines until the second half of 20^{th} century. It was assumed that the lack of storage space forced workers to overfill the existing magazines and partially cover the trusses with salt. Three western magazine units were assessed. Length of each magazine unit is around 41.0 m with various widths of 10.4 – 11.7 m. Structurally, magazines consist of stone perimeter walls with thickness of 125 – 200 cm and timber roof trusses.


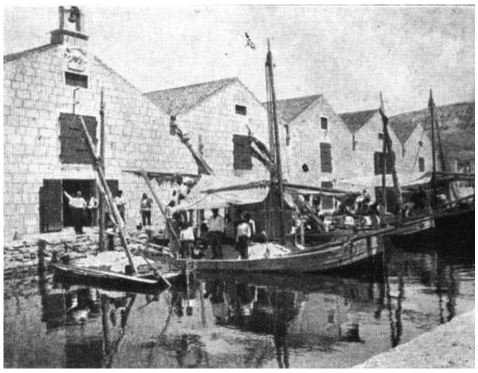

Figure 1: Salt magazines, Pag (left photo taken in 2016, right photo taken in 1923)

2 STRUCTURAL CONCEPT

The roof structure of existing magazines was assessed and examined. It is a typical hanging truss with 1.3 – 1.6 m spacing between the trusses. Clear span of roof structure is 10.4 – 11.7 m. Height of the truss at ridge is 3.45 m. Hanging truss consists of rafters, tie beam, central post and two diagonal struts supporting the rafters at 2/3 length (Fig. 2, 3 and 4). Joints were designed as traditional carpentry joints. Hanging central post and tie beam were joined together with an iron stirrup (tension connector). Trusses are supported on continuous timber wall beams around the perimeter of each magazine. Cross-sections of truss members are 32×32 cm and 34×34 cm and therefore represent unusually large dimensions for solid wood cross-sections even for historic structures. At the time of assessment, the sheeting were asbestos-cement boards [2].

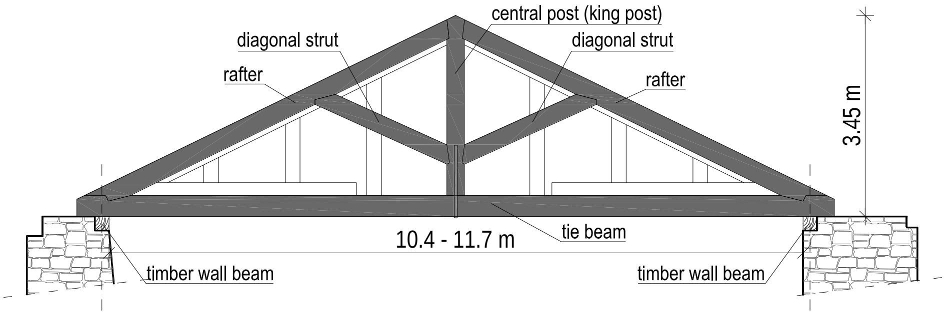

Figure 2: Characteristic cross-section of hanging truss

Figure 3: Magazine 2, inside view

3 ASSESSMENT AND CONDITION OF THE STRUCTURE

Inspection consisted of: the survey of existing structure (geometry, member sizes, joints, connectors, supports); detailed visual inspection (condition of members, joints, supports); laboratory testing and analysis; drawings of existing structure with damage review on roof structure; characteristic truss load-bearing/structural analysis with new load cases; repair and restoration instructions [2].

Timber sampling has been done on the site and testing was performed in certified laboratory [3]. Samples were taken from rafters and tie beams in magazines 1 and 3.

Observed structural deficiencies:

- surface damage of timber trusses due to salt contact;
- removed central post (magazines 2 and 3);
- heavily damaged iron connectors;
- missing members (tie beam, rafter, diagonal strut);
- excessive deflection of tie beam (removed central post);
- inadequate additional strengthening members.

Sea salt is known to have antiseptic action, therefore the presence of salt would contribute to the biological conservation of wood. On the other hand, sea salt has an enhanced hydrolytic action and contributes to mechanical disintegration of wood (through increased abrasion and crystal formation within the wood structure). Moisture content of wood in salt contact is elevated in comparison to normal climatic conditions since the aqueous NaCl solution maintains the level of relative air humidity of 85 %, which would cause the equilibrium moisture content of wood to rise to 17 – 18 %. Accordingly, the mechanical properties of moist wood are somewhat lowered and creep would be enhanced. Additionally, salt causes the corrosion of metals, which presents a crucial risk in maintaining the proper condition of iron or steel connectors.

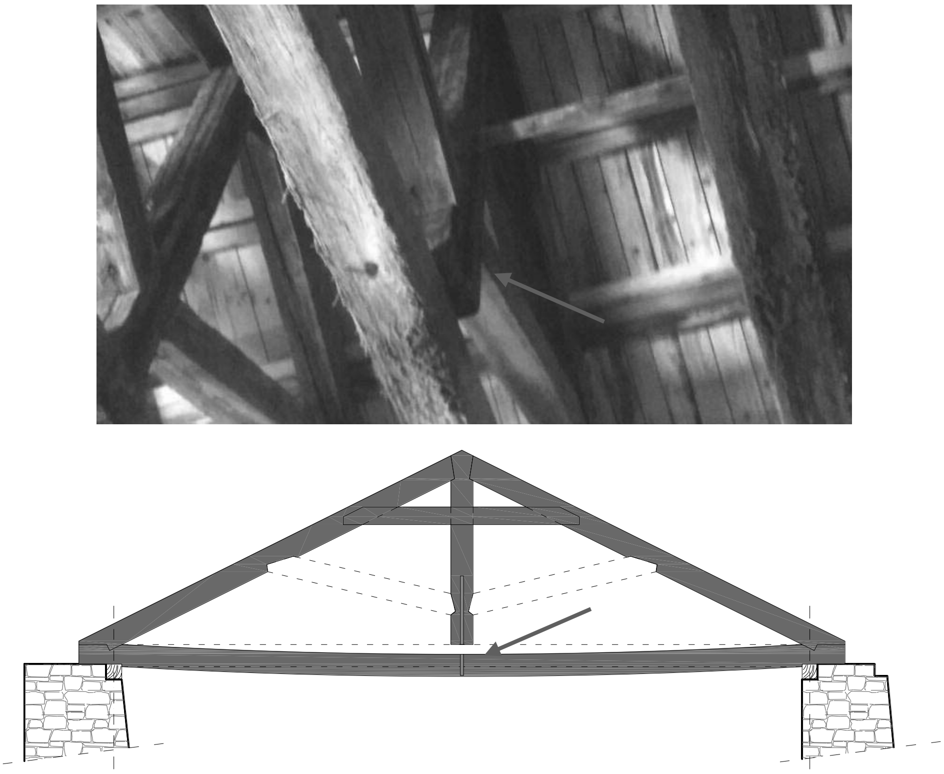

Figure 4: Heavily damaged (broken) iron connector due to corrosion (red arrows)

Overall condition of existing timber structures has been evaluated as poor, but with several applicable restoration options. Specified series of defects and deficiencies are significant in terms of importance for function of the structural systems. Most important deficiencies were found to be missing elements, mostly central posts and diagonal struts. These deficiencies caused major irreversible deformations and deflections of the hanging trusses.

Majority of samples were taken from the third magazine. Sample positions can be seen in Fig. 5 along with the local position in the trusses in Fig. 7, rafter or tie beam. Samples taken from tie beam suffered significantly deeper damage caused by salt than samples taken from rafters. Also, the third magazine suffered more damage than the first and the second magazine. Damaged sheeting or partly removed sheeting on the third magazine roof was the main reason for substantially worse condition of third magazine roof structure. Timber wall beams were not accessible for sampling, but visual inspection proved the suspected poor condition. Timber wall beams weren't isolated from stone wall contact and were severely decayed due to the lack of hydroisolation. It was assumed that moisture content is higher than in the rest of the roof elements. Signs of decay were detected mainly at the positions where timber wall beams supports tie beams. Central posts were removed in places during the installation of transportation lanes that were installed in the middle of the truss (magazine 3). That action altered the structural system and caused excessive deflection of the tie beam of the truss. Tie beam was thus transformed into a simple end-supported beam with insufficient cross-section to support the loads at the span of the given length. Tie beams deflections in magazines 1 and 2 are a consequence of iron connector breaking due to the action of moisture and salt (Fig. 4), which fastened corrosion and degradation process. As confirmed in samples testing, salt influence on timber beams, mostly tie beams, caused only surface damage down to 30 mm of depth (Fig. 6). The inner part of cross section remained sound and dry. Majority of damaged timber elements can be restored or replaced, but certain amount of heavily damaged ones have to be removed and replaced with new ones and properly hydroisolated from the stone wall contact. The exception is the third Magazine, which has to be fully replaced with new timber roof, due to lack of roof sheeting for last several years. Salt damage on the surface of timber beams can be removed down to sound inner part of cross section (Fig. 6).

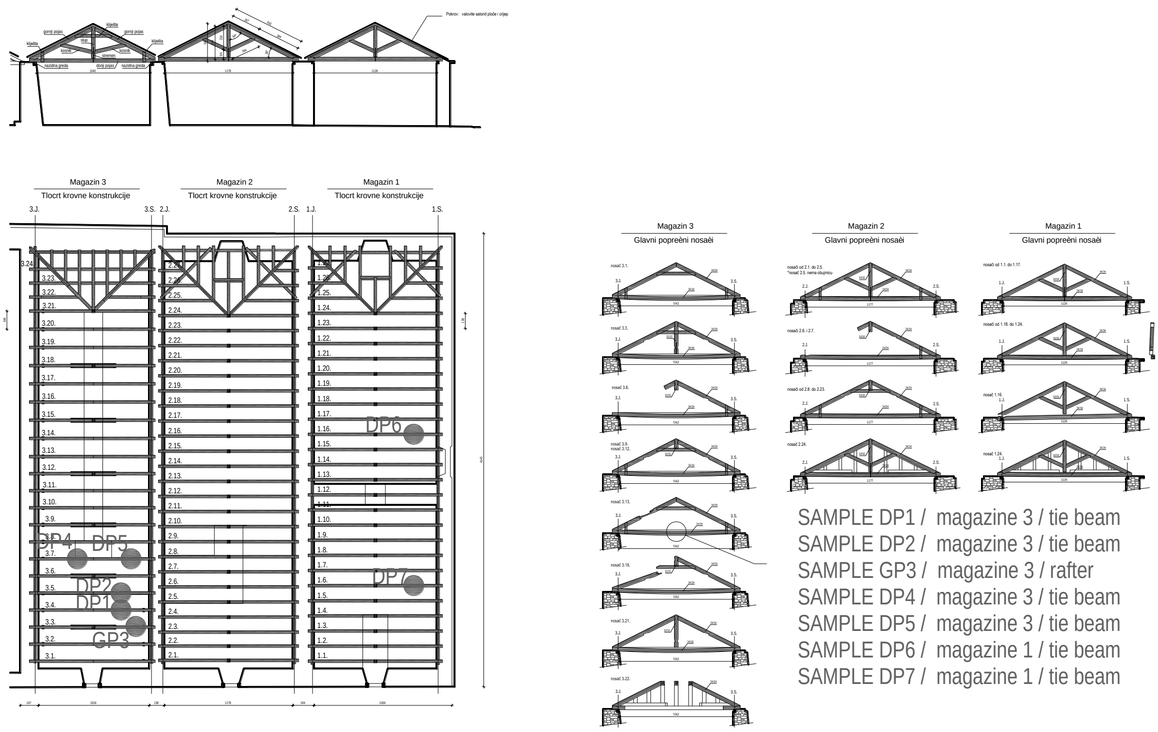

Figure 5: Existing structure plans [2]

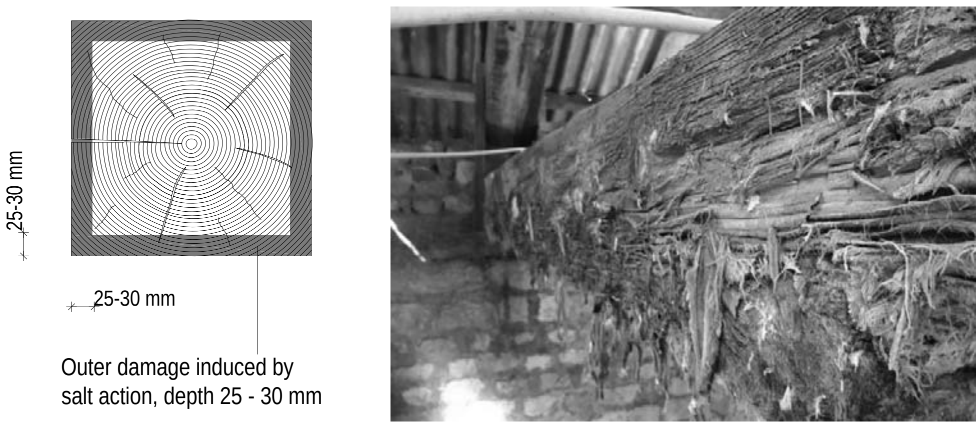

Figure 6: Salt induced damage on cross-section (left) and surface view (right)

4 RESULTS OF LABORATORY TESTING

For laboratory testing, cylindrical samples were drilled down to a depth of 60 mm in different beams in different magazines as presented in the figures 5 and 7. Laboratory tests included examination of the physical properties of taken samples: determination of moisture content, density, growth-rings width, proportion of latewood, determination of timber strength class. Examination of all physical properties of wood and the determination of wood strength class were made in accordance with the relevant EN standards.

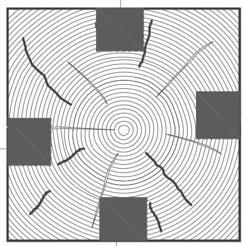

Figure 7: Characteristic cross-section of truss element with sampling positions

According to the determined macroscopic properties of taken specimens and tradition of building with wood at that time in the region of island of Pag, wooden constructions were built of Scots pine (*Pinus sylvestris*) and black pine (*Pinus nigra*) with determined strength class of C50 (according to EN 338; Fig 8, Tab.1).

Figure 8: Cross section of the sample DP 7 (magnification 10 x). Macroscopic anatomical features determine wood as Pine, most probably black pine (*Pinus nigra*) [3]

Health assessment of taken samples was determined using “screening-test” for biological infestation. Tiny pieces of wood were inoculated on sterile nutrient medium in petri dishes (Fig. 9A). After 2 weeks of incubation, petri dishes were visually inspected for contamination and evaluated using light microscopy (Fig 9).

On one hand, mostly brown and greenish-brown powdery mycelia developed in nutrient medium in the petri dishes and the lack of “clamp-connections” between the fungal hyphae lead to the conclusion that taken wood specimens were infected mainly by mold fungi (Fig. 9). On the other hand, mucous cultures developed in nutrient medium reveal bacterial contamination of the specimens which could be from the sea water or contaminated during sampling (Tab. 1). Results of the “screening test” revealed no infection of wood by wood decaying fungi. This biological infestation testing also proved that “screening test” is a good, simple and reliable method for testing of microbiological contamination of wood.

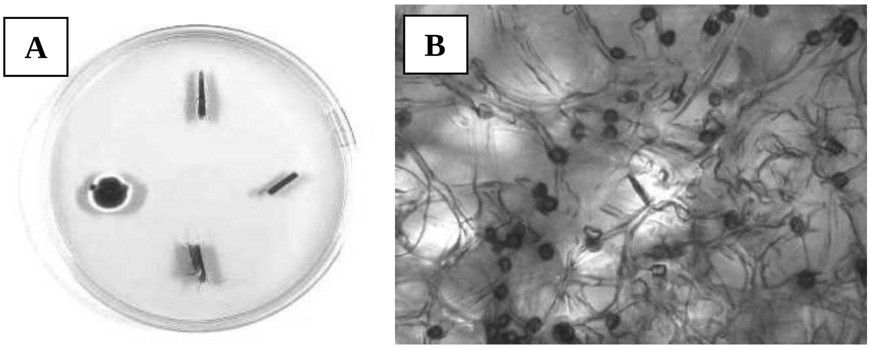

Figure 9: Health inspection of wooden beams: **A)** Chips of wood inoculated on sterile nutrient medium in petri dish (top and bottom chips taken from the surface, left and right chips taken from the 60 mm depth of the wooden beam; **B)** Light microscopy inspection revealed lacking of "clamp-connections" between fungal hyphae

The data of laboratory testing results at measuring positions are presented in the table 1.

Table 1: Surface appearance, health of wood and physical properties of wooden elements in each position of sample withdrawal [2, 3]

Position	Wooden beam surface	Incubated microorganisms cultures	Moisture content [%]	Density, ρ [g/cm^3]	Strength class (EN 338)
DP1			11,93	503	C50
	- salt degradation 25 mm	- low powdery mycelia development - no sign of decay fungi - no biological contamination			
DP2	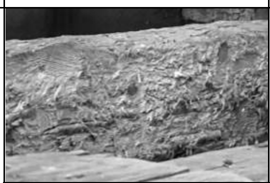		14,84	509	C50
	- salt degradation 20 mm	-low bacterial culture development			
GP3		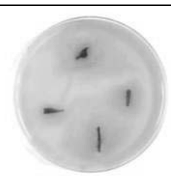	12,69	524	C50
	- salt degradation 10 – 15 mm	-low bacterial culture development			
DP4			-	-	-
	-salt degradation 25 – 30 mm	- low bacterial culture development			

DP5	 -salt degradation 25 mm	 -no biological contamination	14,36	486	C50
DP6	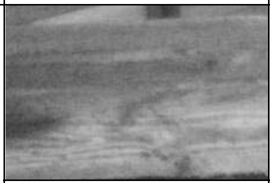 - salt degradation 15 mm	 -no biological contamination	13,26	578	C50
DP7	 -salt degradation 5-10 mm	 -surface powdery mycelia development - no sign of decay fungi - no biological contamination in the middle of the beam	12,51	623	C50

5 STRUCTURAL ANALYSIS

Structural analysis has been performed on existing hanging truss model with reduced cross-sections to dimensions of remaining sound wood central portions, using finite element analysis software “Radimpex Tower 7.0”. Reduced cross-sections have been analyzed due to removal of salt damaged surfaces (overall depth of 25 mm; Fig. 10). According to EN 1995-1-1 and EN 1991-1 with Croatian nationally determined parameters of wind and snow loading, analysis has shown sufficient retention in load bearing capacity (Fig. 11).

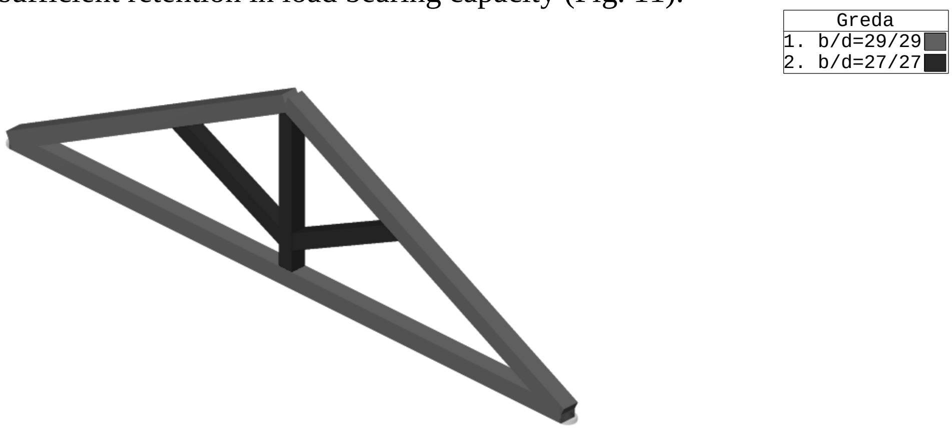

Figure 10: Isometric presentation of structural model

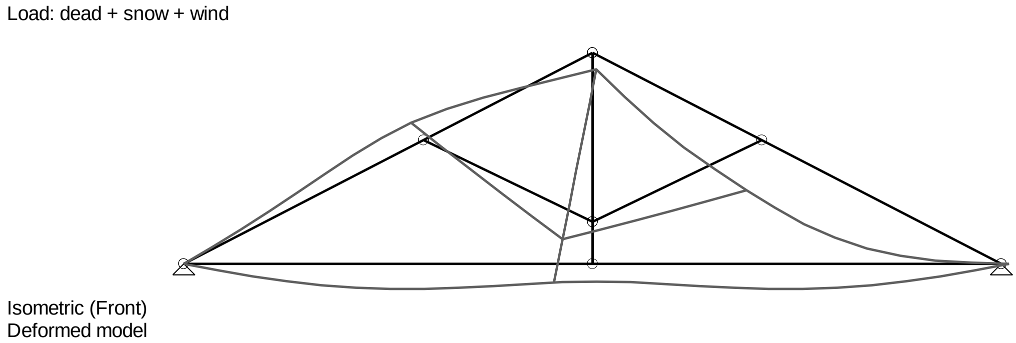

Figure 11: Deformed shape of structural model

6 REPAIR AND REHABILITATION

After investigation process, the following restoration measures have been recommended:
Magazines 1 and 2:

a) Interior scaffolding mounting with temporary support for the roof structure (alternatively, trusses can be placed on floor and after repair process, mounted back).
b) Existing roof sheeting removal.
c) Temporary roof structure installation above existing one.
d) Deconstruction of stone walls above and around timber wall beams.
e) Removal of existing timber wall beams and implementation of new ones, including waterproofing foil insulation.
f) Repair and restoration of existing timber elements (rafters and tie beams, struts, posts) – around 50 %. Repair includes mechanical removal of outer damaged layers with hand tools (scrapers, steel brushes, planning tools). Repair or replacement of iron connectors. New elements must be jointed together exactly like original ones, using traditional carpentry techniques.
g) Installation of missing elements (rafters and tie beams, struts, posts, iron connectors) – around 30 %.
h) Installation of roof sheeting supporting grid.
i) Finishing work of timber elements – biocidal impregnation and decorative coating.
j) Roof sheeting installation.
k) Temporary roof structure removal.

Magazine 3:

Due to heavy damage on timber elements, there was no possibility for repair. Timber structure as a whole must be replaced with the new one.

7 CONCLUSIONS

Existing timber roof structure on salt magazines in Pag (Croatia) was assessed. After field survey with timber sampling, laboratory testing has been carried out along with preliminary structural analysis of the main hanging truss. Overall condition of existing timber structures has been evaluated as poor. Main deficiencies are missing or damaged timber elements made during numerous historic interventions on the structure and salt induced damage on iron connectors and tie beams. In conclusion, repairing and restoration measures have been recommended for magazines 1 and 2, with the exception for magazine 3 which roof must be completely replaced with new one.

8 REFERENCES

[1] *** 2017. Solana Pag (Pag salt pans information leaflet, in Croatian language), online. http://www.solana-pag.hr/povijest.html

[2] Pojatina, J. 2016. "Elaborat o stanju drvenih krovnih konstrukcija" (*Expert report on condition of wooden structures*, in Croatian language). Zagreb

[3] Turkulin, H., Hasan, M. 2016. "Ekspertiza i izvještaj o ispitivanju uzoraka drva konstrukcije krovišta solana u Pagu"(*Testing report and expert opinion on condition of wooden samples of the roof structures of Solana Pag salt pans,* in Croatian language). Zagreb

[4] European Committee for Standardization (CEN): EN 338:2016: Structural timber – Strength classes.

[5] European Committee for Standardization (CEN): EN 1995-1-1:2004+AC:2006+A1:2008: Eurocode 5: Design of timber structures – Part 1-1: General – Common rules and rules for buildings.

[6] European Committee for Standardization (CEN): EN 1991-1-3:2003+AC:2009: Eurocode 1: Actions on structures – Part 1-3: General actions – Snow loads.

[7] European Committee for Standardization (CEN): EN 1991-1-4:2005+AC:2010+A1:2010: Eurocode 1: Actions on structures – Part 1-4: General actions – Wind actions.

SHATIS'17
4th International Conference on
Structural Health Assessment of Timber Structures
20-22 September 2017 Istanbul, Turkey

A DATABASE CONSTRUCTION TOOL FOR SEISMIC VULNERABILITY ASSESSMENT OF TIMBER ROOF STRUCTURES

Maria A. Parisi[1], Chiara Tardini[1], and Davide Vecchi[1]

[1] Politecnico di Milano, Italy

Keywords: Timber roofs, Seismic Vulnerability, Assessment, Inspection database

Abstract

A procedure for the assessment of the seismic vulnerability of timber roof structures previously proposed by the authors is divided into two steps: the first consists in acquiring knowledge of the structure by means of a visual inspection focusing on aspects related to seismic behaviour, while the second elaborates these data to express the vulnerability level of the structural system.

Reference is made to a series of structural characteristics and details that may be considered as vulnerability indicators, among which are the structural typology, the quality of carpentry joints, and the effectiveness of restraints. The original implementation of the procedure made use of paper forms, or templates, for the phase of data collection. The template permits to organize data in a format suitable for use in the vulnerability assessment step, but is also useful as a guide for performing the survey according to predefined and standardized criteria. The survey site conditions, however, are often unfavorable, due to the location of roof structures that may be difficult to reach, with poor environmental and operative conditions, limited access possibly lacking a planking level, dust and subdued light. Paper forms, even if resilient, are often cumbersome to bring along and fill.

The development of new digital technologies, like easily portable computers of small weight and limited dimensions and tablets, has suggested developing a revised digital version of the procedure. The design and implementation of a software tool guiding the survey and recording the observed data into a database has brought to update and improve the original procedure, taking advantage of the possibilities offered by a software support that combines programming language and graphics with great flexibility. The newly developed features of the current prototype system are presented and discussed by means of examples for typical roof structures of the Italian constructional tradition.

1 INTRODUCTION

The many earthquakes that struck Italy in the last decades, from the 1970's up to the most recent one of Central Italy 2016-2017, have shown that the response for traditional masonry buildings is significantly influenced by the behavior of the timber roof structure. The frequent cases of damage related to failure of the roof system or to its interaction with the walls has been counter-balanced by other more positive situations. These corresponded to well-organized and interconnected roof trusses, sometimes strengthened with light interventions, that neither disassembled nor collapsed, but rather kept well-connected with walls, contributing to link them and create a collaborative behavior in the whole building, which is most times the discriminating factor in the final outcome.

This consideration has inspired a research project devoted to timber roof structures under seismic action [1, 2]. The major aim was at investigating the causes and the conditions that would result in seismic vulnerability of the timber roof structure. A parallel objective was to identify simple but effective improvement interventions that could reduce a high vulnerability level [3]

More in general, the work was expected to put into evidence the specific issue of the response of roof structures to seismic action. This action, being of dynamic type and usually with a dominating horizontal component, differs radically from the vertical loads for which roof structures were traditionally conceived. In this situation, the vulnerability assessment of timber roof structures must associate an exam of the features typically related to this material with those pertinent to the problem of seismic behavior with its characteristics, demands, and methods. The main result of this project has been the proposal of a procedure for assessing the seismic vulnerability of timber roof structures.

As a premise, it must be remarked that the seismic vulnerability of a structure, intended as its more or less pronounced tendency to undergo damage or failure in an earthquake, may be expressed at different levels of detail. It may be a rapid single rating based on a very synthetic visual inspection of some particular elements, to be used for pointing out emergency situations. Priority interventions may be decided examining different structures on a comparative basis, as in the case of a territorial survey. Otherwise, vulnerability may concern a more detailed exam of the structure, aimed at a more specific definition of possible criticalities with respect to a dynamic action; the exam of the structure carried out at this level is not yet the assessment that is necessary for design purposes if interventions have to be performed, but is at a time sufficiently detailed to address decisions, and sufficiently synthetic to be performed in a limited amount of time. The latter approach has been followed within this research.

The procedure proposed comprises a first step in which a visual inspection of the structure is performed in order to acquire knowledge on its state and collect data to be used subsequently for the actual seismic assessment. The second step consists in analyzing a series of characteristics of the structural system that have been recognized as significant indicators of its capability of seismic response. Each of the indicators, summarized in the following section, is based on the data and information collected in the first step, which is crucial for an effective assessment.

The visual inspection and data collection phase, which is the center of the present work, has been initially carried out by filling an ad-hoc form that lists all the items to be examined and checked during the process in an organized way.

Visual inspection performed with the basis of a structured form has been used since many years for seismic vulnerability assessment campaigns in various countries, and in Italy in particular. These were related to different kinds of buildings and structures, but did not concern timber. The experience derived from these operations has shown the importance of a well-defined form for an accurate and efficient data collection. The form structure actually guides the surveyor performing the visual analysis, driving to examine with special attention the items that are most critical or most useful for the specific purpose.

In vulnerability assessment applications, so far a printed paper form has generally been used. Some exceptions are starting to arise, like the vulnerability assessment forms alternatively proposed by FEMA as a digital tool [4]. These are, however, intended for a risk estimate crossing vulnerability assessment from the building survey and the local hazard level; the digitized procedure therefore includes a rapid survey and a numerical elaboration of the risk, for which a software program is particularly suited.

The very fast development of digital technologies that now propose highly robust and portable hardware, and on the other side the difficulties encountered in many on-site applications of the survey form in its original paper format have brought to design and implement a new digital version of the form. The possibilities offered by a software approach may solve many of the problems met. At the same time, the resulting enhanced flexibility has permitted to redefine and improve some aspects of the procedure. These aspects are presented and discussed in the following.

2 SEISMIC VULNERABILITY ASSESSMENT FOR TIMBER ROOFS

The level of vulnerability of the roof structure is assessed in the second step of the procedure, after visual inspection [5]. The different structural characteristics and conditions that have been considered most significant for their effect on the seismic response are grouped into the following general indicators; each of them may be further detailed and subdivided pointing out different issues to be considered,

1. The conceptual design: this is the first indicator to be considered; most roof structures, in fact, have been conceived with a load carrying function towards vertical loads; the capability to balance horizontal forces like earthquake-induced inertia forces may have not been considered in the original design, or may be possible but limited altogether; it depends on the structural concept adopted; the first vulnerability indicator concerns, therefore, the structural typology [6].
2. The carpentry joints: the type, details, and conditions of carpentry joints are an important factor in determining the vulnerability of the roof structure; the capability of the joints to hold the connection during cyclic conditions that may reduce compression in the timber elements, and their expected post-elastic behavior must be examined, with the purpose to identify possible failure modes, ending in disassembly or brittle failure.
3. The system of constraints: the types and conditions of the connection of the timber structure to the walls may be considered a major vulnerability indicator; it deals with the effectiveness of the connection in preventing sliding off and loss of support; this kind of failure often triggers progressive failure of the whole building system;
4. The state of the structure: any condition specifically related to the state of the structure that may affect vulnerability is considered here, including the maintenance and conservation state, but also the presence and quality of previously performed strengthening interventions.

The indicators are graded according to a scale that ranges from A to D through B and C. The value A corresponds to the minimum vulnerability of a structure that was designed, executed and maintained according to best practice and incorporates all the positive features in favor of seismic safety, comparable to a new code-designed structure. D is the highest vulnerability level, representing a structure with serious deficiencies that should be promptly remediated by suitable interventions, B and C representing intermediate levels.

Support for grading is given in various forms: for some indicators, reference tables have been developed based on experimental or numerical analysis results, or both, for the most frequent situations; others may be judged referring to the same fundamental concepts; for some other indicators, less developed at the moment, results from case studies are reported as examples. The roof structure typology that is most frequent in Italy is composed of a series of trusses interconnected by ridge beam and purlins, or additionally by diagonal struts and bracing elements. The procedure is particularly tailored on these cases.

The purpose of the first step, the visual inspection, is to obtain the information and data necessary to elaborate the indicators, according to the list above. Some considerations stem from this fact,

1. The inspection considers with particular care some features of the structural system and may simplify others that are usually requiring much attention in the general assessment of timber structures; for instance, the determination of the wood species affects results in a very limited manner, while the presence and effectiveness of metal closures of the joints protecting them from load cycles that may cause a pressure decrease is a priority;

2. Old structures not suitable to balance horizontal loads are not rare; occasional horizontal components are usually absorbed by the actual semirigidity of carpentry joints, or other sources of resilience; yet, these situations are characterized by high uncertainty of behavior and are not reliable; they need to be pointed out and corrected as a most important result of the analysis; other points related to the possibility of the structure to respond to the action concern, for instance, the size of the cross-sections that must be sufficient to carry an increased stress level in their current state; degradation and decay must be considered here, being influential on this issue; given the importance of these situations, the layout of the structure and the relevant data are the first examined and collected.

3 VISUAL SURVEY AND DATA ORGANIZATION

The data and observations gathered during the visual survey are written on site in the data collection form that, consequently guides the inspection. This point is important in order both to direct the inspection to the main items of interest for the intended purpose, and to some extent to homogenize the way the survey is carried out over different cases.

The structure of the collection form must be, then, efficient in considering with due care all the important features and in reducing time and the effort as much as possible.

The survey, and the form, has been conceived with a tree structure, where information is searched with increasing detail, basically going from a structural level to the element and then to the joint level.

As a result, a first page gathers general information identifying the building (type, location, period of construction) and describes its general geometry (dimensions, general layout) and material (brick, stone masonry, etc.). Much of this is compiled out-of-site, before or after the survey.

The wood species present in the roof structure are then specified. A simplified estimate is sufficient here. The presence of biotic attack or degradation for mechanical reasons is posted out at this point for a general view. It will be indicated more specifically in terms of amount and location at element description time.

The type and state of the connections between the roof structure and the supporting walls are examined as a third point.

The next set of data concerns the structural typology, that is, the problem of structural characterization- A timber structure may be conceived as two-dimensional, or 2D, (e.g. trusses interconnected by more or less effective linking elements or substructures) or less frequently as three-dimensional, 3D. From this alternative, down-branching brings to examine more details. For a truss system, 2D, the trusses are individually examined in sequence. For each, the main elements are surveyed, as well as the joints connecting them; down-branching applies as well to joint description.

Similarly, the members linking the trusses are examined. A sketch to be drawn at the start permits to identify the location of trusses and other elements by assigning them a number.

Because the visit on site may not be easily repeatable, an estimate of the paper pages to be brought at roof level is necessary. Following the branches down to joint detail for each truss may require a considerable amount of forms and their compilation may result tedious, fostering errors. Figure 1 shows part of a page collecting data on structural elements..

The data collection procedure has been applied to several roof structures, with good results in terms of the objectives, in spite of the inconveniences mentioned above. After a period of application, its implementation into a software tool seemed to be timely.

18. BIDIMENSIONAL TRUSS (SERIES)						
18. STRUCTURAL ELEMENTS	18.1.1 Rafter				l	r
			circular			
			rectangular			
		Section	other:			
		Dimension:				
		Decay:				
	18.1.2 Parallel rafter				l	r
			circular			
			rectangular			
		Section	other:			
		Dimension:				
		Decay:				
	18.1.3 Tie beam		circular			
			rectangular			
		Section	other:			
		Dimension:				
		Decay:				

Figure 1: Excerpt from paper form

4 ADVANCING THE PROCEDURE

The data collection form that guides the vulnerability assessment according to predefined and standardized criteria was originally on paper for a series of reasons, mostly related to the survey conditions. These paper forms have been used until recently in case studies and applications and have been useful in a first period of development also as a tool to test the procedure. Some inconvenience, however, was experienced in their use, especially in the inspection of large roof structures that required to deal with bulky form packs, a situation aggravated by the usually inhospitable under-roof environment. The state of survey sites is often unfavorable, due to the location of roof structures that may be difficult to reach, with poor environmental and operative conditions, limited access possibly lacking a planking level to walk on, great quantity of dust, subdued light, usually with no possibility to connect to power outlets. Paper forms, even if resilient, become often cumbersome to bring along and impractical to fill. At the same time, the adverse site conditions had suggested to avoid using and even bringing on site a normal and usually delicate portable computer.

Highly portable and robust digital tools of small dimensions and weight, with batteries with long lasting charge have seen a fast development, and are now commonly available. In general, the possibilities offered by mobile technology have fostered various projects for computer-based assessment surveys. With reference to timber structures only, the European Union COST project FP1101 (Forest products) has defined a computer-based data collection template for the assessment of the conditions of timber structures. A first version was implemented in [7]. A template for damage assessment of timber structures of modern design had been presented in [8].

The Mondis project [9], based on the use of tablets, aims at implementing a tool for on-site monitoring of monument damage using mobile devices; it is not, however, intended specifically for timber structures.

This fast development of new digital technologies has suggested developing a revised digital version of the visual inspection and data collection step in the vulnerability assessment procedure [10]. The design and implementation of a software tool recording the observed data into a database has brought to update and improve the original process, taking advantage of the possibilities offered by a software support [11] that combines programming language and graphics with great flexibility.

The new system offers advantages of data digitalization on site and the possibility of a more efficient management of branching down in the data collection phase. The interface with the user is by means of menus for the different items to be considered; the chosen option opens up a new screen with data to be inserted and possibly further branching down. As an example, fig. 2 reports the first screen with general building information and the pointers to more detailed information, like “dimensions and geometry” and the like.

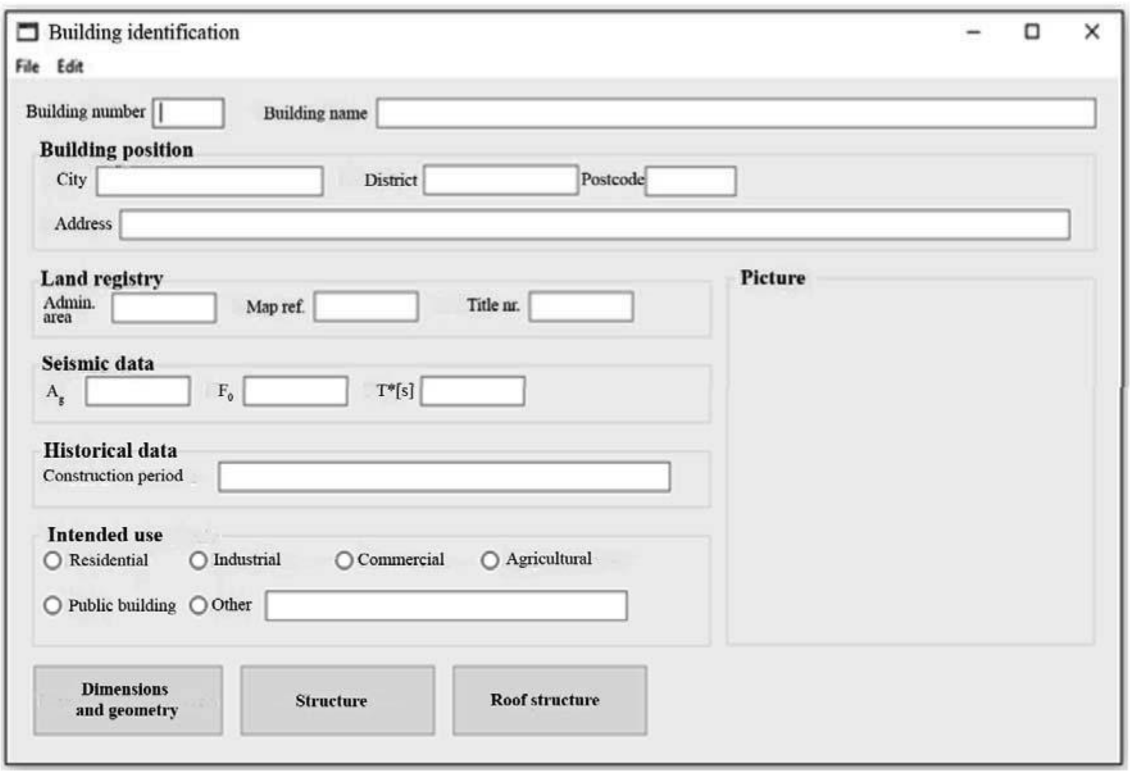

Figure 2: Building information screen

4.1 System implementation

The original data acquisition procedure was organized with a tree-like structure, which is particularly apt to digitalization, and could be easily implemented. In this modality, however, the tree structure may be best exploited with many advantages compared to the original version. In particular, the possibility of

1) moving swiftly along the tree, following down a branch, but also to climb back easily for checking or fixing some information;
2) presenting default values, that may be promptly modified if necessary, simplifying and speeding the process;
3) repeating automatically data for similar elements, intervening only for specific modifications or additions; for instance, if a series of trusses has the same general characteristics, it is possible to define a master truss for which all the data are put in, and generate others, modifying what needed; this operation, as the previous points, is possible also with hard copies, but it becomes extremely time- and paper-consuming; usually paper forms could report the reference case number and only variations, but each form was then partially filled and subsequently completed off-site; errors were likely to occur;
4) inserting new typologies, at different levels (structure types, elements, joints…) which would then appear with the previously defined ones in the menu; this modification of the system is an addition that does not require its total restructuring; this has been the case when, after observing many recurrences, the semi-conical roof structure frequently covering the apse of churches was inserted;

Some other features that are in the development line but are not yet implemented are the possibility of

5) cross checking of entered information, to sort out possible errors;
6) inserting directly sketches, pictures and photos taken at the moment of the survey, that is, on site; now images, as well as comments, documents etc., may be inserted, but usually this is done after the survey; the possibility of taking pictures and insert them with the same instrument will be at best with a tablet or smartphone version of the procedure.

The important general advantage is to obtain directly a database containing in an organized way the data for the case; the database may be accessed by other systems for processing; a module for the evaluation of the indicators, that is, the second step of the procedure is being developed.

The application to practical cases has permitted to test the implemented software and to improve it with some amendments and additions. One of these applications is outlined in the following section.

5 AN APPLICATION

The roof structure of the church of St. Stephen in Vimercate, Milano, in fig. 3, has been used as reference case for testing the new data acquisition procedure.

Figure 3: Views of the church of St. Stephen

Figure 4: View of the roof trusses

The roof covers the central nave of the church and has a typical configuration of 11 parallel trusses ending in a semi-cylindrical roof over the apse. The trusses are interconnected simply with purlins and a ridge beam, as in fig. 4. The roof structure is not visible from below, because it covers a barrel vault that masks it. Not being considered part of the church architecture but only a functional element to support the roof pents, its construction and detailing are not sophisticated. Roof structures of this type have often been considered an artisan element of secondary importance, not understanding their role in some conditions like seismic actions. Figure 5 shows a detail where rudimental manufacturing is evident.

Figure 5: Detail of the rafter and purlin crossing area

The following figures, 6, 7, and 8, are screenshots from the software system. The first gathers general data on the structure and shows its sketch, which was inserted off-site.

Figure 7 concerns the first truss, used as master for the others. Some information like the type of wood remains at this level, others, like the structural elements, branch down. The rafter menu describing the left and right rafter is in fig. 8; space for notes and comments is available, because some observations cannot be condensed in numbers and measures.

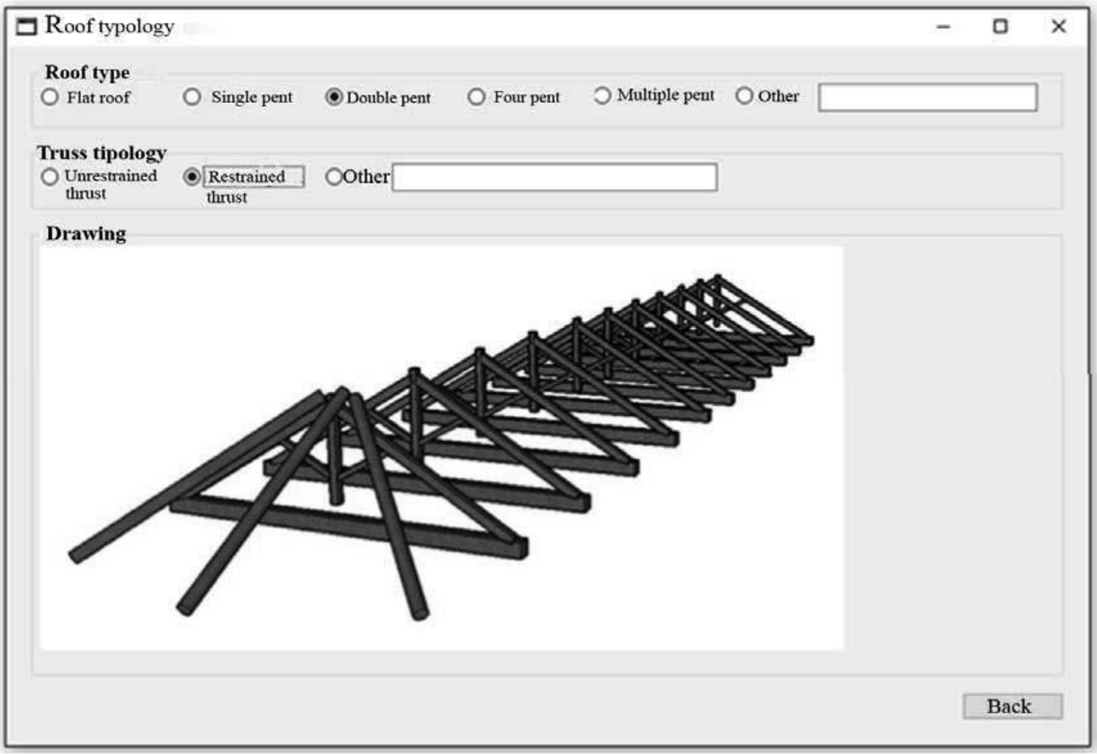

Figure 6: Screen with structure type information

The description of joints follows from the truss page (e.g. fig. 9). Describing a software application synthetically is not effective, but surely the implementation of this case, and some others not described here, were effective in pointing out advantages as well as some limitations. One was the need to include the apse roof among the available typologies, quoted above.

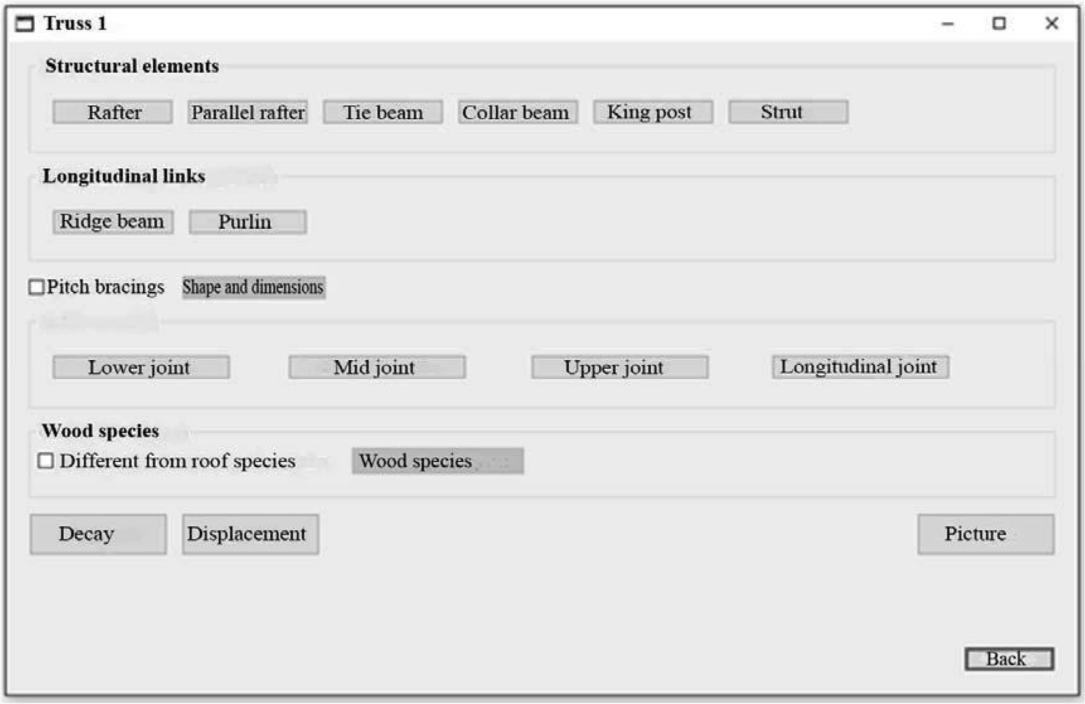

Figure 7: The truss specification with links to its elements

Figure 8: Detailing the rafters

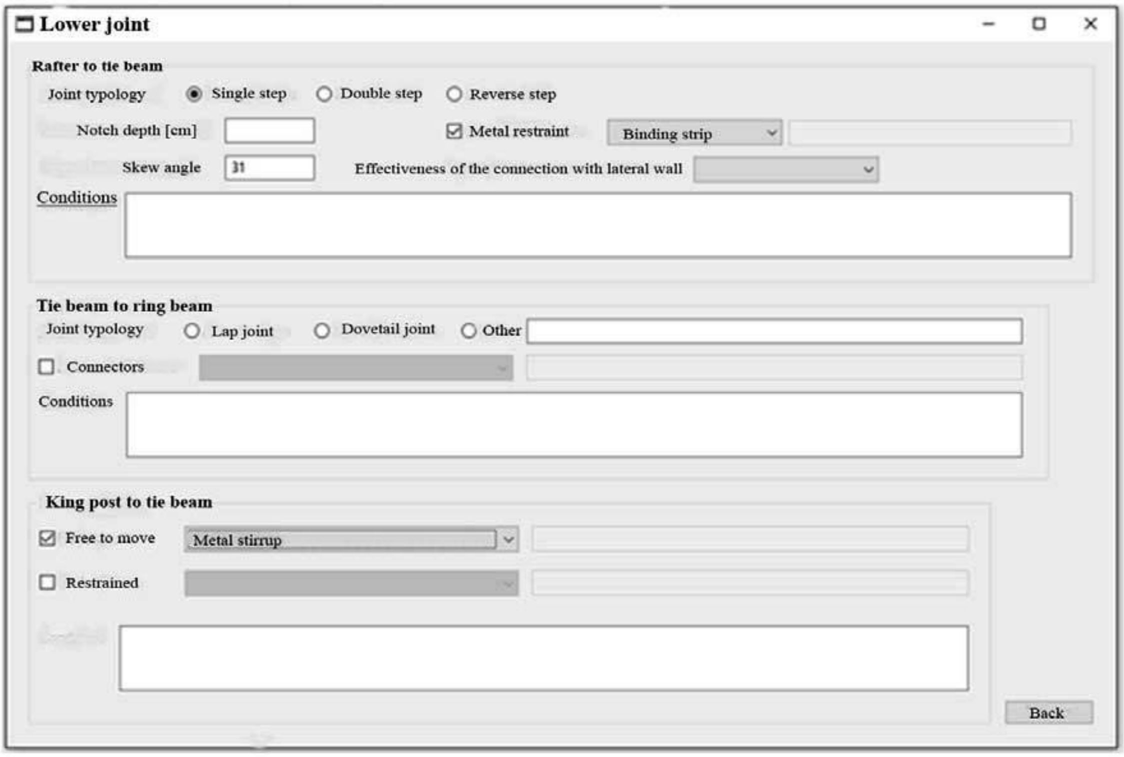

Figure 9: Collecting data on lower truss jonts

6 CONCLUSIONS

The seismic vulnerability assessment of a timber roof structure is a challenging task, for the variety of possible situations and for the influence that details may have on the final outcome. The use of a data collection form that guides in performing the survey in a structured manner helps focusing on the items that are most influential on the seismic behavior.

The use of a digital version of the data collection form initially developed on paper has permitted to enhance flexibility in the operation, reducing significantly the compilation time required, as well as transcription errors, a considerable advantage in the often adverse site conditions.

More features need to be added to the first version that has been implemented, among which is the possibility of data cross-checking and the very basic but powerful possibility of inserting directly at survey time photographic material with views and details that are sometimes better described in a graphic manner.

REFERENCES

[1] Parisi, M. A., Chesi, C., Tardini, C,. Piazza, M., 2008, “Seismic vulnerability assessment for timber roof structures”, *Procs. 14th World Conference on Earthquake Engineering*, Beijing.

[2] Parisi, M.A., Chesi, C., Tardini, C., 2012, “The Role of Timber Roof Structures in the Seismic Response of Traditional Buildings”, paper 2394, *Procs, 15th World Conference on Earthquake Engineering*, Lisbon.

[3] Parisi, M.A., Piazza, M. 2015. “Seismic strengthening and seismic improvement of timber structures”, *Construction and Building Materials*, 97, 55–66.

[4] FEMA P-154, 2014. Rapid observation of vulnerability and estimation of risk, ROVER. Software for use on smartphones".

[5] Parisi, M.A., Chesi, C., Tardini, C., 2013, "Seismic vulnerability of timber roof structures; classification criteria", *Advanced Materials Research,* (778), 1088-1095.

[6] Parisi, M.A., Chesi, C., Tardini C., 2012, "Inferring seismic behaviour from morphology in timber roofs", *International Journal of Architectural Heritage*, 6 (2012), 100-116.

[7] Riggio, M.P., Parisi, M.A., Tardini, C., Tsakanika, E., D'Ayala, D., Ruggieri, N., Tampone, G., Augelli, F., 2015, "Existing timber structures: proposal for an assessment template", *Procs 3rd Intl SHATIS Conf.*, 100-107, Wroclaw, Poland.

[8] Toratti, T. , 2011, "Proposal for a failure assessment template", *Engineering Structures,* 33, 2958-2961.

[9] Cacciotti, M., Blaško, R.,Walach, J.,2015, "A diagnostic ontological model for damages to historical constructions", *Journal of Cultural Heritage*, 16(1):40-48.

[10] Parisi, M.A., Chesi, C., Tardini, C., Vecchi, D., 2017, "Seismic Vulnerability of Timber RoofStructures: an Assessment Procedure", paper 4397, *Procs, 16th World Conference on Earthquake Engineering,* Santiago de Chile.

[11] Rhine, B., 2014. "*Introduction to programming with Xojo*".